

# **MEMBRANE FABRICATION AND MODIFICATION FOR THE TREATMENT OF WASTEWATER USING MEMBRANE DISTILLATION**

**By Minwei Yao**

Thesis submitted in fulfilment of the requirements for  
the degree of

**Doctor of Philosophy**

under the supervision of Ho Kyong Shon and Leonard Tijing

University of Technology Sydney  
Faculty of Engineering and Information Technology

May 2020

## **CERTIFICATE OF ORIGINAL AUTHORSHIP**

I certify that the work in this thesis has not previously been submitted for a degree nor has it been submitted as part of requirements for a degree except as part of the collaborative doctoral degree and/or fully acknowledged within the text. I also certify that the thesis has been written by me.

This research is supported by the Australian Government Research Training Program. Any other help that I have received in my research work and the preparation of the thesis itself has been acknowledged. In addition, I certify that all information sources and literature used are indicated in the thesis.

Production Note:

Signature of Student: Signature removed prior to publication.

Date: 26/05/2020

## ACKNOWLEDGEMENTS

During my journey from objective to goal, I have experienced showers of guidance, inspiration, and blessing from family, colleagues, and friends. Hereby, I offer flowers of gratitude to the almighty, which has been the source of strength throughout my research life.

First of all, I would like to express my gratitude to my family, who are always my backbone of my life and work. Their unconditional love, generous services, and moral supports shape me and my research work.

I would like to express my heartfelt gratitude to my supervisor Prof. Ho Kyong Shon, School of Civil and Environmental Engineering, Faculty of Engineering and Information Technology. He is the main reason that I have the opportunity to pursue my dream of research journey. He is a lighthouse that guides me navigating research fields with big uncertainties. Also, he is both resourceful and generous, so I could enjoy convenience in research life free of many trivial matters. I would also like to thank my co-supervisor Dr. Leonard D. Tijing for his kind support and guidance. His valuable suggestions greatly helped me in successful completion of the PhD journey.

I wish to give my special thanks to Dr. Yunchul Woo who guided and accompanied me throughout a large part of my PhD course. Without him, the journey would be much more challenging. It is very lucky for me to have a mentor like him who could give me valuable guidance and constant encouragement. He is also a very generous and resourceful mate.

I will express my sincere thanks to the external facilities and personnel who provided generous support to me. I would like to say many thanks to Dr. Pierre Le Clech and Dr. Yun Ye, School of Chemical Engineering, the University of New South Wales, Sydney, for providing the excellent facilities for my work including capillary flow porometry measurement. I wish to express my sincere gratitude to Prof. Yuan Chen and Ziwen Yuan, School of chemical and Biomolecular Engineering, the University of Sydney, Sydney, for their kind support. Also, I want to acknowledge Dr. Michael Dong Han Seo, CSIRO, Sydney, for his generous help.

With deep sense of gratitude and humbleness I would like to say many thanks to fellow research members in our school, who made my research journey memorable. I would like to thank Jiawei Ren, Dr. Youngjin Kim, Dr. Gayathri Danasamy, Dr. Sherub Phuntsho and Dr, Laura

Chekli, Dr. Myoung Jun Park, Dr. Jung-Eun Kim, Dr. Sungil Lim, Aaron Katz, Van Huy Tran, Sayed Mukit Hossain, Federico Volpin, Nawshad Akther, Syed Muztuza Ali, Ugyen Dorji, Pema Dorji, Ralph Rolly Gonzales, Mekdim Mezemir, David Inhyuk Kim, Jade Jiayi Jiang, Idris Ibrahim, Youngkwon Choi, and Seongchul Ryu. Throughout the course of my research life, I met lots of amazing friends who offered me joys, encouragements, and inspiration. I would like to express my sincere gratitude to Lay, Jackie, Alex, Yang, Jun, Yiwen, Kireesan, and many other nice guys. The profound connections between us are as precious as my academic achievement.

I would also like to acknowledge Mohammed Johir, Nirenkumar Pathak, Mohammad Boshir Ahmed, Bentuo Xu, Katie McBean, Herbert Yuan, Mark Berkahn, Mark Lockrey, and Alexander Angeloski for their professional laboratory support. I would also like to give thanks to Van Le, Minnie Wan, and Alex Chen for their administrative supports.

I would like to thank the Department of Education, Australian Government for offering me the Australian Government Research Training Program Scholarship towards the completion of the thesis. My work is also supported by a grant (code 18IFIP-C146666-01) from Industrial Facilities & Infrastructure Research Program funded by the Ministry of Land, Infrastructure and Transport of the Korean government; I expressed grateful thanks to them.

Last, but not least, I express my gratitude and apologize to everybody whose contributions I could not mention in this page.

The expertise and achievement in this study belongs to those acknowledged above, and all errors are mine.





## The format of this thesis: Thesis by compilation

### Journal articles included in this thesis:

1. **Yao, M.**, Tijing, L.D., Naidu, G., & Shon, H.K. 2019, 'A review of membranes with special wettability for the treatment of saline wastewater deploying membrane distillation', *Desalination*, vol. 479, pp. 1143-12.
2. **Yao, M.**, Ren, J., Akther, N., Woo, Y.C., Tijing, L.D., Kim, S.H. & Shon, H.K. 2019, 'Improving membrane distillation performance: Morphology optimization of hollow fiber membranes with selected non-solvent in dope solution', *Chemosphere*, vol. 230, pp. 117-26.
3. **Yao, M.**, Woo, Y.C., Ren, J., Tijing, L.D., Choi, J.S., Kim, S.H. & Shon, H.K. 2019, 'Volatile fatty acids and biogas recovery using thermophilic anaerobic membrane distillation bioreactor for wastewater reclamation', *Journal of Environmental Management*, vol. 231, pp. 833-42.
4. **Yao, M.**, Woo, Y.C., Tijing, L.D., Choi, J.S. & Shon, H.K. 2018, 'Effects of volatile organic compounds on water recovery from produced water via vacuum membrane distillation', *Desalination*, vol. 440, pp. 146-55.
5. **Yao, M.**, Woo, Y.C., Tijing, L.D., Cesarini, C. & Shon, H.K. 2017, 'Improving nanofiber membrane characteristics and membrane distillation performance of heat-pressed membranes via annealing post-treatment', *Applied Sciences (Switzerland)*, vol. 7, no. 1.
6. **Yao, M.**, Woo, Y.C., Tijing, L.D., Shim, W.G., Choi, J.S., Kim, S.H. & Shon, H.K. 2016, 'Effect of heat-press conditions on electrospun membranes for desalination by direct contact membrane distillation', *Desalination*, vol. 378, pp. 80-91.

\*All the papers have been published.

\*\*As the first author, I am the main contributor of the papers mentioned above.

## ABSTRACT

Owing to both water shortage and environmental protection, the government around the world is creating policies to regulate the release of wastewater into natural bodies of water. Therefore, there is a growing requirement of highly efficient wastewater treatment technologies.

Currently, centralized wastewater treatment plants were used in most cities and towns globally. The on-site treatment of domestic wastewater is consistently gaining interests because it reduces the needs of central treatment plants, which require large footprint and high maintenance. In addition, the potential use of the reclaimed water for non-potable purposes reduces the stress in local water supply, and hence the cost of freshwater production and transportation. However, conventional wastewater treatment technologies used in the centralized treatment plant are not feasible to be implemented in the decentralized treatment facilities owing to its large footprint and long retention time. Currently membrane bioreactor (MBR) has been developed for wastewater treatment facilities with small footprint. However, the quality of permeate discharged from MBR system is not high enough for direct use. Therefore, additional treatment such as UV and reverse osmosis (RO) are essential, which requiring more footprint and energy consumption. To address these issues, the overall aim of my PhD study is to develop highly efficient membrane system to treat wastewater with special designed membranes. Membrane distillation (MD) has many advantages over conventional microfiltration (MF) such as high quality permeates, leading to potentially high energy efficiency for the whole wastewater treatment plant. So, it is critical to evaluate the possibility of MD to replace MF in MBR, as MD has unique mechanism which provides several advantages over MF. Hereby, following research objectives have been developed to meet the aim: 1. to develop the first thermophilic anaerobic membrane distillation bioreactor (anMDBR) for the treatment of municipal wastewater. 2. to improve the permeation performance of hollow fiber membranes. 3. to investigate the behavior (mass transport, fouling, and rejection) of organic compounds in MD processes regarding fouling and mass transfer.

During my PhD studies, I have successfully developed the first anMDBR system in lab-scale. High inorganic and organic compounds rejection of 99.99% could be achieved using this system. Based on the results, I recommend 45 °C as optimal bioreactor temperatures for its stable flux performance and resource recovery. It was found that salinity of the mixed liquor had minimal impact on anMDBR. The potential recovery of biogas and volatile fatty acids

offered economic benefits. Some challenges were realized when developing an MDBR system:

1. Permeation flux was very low (~2 LMH).
2. Impact of volatile organic compounds (VOCs).
3. Membrane fouling issues.

Hence, following solutions have been suggested:

1. Development of membrane with high permeability.
2. Study of VOCs behavior.
3. Development of membranes with anti-fouling properties.

Therefore, in next stage of my study, I developed hollow fiber membranes with bicontinuous structure and porous skin without using weak solvent in coagulation bath. The open pore morphology improved permeation performance in membrane distillation due to high porosity and mean pore size. Also, I found that non-solvents in the dope solution affect the morphology of hollow fiber membranes. It can be concluded that this is a simple and cost-effective technique, which is suitable for mass production. Then I investigated the behavior of VOCs in feed tank. It was found that VOCs with surfactant properties existing in the feed have high mobility and could cause rapid wetting. Also, the total flux of VMD was increased with the addition of VOCs into the feed. And VOCs showed negative impacts on the permeate quality as they could penetrate membranes. I also conducted some research regarding permeation performance improvement using heat-treatment and optimal conditions had been determined. Recommendations for future study have also been addressed in this thesis.

## LIST OF ABBREVIATIONS

2-BE	2-Butoxyethanol
anMDBR	anaerobic membrane distillation bioreactor
AF	Anti-fouling
AgNP <sub>s</sub>	Silver nanoparticles
AFM	Atomic force microscopy
AGMD	Air gap membrane distillation
Al <sub>2</sub> O <sub>3</sub> NPs	Alumina nanoparticles
ATR-FTIR	Attenuated total reflectance – Fourier transform infrared spectroscopy
AW	Anti-wetting
BAU	Business as usual
C <sub>6</sub> Cl <sub>3</sub>	Alcyone
CA	Contact angle
CBD	Chemical bath deposition
CDI	Capacitive deionization
CF <sub>4</sub>	Tetrafluoromethane
CFP	Capillary flow porometry
CNTs	Carbon nanotubes
COD	Chemical oxygen demand
CSG	Coal seam gas
CVD	Chemical vapor decomposition
DBP	Dibutyl phthalate
DCMD	Direct contact membrane distillation
DI	De-ionized water
DMAc	N, N-Dimethylacetamide
DMF	N, N-Dimethylformamide
DS	Desalination
DSC	Differential scanning calorimetry
EDX	Energy dispersive x-ray spectroscopy
ENM	Electrospun nanofiber membrane
FAS17	1H, 1H, 2H, 2H-Perfluorodecyltrimethoxysilane
FAS21	1H, 1H, 2H, 2H-Perfluorododecyltrichlorosilane

FO	Forward osmosis
FDTS	1H, 1H, 2H, 2H-Perfluorodecyltrichlorosilane
FTCS	1H, 1H, 2H, 2H-Perfluorododecyltrichlorosilane
GC-MS	Gas chromatography-mass spectrometry
GOR	Gain output ratio
HA	Humic acid
HF	Hollow fiber
HP	High permeability
IPA	Isopropyl alcohol
IW	Industrial wastewater
LBL	Layer-by-layer
LEP	Liquid entry pressure
LNG	Liquefied natural gas
L-L	Liquid-liquid
MBR	Membrane bioreactor
MCr	Membrane crystallization
MD-BR	Membrane distillation-membrane bioreactor
MD	Membrane distillation
MF	Microfiltration
N6	Nylon-6
NaCl	Sodium chloride
NaOH	Sodium hydroxide
NH <sub>4</sub> <sup>+</sup>	Ammonium
NIPS	Non-solvent induced phase separation
NF	Nanofiltration
NMP	N-Methyl-2-pyrrolidone
NP	Nanoparticle
NS	Non-solvent
OH	Hydroxyl
OMBR	osmosis membrane bioreactor
OTMS	Octadecyltrimethoxysilane
PA	Polyamide
PAM	Polypropylene acid ammonium

PAN	Polyacrylonitrile
PDEs	Partial differential equations
PDMS	Polydimethylsiloxane
PFDT	1H, 1H, 2H, 2H-Perfluorodecanethiol
PFOTCS	1H, 1H, 2H, 2H-Perfluorooctyl-trichlorosilane
PFOTES	1H, 1H, 2H, 2H-Perfluorooctyltriethoxysilane
PFTES	1H, 1H, 2H, 2H-Perfluorodecyltriethoxysilane
PEI	Polyetherimide
PES	Polyether sulfone
PET	Polyethylene terephthalate
PFPE	Perfluoropolyether
PGMD	Permeate gap membrane distillation
PP	Polypropylene
PRO	Pressure retarded osmosis
PS	Polystyrene
PSD	Pore size distribution
PSf	Polysulfone
PTFE	Polytetrafluoroethylene
PTFE	
-AF 2400	Poly[4,5-difluoro-2,2-bis(trifluoromethyl)-1,3-dioxole-co-tetrafluoroethylene]
PVA	Polyvinyl alcohol
PVAc	Polyvinyl acetate
PVC	Polyvinyl chloride
PVDF	Polyvinylidene fluoride
PVDF-HFP	Polyvinylidene fluoride-co-hexafluoropropylene (PVDF-co-HFP)
RO	Reverse osmosis
SDS	Sodium dodecyl sulfate
SEC	Specific energy consumption
SEM	Scanning electron microscopy
SFE	Surface free energy
SGMD	Sweeping gas membrane distillation
SiNPs	Silica nanoparticles
SiO <sub>2</sub>	Silicon dioxide

SMM	Surface modifying macromolecules
SWRO	Seawater reverse osmosis
S-L	Solid-liquid
TEM	Transmission electron microscopy
TEP	Triethyl phosphate
TIPS	Thermally induced phase separation
TiO <sub>2</sub>	Titanium oxide
TGA	Thermogravimetric analysis
TOC	Total organic carbon
TPC	Temperature polarization coefficient
TiO <sub>2</sub>	Titanium dioxide
UF	Ultrafiltration
VFA	Volatile fatty acids
VIPS	Vapor induced phase separation
VMD	Vacuum membrane distillation
VOC	Volatile organic compound
x-DVLO	Extended Derjaguin Landau Verwey Overbeek
XRD	X-ray diffraction
ZnO NPs	Zinc oxide nanoparticles



## LIST OF SYMBOLS

$A$	Effective area of the membrane
$B$	Pore geometry coefficient
$B'$	Membrane coefficient
$C$	Cold fluid
$C_p$	Permeate concentration
$C_f$	Feed concentration
$C_m$	Membrane mass transfer coefficient
$C_p$	Specific heat capacity
$D_{AB}$	Water vapor diffusion coefficient
$d_h$	Equivalent hydraulic diameter
$f$	fraction of solid surface projections under liquid droplets
$Flux_E$	Flux of each point
$Flux_I$	Flux of the initial point
$g$	Gravity
$h$	Heat transfer coefficient
$H$	Hot fluid
$I_D$	D band
$I_G$	G band
$J$	Water vapor flux
$J_{AGMD}$	Water vapor flux by AGMD
$J/J_o$	Normalized flux
$k_x$	Transversal thermal conductivity
$k_z$	Axial thermal conductivity
$L$	Channel length
LMH	L/m <sup>2</sup> h
$M_w$	Molecular mass of water
$P_{avgm}$	Log mean air pressure based from both sides of the membrane
$P_{avgma}$	Log mean air pressure within the air gap
$P_C$	Water vapor pressure on the air gap layer
$P_H$	Water vapor pressure on the membrane surface
$P_0$	Water vapor pressure in the vacuum side

$P_v(T'_w)$	Water vapor pressure at the membrane shell surface at the relative temperature
$Pr$	Prandtl number
$P_T$	Total pressure of water vapor and air
$P_w$	Vapor pressure of pure water
$r$	Membrane pore radius
$r_f$	Roughness ratio of wetted areas
$R$	Universal gas constant
$R_a$	Mean roughness
$R_{AGMD}$	Total mass transfer resistance in the AGMD
$\gamma_L$	Surface tension of liquid in contact with air
$\gamma_{SL}$	Solid-liquid interfacial energy
$\gamma_{SV}$	Solid-vapor interfacial energy
$\gamma_{LV}$	Liquid-vapor interfacial energy
$Re$	Reynolds number
$R_c$	Cake layer resistance
$R_G$	Molecular diffusion resistance related with the graphene effect
$R_K$	Knudsen diffusion resistance
$R_m$	Membrane resistance
$R_M$	Molecular diffusion resistance
$R_{M-air}$	Molecular diffusion resistance in the air gap
$R_t$	Total mass transfer resistance
$R_{tp}$	Temperature polarization resistance
$RT$	Room temperature
$SR$	Salt rejection ratio
$T_{avg,a}$	Average temperature based from both sides of the membrane
$T_{avg,m}$	Average temperature at the air gap
$u$	Flow velocity
$W_1$	Weight of the saturated membrane
$W_2$	Weight of the dry membrane
$x_{NaCl}$	Mole fraction of NaCl
$x_w$	Mole fraction of water
$\beta$	Enrichment factor
$t$	Operating duration

$\gamma_w$	Activity coefficient of water
$\delta$	Thickness
$\tau$	Pore tortuosity
$\delta_m$	Membrane thickness
$\delta_a$	Air gap thickness
$\theta_Y$	Young contact angle
$\theta_C$	Apparent contact angle
$\Delta g$	Mass of permeate
$\varepsilon$	Membrane porosity
$k$	Thermal conductivity
$\lambda$	Latent heat of water
$\mu$	Viscosity
$\rho$	Liquid density
$\rho_e$	Density of ethanol
$\rho_d$	Density of PVDF material
$\tau_m$	Membrane pore tortuosity
$f$	Feed
$fl$	Fluid
$m$	Porous membrane
$si$	Solid membrane
$\Phi_{outer}$	Outer diameter
$\Phi_{inner}$	Inner diameter

# TABLE OF CONTENTS

ACKNOWLEDGEMENTS .....	iii
ABSTRACT .....	vii
LIST OF ABBREVIATIONS .....	ix
LIST OF SYMBOLS .....	xiii
TABLE OF CONTENTS .....	xvi
LIST OF FIGURES .....	xxi
LIST OF TABLES .....	xxvi
CHAPTER 1 .....	1
Introduction .....	1
1.1 Introduction .....	2
1.2 Objectives and scope of the research .....	3
1.3 Structure of the study .....	4
CHAPTER 2 .....	5
Literature Review .....	5
2.1 Introduction .....	6
2.2 Membrane distillation and wetting phenomena .....	8
2.2.1 Principle of membrane distillation .....	8
2.2.2 Membrane wetting in membrane distillation .....	8
2.2.3 Membrane properties deciding wettability .....	10
2.2.3.1 Contact angle (CA) .....	11
2.2.3.2 Surface roughness and morphology .....	14
2.2.3.3 Surface tension .....	15
2.2.3.4 Surface charge .....	16
2.3 Special wettability .....	17
2.3.1 Superhydrophobic membrane surfaces .....	17
2.3.2 Omniphobic membrane surfaces .....	20
2.3.3 Janus membranes .....	23
2.4 Membranes with special surface wettability for membrane distillation .....	26
2.4.1 Nanocomposite membranes .....	26
2.4.1.1 Fabrication method .....	27
2.4.1.2 Application .....	30
2.4.1.3 Challenges .....	31
2.4.2 Surface-modified commercial membranes .....	31
2.4.2.1 Modification method .....	31
2.4.2.2 Application .....	38

2.4.2.3	Challenges.....	39
2.4.3	Synthesized membranes with special wettability.....	40
2.4.3.1	Modification method.....	40
2.4.3.2	Application.....	45
2.4.3.3	Challenges.....	46
2.4.4	Surface-modified ceramic membranes.....	47
2.4.4.1	Modification method.....	47
2.4.4.2	Application.....	50
2.4.4.3	Challenges.....	50
2.5	Concluding remarks and future perspectives .....	51
CHAPTER 3 .....		52
Materials and Methods.....		52
3.1	Introduction.....	53
3.2	Experimental materials .....	53
3.3	Electrospinning device.....	53
3.4	Membrane distillation setup.....	54
3.4.1	Direct contact membrane distillation (DCMD).....	54
3.4.2	Vacuum membrane distillation .....	56
3.5	Analytic methods used in experiments .....	57
3.5.1	Scanning Electron Microscope (SEM) and energy dispersive X-ray spectroscopy (EDX) 57	
3.5.2	Membrane thickness .....	57
3.5.3	Contact angle .....	57
3.5.4	Mechanical strength.....	57
3.5.5	Liquid entry pressure (LEP).....	57
3.5.6	Pore size .....	58
3.5.7	Porosity .....	59
3.5.8	Fourier-transform infrared (FT-IR).....	59
3.5.9	X-ray diffraction (XRD) .....	59
3.5.10	Total organic carbon (TOC).....	59
CHAPTER 4 .....		60
Wastewater Reclamation Utilizing Membrane Distillation with Resource Recovery .....		60
4.1	Introduction.....	61
4.2	Experimental method.....	63
4.2.1	Set-up .....	63
4.2.2	MD and anMDBR.....	64
4.2.3	Analytical methods .....	65

4.2.4	Mass transfer resistance .....	65
4.2.5	Removal ratio and enrichment factor, $\beta$ .....	67
4.3	Effects of bioreactor (feed side) temperature (45, 55, & 65 °C) on anMDBR performance ....	67
4.3.1	Flux comparison and inorganic compounds rejection for 7 days.....	67
4.3.2	Membrane fouling analysis in membrane distillation bioreactors .....	70
4.3.3	Change of TOC, NH <sub>4</sub> , pH, and VFA concentrations in the permeate and mixed liquor at various feed temperatures .....	74
4.4	Effects of various salinity on anMDBR.....	76
4.4.1	Effects of bioreactor initial salinities on the permeate flux and membrane fouling morphologies.....	76
4.4.2	Removal efficiency .....	77
4.4.3	Performance of anMDBR compared with MD .....	77
4.5	Bioresource recovery .....	79
4.5.1	VFAs recovery from the permeate.....	79
4.5.2	Biogas recovery from the thermophilic anMDBR.....	81
4.6	Conclusions.....	82
CHAPTER 5 .....		84
Behavior of Volatile Organic Compounds in Membrane Distillation .....		84
5.1	Introduction.....	85
5.2	Experimental method.....	87
5.2.1	Chemicals.....	87
5.2.2	Vacuum membrane distillation (VMD) configuration.....	88
5.2.3	Characterizations.....	88
5.3	Results and discussions.....	89
5.3.1	Optimization of VMD process.....	89
5.3.2	Effects of VOCs on MD performance .....	90
5.3.3	VMD treatment of synthetic brine water .....	90
5.3.4	Comparison of flux using various VOCs as feed.....	91
5.3.5	Mass transfer of VOC from feed to permeate.....	92
5.4	Effect of VOCs on the membranes .....	93
5.4.1	Penetration of VOCs and water into the membranes .....	93
5.4.2	Contact angle .....	94
5.5	Long-term operation performance with feed containing 2-BE .....	95
5.5.1	Flux .....	95
5.5.2	Penetration of 2-BE and water through the membrane .....	96
5.5.3	Contact angle .....	98
5.6	Mechanism of penetration of VOCs .....	98

5.7	Conclusion .....	100
CHAPTER 6 .....		101
Improving Membrane Distillation Permeation Performance by Optimizing Non-solvent in Dope Solution.....		101
6.1	Introduction.....	102
6.2	Experimental method .....	104
6.2.1	Determination of dope solution recipes .....	104
6.2.2	Preparation of dope solution and fabrication of PVDF hollow fiber membranes.....	106
6.2.3	Characterizations.....	108
6.3	Results and discussion .....	108
6.3.1	Effect of various NS on the inner structure of the hollow fiber membranes.....	108
6.3.2	Porosity and pore size distribution.....	112
6.3.3	Polymer crystallinity and mechanical strength .....	114
6.3.4	Surface morphology, contact angle, and surface roughness .....	116
6.3.5	MD flux performance.....	118
6.3.5.1	Comparison of MD performance using various membranes .....	118
6.3.5.2	Long-term operation of membrane distillation .....	119
6.4	Conclusions.....	120
CHAPTER 7 .....		122
Improving Permeation Performance of Membrane Distillation by Heat-Pressing on Membranes ....		122
7.1	Introduction.....	123
7.2	Experimental method .....	125
7.2.1	Membrane fabrication by electrospinning .....	125
7.2.2	Heat-press post-treatment .....	125
7.2.3	Experiment design.....	125
7.3	Results and discussion .....	127
7.3.1	Effect of heat-press temperature on the membranes .....	127
7.3.1.1	Effect of temperature on morphology .....	128
7.3.1.2	Effect of temperature on the characteristics.....	129
7.3.2	Effect of heat-press pressure on the membranes.....	131
7.3.2.1	Effect of pressure on the morphology .....	132
7.3.2.2	Effect of pressure on the characteristics.....	133
7.3.3	Effect of heat-press duration on the membranes.....	135
7.3.3.1	Effect of duration on the morphology .....	136
7.3.3.2	Effect of duration on the characteristics.....	137
7.3.4	Effect of heat-press on membrane with various thickness.....	139
7.3.4.1	Effect of heat press on morphology and characteristics.....	139

7.3.5	MD performance of heat-pressed membrane with various thicknesses .....	143
7.3.5.1	Comparison of permeation performance of heat-pressed and commercial membranes with their Characteristics and MD setting up parameters .....	145
7.4	Conclusion .....	147
CHAPTER 8 .....		149
Improving Membrane Properties for Membrane Distillation by Annealing .....		149
8.1	Introduction .....	150
8.2	Experimental method .....	151
8.2.1	Heat-press treatment .....	151
8.2.2	Annealing .....	151
8.3	Results and discussion .....	152
8.3.1	DCMD performance .....	152
8.3.2	Increased crystallinity and appearance of $\alpha$ phase after annealing .....	153
8.3.3	Further detection of phase conversion by XRD .....	155
8.3.4	Improvement of membrane properties .....	157
8.3.4.1	Pore size distribution and porosity .....	157
8.3.5	Improvement of liquid entry pressure (LEP) and hydrophobicity .....	158
8.4	Conclusion .....	159
CHAPTER 9 .....		160
Conclusions and Recommendations .....		160
9.1	Conclusions .....	161
9.2	Recommendations .....	162
REFERENCES .....		165



## LIST OF FIGURES

<b>Figure 1.</b> Water scarcity of various types in the world (Gude 2017) .....	3
<b>Figure 2.</b> Schematic of pore wetting (partial or fully-wetted) caused by surfactants in wastewater; the surfactants have hydrophobic tails and hydrophilic heads.....	9
<b>Figure 3.</b> Factors affecting membrane wetting: (a) membrane surface properties (wettability, roughness, surface tension, pore size, surface charge, and surface functional group); (b) hydrodynamics (flow velocity, motion direction, temperature, hydrostatic pressure), and; (c) feed characteristics (mole fraction, diffusivity, species concentration, charge, pH) .....	11
<b>Figure 4.</b> Schematic of a liquid drop indicating the thermodynamic equilibrium in terms of Young equation.....	12
<b>Figure 5.</b> (a) Wenzel and (b) Cassie-Baxter model of surface wetting regime .....	13
<b>Figure 6.</b> Kao diagrams of a sample membrane with fixed roughness showing the relationship between surface tension and wetting regimes (Kujawa & Kujawski 2016). .....	14
<b>Figure 7.</b> Requirement of CA to suspend water: a) simple topology; b) re-entrant topology .....	15
<b>Figure 8.</b> Comparison of in-air water contact angle (CA), underwater oil CA on the pristine and surface-modified composite membranes. The underwater oil CA on PDDA/SiNPs-PVDF membrane decreases continuously for 30 min (Wang, Jin, et al. 2016). .....	16
<b>Figure 9.</b> Summary of membranes with special wettability for membrane distillation. ....	17
<b>Figure 10.</b> a) Low- resolution scanning electron microscopy (SEM) of nanopiked microchannels glass membrane surface that are etched in 1% hydrofluoric acid for 30 mins; b) high-resolution SEM of nanopiked microchannels; c) array of cone-shaped nanopikes; d and e) high CAs on superhydrophobic membranes (Ma et al. 2009).....	18
<b>Figure 11.</b> a) Various liquid droplets on PVDF membrane before and after surface modifications (transparent: Milli-Q water, brown: humic acid solution, pink, blue, and green: buffer solutions with pH of 4, 7, and 14, respectively); (b) acquired low tilt angles after surface modifications by fluorination (Razmjou et al. 2012).....	19
<b>Figure 12.</b> Comparison of contact angles of liquids with various surface tension on hydrophobic PTFE and omniphobic membranes. Photos below show wetting behavior of both membranes: PTFE membrane is susceptible to rapid wetting against low surface tension liquids while omniphobic membrane is able to repel the liquids (Lin et al. 2014).....	21
<b>Figure 13.</b> SEM images of the surface morphology of A) pristine glass fiber membrane; B) omniphobic surface on glass fiber after modifications. The inset image in B displays the same sample at lower magnification. (Lin et al. 2014) .....	22

<b>Figure 14.</b> Contact angles of ethylene glycol, mineral oil, and methanol on neat and plasma-treated electrospun nanofiber membranes. The surface tensions of the liquids are 47.7, 30.0, and 22.7 mN/m, respectively (Chul Woo et al. 2017) .....	23
<b>Figure 15.</b> Contact angle measurements of the developed hollow fiber. A) Force per unit length of fiber vs. immersion depth. Wetting state and contact angle of water droplet on flat sheet membrane using dope solution B) for hollow fiber shell layers; C) for hollow fiber lumen layers (Bonyadi & Chung 2007).....	24
<b>Figure 16.</b> a) surface of a virgin PVDF membrane; b) surface of a PEG-grafted PVDF membrane; surface of a TiO <sub>2</sub> -coated membrane surface-grafted by PEG that is c) just modified; d) after 5 min ultrasonic treatment (Zuo & Wang 2013) .....	25
<b>Figure 17.</b> a) SEM images of dual-biomimetic PS nanofiber membranes; b) the dotted circle showed nanopapillous and nanoporous structures; c) the effect of membrane thickness on pore size distribution; d) the comparison of flux between superhydrophobic nanofiber PS membrane with a commercial PVDF membrane (Li et al. 2014).....	28
<b>Figure 18.</b> a) resistance against water and n-hexane droplets; b) oil/water separation processes using neat nanofiber PVDF and superhydrophobic nanofiber membranes; c) DCMD configuration and permeation performance comparison (Su et al. 2016) .....	30
<b>Figure 19.</b> Topographies of a,b) pristine commercial PVDF membrane; c,d) fluorinated AgNPs deposited membrane (Shan et al. 2018) .....	32
<b>Figure 20.</b> a) Pore size distribution of virgin PTFE membrane, the PVA coated PTFE membrane, and cross-linked surface-modified membrane; b) in-air water contact angle and underwater contact angle of these membranes (Wang, Hou, et al. 2018).....	37
<b>Figure 21.</b> a) Force-displacement curves showing the patterns where a mineral oil droplet interacted with the composite Janus membrane (black curve) and hydrophobic membrane (red curve); b) the five stages in the patterns (Wang, Hou & Lin 2016a).....	38
<b>Figure 22.</b> SEM of the surface layer of the electrospun nanofiber PVDF membranes that are coated with a layer of PDMS (An et al. 2017) .....	43
<b>Figure 23.</b> Schematic illustrations of pristine and CF <sub>4</sub> plasma modified electrospun nanofiber membranes regarding contact angles of liquids with various surface tensions (Chul Woo et al. 2017) .....	44
<b>Figure 24.</b> a) Normalized flux and salt rejection membranes in the MD treatment of 1,000 ppm o/w emulsion as feed solution using a) hydrophobic and omniphobic and c) Janus (hydrophilic-on-hydrophobic) and Janus (hydrophilic-on-omniphobic) membranes; before and after MD test for b) hydrophobic membranes and d) Janus (hydrophilic-on-omniphobic) membranes (Huang et al. 2017)45	
<b>Figure 25.</b> The DCMD performance of carbon nanotube coated membranes as a function of a) salt concentration and b) time; the flux of DCMD treating feed water containing humic acid and sodium	

chloride when the membrane work as open-circuit, cathode, or anode regarding c) flux and d) salt rejection; e-g) the surface morphology and water contact angle of the coated membranes used as various electrodes after 12 h DCMD operation; h-j) schematic figures of electrostatic interaction between organic foulants and the surface modified membranes at various modes (Dong et al. 2018)	49
<b>Figure 26.</b> Schematic diagram of electrospinning configuration used in the experiments .....	54
<b>Figure 27.</b> Schematic diagram of DCMD process .....	55
<b>Figure 28.</b> Schematic diagram of vacuum membrane distillation in this study .....	56
<b>Figure 29.</b> Schematic setup of the LEP apparatus (Woo, Kim, et al. 2016) .....	58
<b>Figure 30.</b> Schematic diagram of the anaerobic membrane distillation bioreactor used in the present study.....	64
<b>Figure 31.</b> Anaerobic membrane distillation bioreactor flux performance at various bioreactor temperatures. (anMDBR-45, anMDBR-55, and anMDBR-65 are membrane distillation bioreactor operated at 45, 55, and 65 °C, respectively) .....	68
<b>Figure 32.</b> SEM images of the shell sides of hollow fiber membrane surfaces for: (a) virgin membrane, and for anMDBR at various temperatures after 7-day operation: (b)45°C, (c)55°C, (d)65°C.....	70
<b>Figure 33.</b> FTIR analysis of shell and lumen sides of hollow fiber membranes after 7 days' operation (a. FTIR analysis on the shell sides of the membranes; b. on the lumen sides).....	72
<b>Figure 34.</b> Total organic compounds and N-NH <sub>4</sub> concentrations in permeate and mixed liquor at (a)45°C; (c)55°C; (e)65°C, pH and total volatile fatty acid concentrations in permeate and mixed liquor at b)45°C; (d)55°C; (f)65°C .....	74
<b>Figure 35.</b> Flux of anMDBR-55 operated at various initial salinity .....	77
<b>Figure 36.</b> Flux comparison between membrane distillation and anaerobic membrane distillation bioreactor at various temperatures (MD-45 means MD operated at 45 °C; AnMDBR-45 means anMDBR operated at 45 °C; same rule of calling is used in the other items in the legend).....	78
<b>Figure 37.</b> Enrichment ratio of each individual volatile fatty acid (VFA) and their relationship with the partition coefficient.....	80
<b>Figure 38.</b> Biogas yield and methane percentage in bioreactors at (a)45 °C; (b)55 °C; (c)65 °C, and (d) their biogas components at day 7 .....	82
<b>Figure 39.</b> Effects of A) 2-butoxyethanol on flux when treating de-ionized water and synthetic produced water; B) various volatile organic compounds on flux when treating de-ionized water.....	90
<b>Figure 40.</b> Changes in concentrations of various volatile organic compounds in A) permeate; and B) feed sides.....	92
<b>Figure 41.</b> FTIR analysis of membranes after 24 h operation: (A) shell side (feed) (B) lumen side (permeate) .....	94
<b>Figure 42.</b> Contact angle of membranes after treating various VOCs for 24 h in VMD .....	95

<b>Figure 43.</b> Flux of VMD treating synthetic CSG RO brine containing 2-BE for 72 h .....	96
<b>Figure 44.</b> FTIR analysis of both a) shell and b) lumen sides of membranes after 24 h and 72 h operations using feed with and without 2-BE addition.....	97
<b>Figure 45.</b> Contact angle of HF membranes after treating synthetic produced water containing 2-BE after 24 and 72 h operation via VMD .....	97
<b>Figure 46.</b> Mechanism of the penetration of VOCs: A) 2-butoxyethanol (2-BE) molecules was attracted and adhered onto the membranes surface due to hydrophobic interactions between the alkyl head on the 2-BE and the hydrophobic surface of the membrane polymer; B) three hydrogen bonds were formed between the 2-BE and water molecules; C) the water vapors “pushed” the 2-BE molecules moving forward through the membrane pores; D) pore wetting started to appear due to the surfactant properties of 2-BE .....	99
<b>Figure 47.</b> SEM images displaying the cross-section of hollow fiber membranes cast from (a-c) 11 wt.% PVDF in NMP; (d-f) 11 wt.% PVDF in TEP; 11 wt.% PVDF in TEP with 17.8 wt.% NS of (g-i) acetone; (j-l) DBP and (m-o) toluene.....	110
<b>Figure 48.</b> Viscosity of various dope solutions.....	111
<b>Figure 49.</b> SEM images displaying the surface morphology of hollow fiber membranes cast from (a) 11 wt.% PVDF in NMP; (b)11 wt.% PVDF in TEP; 11 wt.% PVDF in TEP with NS of (c), (d) acetone; (e), (f) DBP; (g), (h) toluene.....	117
<b>Figure 50.</b> Contact angle of hollow fiber membrane shell surface by using dope solutions containing various NSs .....	118
<b>Figure 51.</b> Flux permeation comparison of membrane samples prepared by using dope solutions containing various NS in direct contact membrane distillation .....	119
<b>Figure 52.</b> Flux performance of the commercial membrane, NMP0 and TEPT-2.....	120
<b>Figure 53.</b> SEM images of as-spun and heat-pressed PVDF-HFP membrane at magnifications of 10K and 50K: (a)as-spun neat membrane (Neat); membranes heat-pressed under (b)140 °C (M0); (c)150 °C (M1); (d)160 °C (M2). .....	128
<b>Figure 54.</b> Fiber distributions of as-spun and membrane samples heat-pressed under various temperatures.....	129
<b>Figure 55.</b> Effects of temperature on thickness, porosity and contact angle.....	129
<b>Figure 56.</b> SEM images of heat-pressed PH membrane at magnifications of 10K and 50K: membranes heat-pressed under (a)0.7 kPa (M1-A); (b)2.2 kPa (M1-B); (c)6.5 kPa (M1-C); (d)9.8 kPa (M1-D). .....	132
<b>Figure 57.</b> Fiber distributions of as-spun and membrane samples heat-pressed under various pressures.....	133
<b>Figure 58.</b> Effects of pressure on thickness, porosity and contact angle.....	133

<b>Figure 59.</b> SEM images of heat-pressed PVDF-HFP membrane at magnifications of 10K and 50K: membranes heat-pressed for (a)1 h (M1-B-1); (b)2 h (M1-B-2); (c)4 h (M1-B-3); (d)8 h (M1-B-4).	136
<b>Figure 60.</b> Fiber distributions of as-spun and membrane samples heat-pressed for various durations. .....	137
<b>Figure 61.</b> Effects of pressure on thickness, porosity and contact angle.....	137
<b>Figure 62.</b> SEM cross section images of as-spun (a: 400k) and heat-pressed membrane (b: 350k; c: 1500k) .....	139
<b>Figure 63.</b> Effects of heat-press with optimal conditions on porosity and contact angles of membranes with various thicknesses .....	141
<b>Figure 64.</b> Comparison of DCMD permeation performance of selected membrane samples.....	144
<b>Figure 65.</b> Comparison of flux performance between post-treated& as spun electrospun membranes and commercial ones (feed: 60 °C, permeate: 20 °C) .....	152
<b>Figure 66.</b> FT-IR spectra of as-spun and thermal treated electrospun membranes .....	153
<b>Figure 67.</b> XRD patterns (2 $\theta$ spectra) of as-spun and thermal treated electrospun membranes .....	156
<b>Figure 68.</b> Pore diameter distribution of as spun and post-treated electrospun membranes .....	157
<b>Figure 69.</b> Comparison of LEP, CA and average pore diameter of as-spun, heat-pressed, and annealed membranes .....	159

## LIST OF TABLES

<b>Table 1.</b> Published reports in the literature about nanocomposite membranes with special wettability(superhydrophobicity) categorized by application.....	26
<b>Table 2.</b> Various chemical compounds for fluorination.....	33
<b>Table 3.</b> Published reports in the literature about surface-modified commercial membranes with special wettability for MD. ....	35
<b>Table 4.</b> Published reports in the literature about surface-modified synthesized membranes with special wettability for MD .....	40
<b>Table 5.</b> Published reports in the literature about surface-modified inorganic membrane with special wettability for MD .....	47
<b>Table 6.</b> Mass transfer resistance analysis between bioreactors operated at various temperatures.....	73
<b>Table 7.</b> Properties of VOCs and concentrations of ion components of the synthetic produced water used in this study.....	87
<b>Table 8.</b> Hansen solubility parameters at 25°C, molecular weight, density, partition coefficient, and viscosity of various chemicals used in this study .....	105
<b>Table 9.</b> Name conventions and dope solution compositions for hollow fiber membrane fabrication in this study. ....	106
<b>Table 10.</b> PVDF hollow fiber spinning conditions.....	107
<b>Table 11.</b> Comparison of porosity, mean pore size, thickness, and inner and outer diameters of hollow fiber membranes using various dope solutions .....	113
<b>Table 12.</b> Comparison of mechanical strength and crystallinities of hollow fiber membranes using various dope solutions.....	115
<b>Table 13.</b> Heat-press conditions and name conventions used in the present study. ....	126
<b>Table 14.</b> Characteristics of the membranes after heat-press at different temperatures.....	130
<b>Table 15.</b> Characteristics of the membranes after heat-press at different pressures.....	134
<b>Table 16.</b> Characteristics of the membranes after heat-press at different durations.....	138
<b>Table 17.</b> Thickness of various membrane samples before and after heat-press .....	140
<b>Table 18.</b> Characteristics of the membranes with various thicknesses after heat-press .....	142
<b>Table 19.</b> Comparison of Heat-pressed MD flat-sheet membranes for desalination with commercial PVDF membrane .....	145
<b>Table 20.</b> Sample naming and their thicknesses.....	151

# **CHAPTER 1**

## **Introduction**

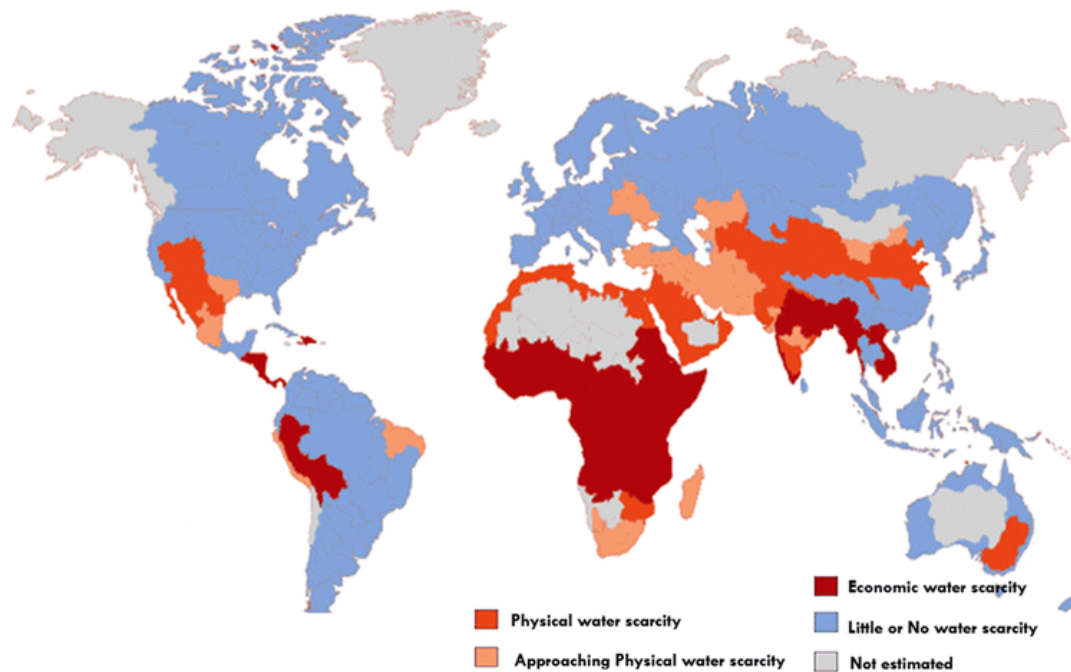
## 1.1 Introduction

Water scarcity has been one of most serious issues in global societies (Boulay et al. 2018). Specifically, water scarcity is defined as “lack access to clean freshwater”. Currently, the issue is being worsened owing to a tilting supply-demand balance. Although the earth is a planet having abundant liquid water, only 3% of them is freshwater, and some of them is steadily becoming unrecyclable owing to pollution, global warming and other human activities, which lessen the water supply; on the other hand, the rapidly-growing population of humans greatly increase the demand of water resources. **Figure 1** shows that water scarcity is a serious issue in some regions of the world and it can be classified into physical water scarcity and economic water scarcity (Gude 2017). Physical water scarcity is becoming more severe due to the global warming issue which affects freshwater sources. There are two main approaches to solve physical water scarcity: desalination and wastewater reuse (Gude 2016; Wang et al. 2017). Environmental-friendly water purification methods with low cost and energy consumption are highly desirable. Currently, membrane technology (membrane filtration) is dominant in desalination and play an important role in wastewater treatment field owing to its high efficiency, ease of operation and relatively small footprint. Specifically, seawater reverse osmosis (SWRO) is widely implemented for desalination. Regarding wastewater reuse, microfiltration (MF), ultrafiltration (UF), nanofiltration (NF), reverse osmosis (RO), and membrane bioreactor (MBR) are being implemented for wastewater treatment and the choice of technology is depending on the characteristics of wastewater and the requirement of permeate quality (Singh & Hankins 2016).

Membrane distillation (MD) is an emerging membrane technology. As the mass transfer of water is driven by temperature gradient, it has a very distinct mechanism from conventional pressure-driven membrane technology. Therefore, MD is capable of treating wastewater which conventional membrane technology cannot deal with (Warsinger et al. 2015). The potential use of waste heat and thermal heat makes the technology more efficient. Researchers have implemented MD in various applications including desalination, the treatment of produced water and industrial wastewater, brine treatment, forward osmosis draw solution recovery, etc. (Duong et al. 2015a; Kim et al. 2019; Quist-Jensen et al. 2017). However, several challenges have been found before MD being fully commercialized. First, MD has low permeation performance especially when considering the use of high thermal energy. Secondly, currently available MD membranes are prone to membrane wetting. Thirdly, MD membranes may suffer



more severe organic fouling due to hydrophobic interaction between hydrophobic membranes and organic foulants (Deshmukh et al. 2018; McGinnis & Elimelech 2008).



**Figure 1.** Water scarcity of various types in the world (Gude 2017)

Therefore, there is a strong need to develop membranes with high permeability and improved wetting and fouling resistance. Two types of membranes are being substantially studied: flat sheet and hollow fiber (HF) membranes. Flat sheet membranes can be fabricated through various methods including non-solvent induced phase separation (NIPS), thermally induced phase separation (TIPS), electrospinning, etc., while hollow fiber membranes can be fabricated mostly via wet-spinning, which is a type of NIPS (Khayet & Matsuura 2003; Wang, Zheng, et al. 2016). In addition, surface modifications are widely implemented to impart special wettability on membrane surfaces for stable high flux performance against more challenging wastewater (Wang, Hou & Lin 2016b; Wang & Lin 2017).

## 1.2 Objectives and scope of the research

As an emerging membrane technology, MD should have new potential wastewater treatment applications for its fully commercialization. Further studies should also be carried out to improve the system, which including studies on process optimization and MD membrane development. Specific objectives of the present study during my PhD study are listed below:

- To develop a thermophilic anaerobic membrane distillation bioreactor (anMDBR) for the treatment of municipal wastewater
- To investigate the behavior of volatile organic compounds in MD processes
- To improve the permeation performance of NIPS membranes by adjusting non-solvents in dope solutions
- To improve the permeation performance of electrospun membranes by post treatment

### **1.3 Structure of the study**

This thesis consists of nine chapters. Research backgrounds, research objectives and scope of the study are presented in Chapter 1 (Introduction).

Chapter 2 demonstrates literature reviews about development of MD membranes with special wettability for the treatment of challenging wastewater.

Chapter 3 covers general materials and characterizations used in experiments during the PhD study.

Chapter 4 introduced the development of anMDBR for the treatment of municipal wastewater. The advantage and disadvantage of the usage of MD HF membranes in the system are discussed.

Chapter 5 demonstrates the volatile organic compounds behavior in an MD system and its assumed mechanism.

Chapter 6 illustrates the improvement of structure and surface morphology of HF membranes for enhanced permeability in MD.

Chapter 7 introduces heat-press as post-treatment on electrospun nanofiber membrane for improved wetting resistance and flux performance.

Chapter 8 further explores the favored effects of annealing on the heat-pressed nanofiber membranes.

Chapter 9 summarizes the findings and challenges in Chapter 4-8; outlook on future researches and recommendations are also addressed in this chapter.

# **CHAPTER 2**

## **Literature Review**

## 2.1 Introduction

Presently, significant research focus is being placed on next generation water and wastewater treatment technologies to address global water shortage issues (Tijing, Choi, et al. 2014; Wirth & Cabassud 2002). Among the current water and wastewater treatment technologies, membrane processes play a dominant role in the global market due to their relatively higher energy efficiency and smaller footprint, (Lonsdale 1982; Wang & Chung 2015). Conventional membrane technologies are mainly pressure-driven processes, such as reverse osmosis (RO) and nanofiltration (NF). Recently, innovative membrane technologies driven by other driving forces have been extensively developed. Among them, membrane distillation (MD) has attracted wide attention (Camacho et al. 2013a). MD is driven by vapor pressure gradient induced by temperature difference. Its distinct working mechanism makes it capable of treating challenging wastewater (e.g. brine) where conventional pressure-driven membrane processes are struggling to deal with (Xie et al. 2016). The other major advantage of MD is its potential to be coupled with alternative heat sources such as solar and low-grade waste heat, making the process more energy efficient (Al-Obaidani et al. 2008; Duong et al. 2015b). Also, MD can be integrated with other water treatment technologies towards zero liquid discharge - an ideal condition for sustainable concentrate treatment (Onishi et al. 2018; Tufa et al. 2015).

However, MD is still in the stage of laboratory research and only has a few pilot-scale demonstrations with limited success of commercialization, due to several reasons. One of the reasons is the lack of suitable membranes (Lalia, Guillen-Burrieza, et al. 2013a; Zuo, Bonyadi & Chung 2016). Along with high permeability, an appropriate membrane for MD should have high wetting resistance, i.e., only water vapor is allowed to pass through the membrane structures (Eykens, De Sitter, Dotremont, De Schepper, et al. 2017; Zhang, Song, et al. 2013). Conventionally, commercial hydrophobic microfiltration membranes have been widely evaluated in various MD applications. However, these membranes still suffer low permeation flux and are prone to wetting issues especially when high feed temperature and feed flow rates are applied (Boubakri et al. 2015; Lalia, Kochkodan, et al. 2013). The process becomes more challenging when treating wastewater which contains high salinity or concentrations of low surface tension compounds including surfactants and oil (e.g., textile wastewater, produced water, seawater brine, municipal wastewater, etc.). These feed solutions cause the membranes to suffer rapid wetting and fouling which may lead to membrane damage, necessitating early membrane replacement. This inevitably incurs additional operation cost (Alkhudhiri, Darwish

& Hilal 2013a; El-Abbassi et al. 2009; Goh et al. 2013b; Van der Bruggen 2013). Due to the inability of the commercial membrane to have stable flux and rejection performance, there is a need to fabricate new membranes that have high wetting and fouling resistance, while maintaining adequate flux and superior salt rejection (Chew, Zhao, Loh, et al. 2017; Zuo et al. 2017).

Enormous research efforts have been dedicated towards developing MD membranes with the desired robust properties. Among them, membranes with special wettability have been found to be the most effective for the improvement of fouling and wetting resistance (Lu et al. 2017). Inspired by nature, the special wettability on MD membranes has been realized by adjusting surface roughness and chemical compositions via surface engineering, supported by the advances in nanomaterial synthesis and modification techniques (Kang & Cao 2014).

In recent years, many researchers have made remarkable achievements in the fabrication of membranes with special wettability. Some researchers have successfully developed membranes with improved flux and stability in MD operations (Drioli, Ali & Macedonio 2015); while others were geared towards the development of membranes to deal with highly saline wastewater with low surface tension components (Dow et al. 2017; Duong et al. 2015b). These membranes with special wettability were found to have high wetting and fouling resistance, which make MD more viable in real applications (Lu et al. 2016; Razmjou et al. 2012).

Recently, a few review articles have reported some advances in membrane fabrication and modification for MD application; however, none of which have focused discussion on membranes with special wettability. As the development of membranes with high wetting and fouling resistance is essential for the success of MD applications (especially in the treatment of challenging wastewater), there is a strong need to review innovation in membranes with special wettability from perspectives of both material science and practical engineering. This review includes an overview of surface wettability and its fundamentals, a literature review of various types of surface special wettability, and a summary of fabrication methods and MD applications of membranes with special wettability.

## **2.2 Membrane distillation and wetting phenomena**

### **2.2.1 Principle of membrane distillation**

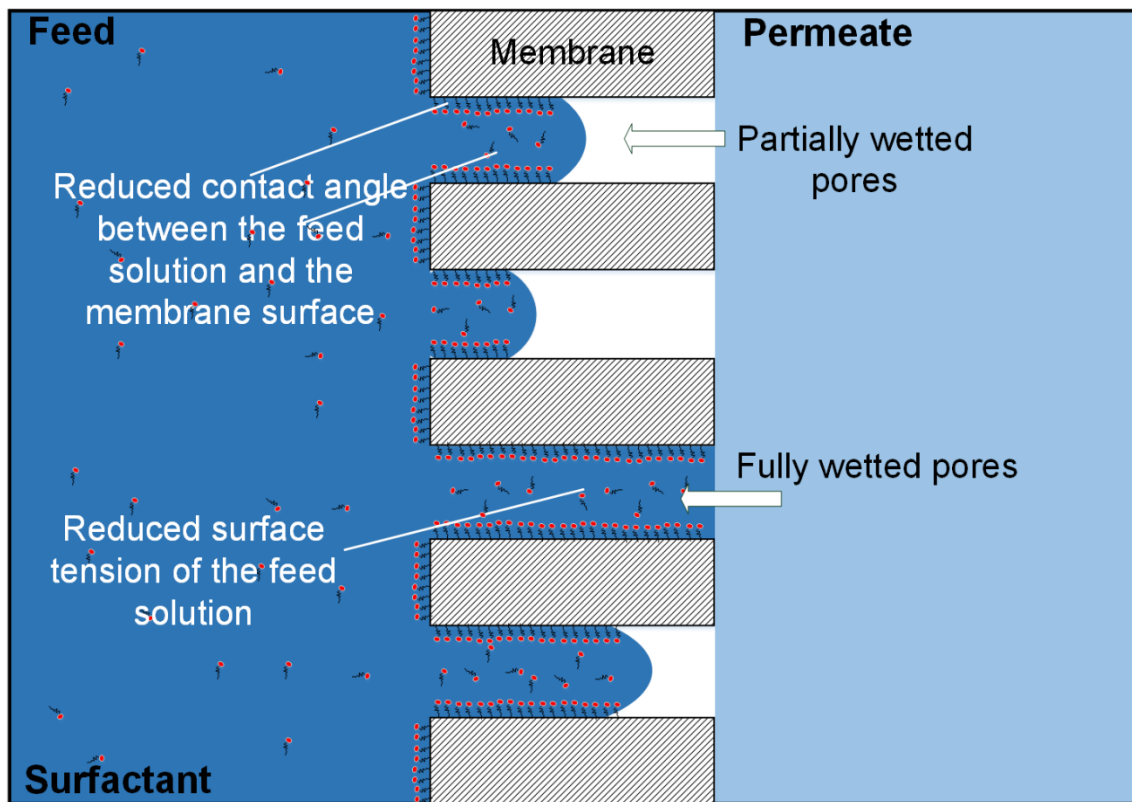
MD is a membrane separation process where water vapor instead of liquid water passes through a hydrophobic, porous membrane and is condensed in the permeate side (Khayet 2011). The mass transfer of volatile liquids is driven by partial vapor pressure difference induced by the temperature differences between feed and permeate sides. This unique mechanism makes MD viable in some applications where conventional technologies are struggling. Moreover, the energy efficiency of MD can be greatly improved when low grade waste heat is available. Theoretically, permeate of MD can reach 100% rejection of non-volatile components (Alkhudhiri, Darwish & Hilal 2012).

The detailed transport mechanism of MD is described in the following steps: (1) liquid water evaporates at the hot feed water-membrane interface; (2) driven by temperature gradient, the water vapor passes through membrane pores; then, (3) the water vapor condenses at the cold permeate side (Qtaishat et al. 2008). MD can be configured in various ways depending on how water vapor is condensed. Direct contact MD (DCMD) is the most studied configuration owing to the convenience of setup, where both feed water and permeate water are touching the membrane at both sides. For comparison, both air gap and permeate gap MD (AGMD & PGMD) configurations require condensation plates set inside modules, and vacuum and sweeping gas MD (VMD & SGMD) require external condensers to liquefy water vapor (Alkhudhiri, Darwish & Hilal 2012; Cerneaux et al. 2009). Generally, higher liquid entry pressure (LEP) and wetting resistance are required for membranes used in the configurations of VMD and SGMD owing to additional external pressures on the permeate side of membrane surfaces; hence, membranes used in VMD and SGMD usually have higher hydrophobicity and smaller average pore size (Khayet, Godino & Mengual 2000; Xu, Zhu & Xu 2006).

### **2.2.2 Membrane wetting in membrane distillation**

Membrane wetting is generally defined as liquid contacting with a solid membrane surface through intermolecular interaction between the phases of gas, liquid, and solid (Krupenkin et al. 2004). Specifically, wetting of porous membranes sees liquids penetrating the pores of membrane. As a result, the flux either declines (partial pore wetting) or steeply rises (complete wetting) while salt rejection keeps decreasing sharply (Saffarini et al. 2013). **Figure 2** shows

the pore wetting potential (partial- or fully-wetted) for MD membranes. This wetting phenomenon is especially unique for MD since phase change is necessary, i.e., forming into water vapor, rather than allowing liquid water to penetrate through the membrane. It is interesting to note that recent studies found that some non-volatile organic compounds could still pass through membranes easily without the occurrence of membrane wetting via a so-called “adsorption-desorption-adsorption” mechanism (Meng, Ye, et al. 2014; Naidu, Jeong & Vigneswaran 2015; Yao et al. 2018).



**Figure 2.** Schematic of pore wetting (partial or fully-wetted) caused by surfactants in wastewater; the surfactants have hydrophobic tails and hydrophilic heads

Hydrophobic membranes are widely used to lessen the possibility of liquid water penetration in MD. As requirement, at least one layer of the MD membrane should be hydrophobic, commonly the one facing the feed solution. Therefore, hydrophobic polymers such as polyvinylidene fluoride (PVDF), polytetrafluoroethylene (PTFE), and polypropylene (PP) are favored to be used as MD membrane materials (Li et al. 2003; Tang et al. 2010; Yang et al. 2011; Zhu et al. 2013). It is widely accepted that the primary metric for determining membrane

wetting (wicking) resistance is  $LEP$ , and membrane wetting occurs when transmembrane pressure ( $\Delta P$ ) exceeds the  $LEP$  of membrane against a specific liquid (Wang, Chen & Lin 2018):

$$\Delta P \geq LEP \quad (1)$$

In other words,  $LEP$  is the maximum transmembrane pressure that a membrane pore can sustain (i.e. the minimum pressure for liquids to penetrate membrane pores). It is defined as (García-Payo, Izquierdo-Gil & Fernández-Pineda 2000; Rezaei et al. 2018):

$$LEP = - \frac{B\gamma_L \cos\theta}{r_{max}} \quad (2)$$

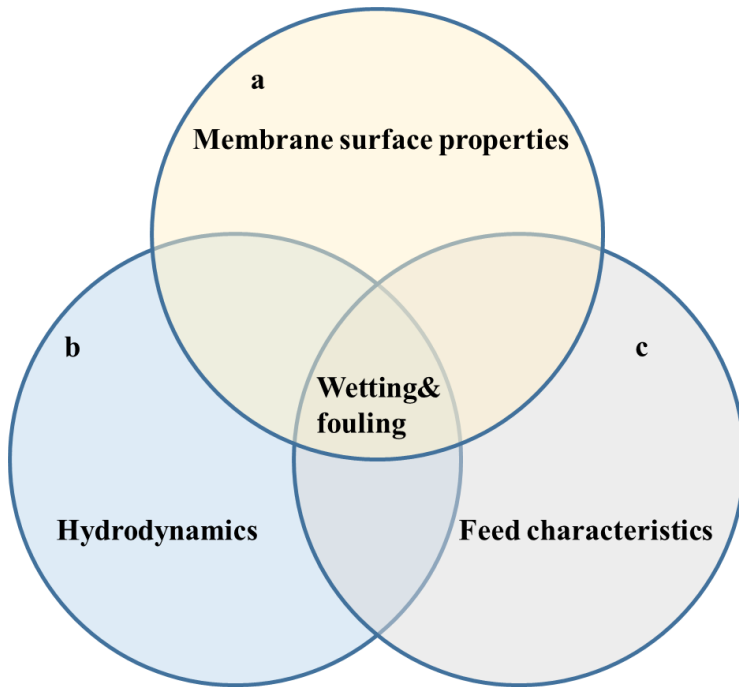
where  $\gamma_L$  is the surface tension of a liquid,  $\theta$  is the apparent contact angle (CA) between feed solution and membrane surface,  $r_{max}$  is the maximum pore size of the membrane, and  $B$  is the pore geometry coefficient (e.g., stretched membranes such as PTFE with small curvature radius has  $B$  value of  $\sim 0.4 - 0.6$ ).

Recent studies found that the existence of low surface tension chemicals in feed solutions play a significant role in membrane pore wetting as it can affect both membrane surface properties and feed characteristics (Chew, Zhao, Loh, et al. 2017; Vazquez, Alvarez & Navaza 1995; Wang, Chen, et al. 2018). As shown in **Figure 2**. Schematic of pore wetting (partial or fully-wetted) caused by surfactants in wastewater; the surfactants have hydrophobic tails and hydrophilic heads, the deposition or adsorption of surfactants on membrane surfaces can reduce its  $LEP$  by reducing both the CA on membrane surfaces and the surface tensions of feed water, so the membranes can be easily wetted (Gryta et al. 2009).

### 2.2.3 Membrane properties deciding wettability

Major factors that influence fouling and wetting in MD can be grouped into: (a) membrane surface properties (wettability, roughness, surface tension, pore size, surface charge, and surface functional group); (b) hydrodynamics (flow velocity, motion direction, temperature, hydrostatic pressure), and; (c) feed characteristics (mole fraction, diffusivity, species concentration, charge, pH) (see **Figure 3**). The present review article focuses on the development of membranes with specific surface properties (various special wettability) to address the challenges in potential MD applications.





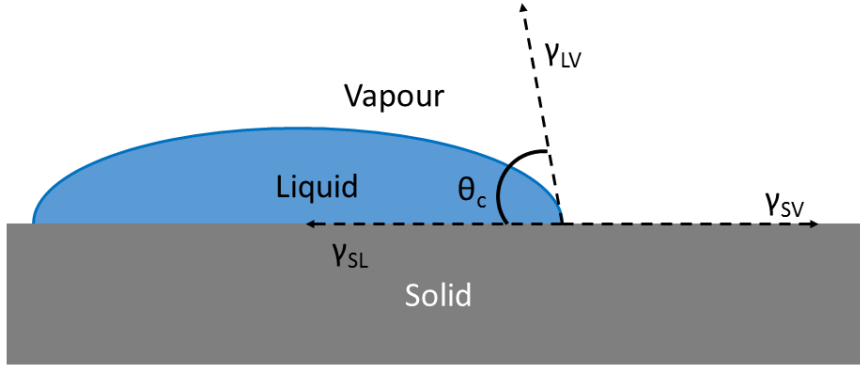
**Figure 3.** Factors affecting membrane wetting: (a) membrane surface properties (wettability, roughness, surface tension, pore size, surface charge, and surface functional group); (b) hydrodynamics (flow velocity, motion direction, temperature, hydrostatic pressure), and; (c) feed characteristics (mole fraction, diffusivity, species concentration, charge, pH)

#### 2.2.3.1 Contact angle (CA)

CA is the angle where liquid-vapor interface meets solid-liquid interface. It is generally used to quantify the wettability of a membrane surface against specific liquids (Cassie & Baxter 1944). As the CA in equilibrium reflects the strength of molecular interaction between solids, liquids, and vapors, the surface tension of a material can be calculated based on the Young equation with the CA acquired on a rigid surface (Choi et al. 2009; Marmur 2008):

$$\gamma_{SL} - \gamma_{SV} - \gamma_{LV} \cos \theta_c = 0 \quad (3)$$

where  $\gamma_{SL}$  is solid-liquid interfacial energy,  $\gamma_{SV}$  is solid-vapor interfacial energy, and  $\gamma_{LV}$  is liquid-vapor interfacial energy (see schematic in **Figure 4**).



**Figure 4.** Schematic of a liquid drop indicating the thermodynamic equilibrium in terms of Young equation

Wenzel or Cassie-Baxter model should be introduced when CA is measured on a rough surface such as the surface of porous membranes (Yuan & Lee 2013). A relationship between the Young CA and the apparent CA of water on a rough surface has been developed depending on the state of surface wettability (Wenzel or Cassie-Baxter) (Marmur 2003; McHale 2007). In both models, roughness plays an important role determining apparent CA. Wenzel state, a homogeneous wetting regime, occurs when liquids completely reach roughness valleys (**Figure 5a**), which is represented by the following equation:

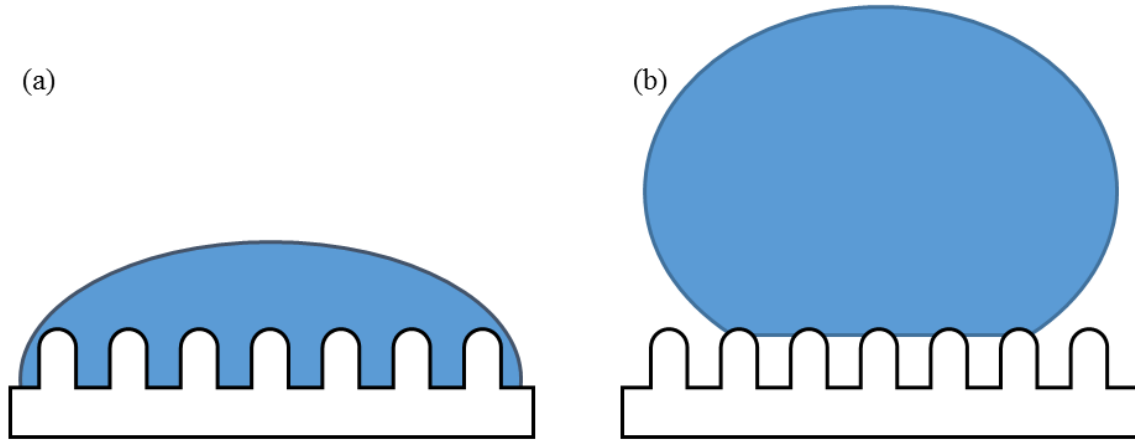
$$\cos\theta_C = r\cos\theta_Y \quad (4)$$

where  $r$  is the roughness ratio, defined as the ratio between actual and projected solid surface areas,  $\theta_Y$  is the Young CA when the liquid is placed on ideal smooth surface in thermodynamic equilibrium systems, and  $\theta_C$  is the apparent CA.

Cassie-Baxter, on the contrary, is a heterogeneous wetting regime as air remained trapped inside the roughness valleys under liquids (see **Figure 5b**), expressed as:

$$\cos\theta_C = r_f f \cos\theta_Y + f - 1 \quad (5)$$

where  $f$  is the fraction of solid surface projections under liquid droplets, and  $r_f$  is the roughness ratio of wetted areas;  $\theta_Y$  is the Young's CA when same ideal solid surface is applied in thermodynamic equilibrium systems, and  $\theta_C$  is the apparent CA. The Cassie-Baxter equation can be converted into the Wenzel equation when  $f = 1$ ,  $r_f = r$ .

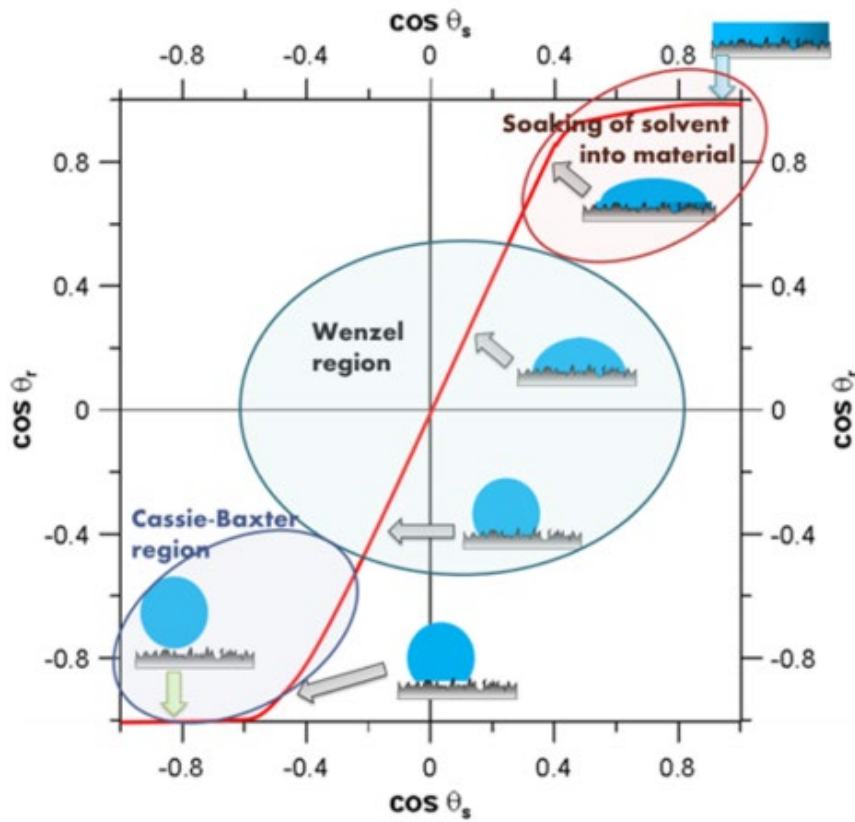


**Figure 5.** (a) Wenzel and (b) Cassie-Baxter model of surface wetting regime

In addition, sliding angle is applied to determine the surface wettability, defined as the minimum tilt angle required for water droplets to slide down an inclined plate. Lower sliding angles can be usually observed when membrane surfaces have higher apparent CAs. The Cassie-Baxter state of surface has much lower sliding angle than Wenzel state at the same apparent CAs due to air trapped in surface structures (Miwa et al. 2000).

It is concluded that surface wettability is strongly affected by surface roughness and morphology. Kao diagram (**Figure 6**) is introduced to illustrate a relationship between the Young CA (representing surface tension) and the apparent CA in terms of the surface wettability state (Wenzel/Cassie-Baxter) of membranes (Kujawa & Kujawski 2016; Onda et al. 1996). The Kao diagram illustrates that the hydrophobicity of hydrophobic surfaces or hydrophilicity of hydrophilic surfaces is amplified by surface roughness. The cosine values of the apparent CA ( $\theta_r$ ) is plotted against the cosine values of the Young CA on rigid smooth surfaces ( $\theta_s$ ). Given a fixed surface roughness, changes in the Young CA (i.e. the change of surface tension) results in amplified changes in the apparent CA. However, the effects of the Young CA on the apparent CA diminishes dramatically at both ends of  $\cos\theta_r$  ranges (Füstner et al. 2005; Kujawa & Kujawski 2016). Usually, a larger surface roughness leads to a sharper gradient in terms of relationships between the apparent CA and the Young CA due to the effects of additional air trapped in surface structures (Onda et al. 1996). It is concluded that both low surface tension and high roughness contribute to the Cassie-Baxter state on membrane surface,

which is generally necessary for superhydrophobic and omniphobic surfaces having high CA and low sliding angle of water droplet.



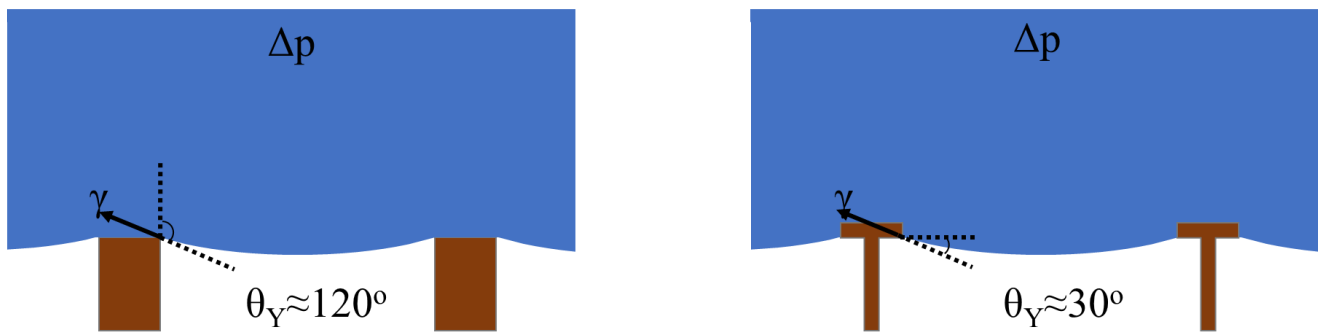
**Figure 6.** Kao diagrams of a sample membrane with fixed roughness showing the relationship between surface tension and wetting regimes (Kujawa & Kujawski 2016).

#### 2.2.3.2 Surface roughness and morphology

Surface roughness is used to represent irregularities at the surface of the material during the fabrication process (Öktem, Erzurumlu & Kurtaran 2005). Roughness statistics obtained from instrumental analyses (atomic force microscopy) gives quantitative insights into membrane morphology. Generally,  $R_{RMS}$  and  $R_{average}$ , which are both functions of height deviations from mean surface levels, are used to represent membrane surface roughness.

In addition to surface roughness, membrane morphology is another physical property affecting surface wettability. Generally, the achievement of multi-scale surface structures leads to improved hydrophobicity on membrane surfaces. Re-entrant structures are most favored for MD membranes as such morphology can easily achieve Cassie-Baxter state against most liquid

even it has low surface tension, owing to the large amounts of air pockets on the membrane topology (Kwon, Shin & Chu 2014). **Figure 7(a)** shows that a topology without re-entrant structures requires surface materials having higher than  $90^\circ$  Young CA to suspend water. On the other hand, re-entrant topology can suspend water with a surface material having the Young CA much lower than  $90^\circ$  by reducing solid-liquid contact (**Figure 7(b)**). It means that, by changing surface structure alone, a membrane can suspend or repel low surface tension liquids including oil and surfactants (Boo, Lee & Elimelech 2016). In summary, for membranes with hierarchical topology, increases in the fraction of trapped air greatly reduce the requirement of material's inherent wettability for the suspension or repellency of liquids. If the air fraction is extremely high ( $>94\%$ ), a membrane made of hydrophilic materials but with re-entrant topology can repel very low surface tension liquids, although the achievement of such topology is very difficult (Liu & Kim 2014).



**Figure 7.** Requirement of CA to suspend water: a) simple topology; b) re-entrant topology

### 2.2.3.3 Surface tension

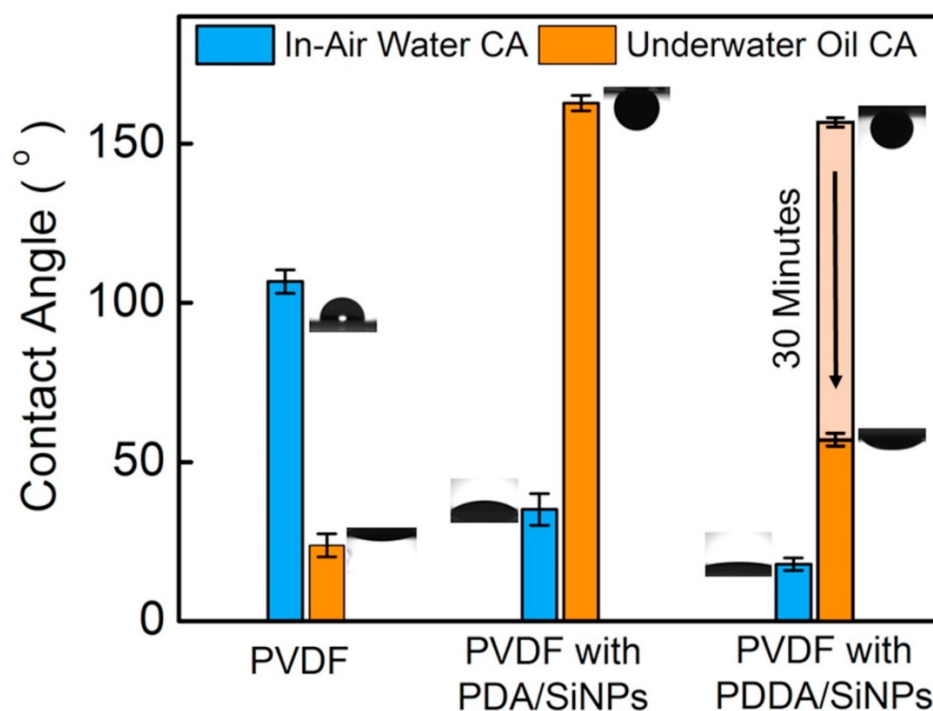
Surface tension (surface energy) quantifies the required energy to create a surface by disrupting intermolecular bonds (Owens & Wendt 1969). Surface tension plays a critical role in surface wetting: a solid surface with low surface tension has generally less wetting tendency. Surface tension can be worked out using eq. (3) with Young's CA, which is stated in section 2.3.1.

Commercial hydrophobic membranes widely used in MD experiments are made of polymers with low surface tension. However, these membranes are prone to fouling by organic pollutants such as mineral oils or to wetting by surfactant due to hydrophobic interaction (Goh et al. 2013b).

#### 2.2.3.4 Surface charge

The surface charge of a membrane surface is the electrical potential difference between the membrane surface immersed in a conducting liquid and the bulk of the liquid (Wang, Jin, et al. 2016). The surface charge of membrane greatly affects the wettability against low surface tension liquid due to hydration forces, which can be explained by Extended Derjaguin Landau Verwey Overbeek (x-DVLO). The surface charge of membrane varies greatly depending on feed water chemistry including pH, electrolyte concentrations, and the presence of organic compounds. Surface charge is determined by zeta potential measurements.

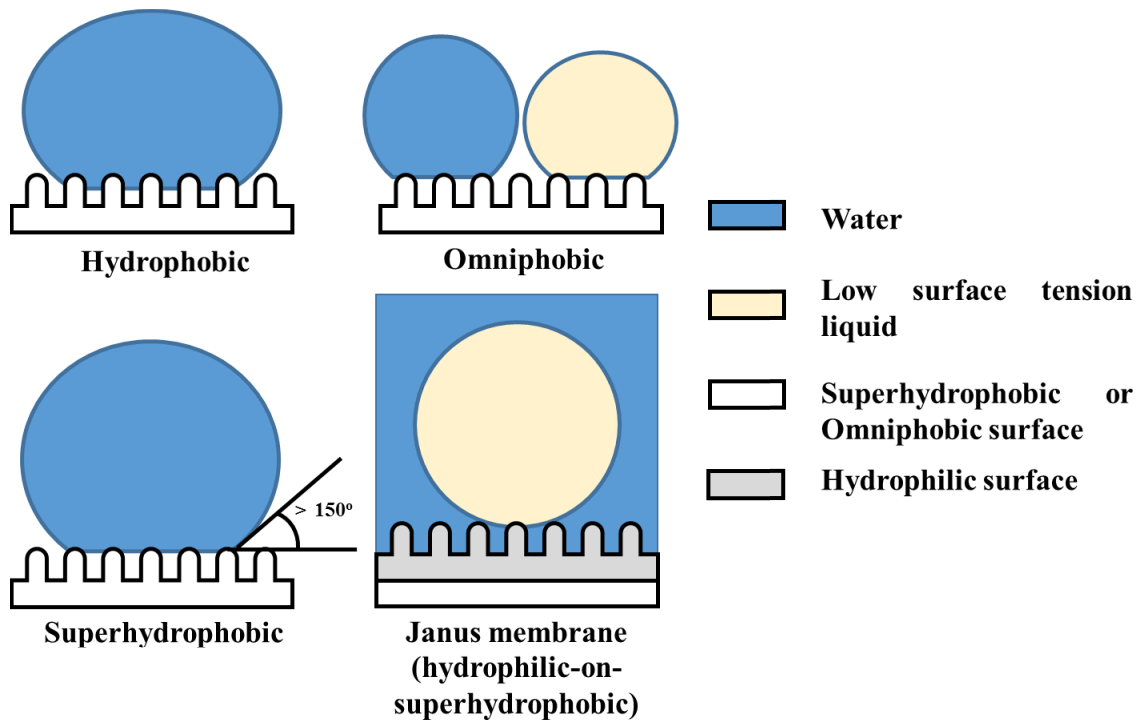
Surface charge has strong impacts on the wettability of certain liquid compounds. **Figure 8** shows that a positively-charged (PVDF with PDDA/SiNPs) composite membrane has low underwater oil CA after 30 min while a negatively-charged composite membrane (PVDF with PDA/SiNPs) maintains underwater superoleophobicity although both composite membranes were coated with hydrophilic layers (Wang, Jin, et al. 2016).



**Figure 8.** Comparison of in-air water contact angle (CA), underwater oil CA on the pristine and surface-modified composite membranes. The underwater oil CA on PDDA/SiNPs-PVDF membrane decreases continuously for 30 min (Wang, Jin, et al. 2016).

## 2.3 Special wettability

Various types of special surface wettability have been demonstrated to improve the MD stability against wetting and fouling issues (**Figure 9**). In this section, special wettability on membrane surfaces for MD applications is discussed. Novel Janus membranes with special wettability are also covered in this section. Details about their definition, working principles, and fabrication approaches are presented and analyzed. Evaluation and insights of the special wettability are also discussed.

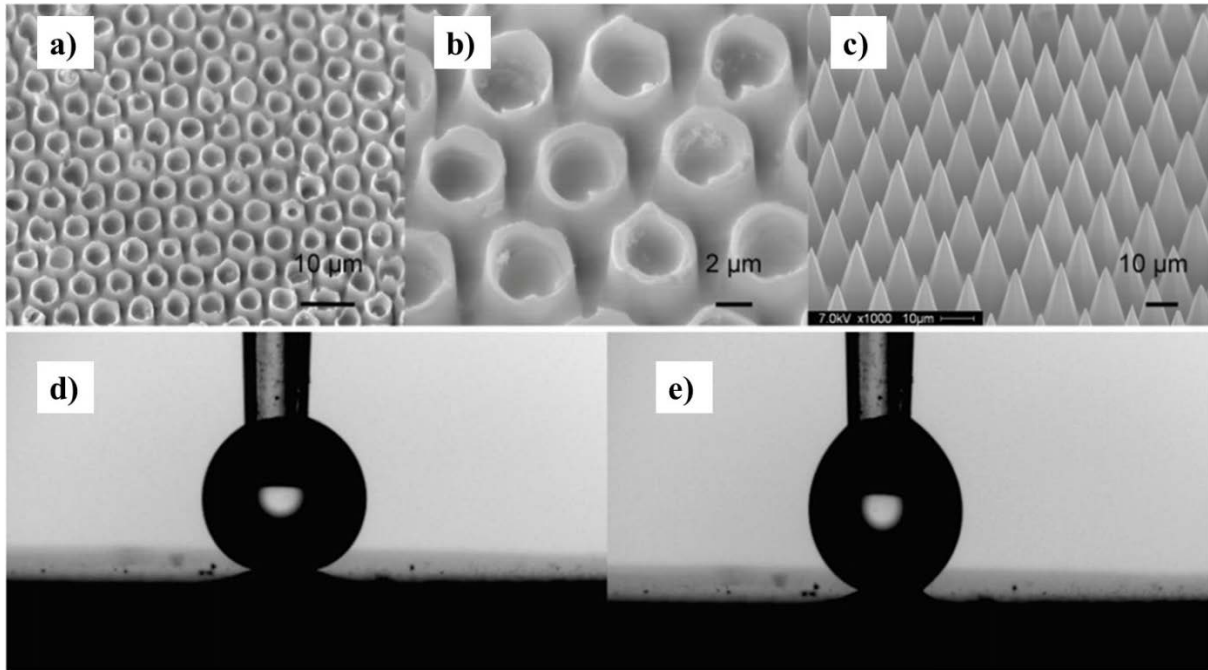


**Figure 9.** Summary of membranes with special wettability for membrane distillation.

### 2.3.1 Superhydrophobic membrane surfaces

Superhydrophobic surfaces are inspired from natural phenomena such as the lotus effect for its self-cleaning property. A superhydrophobic surface is generally defined by an apparent water CA of more than  $150^\circ$  (Crick & Parkin 2011; Razmjou et al. 2012). However, the CA varies greatly depending on various measurement techniques. In addition, two distinctly different wetting states, Wenzel and Cassie-Baxter, can share the same apparent angles. To clear the ambiguity, some researchers argued that superhydrophobic membranes should have a Cassie-Baxter wetting state. Therefore, a more explicit definition of superhydrophobicity is that in

addition to high apparent CAs, water droplets should be able to bounce or have very low sliding angles (i.e. tilt angle) on the superhydrophobic surfaces (Crick & Parkin 2011; Marmur 2004).



**Figure 10.** a) Low- resolution scanning electron microscopy (SEM) of nanospiked microchannels glass membrane surface that are etched in 1% hydrofluoric acid for 30 mins; b) high-resolution SEM of nanospiked microchannels; c) array of cone-shaped nanospikes; d and e) high CAs on superhydrophobic membranes (Ma et al. 2009)

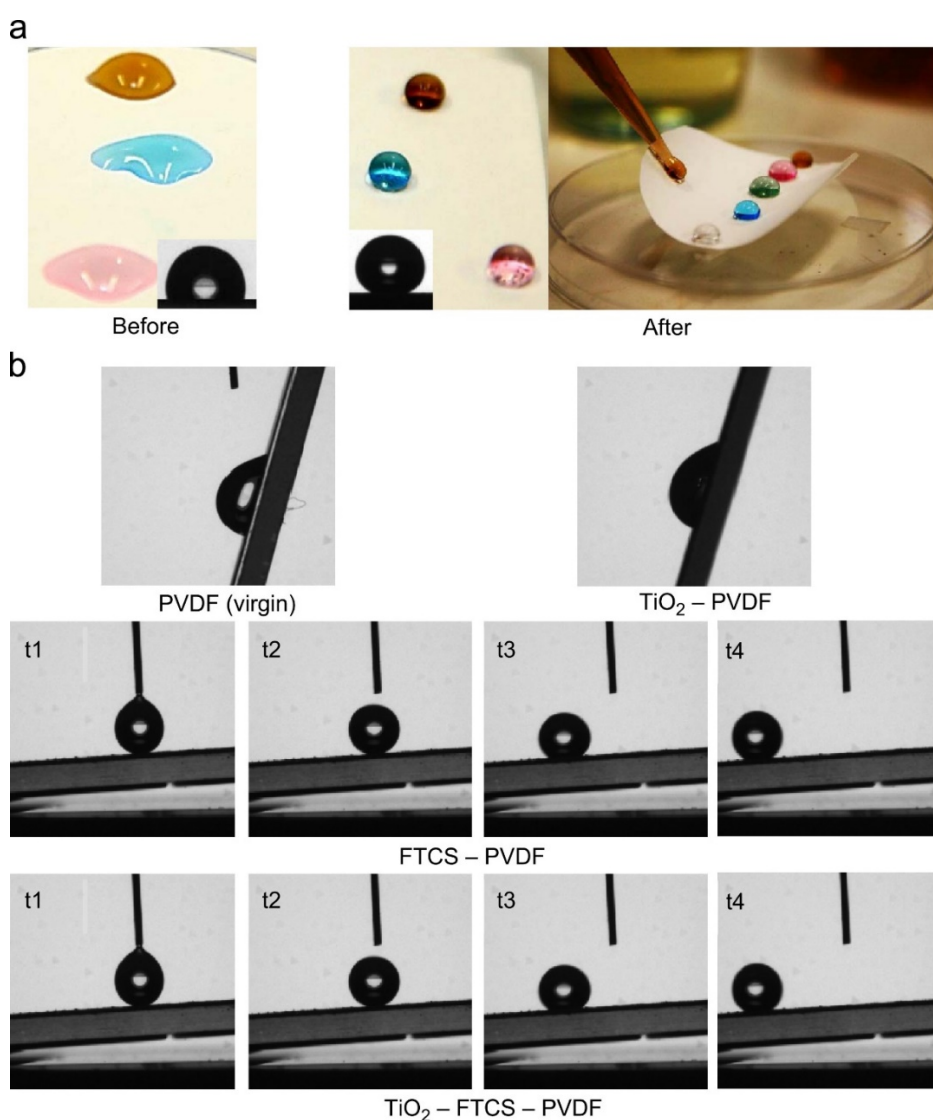
Recently, superhydrophobic MD membranes have been developed to address challenges in MD applications. Membranes with superhydrophobic surface tend to have improved flux and suffer much less flux reduction in long-term MD operation due to its much higher wetting resistance and self-cleaning properties. In some cases, superhydrophobic membranes also have improved wetting resistance against feed solution containing low surface tension components (Yan et al. 2017).

One of the first superhydrophobic membranes for MD was developed by Ma et al. in 2009 by creating ordered arrays of nanospiked microchannels on glass membrane surface followed by the fluorination on membrane surfaces (Ma et al. 2009) (see **Figure 10**). The membrane surface had a high water CA of over 160°. It is believed that the nanostructures at the membrane surface



contributed to the improvement of CAs. Varying surface morphology by increasing cone angles led to much improved superhydrophobicity.

Razmjou et al. developed a superhydrophobic membrane by incorporating fluorinated  $\text{TiO}_2$  nanoparticles (NPs) onto PVDF membranes (**Figure 11**) (Razmjou et al. 2012). The membrane surface had hierarchical structure with multilevel roughness, exhibiting a water CA of  $163^\circ$ , a glycerol CA of  $166^\circ$ , and a 30% (vol.) mono-ethanol amine CA of  $150^\circ$ . In principle, a superhydrophobic surface can be achieved in two steps: 1) increasing surface roughness with hierarchical structures, and; 2) decreasing surface tension with tailored chemical compositions on membrane surfaces.



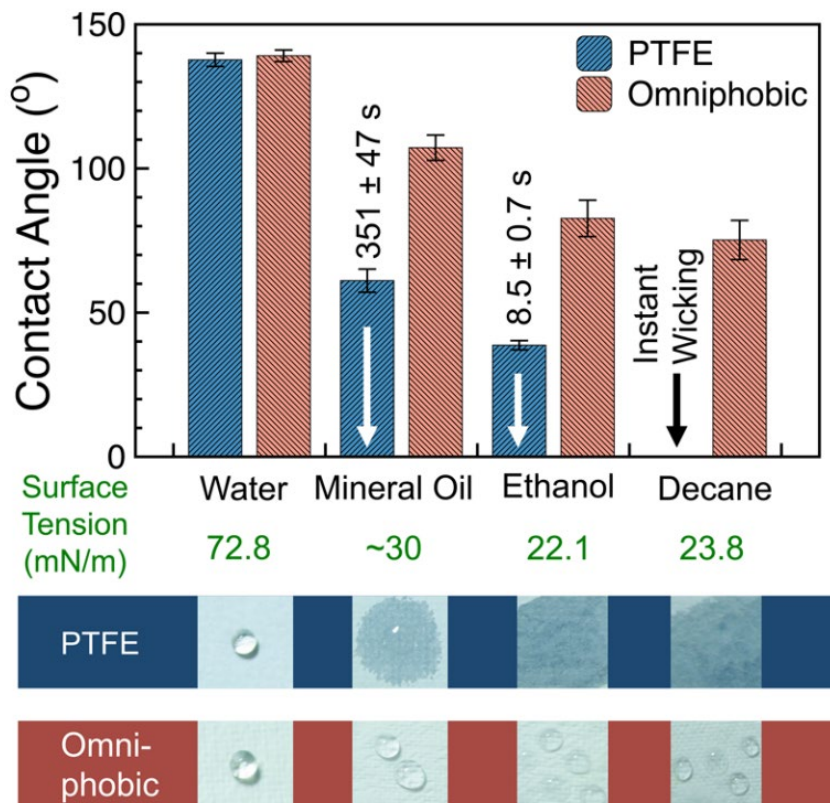
**Figure 11.** a) Various liquid droplets on PVDF membrane before and after surface modifications (transparent: Milli-Q water, brown: humic acid solution, pink, blue, and green:

buffer solutions with pH of 4, 7, and 14, respectively); (b) acquired low tilt angles after surface modifications by fluorination (Razmjou et al. 2012)

Although better MD performance has been achieved with superhydrophobic membranes for its improved permeability and wetting resistance, there are still challenges due to its intrinsic limitations. Like hydrophobic surface, superhydrophobic surfaces are prone to severe organic fouling especially when oil emulsion exists in the feed water. Flux will quickly decline when membrane fouling occurs which is caused by oil adsorption on membrane surfaces.

### **2.3.2 Omniphobic membrane surfaces**

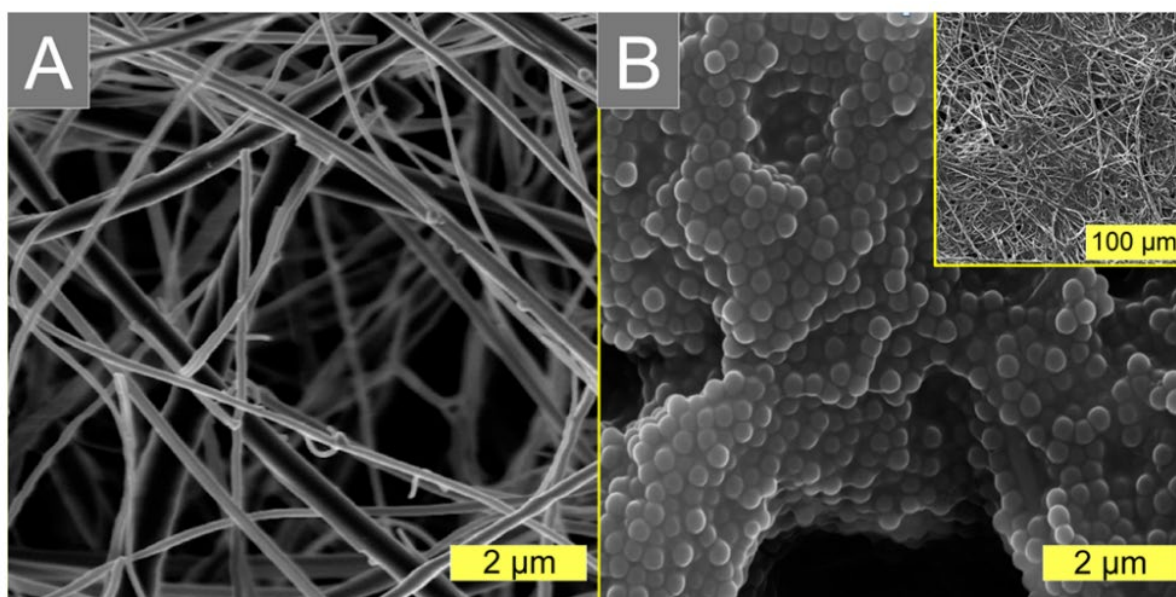
Omniphobic surfaces can repel liquids in a broad range of surface tensions and polarities, exhibiting high CA of these liquids such as mineral oils, decane, ethanol, etc. Compared with superhydrophobic surfaces, omniphobic surfaces generally have even lower surface tension. In addition, hierarchical structures with reentrant features are generally found on omniphobic surfaces, to achieve Cassie-Baxter state for liquid-solid-vapor interfaces (Lu, Zuo, et al. 2018). Such wettability have properties including self-cleaning, bio and mineral fouling resistance, and stain resistance (Boban et al. 2018; Yong et al. 2017). To address fouling and wetting issues when treating low surface tension feeds via MD, omniphobic membranes have been developed. **Figure 12** compares the CAs of liquids with various surface tension on hydrophobic PTFE and omniphobic membranes. Photos below the CA chart shows wetting behavior of both membranes: PTFE membrane is susceptible to rapid wetting against low surface tension liquids while omniphobic membrane is able to repel the liquids (Lin et al. 2014).



**Figure 12.** Comparison of contact angles of liquids with various surface tension on hydrophobic PTFE and omniphobic membranes. Photos below show wetting behavior of both membranes: PTFE membrane is susceptible to rapid wetting against low surface tension liquids while omniphobic membrane is able to repel the liquids (Lin et al. 2014)

Lin et al (Lin et al. 2014) fabricated first omniphobic MD membrane by coating silica nanoparticles on glass membranes followed by fluorination. The modified surface illustrated

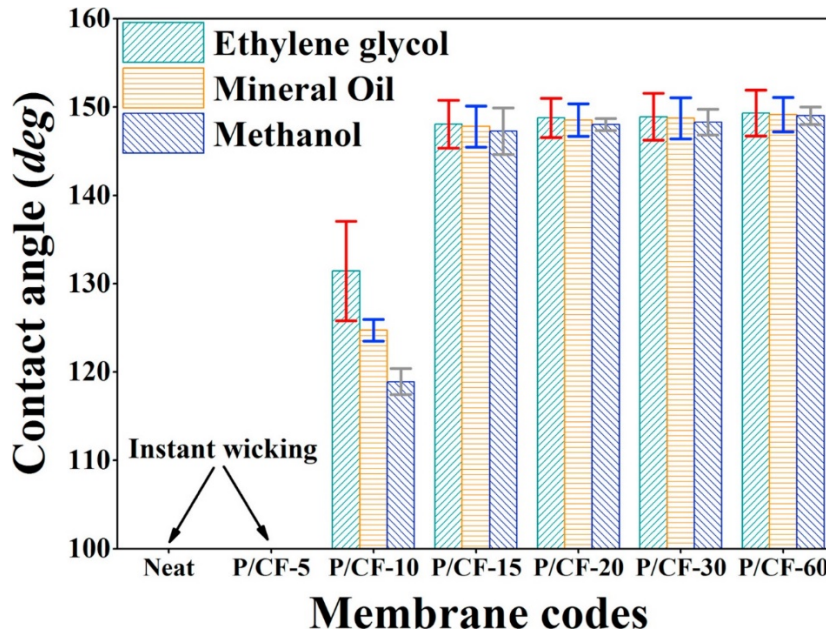
high CA towards low surface tension chemical liquids including mineral oil, ethanol, and decane, due to the air trapped inside reentrant structures (see **Figure 13**).



**Figure 13.** SEM images of the surface morphology of A) pristine glass fiber membrane; B) omniphobic surface on glass fiber after modifications. The inset image in B displays the same sample at lower magnification. (Lin et al. 2014)

Woo et al. developed omniphobic MD membrane surfaces without reentrant structures by modifying the electrospun nanofiber membranes with  $\text{CF}_4$  plasma treatment. The omniphobic surface displayed water CA  $> 160^\circ$ , and high CA ( $147 - 149^\circ$ ) towards ethylene glycol, mineral oil, and methanol (**Figure 14**). Increase in the duration of  $\text{CF}_4$  plasma treatment resulted in improved omniphobicity by reducing surface tension through the formation  $\text{CF}_3$  and  $\text{CF}_2\text{-CF}_2$  bonds.

Omniphobic membranes provide additional wetting resistance against both water and low surface tension liquids, so the inorganic fouling issues are mitigated. However, it is challenging to fabricate chemically and mechanically robust omniphobic membranes. Moreover, omniphobic membranes usually contain toxic compounds (e.g. fluorine) which makes them unsuitable for potable water production.



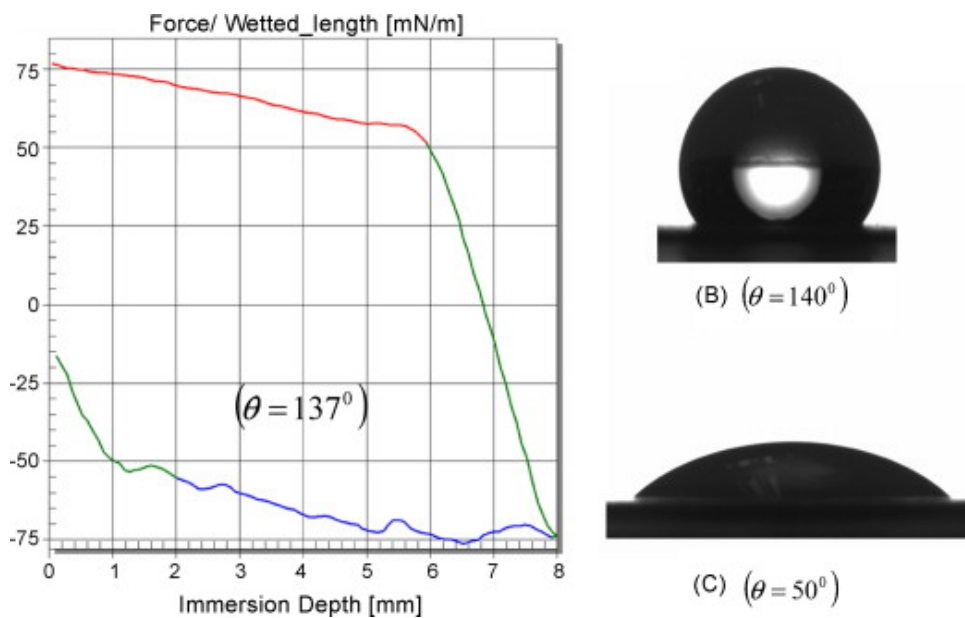
**Figure 14.** Contact angles of ethylene glycol, mineral oil, and methanol on neat and plasma-treated electrospun nanofiber membranes. The surface tensions of the liquids are 47.7, 30.0, and 22.7 mN/m, respectively (Chul Woo et al. 2017)

### 2.3.3 Janus membranes

Janus membrane structures allow opposite properties at the two sides working collaboratively, exhibiting distinctive mass transfer mechanism with integrated selectivity. In broad sense, the properties of both sides in a Janus membrane can differ in chemical and physical aspects such as morphology, surface charge, component, etc. Recently, the definition of Janus membrane is becoming more specific. To be in line with literature, Janus membranes are defined as the ones having opposing wettability at each side (Yang et al. 2016) and can be configured in three approaches: 1) A-on-B: one side is significantly thinner than the other; 2) A-and-B: Both sides share similar thicknesses; sandwich membrane including one additional middle layer is also counted as one special form of Janus membrane; 3) A-to-B: gradient across the membrane cross-section can be observed between the two sides. In general, there are two approaches to fabricate Janus membranes: asymmetric fabrication and asymmetric decoration, depending on whether Janus structures are achieved during the formation of membranes (Huang et al. 2017).

Decided by the configurations and the composition of each layer, Janus membranes can exhibit various surface wettability and mass transfer mechanism.

Khayet et al. developed a flat-sheet Janus membrane for MD with a configuration of “hydrophobic layer over hydrophilic layer”. The membrane was prepared by a single phase inversion casting step with a hydrophilic polymer dope solution containing hydrophobic fluorinated surface-modifying macromolecules (Khayet, Mengual & Matsuura 2005). Bonyadi and Chung also developed a Janus membrane but in a HF membrane configuration with similar structure: hydrophobic layer on hydrophilic layer (Zuo, Bonyadi & Chung 2016). **Figure 15** shows the contact angle measurements of the HF Janus membrane, having two different values at opposite sides of the membrane.



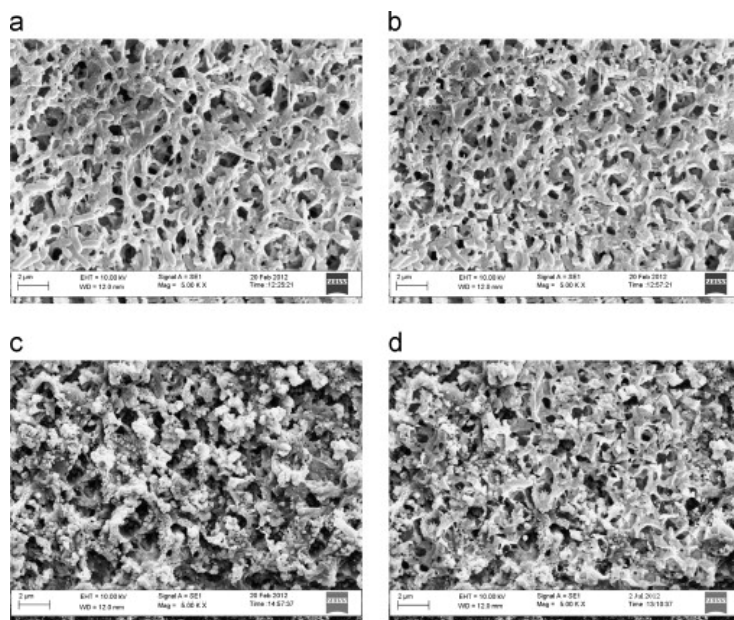
**Figure 15.** Contact angle measurements of the developed hollow fiber. A) Force per unit length of fiber vs. immersion depth. Wetting state and contact angle of water droplet on flat sheet membrane using dope solution B) for hollow fiber shell layers; C) for hollow fiber lumen layers (Bonyadi & Chung 2007)

Meanwhile, Peng et al. reversed the layer design and fabricated a membrane with hydrophilic layer on hydrophobic layer (Peng, Fane & Li 2005). The approach was designing PVA/PEG hydrophilic layers with a thickness of 6  $\mu\text{m}$  coated on top of hydrophobic PVDF substrates (Peng, Fane & Li 2005). Recently, interest in this configuration has been increasing due to their improved wetting and fouling resistance against oils and other low surface tension liquids,



which is essential for the potential usage of MD in the treatment of produced water. Zuo and Wang conducted a detailed investigation on the development of Janus membrane with the configuration of “hydrophilic layer on hydrophobic layer” in terms of fouling resistance. The hydrophilic layer exhibits very low in-air water CA but high underwater oil CA. The membranes were fabricated by grafting a hydrophilic layer made from PEG on top of a hydrophobic PVDF flat sheet membrane (Zuo & Wang 2013). The top and bottom sides of Janus membrane showed water CA of 25.2° and 120.1°, respectively, as the deposition of TiO<sub>2</sub> particles on hydrophilic layers further improved the hydrophilicity of the membrane surfaces by the incorporation of multi-level structures. Plasma was then applied on the coated membrane to improve the stability of the hydrophilic layer. The Janus membrane showed strong attachment of the hydrophilic layer onto the hydrophobic layer as surface morphology hardly changed after 5 min of ultrasonic treatment (**Figure 16**). Like omniphobic membranes, Janus membranes with “hydrophilic layer on hydrophobic layer” configuration exhibit improved fouling resistance against low surface tension liquids and wetting resistance against surfactants.

Although Janus membranes exhibit unique properties beneficial to MD applications, its fabrication approaches in large scale are still challenging. Also, some unknown influencing factors such as stimuli-responsive effects on Janus configurations need further investigation.



**Figure 16.** a) surface of a virgin PVDF membrane; b) surface of a PEG-grafted PVDF membrane; surface of a TiO<sub>2</sub>-coated membrane surface-grafted by PEG that is c) just modified; d) after 5 min ultrasonic treatment (Zuo & Wang 2013)

## **2.4 Membranes with special surface wettability for membrane distillation**

The development of MD membranes with special wettability has drawn significant attention in recent years. In addition to the satisfaction of the desired membrane properties, the provision of special wettability on MD membrane surface contributes to synergetic effects which may benefit the overall MD processes. For example, superhydrophobic MD membranes designed with anti-wetting property usually have improved permeability and selectivity (Razmjou et al. 2012; Su et al. 2016). This section comprehensively discusses details on the fabrication methods to achieve MD membranes with special wettability. Further, enhancement in MD performance for various application using these MD membranes with special wettability features is highlighted.

We categorized the membrane fabrication techniques to produce surface with special wettability into four subgroups: nanocomposite membranes, surface-modified commercial polymer membranes, surface-modified synthesized polymer substrates, and surface-modified inorganic membranes. Nanocomposite membranes are one-step fabricated membranes, by which the membrane matrix and its surface special wettability features are created simultaneously. Meanwhile, the three other subgroups are membranes requiring surface modification, which are categorized based on the types of their substrates.

### **2.4.1 Nanocomposite membranes**

This section covers all MD nanocomposite membranes with special wettability which are fabricated via one-step fabrication methods. All these membranes have superhydrophobic surfaces (Table 1).

**Table 1.** Published reports in the literature about nanocomposite membranes with special wettability(superhydrophobicity) categorized by application



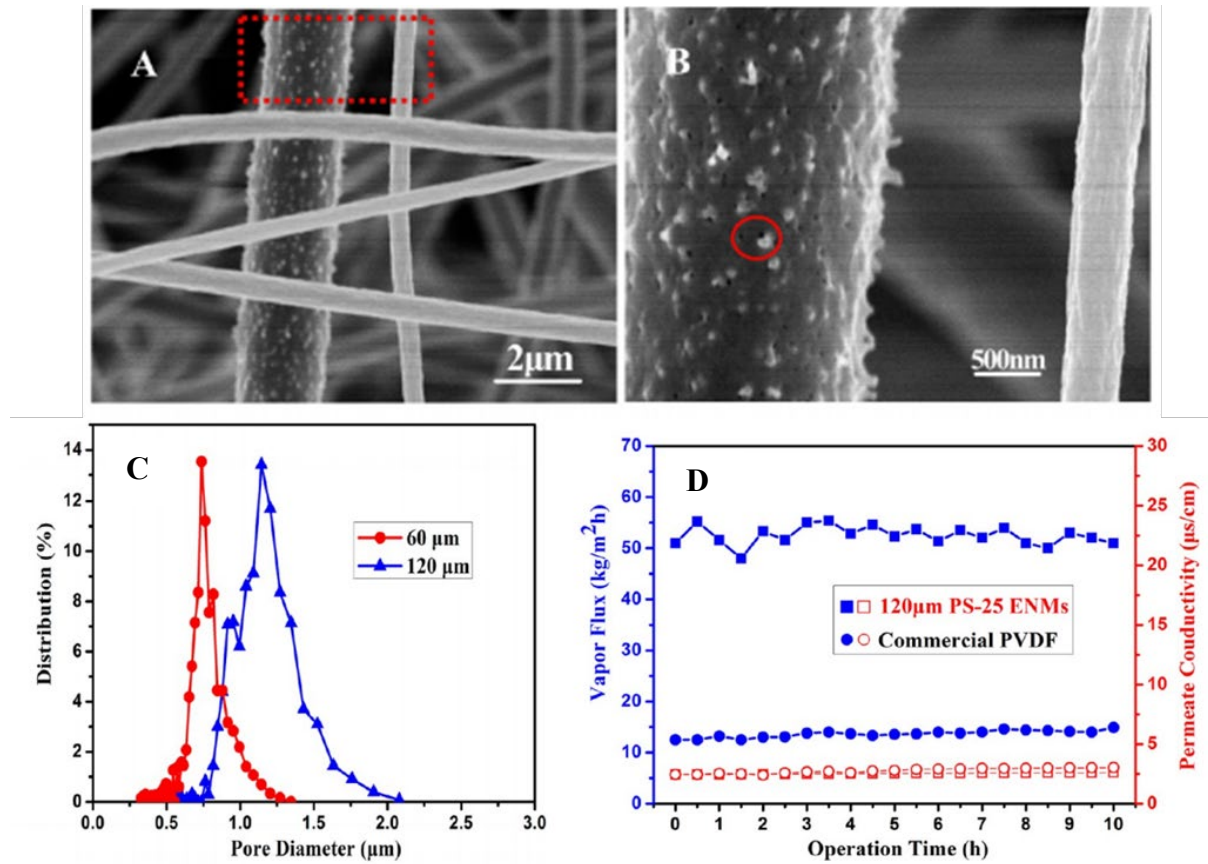
<b>Polymer and additives</b>	<b>Fabrication method</b>	<b>Contact angle (°)</b>	<b>Mean pore size (μm)</b>	<b>Application</b>	<b>Benefit</b>	<b>Ref.</b>
<b>PVDF /hydrophobic silica</b>	Electrospinning	150	0.36	DS	AW	(Liao et al. 2014)
<b>PVDF</b>	Electrospinning (electrospraying hydrophobic silica simultaneously)	163	n/a	DS	HP	(Su et al. 2016)
<b>PVDF/ PTFE</b>	Electrospinning	152	0.49±0.15	DS	AW	(Dong et al. 2014b)
<b>PVDF-HFP /carbon nanotubes</b>	Electrospinning	159	0.29±0.01	DS	AW	(Tijing et al. 2016)
<b>PVDF-HFP /graphene</b>	Electrospinning	163	0.86±0.02	DS	AW	(Woo, Tijing, et al. 2016)
<b>PS</b>	Electrospinning	150	1.15	DS	HP	(Li et al. 2014)
<b>PMMA/PDMS</b>	Electrospinning	163	8.03	DS	AW	(Ren et al. 2017)

Note: DS = desalination, IW = industrial wastewater, AF = anti-fouling, AW = anti-wetting, HP = high permeability

#### 2.4.1.1 Fabrication method

Nanocomposite membranes are fabricated using electrospinning technique as nanofiber membranes generally have rough surfaces. Electrospinning technique offers a relatively easy and straightforward fabrication method for achieving nanocomposite membranes with large pore sizes, and superhydrophobicity that greatly improve wetting resistance while maintaining high permeability. For nanofiber membrane fabrication, the material parameters (such as dope solution concentration), process parameters (such as applied voltage, tip-to-collector distance

and fabrication time), and environmental parameters (such as humidity) should be optimized to attain the desired membrane morphology that will effectively enhance MD performance.

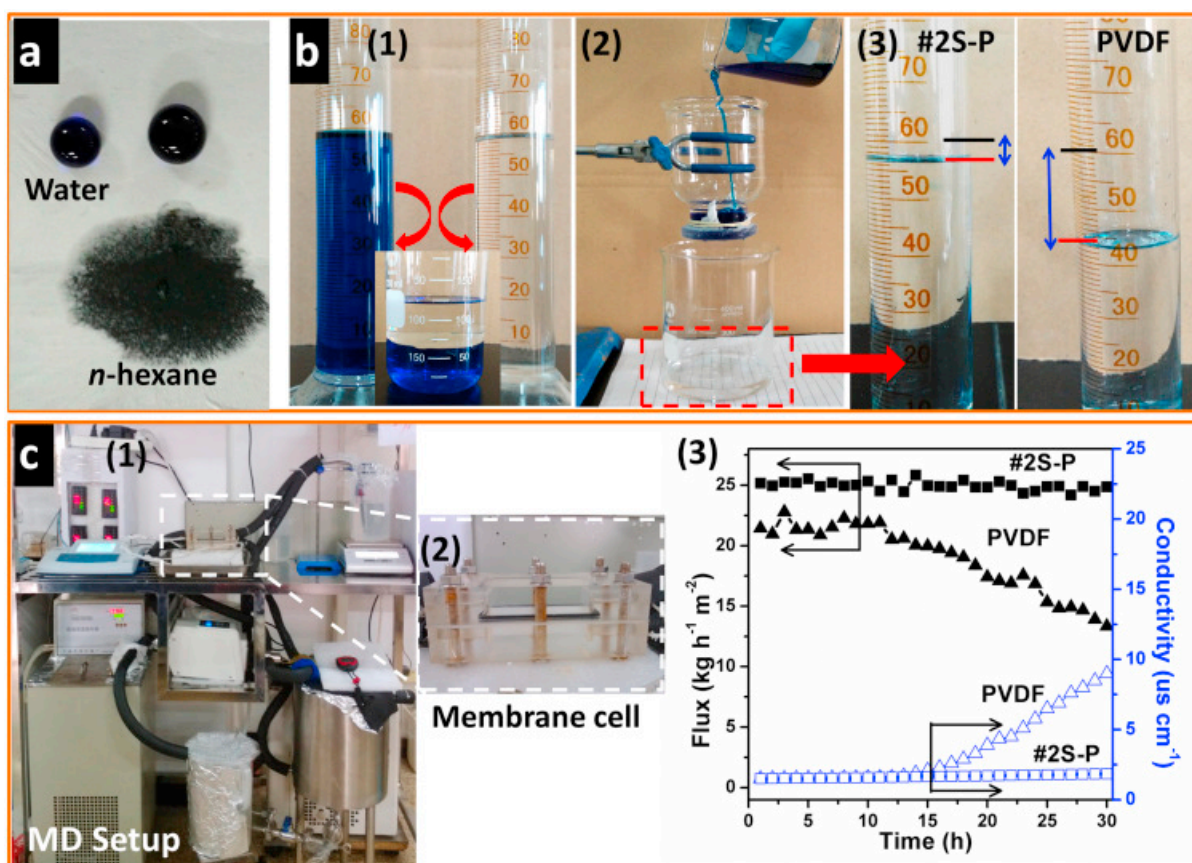


**Figure 17.** a) SEM images of dual-biomimetic PS nanofiber membranes; b) the dotted circle showed nanopapillae and nanoporous structures; c) the effect of membrane thickness on pore size distribution; d) the comparison of flux between superhydrophobic nanofiber PS membrane with a commercial PVDF membrane (Li et al. 2014)

Hierarchical structures on the surface of nanocomposite membranes can significantly enhance its performance. Li et al. successfully developed electrospun polystyrene (PS) nanofiber membranes with micro/nanoscale roughness, which are inspired by the lotus effect (**Figure 17**). The nanofiber membranes showed high CA ( $\sim 150^\circ$ ), which led to very high flux (105 LMH) under feed/permeate temperature difference of 50 °C (Li et al. 2014). A common method for creating hierarchical structure on the surface of nanocomposite membranes is by adding hydrophobic micro/nanoparticles into dope solutions. For instance, Woo et al. added two-dimensional graphene nanoparticles into the PVDF dope solution for electrospinning (Woo, Tijing, et al. 2016). With an optimal graphene concentration of 5 wt.%, the nanofiber

membranes obtained a very high contact angle of  $163^{\circ}$  with high LEP of 187 kPa due to protruding nanoparticles on electrospun nanofibers. However, further increase in nanoparticle concentrations caused aggregation issues, leading to decrease in porosity and mean pore size; thereby, reducing the MD flux. Other hydrophobic particles that are added into dope solution include micro-size polymers (PTFE, PDMS), one-dimension nanomaterials (carbon nanotube), and three-dimensional nanomaterials (surface modified silica) (Dong et al. 2014b; Liao et al. 2014; Ren et al. 2017; Tijing et al. 2016).

Apart from electrospinning technique for the blended dope solution, simultaneous electrospraying of the nanocomposite dope solution while electrospinning nanofibrous membranes can also result in favorable membrane surface property. Su et al. fabricated a membrane with low sliding angle of  $3^{\circ}$  and high LEP of 280 kPa by electrospraying surface modified silica while electrospinning PVDF membrane (Su et al. 2016). The nanofiber membrane also showed superoleophilicity (**Figure 18**).



**Figure 18.** a) resistance against water and n-hexane droplets; b) oil/water separation processes using neat nanofiber PVDF and superhydrophobic nanofiber membranes; c) DCMD configuration and permeation performance comparison (Su et al. 2016)

#### 2.4.1.2 Application

Nanocomposite membranes are usually superhydrophobic; illustrating excellent permeability with high selectivity and wetting resistance. As such, they are highly suitable to be applied for high salinity treatment such as seawater desalination and brine concentration as shown in Table 1. Upon surface modification, these nanocomposite membranes exhibit improved permeability (Li et al. 2014; Su et al. 2016), as well as enhanced MD permeate fluxes compared with commercial PVDF membranes. Also, nanocomposite membranes achieve better LEP and wetting resistance in long-term operation (Ren et al. 2017; Woo, Tijng, et al. 2016). These surface-modified membranes illustrated stable performance for 60 h in the configuration of AGMD with the salt rejection of 99.99%.

### 2.4.1.3 Challenges

Although nanocomposite membranes may have surface superhydrophobicity, the equilibrium of water droplets on these membranes are usually at Wenzel state, as the droplet cannot bounce or have very low sliding angles. As such, the hydrophobicity of these membranes is compromised, leading to lower wetting resistance. Further, although embedding nanoparticles enhances the characteristics of nanocomposite membranes, it still does not resolve the large pore size and low LEP issues of electrospun membranes. Therefore, long-term MD operation for these membranes is still a challenge.

As nanocomposite membranes can only attain one special wettability feature, which is superhydrophobicity, their application is highly limited towards desalination. This is because, superhydrophobic membranes are prone to organic fouling (as mentioned in previous sections). The minimal organic content in seawater does not affect the performance of nanocomposite membranes. Also, scaling up electrospinning technique into industrial level is a major challenge.

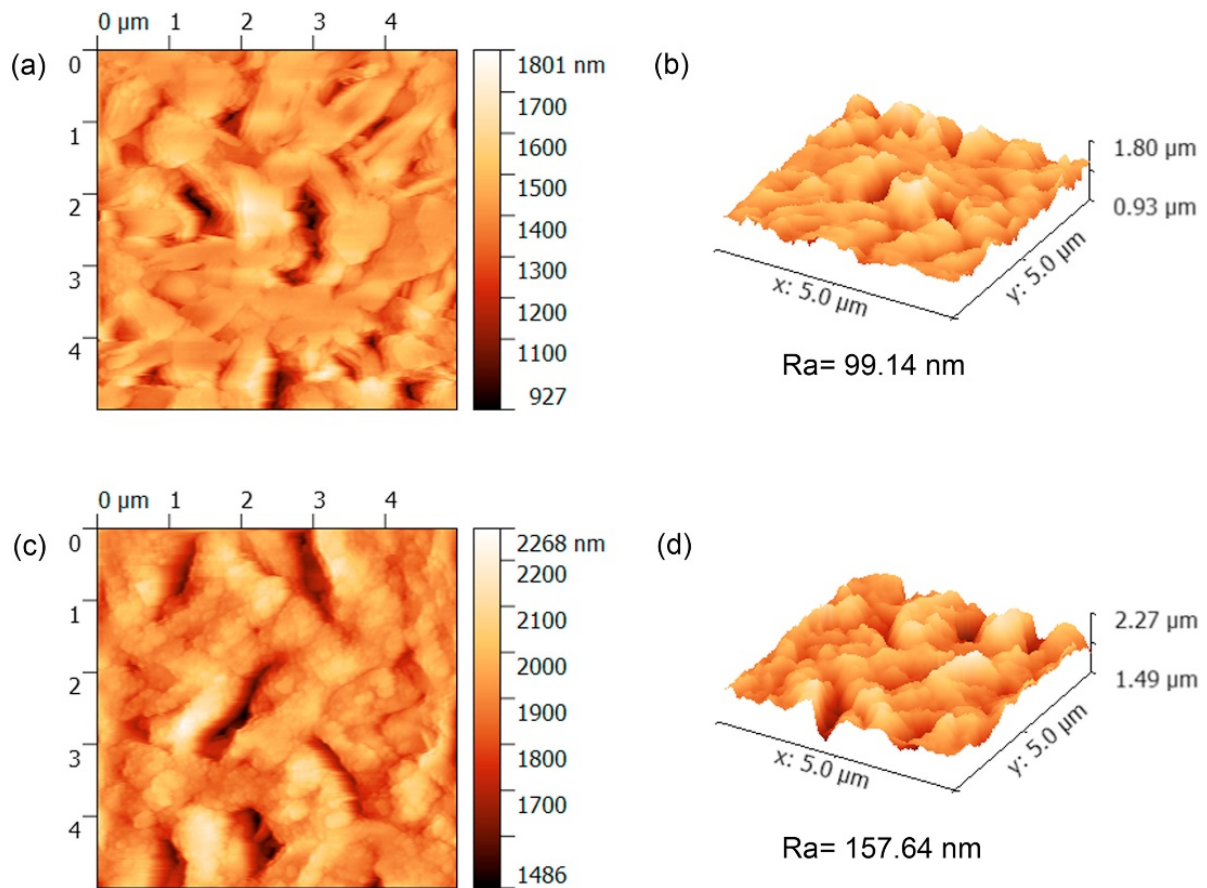
## 2.4.2 Surface-modified commercial membranes

This section covers discussions on surface-modified commercial membranes with special wettability for MD. Due to their low cost, stable quality, and wide availability, hydrophobic commercial membranes mostly made of PVDF with surface pore sizes ranging from 0.2- 0.45  $\mu\text{m}$  have been utilized for surface modification to enable improved properties and hence performance for MD.

### 2.4.2.1 Modification method

Commercial membranes can attain superhydrophobicity and omniphobicity by increasing the surface roughness and providing multi-level structures. A favorable manner to achieve these conditions is by incorporating nanoparticles (e.g.  $\text{TiO}_2$ , silica, etc.) on the surfaces of the commercial membrane surfaces. Nanoparticles can be incorporated onto a commercial membrane surface via dip-coating or by adhesive-deposition (such as using polydopamine (PDA) as adhesive). For example, Shan et al. deposited Ag nanoparticles (AgNPs) on commercial PVDF membrane using PDA as adhesive (Shan et al. 2018). As a result, the roughness of the commercial membrane increased from 99.1 to 157.6 nm, and the CA increased from  $126^\circ$  to  $136^\circ$ . The deposition of composite particles with multiscale roughness on

membrane surfaces has also been explored to obtain MD membranes with hierarchical structure. Zheng et al. firstly fabricated polystyrene (PS) microspheres with silica NPs deposited on their surfaces; then coated the composite particles onto commercial membrane using the adhesive polymer 3-methacryloxypropyltrimethoxysilane. The hierarchical membrane achieved a significantly increased surface roughness,  $R_a = 343$  nm, while the silica-coated membrane and pristine membrane have a roughness of 142 and 99 nm, respectively (Zheng et al. 2018). With the aid of fluorination, the imparted re-entrant structure on the membrane surface maintained a Cassie-Baxter state of wettability. It had a very high water CA of  $176.5^\circ$  and low sliding angle of  $7^\circ$ , and water droplet could bounce back when falling on the membrane surface. The modification approaches using NPs can also enhance the permeability of MD membranes due to the large surface areas of NPs if well designed.

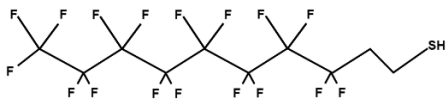
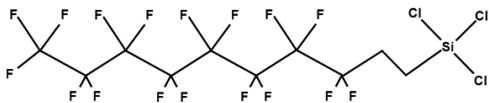
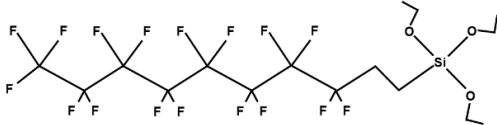


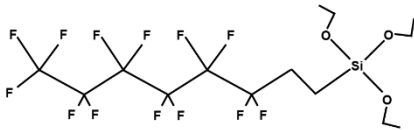
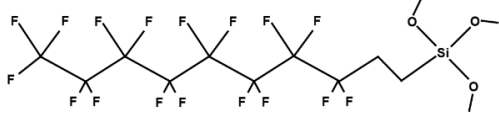
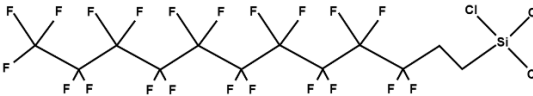
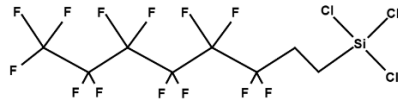
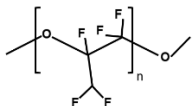

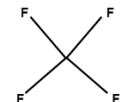
**Figure 19.** Topographies of a,b) pristine commercial PVDF membrane; c,d) fluorinated AgNPs deposited membrane (Shan et al. 2018)

Commonly, the nanoparticle-coated commercial membranes are then fluorinated to achieve superhydrophobicity or omniphobicity. **Table 2** shows various compounds used for

fluorination, mostly long-chain fluoroalkyl silanes. Razmjou et al. fluorinated the TiO<sub>2</sub> coated membrane with 1H, 1H, 2H, 2H-perfluorodecyltrichlorosilane (FTCS) (Razmjou et al. 2012). This new membrane illustrated self-cleaning property as indicated by the significantly decreased sliding angles (**Figure 19**). Fluorination of NPs coated membranes with re-entrant structures renders them omniphobic surfaces. The fluorinated multiscale membranes showed strong resistance against low surface tension liquids: 156° on oil emulsion, 133° on diiodomethane, and 138° on hexadecane (**Table 3**), making the membrane capable of treating feed water containing low surface tension components (Zheng et al. 2018). Generally, the fluorinated NPs coated commercial membranes have much improved wetting and fouling resistance due to the multi-scale roughness on the surface. The wettability is maintained at Cassie-Baxter state for all these membranes, which means they have very high contact angle and low sliding angles.

**Table 2.** Various chemical compounds for fluorination.

Chemical name	CAS no.	Chemical structure	Ref.
<b>1H,1H,2H,2H-Perfluorodecanethiol (PFDT)</b>	34143-74-3		(Lu, Su, et al. 2018; Shan et al. 2018)
<b>1H,1H,2H,2H-Perfluorodecyltrichlorosilane (FDTs)</b>	78560-44-8		(Boo, Lee & Elimelech 2016; Kujawa et al. 2017; Lee et al. 2016; Subramanian et al. 2019)
<b>1H,1H,2H,2H-Perfluorodecyltriethoxysilane (PFTES)</b>	101947-16-4		(An, Liu & Hu 2018; Hubadillah et al. 2019; Woo et al. 2018; Zhong et al. 2017; Zhu, Liu,

			Hou, et al. 2018)
<b>1H,1H,2H,2H-Perfluorooctyltriethoxysilane (PFOTES)</b>	51851-37-7		(Xu et al. 2017)
<b>1H,1H,2H,2H-Perfluorodecyltrimethoxysilane (FAS17)</b>	83048-65-1		(Chen et al. 2018; Dong et al. 2015; Zheng et al. 2018)
<b>1H,1H,2H,2H-Perfluorododecyltrichlorosilane (FAS21, FDDTS)</b>	102488-49-3		(Deng et al. 2018; Lin et al. 2014; Meng, Mansouri, et al. 2014; Razmjou et al. 2012)
<b>1H,1H,2H,2H-Perfluorooctyl-trichlorosilane (PFOTCS)</b>	78560-45-9		(Lu et al. 2016; Ma et al. 2009)
<b>Perfluoropolyether (PFPE)</b>	69991-67-9		(Liao et al. 2014; Liao, Wang & Fane 2014)
<b>Poly[4,5-difluoro-2,2-bis(trifluoromethyl)-1,3-dioxole-co-tetrafluoroethylene] (PTFE AF 2400)</b>	37626-13-4		(Lu, Zuo, et al. 2018)
<b>Tetrafluoromethane (CF4)</b>	75-73-0		(Chul Woo et al. 2017; Yang et al. 2014)

Apart from the use of nanoparticles coating and fluorination, other modification treatments have also been implemented to acquire superhydrophobicity on commercial membrane. Yang et al. obtained a superhydrophobic membrane by applying CF<sub>4</sub> plasma-modification, which had improved CA of 162° (Yang et al. 2014). The membrane surface roughness and structures



are not affected by plasma modification, so the surface wettability remains at Wenzel state; low sliding angle of water droplets has not been observed.

**Table 3.** Published reports in the literature about surface-modified commercial membranes with special wettability for MD.

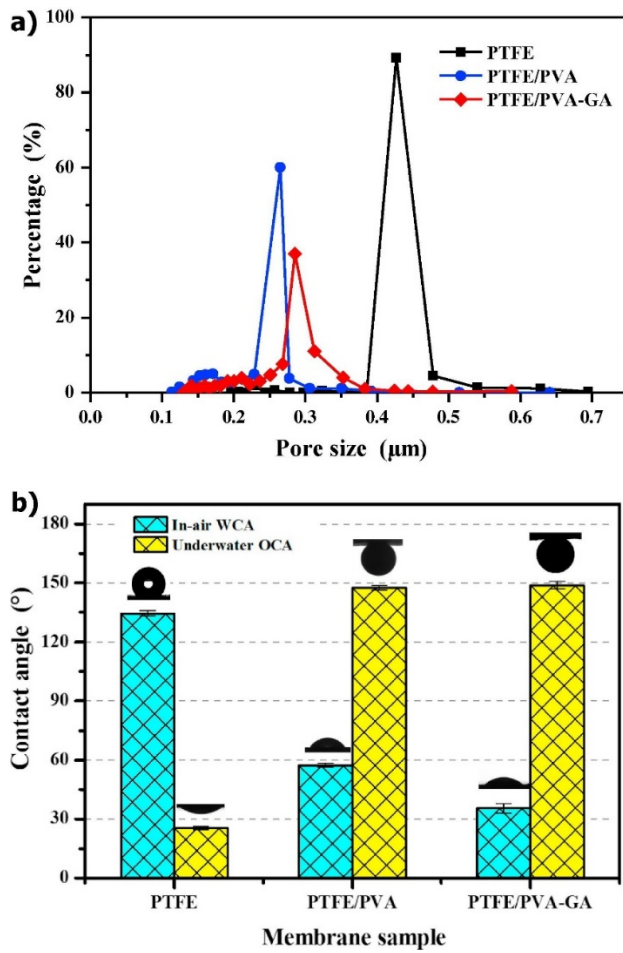
Substrate	Modification methods	Special wettability	Contact angle (°)	Mean pore size (μm)	Application	Benefits	Ref.
PVDF	Plasma-modifying (CF <sub>4</sub> )	superhydrophobic	162	0.25	DS	HP	(Yang et al. 2014)
PVDF	Dip-coating (TiO <sub>2</sub> )/ f	superhydrophobic	163	0.39±0.03	DS	AF	(Meng, Mansouri, et al. 2014; Razmjou et al. 2012)
PP (hf)	PDA-depositing (SiNPs)/ f	superhydrophobic	157	0.2	DS	AW	(Xu et al. 2017; Zhong et al. 2017)
PVDF	Dip-coating (SiNPs)/ f	omniphobic	167 141-MI	0.40±0.02	SF	AW	(Boo, Lee & Elimelech 2016; Lu et al. 2016)
PVDF	P (A 174)-depositing (SiNPs@PS)/ f	omniphobic	177 156-oil emulsion 133-MI 138-HXD	0.26±0.05	SF	AF/AW	(Zheng et al. 2018)
PVDF	PDA-depositing (AgNPs)/ f	omniphobic	168 137- rapeseed oil	0.38	SF	AF/AW	(Shan et al. 2018)
PVDF	Dip-coating (TiO <sub>2</sub> )/ plasma modifying (He)	Janus (hydrophilic-on-hydrophobic)	25.2	0.18	OW	AF/AW	(Zuo & Wang 2013)
PVDF	Spraying-coating (CTS-PFO/SiNPs)	Janus (hydrophilic-on- hydrophobic)	0 UW 150-crude oil	0.39±0.03	OW	AF	(Wang, Hou & Lin 2016a)

<b>PVDF</b>	Spraying (SiNPs)/ PDA-depositing	Janus (hydrophilic-on- hydrophobic)	35 UW 163- crude oil	0.4	OW	AF	(Wang, Jin, et al. 2016)
<b>PVDF</b>	Dip-coating (PVA)	Janus (hydrophilic-on- hydrophobic)	0	-	SF	AF/AW	(Lu et al. 2017)
<b>PVDF</b>	Filtration-coating (graphene oxide)	Janus (hydrophilic-on- hydrophobic)	125	0.69	SF	AF	(Qiu et al. 2018)
<b>PTFE</b>	Electrospinning (PVA)	Janus (hydrophilic-on- hydrophobic)	36 UW 149- crude oil	0.28±0.04	OW	AF	(Wang, Hou, et al. 2018)
<b>PVDF (hf)</b>	PDA-depositing (PEI)	Janus (hydrophilic-on- hydrophobic)	26,13	0.02	OW	AF/AW	(Chew, Zhao, Malde, et al. 2017; Chew et al. 2018)

Note: hf = hollow fiber, f = fluorination, DS = desalination, MI = diiodomethane, HXD = hexadecane, IW = industrial wastewater, SF = surfactants removal, OW = oil/water separation, AF = anti-fouling, AW = anti-wetting, HP = high permeability

Janus (hydrophilic-on-hydrophobic) membranes can be acquired by coating a layer of highly hydrophilic compounds (i.e. high surface tension) on the commercial membranes. Wang et al. successfully coated one layer of PVA on PTFE membrane using electrospinning. After crosslinking, the Janus membrane had a low in-air water CA of 35.5° and high underwater oil CA of 148.7°. However, its pore size significantly decreased from 0.45 to 0.28 µm (**Figure 20**). Owing to the low roughness of commercial membranes, NPs have also been employed to impart multi-scale structures to the membrane surfaces. Wang et al. created a hierarchical structure on commercial PVDF membrane using silica NPs. As a result, the composite membrane had a very high underwater oil CA of 163°. **Figure 21** shows that, unlike hydrophobic and superhydrophobic membrane surfaces, the composite Janus membrane had minimal interaction with oil droplets due to low attraction between them; therefore, there was no physical contact between the oil droplet and membrane surface (Wang, Hou & Lin 2016a). The surface charge of the Janus membranes must be taken into consideration as it affects the wettability of oil significantly. Wang et al. found that a negatively charged Janus membrane could maintain high oil CA at 163° consistently while the positively charged one failed. Also

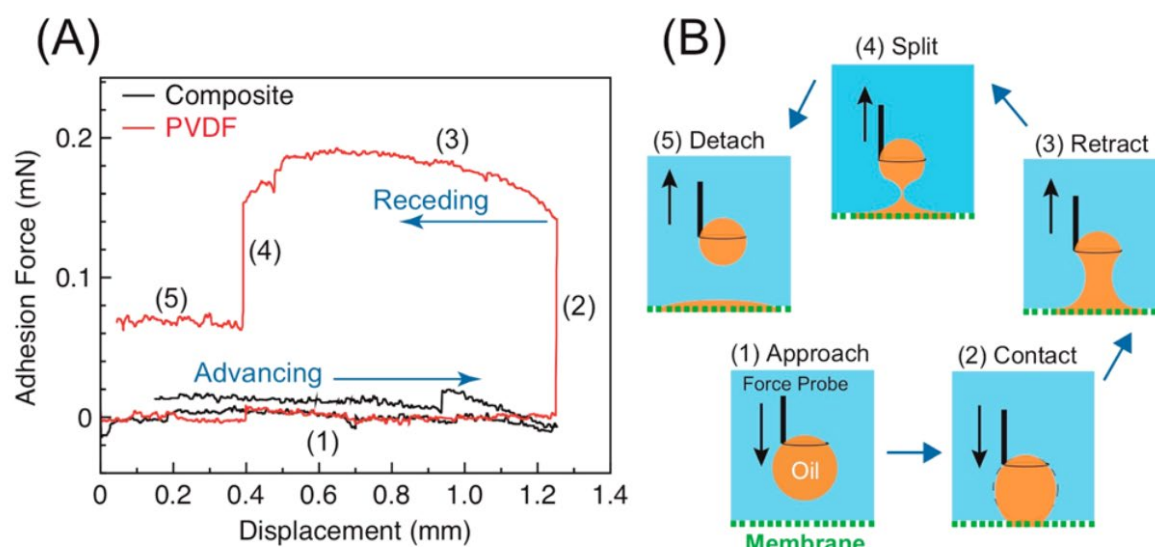
in DCMD experiments, only the negatively-charged composite membranes could maintain high flux stably when treating saline solution containing crude oil (Wang, Jin, et al. 2016).



**Figure 20.** a) Pore size distribution of virgin PTFE membrane, the PVA coated PTFE membrane, and cross-linked surface-modified membrane; b) in-air water contact angle and underwater contact angle of these membranes (Wang, Hou, et al. 2018)

After surface modification, nearly all the commercial membranes still maintain their high mechanical strength, making them viable in long-term operation. However, the pore size of

these surface-modified commercial membranes become even smaller after the modification; therefore, they have relatively lower flux than superhydrophobic nanocomposite membranes.



**Figure 21.** a) Force-displacement curves showing the patterns where a mineral oil droplet interacted with the composite Janus membrane (black curve) and hydrophobic membrane (red curve); b) the five stages in the patterns (Wang, Hou & Lin 2016a)

#### 2.4.2.2 Application

The commercial membranes that were imparted with superhydrophobicity are used for desalination. Depending on the modification approaches, these membranes can have improved permeability, wetting resistance, or scaling resistance (Meng, Mansouri, et al. 2014; Razmjou et al. 2012; Yang et al. 2014). The commercial membranes that were imparted with omniphobicity are used to treat highly saline oil-field produced water containing surfactants. The surface modified membranes have improved wetting and fouling resistance against sodium dodecyl sulfate (SDS) with concentration up to 0.5 mM in feed wastewater (Lu et al. 2016; Shan et al. 2018; Zheng et al. 2018). Also, the surface-modified commercial membranes with omniphobicity can deal with wastewater containing oil emulsion. More specifically, as oil emulsion can be prepared by surfactant or physical emulsification, the capacity of omniphobic MD membranes treating the oil emulsion varies. Oil-emulsion (prepared by surfactant) with the addition of oil up to 0.005 %v/v into the wastewater can be treated with stable MD permeation performance (Boo, Lee & Elimelech 2016). Wastewater containing oil emulsion that are prepared physically using high concentration of crude oil (1,000 ppm) can also be

treated by the surface-modified membranes (Wang, Hou & Lin 2016a). On the other hands, produced water or oil-emulsion wastewater can also be treated by Janus membranes (hydrophilic-on-hydrophobic) after surface-modifying commercial membranes. The membranes showed improved fouling and wetting resistance against wastewater containing high crude oil (~ 1000 mg/L) and salinity (~ 35 g/L NaCl) (Qiu et al. 2018; Wang, Hou & Lin 2016a; Wang, Jin, et al. 2016).

#### 2.4.2.3 Challenges

The approaches towards achieving surface-modify commercial membranes face several challenges. First, permeation of MD membrane may be decreased when polymers are used as adhesive to deposit NPs on the commercial membranes as the polymers can block membrane pores and hence reduce the mean pore size of the membranes. For these reasons, the thickness of NPs layers must be controlled precisely. Secondly, the strength of attachment between the NPs and the membrane substrates is compromised. Currently, PDA-depositing membranes showed the highest stability; the membranes show high stability as they remain intact after undergoing ultrasonic tests. However, in real applications using membrane technology, chemical cleaning is a commonly applied practice. Chemical cleaning reduces the strength of attachment of NPs on the surface modified membranes (Wu, Mansouri & Chen 2013). The detached nanoparticles into treated water expose strong risks to human health, making NPs deposited membranes not viable for potable water treatment. Thirdly, most nanoparticles have low hydrophobicity, which means further modification approaches are required to reduce their surface tension. Fluorination is an effective technique for the development of MD membrane with desired wettability, but several issues hinder its potentials in industrial usage. The stability of the deposited fluorine compounds on membrane surface can be severely challenged by chemical cleaning during water-treatment cycles. Especially, in terms of fluorinated NPs coated membranes, the potential detachment of fluorinated NPs makes the membrane only viable for industrial usage. Also, most fluorine compounds have extremely poor degradability in the environment, and they can easily accumulate in living organisms and cause long-term harms. As stricter regulations on fluorine compounds are being proposed by many governments, it can further hinder their implication in the membrane modification. For these reasons, it is important to evaluate the potential of using chemicals that are less toxic such as octamethylcyclotetrasiloxane (D4) as a substitute to fluorine compounds to reduce surface tension.

### 2.4.3 Synthesized membranes with special wettability

This section discusses developments in lab-synthesized membranes with special wettability for MD. Most of the published research are directed towards developing new membranes that can address the challenges for long-term MD application. Two most commonly utilized techniques for substrates are by phase inversion (casting) and electrospinning. Generally, casted membranes have much smaller pore sizes compared to electrospun nanofiber membranes.

#### 2.4.3.1 Modification method

Various special wettability can be achieved on synthesized membranes via surface modification. As discussed in the last section, the common approaches of imparting superhydrophobicity or omniphobicity on commercial membranes are to coat nanoparticles onto the membrane surface followed by fluorination. This approach is also utilized in synthesized membranes. Aside from fluorination, some other low surface tension chemicals had been deposited on the membrane surface to acquire superhydrophobicity (**Table 4**).

**Table 4.** Published reports in the literature about surface-modified synthesized membranes with special wettability for MD

Substrate	Substrate type	Modification methods	Special wettability	Contact angle (°)	Mean pore size (μm)	Applications	Benefits	Ref.
PVDF	NIPS	Dip-coating (OTMS)	superhydrophobic	160	0.05	DS	AW	(Ray et al. 2018)
PVDF	NIPS	Spraying (PDMS and hydrophobic SiNPs)	superhydrophobic	156	0.36±0.02	BT	AF	(Zhang, Song, et al. 2013)
PVDF (hf)	NIPS	Ultrafiltration-coating (etched PVDF particles)	superhydrophobic	164	n/a	SF	AW	(Yan et al. 2017)
PVDF-HFP	Elec	Electrospraying (PDMS)	superhydrophobic	155 157	0.49, 0.40±0.05	IW	AF/AW	(An et al. 2017; Lee et al. 2017)
PVDF	Elec	Dip-coating (AgNPs)/ (1-Dodecanethiol)	superhydrophobic	153	0.34±0.01	DS	HP	(Liao, Wang &

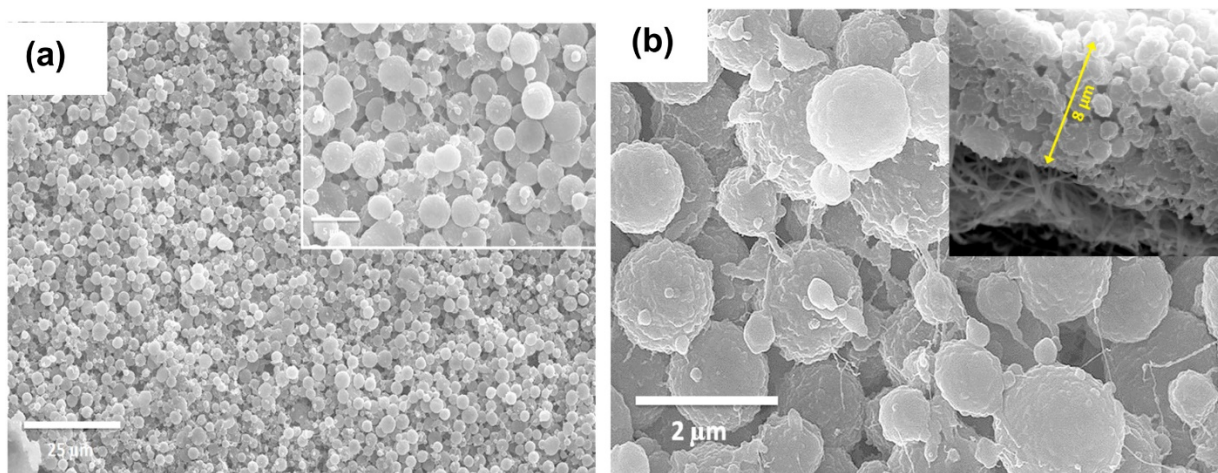
								Fane 2013)
<b>PVDF</b>	Elec	Electrospinning (hydrophobic SiNPs)	superhydrophobic	156 152	0.69±0.02, 0.61	DS	AW	(Li et al. 2015; Liao, Wang & Fane 2014)
<b>PVDF</b>	Elec	Electrospinning (hydrophobic Al <sub>2</sub> O <sub>3</sub> NPs)	superhydrophobic	150 154	0.37 0.39	IW	AF	(Attia et al. 2017; Attia et al. 2018)
<b>PVDF</b>	NIPS	LBL (Si aerogel)/ f	omniphobic	177  163-mineral oil  160-methanol	0.09±0.01	SF	AW	(Woo et al. 2018)
<b>PVDF (hf)</b>	NIPS	Chemical modifying (SiNPs)/ f	omniphobic	142  100-cooking oil  75-ethanol	0.20±0.02	SF	AW	(Lu, Zuo, et al. 2018)
<b>PVDF</b>	Elec	Plasma-modifying (CF <sub>4</sub> )	omniphobic	161 158-MI	0.80±0.02	SF	AF/AW	(Chul Woo et al. 2017)
<b>PVDF-HFP</b>	Elec	f	omniphobic	138  127-soybean oil	0.84	SF	AW	(An, Liu & Hu 2018; Lu, Su, et al. 2018)
<b>PVDF</b>	Elec	Dip-coating (FTCS)/ f	omniphobic	160  130-mineral oil	0.26	SF	AW	(Deng et al. 2018)
<b>PVDF</b>	Elec	Dip-coating (SiNPs)/ f	omniphobic	150  138-mineral oil	0.42	SF	AW	(Lee et al. 2016)
<b>PVDF-HFP</b>	NIPS	Spraying CTS/PFO)/ (SiNPs-heat-treatment	Janus (hydrophilic-and- omniphobic)	15  UW 150-crude oil	n/a	OW	AF/AW	(Huang et al. 2017)

<b>PVA</b>	Elec	f	Janus (superhydrophobic - on-hydrophilic)	158	0.46±0.01	DS	AF	(Don g et al. 2015)
<b>PI</b>	Elec	PDA-depositing (SiNPs)/ f	Janus (omniphobic - on-hydrophilic)	152	2.23	SF	AF/AW	(Zhu, Liu, Hou, et al. 2018)
<b>PVDF</b>	Elec	Electrospraying (SiNPs@PAN)	Janus (hydrophilic- and- superhydrophobic)	0 UW 164- soybean oil	1.45	OW	AF/AW	(Zhu, Liu, Zhong, et al. 2018)

Note: NIPS = non-solvent induced phase separation, Elec = electrospinning, hf = hollow fiber, f = fluorination, DS = desalination, MI = diiodomethane, BT = brine treatment, IW = industrial wastewater, SF = surfactants removal, OW = oil/water separation, AF = anti-fouling, AW = anti-wetting, HP = high permeability

Besides inorganic nanoparticles, polymer particles have also been coated on synthesized membranes to create multi-scale morphology. Yan et al. deposited etched PVDF particles on HF membranes using ultrafiltration coating process to create lotus effect. The coating layer significantly increased its water CA to 164°, without blocking the membrane pores (Yan et al. 2017). Some other researchers obtained superhydrophobic nanofiber membranes by electrospraying polydimethylsiloxane (PDMS) polymeric microspheres onto membrane surfaces (An et al. 2017; Lee et al. 2017). After the PDMS deposition, re-entrant hierarchical structures were created on the membrane surfaces (**Figure 22**), leading to increased water CA and significantly decreased sliding angle. The polymeric particles used in the modification are hydrophobic, so there is no requirement of reducing surface tension, which means the modification procedure is simpler.



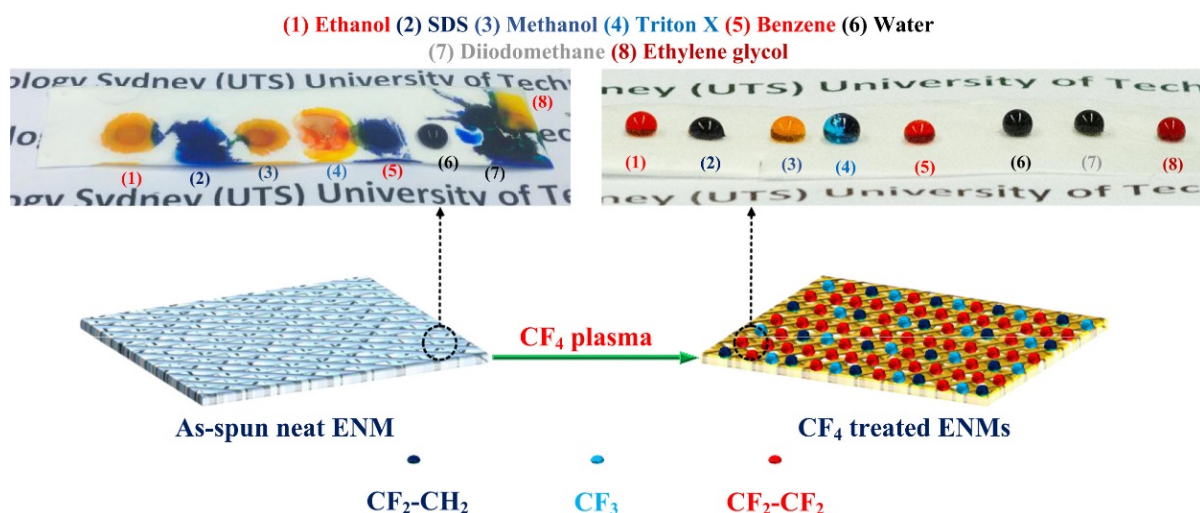


**Figure 22.** SEM of the surface layer of the electrospun nanofiber PVDF membranes that are coated with a layer of PDMS (An et al. 2017)

As nanofiber membranes have advantages of high surface roughness with multi-scale structures, it is possible for these membranes to achieve omniphobicity with single-step surface modification. An et al. obtained omniphobic membranes by fluorinating electrospun PVDF-HFP nanofiber membranes, and the membranes gained the ability to repel soybean oil with a contact angle of  $127^\circ$ . Woo et al. obtained an omniphobic electrospun nanofiber membrane by  $\text{CF}_4$  modifying. **Figure 23** shows that the surface-modified nanofiber membrane can repel low surface tension liquids including ethanol and diiodomethane. Comparatively the same surface modified technique with commercial PVDF membranes failed to perform. The failure is attributed to air trapping on the hierarchical structures of nanofiber membrane surfaces. Also, the  $\text{CF}_4$  plasma modified nanofiber membranes had much higher mean pore size than the commercial membranes (0.80 vs. 0.25  $\mu\text{m}$ ). Aside from fluorination, some other low surface tension chemical had been deposited on the membrane surface to acquire superhydrophobicity. Ray et al. coated synthesized NIPS membranes with octadecyltrimethoxysilane (OTMS), resulting in the acquirement of superhydrophobicity with much improved wetting resistance (Ray et al. 2018).

In contrast, more complicated approaches have been developed to impart omniphobicity on polymeric substrates. Woo et al. developed a layer-by-layer (LBL) assembly technique to create hierarchical structures with reduced surface tension on NIPS membranes. Via electrostatic interaction, layers of PDDA, silica aerogel, PDDA, and FTCS were coated on the membrane surface in sequence (Woo et al. 2018). Although the deposited multiple layers on

the membrane reduced its pore size from 0.20 to 0.09  $\mu\text{m}$ , the LBL membrane achieved a very high water CA of 177° and oil CA of 163°.

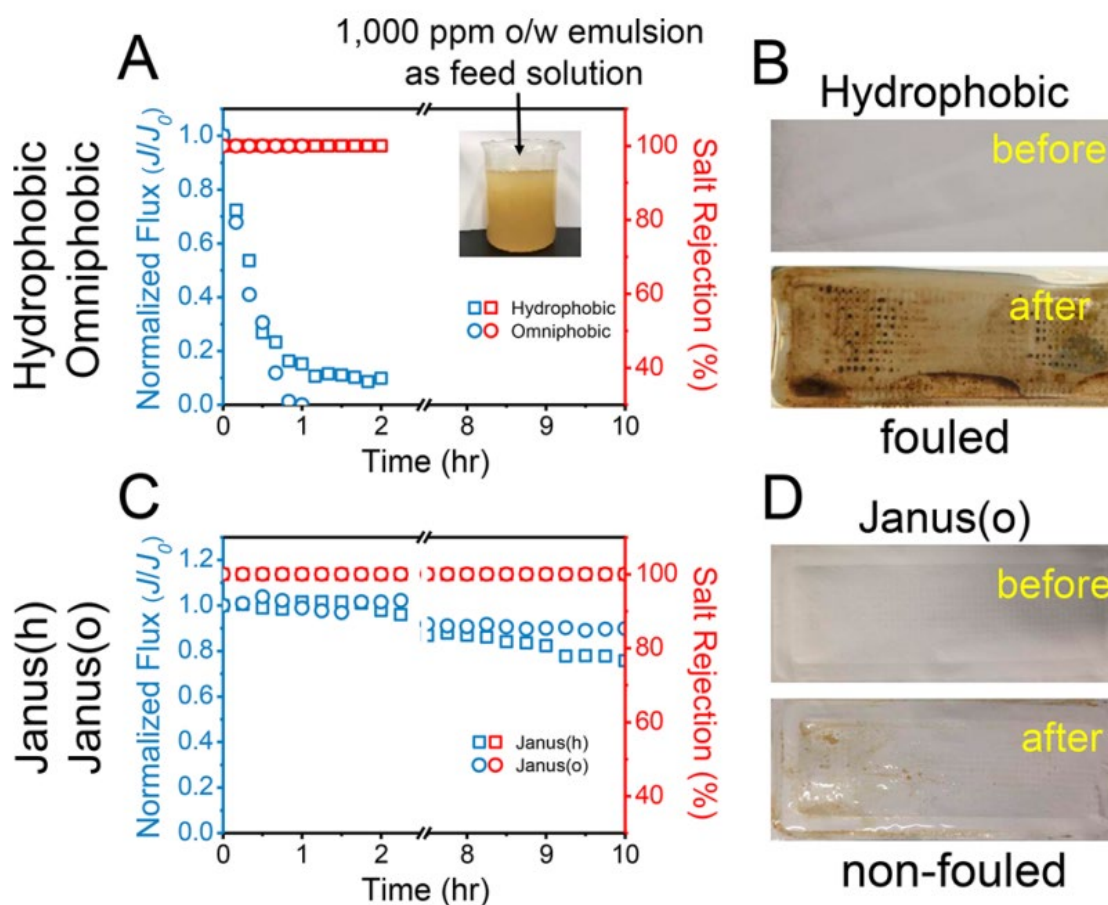


**Figure 23.** Schematic illustrations of pristine and  $\text{CF}_4$  plasma modified electrospun nanofiber membranes regarding contact angles of liquids with various surface tensions (Chul Woo et al. 2017)

In addition to omniphobic membrane, two special types of Janus membrane: hydrophilic-on-superhydrophobic, and hydrophilic-on-omniphobic designs have also been developed based on synthesized membranes to deal with low surface tension foulants in wastewater. The customized substrates offer additional benefits which cannot be achieved by Janus (hydrophilic-on-hydrophobic) membranes based on commercial membranes. Huang et al. developed omniphobic nanofiber substrates by fluorinating silica-coated electrospun membranes; then a hydrophilic layer of silica chitosan with perfluorooctanoate was sprayed on the omniphobic substrates to obtain the Janus membrane (hydrophilic-on-omniphobic) (Huang et al. 2017).

**Figure 24** shows that the omniphobic membrane had strong wetting resistance against oil/water emulsion but was still prone to organic fouling, and the coated hydrophilic layer on the top

could improve its fouling resistance with minimal impact on flux performance.



**Figure 24.** a) Normalized flux and salt rejection membranes in the MD treatment of 1,000 ppm o/w emulsion as feed solution using a) hydrophobic and omniphobic and c) Janus (hydrophilic-on-hydrophobic) and Janus (hydrophilic-on-omniphobic) membranes; before and after MD test for b) hydrophobic membranes and d) Janus (hydrophilic-on-omniphobic) membranes (Huang et al. 2017)

#### 2.4.3.2 Application

The superhydrophobic synthesized membranes offers a wide application for the field for desalination, treatment of brine water and industrial wastewater. The membrane exhibits stable permeation flux and high salt rejection for 180 h in treating highly concentrated brine water (25 wt.%). It had significant anti-scaling properties as the post-tested membranes hardly showed any sign of foulants on the SEM images of the relative samples (Zhang, Song, et al. 2013). Superhydrophobic synthesized membranes can also be used to treat industrial wastewater. The PDMS coated membranes showed high flux recovery with water flushing in

the treatment of single dye (crystal violet) in the configuration of DCMD with much mitigated fouling issues. Also, their permeability was higher than commercial membranes due to the large mean pore size and porosity of the synthesized electrospun substrates (An et al. 2017). Industrial wastewater containing heavy metals (Pb, Cd, Zn, etc.) with concentrations up to 600 ppm can also be treated (Attia et al. 2017; Attia et al. 2018).

On the other hand, omniphobic and Janus (hydrophilic-on-hydrophobic) synthesized membranes can be used to treat wastewater water containing low surface tension chemicals such as surfactants and oil emulsion. Usually, these membranes have higher permeability than surface-modified commercial membranes due to their large mean pore size and porosity (Chul Woo et al. 2017; Zhong et al. 2017). The omniphobic synthesized membranes achieved a high flux around 20 LMH with a feed solution temperature of 65 °C when treating synthetic wastewater containing 0.1 mM SDS (An, Liu & Hu 2018). By sacrificing the permeation performance, even higher fouling and wetting resistance against low surface tensions feeds can be achieved. The hierarchical composite membranes had much improved wetting resistance as it can treat feed water containing SDS of concentration up to 0.5 mM without performance deterioration; also, these membranes could treat RO brine from coal seam gas produced water stably for 72 h.

#### 2.4.3.3 Challenges

Development of synthesized membranes with special wettability is still a major challenge. Like the surface modified commercial membranes, the coating layers involving nanoparticles suffer loose attachment issue.

Electrospun nanofiber membranes are highly favored as synthesized substrates as they offer high roughness, large mean pore size and porosity, and they are convenient for customization. However, the mechanical strength of nanofiber substrate-based membranes needs improvement for larger scale application; Moreover, there is still a lot of challenges in the upscaling of electrospinning due to device limitation.

LBL membranes are robust with high wetting and fouling resistance. However, they have relatively low permeation performance due to small pore sizes, making it limited to niche applications. Therefore, further optimization should be investigated to develop LBL membranes with large mean pore size without compromising the omniphobic property.

#### 2.4.4 Surface-modified ceramic membranes

Ceramic membranes have also been extensively developed for use in MD. **Table 5** presents various studies using modified ceramic membranes with special wettability. In terms of characteristics, ceramic membranes generally exhibit high chemical, thermal, and mechanical stability. These characteristics make them especially suitable for applications in harsh environment such as corrosive and high temperature conditions.

##### 2.4.4.1 Modification method

Typically, inorganic materials such as glass, silica, alumina, titanium oxide, etc. are used to make ceramic membranes for MD. Surface modification must be applied onto the ceramic membranes to prevent membrane wetting as they are naturally hydrophilic. A superhydrophobic or omniphobic layer can be coated on these membranes, to form either (superhydrophobic-on-hydrophilic) or (omniphobic-on-hydrophilic) Janus membranes, respectively. Fluorination is the most common approach adopted to attain superhydrophobicity on ceramic membranes. In its natural condition, the surface of inorganic ceramic membrane contains hierarchical structures. As such, superhydrophobicity (high water CA of  $160^\circ$ ) can be easily achieved in ceramic membrane with fluorination alone. Hubadillah mimicked the lotus effect by simply fluorinating silica membrane with FAS; the surface modified membrane had high water CA of  $161^\circ$ , and a significantly reduced pore size from 1.43 to 0.54  $\mu\text{m}$ , exhibiting high arsenic rejection of 99.6% in DCMD (Hubadillah et al. 2019). Also, other hydrophobic compounds can be deposited on the surface of ceramic membranes to achieve Janus (superhydrophobic-on-hydrophilic). Dong et al. developed Janus (superhydrophobic-on-hydrophilic) ceramic membranes by depositing carbon nanotubes (CNT) on nickel aluminate substrates via chemical vapor decomposition (CVD) (Dong et al. 2018). The superhydrophobic membranes illustrated improved fouling resistance. **Figure 25** shows that the organic fouling resistance could be further improved by changing the surface charge of the CNT-coated superhydrophobic membranes: the membranes working as cathode led to stable permeation for the treatment of brine solution containing 30  $\text{mg L}^{-1}$  humic acid.

**Table 5.** Published reports in the literature about surface-modified inorganic membrane with special wettability for MD

Substrate	Modification methods	Special wettability	Contact angle (°)	Mean pore size (μm)	Applications	Benefits	Ref.
Glass	Glass fiber drawing/ f	Janus (superhydrophobic-on-hydrophilic)	165	3.4	DS	AF/HP	(Ma et al. 2009)
Glass	Chemical modifying (SiNPs)/ f	Janus (omniphobic-on-hydrophilic)	140 108-mineral oil 80-ethanol	0.7	SF	AW	(Lin et al. 2014)
Glass	CBD depositing (ZnO NPs)/ f	Janus (omniphobic-on-hydrophilic)	153 110-ethanol	0.4	SF	AW	(Chen et al. 2018)
TiO <sub>2</sub>	f	Janus (superhydrophobic-on-hydrophilic)	147	0.2	IW	AF/AW	(Kujawa et al. 2017)
Alumina	Sol-gelling (fluorinated Al <sub>2</sub> O <sub>3</sub> NPs)	Janus (superhydrophobic-on-hydrophilic)	158	0.4	DS	HP	(Huang et al. 2018)
Nickel aluminate	CVD (CNT)	Janus (superhydrophobic-on-hydrophilic)	170	0.15	BT	AF/AW	(Dong et al. 2018)
Silica	f	Janus (superhydrophobic-on-hydrophilic)	161	0.54	IW	AW	(Hubadillah et al. 2019)
Anodized alumina	f	Janus (superhydrophobic-on-hydrophilic)	162	0.08	DS	HP	(Subramanian et al. 2019)
Alumina	Dip-coating (C <sub>6</sub> Cl <sub>3</sub> )	Janus (superhydrophobic-on-hydrophilic)	154	0.81	DS	AW	(Kujawa 2019)

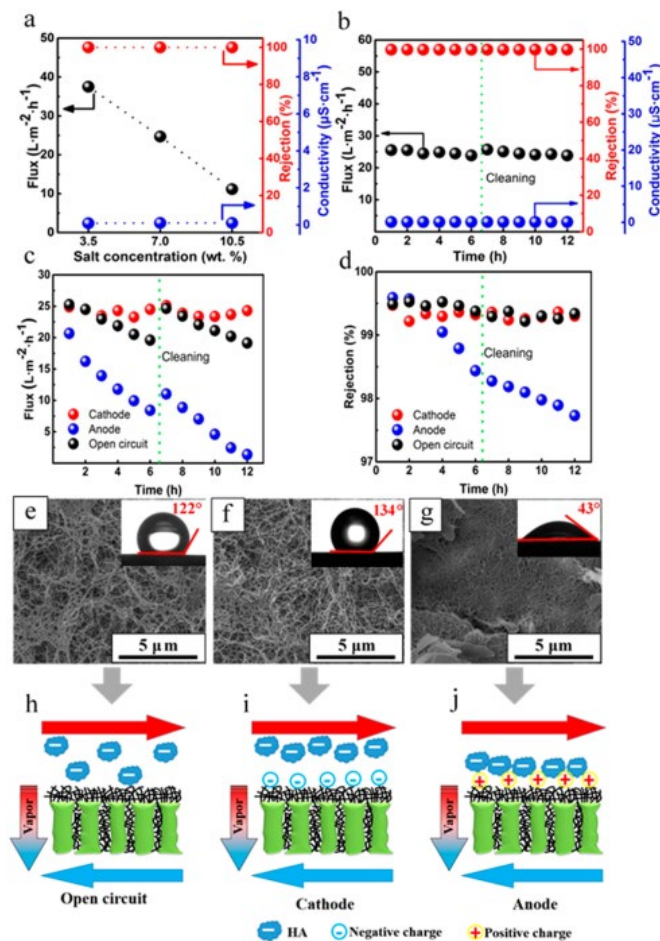
Note: hf = hollow fiber, f = fluorination, DS = desalination, BT = brine treatment, IW = industrial wastewater, AF = anti-fouling, AW = anti-wetting, HP = high permeability

To achieve even higher wetting resistance, the achievement of Cassie-Baxter wetting state is required. Therefore, re-entrant structures should be created on the membrane surfaces before being fluorinated. Directly changing the morphology of ceramic substrate is also an option that can be explored. For instance, Ma et al. developed superhydrophobic glass membranes with ordered arrays of nanospiked microchannel using a process involving multiple chemical and physical techniques, and the surface-modified membrane has high water CA of 165° (Ma et al.



2009). Alternatively, NPs can be deposited onto ceramic membranes, which is a common technique used on polymeric membranes as discussed in previous sections. ZnO NPs was successfully deposited on glass membranes using chemical bath method to create hierarchical re-entrant structures, then FAS17 was applied on the NP-coated membrane to achieve omniphobic surface (Chen et al. 2018). When treating saline water containing 0.3 mM SDS using this omniphobic membrane, a stable water flux was maintained for 8 h, while superhydrophobic glass membranes failed at the same operation conditions. Both approaches for improving surface roughness are complex, involving multiple chemical or physical techniques. Considering that the attachment of the deposited layer on ceramic substrates are less stable, the first approach is more attractive for the creation of re-entrant structures.

Ceramic membrane with special wettability can be very promising for MD due to their appropriate pore sizes. Also, they demonstrate strong robustness in harsh working environment.



**Figure 25.** The DCMD performance of carbon nanotube coated membranes as a function of a) salt concentration and b) time; the flux of DCMD treating feed water containing humic acid

and sodium chloride when the membrane work as open-circuit, cathode, or anode regarding c) flux and d) salt rejection; e-g) the surface morphology and water contact angle of the coated membranes used as various electrodes after 12 h DCMD operation; h-j) schematic figures of electrostatic interaction between organic foulants and the surface modified membranes at various modes (Dong et al. 2018)

#### 2.4.4.2 Application

Janus ceramic membranes (superhydrophobic-on-hydrophilic) are versatile which can be used for desalination, brine treatment and industrial wastewater treatment. When used for desalination, high water flux around 30 LMH and salt rejection rate of 99.9% can be achieved due to the large pore size of the membranes (0.4  $\mu\text{m}$ ) (Huang et al. 2018). A Janus membrane based on Nickel aluminate can treat highly saline wastewater with NaCl concentration up to 105  $\text{g}\cdot\text{L}^{-1}$ . The membrane exhibited high flux performance of 24 LMH and salt rejection of 99.6% in 12 h DCMD operation (Dong et al. 2018). Another application is the removal of volatile organic compounds (butanol, methyl-tert-butyl ether, and ethyl acetate) from binary aqueous solutions. A silica based Janus membrane (superhydrophobic-on-hydrophilic) showed much improved removal efficiency (Kujawa et al. 2017).

Janus ceramic membranes (omniphobic-on-hydrophilic) can be used to treat produced water having low surface tension. Wastewater containing 1 M NaCl and 0.3mM SDS can be treated in DCMD with stable permeation and salt rejection using omniphobic glass fiber membranes based on ZnO nanoparticles modification (Chen et al. 2018).

#### 2.4.4.3 Challenges

Several challenges must be addressed before surface-modified ceramic membranes can achieve full commercialization. Currently, the technique used to fabricate ceramic membranes are energy-intensive. Moreover, they must be surface modified before being used in MD due to the hydrophilic nature of ceramic membranes.

Processes that render ceramics hydrophobic requires specialized resources and skills as chemicals used for surface modification may block membrane pores if not properly applied. Therefore, the fabrication and modification approaches should be optimized to develop ceramic membranes for MD. Simpler chemical or physical approaches should be explored to reduce the cost of fabrication processes.



## **2.5 Concluding remarks and future perspectives**

The success of MD system relies on the development of approximate membranes having high wetting –resistance in long-term operation. Specifically, wastewater containing surfactant and low surface tension chemical contaminants poses more serious challenges. Therefore, MD membranes with special wettability have been developed to take on them.

## **CHAPTER 3**

### **Materials and Methods**

### 3.1 Introduction

The experimental work covers both MD processes and membrane fabrication. General materials and methods used in the experiment are illustrated in this chapter while detailed specific methods are illustrated in each individual chapter relevantly.

### 3.2 Experimental materials

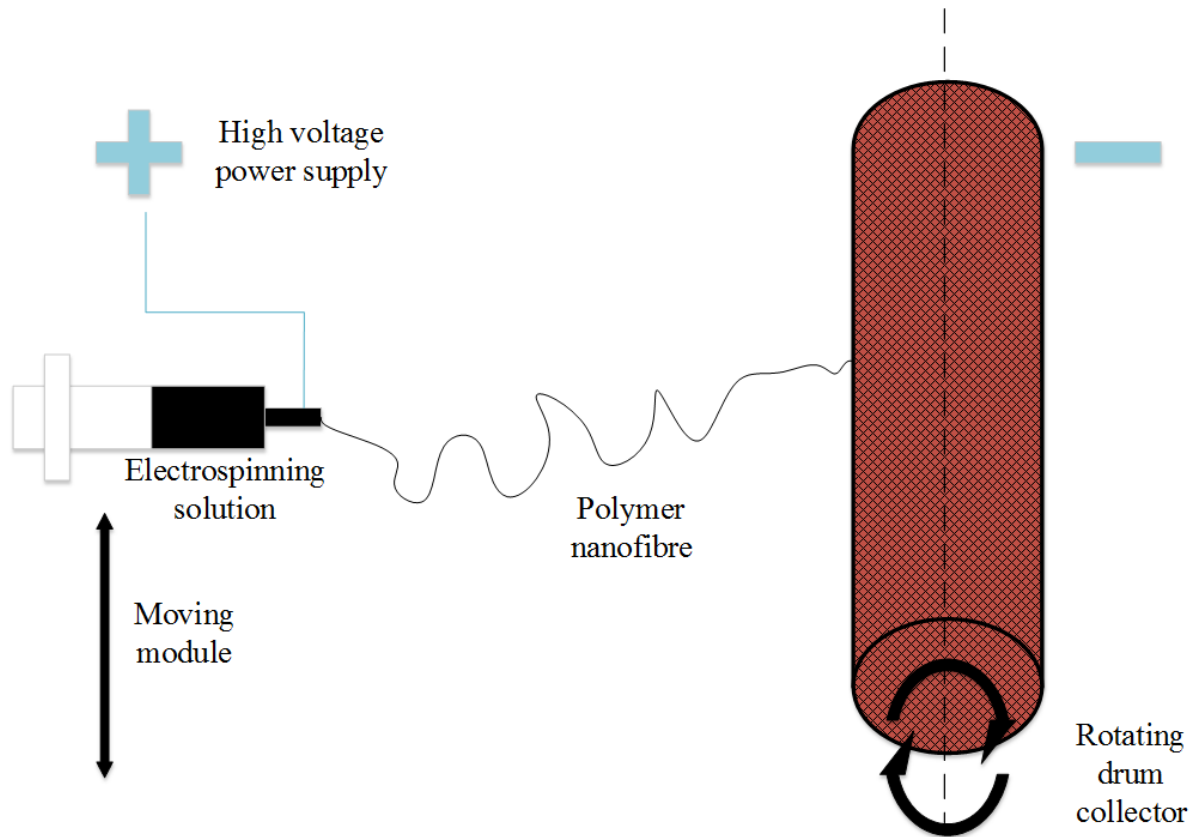
The polymer used for the fabrication of nanofiber membranes was polyvinylidene fluoride-co-hexafluoropropylene (referred herein as PH, MW = 455,000), and it was purchased from Sigma-Aldrich, USA. For membrane fabrication using NIPS, high molecular weight PVDF polymer pellets (Kynar® HSV900) were kindly provided by Arkema Inc. Triethyl phosphate (TEP, 99%), N-methyl-2-pyrrolidone (NMP, 99.5%), ethanol (100%), acetone (99.5%) and dibutyl phthalate (DBP, >97%) were all purchased from Chem-Supply. N, N dimethylacetamide (DMAc, 99.5%) and toluene (>99.5%) were used as solvent and co-solvent, respectively; both were purchased from Sigma-Aldrich. All the chemicals were used as received without further purification.

For the comparison of flat sheet membranes, commercial microfiltration membrane (pore size = 0.22  $\mu\text{m}$ , porosity = 70%, GVHP) bought from Millipore was used; for HF membranes, Polyvinylidene fluoride (PVDF) membrane was manufactured and provided by Econity, Republic of Korea. The HF membranes had inside and outside diameters of 0.77 mm and 1.3 mm, respectively. Mean pore size, liquid entry pressure, and porosity of the membranes were 0.1  $\mu\text{m}$ , 2.3 bar, and 63%, respectively. Both membranes were used as received without any modification and treatment.

### 3.3 Electrospinning device

**Figure 26** illustrates the configuration of the electrospinning device used in this study. The polymer solution was pulled out of the syringe by the syringe pump and formed whipping fibers within a high voltage electrical field (applied voltage = 21 kV). Then fibers were collected onto the rolling drum after most contained solvent evaporated during the whipping process. During electrospinning process, the nozzle was continuously moving inwards and outwards parallel to the axis of the rotation of the drum. The setting operation conditions for electrospinning were constant throughout the study in all the experimental stage: The distance between the nozzle

tip and collector was set at 20 cm. The syringe pump had a pushing rate of 1 ml/h and had been running continuously.



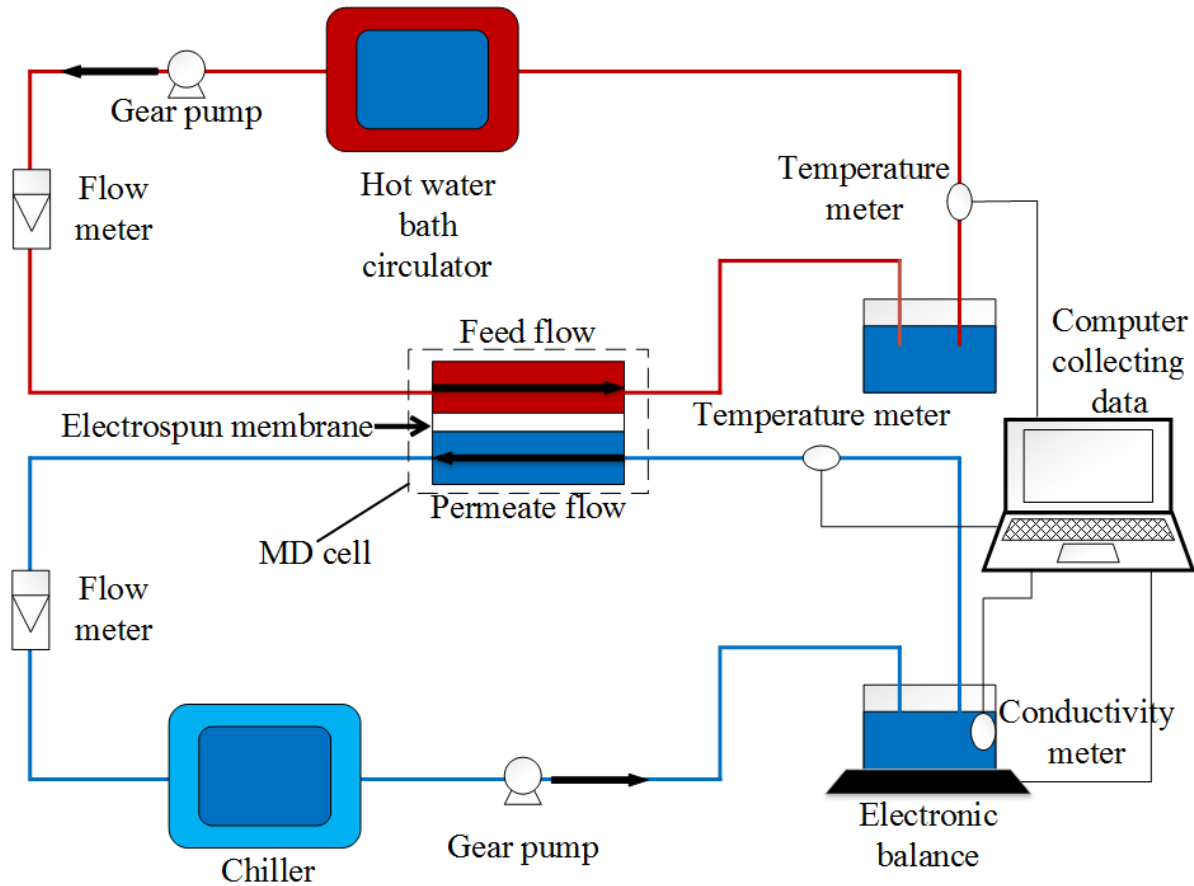
**Figure 26.** Schematic diagram of electrospinning configuration used in the experiments

### 3.4 Membrane distillation setup

#### 3.4.1 Direct contact membrane distillation (DCMD)

Membranes were tested in DCMD setup shown in **Figure 27**, the membrane samples were fixed in the DCMD cell module. The length and width of both feed and permeate channels were 77 mm and 26 mm respectively, making up an effective membrane area of 20 cm<sup>2</sup>. The module was placed horizontally and ran in counter-current mode with feed flow on top side. Sodium chloride (NaCl) at a concentration of 3.5 wt.% in water was used in the feed side, and its temperature was being maintained at 60 °C by a heating bath. Deionized (DI) water was used in the permeate side, and its temperature was being kept at 20 °C by a chiller. The mass flow rates in both permeate and feed sides were being maintained at 400 ml/min via a gear pump. The running conditions and parameters of DCMD were being kept unchanged in the whole experiment, and each condition of heat-press was tested three times with a new sample

for ensuring experimental reproducibility. A desktop computer was setup to collect the data of temperatures in both feed and permeate sides automatically via thermocouples connected to the flow lines. The flux was calculated by dividing the change of mass in the permeate container by the duration of change while the reading of mass was collected automatically once every minute on the linked electronic balance (Eq. (6)), and salt rejection was calculated using Eq. (7).



**Figure 27.** Schematic diagram of DCMD process

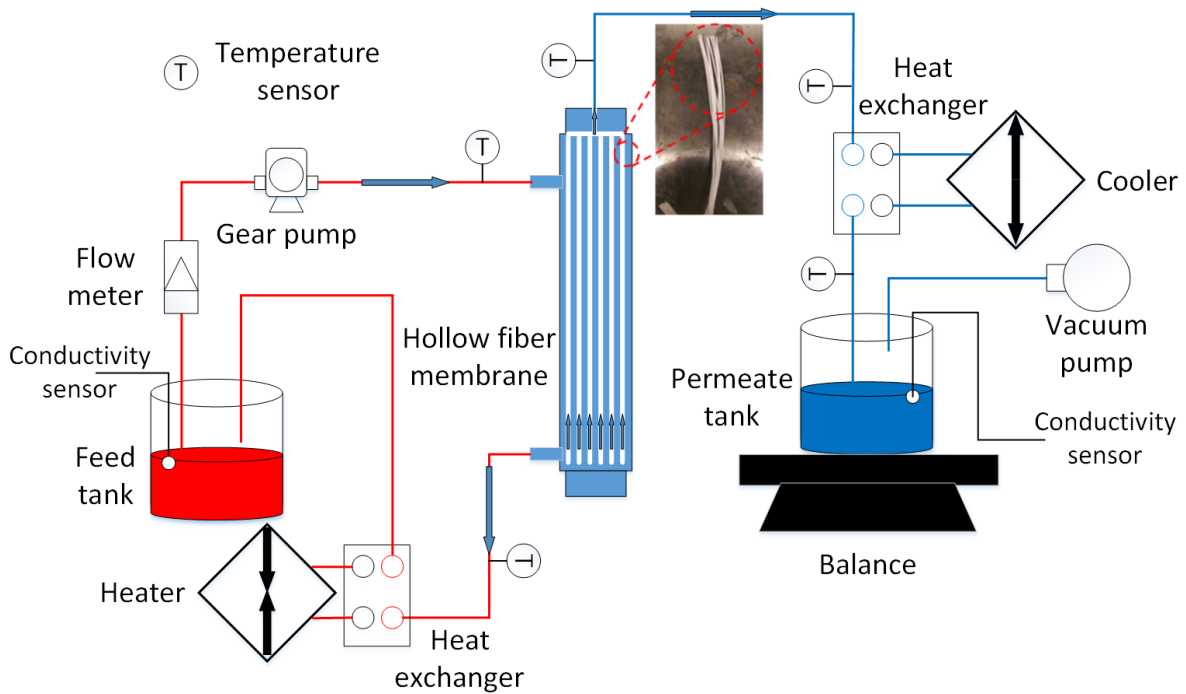
$$J = \frac{\Delta g}{A \times \Delta t} \quad (6)$$

$$\text{Salt rejection} = \left(1 - \frac{c_p}{c_f}\right) \times 100\% \quad (7)$$

where  $J$ ,  $\Delta g$ ,  $A$ ,  $t$ ,  $SR$ ,  $C_f$ , and  $C_p$  represent the water permeate flux ( $\text{L/m}^2\text{h}$  or  $\text{LMH}$ ), mass of permeate water ( $\text{L}$ ), effective total membrane area ( $\text{m}^2$ ), operation time ( $\text{s}$ ), salt rejection (%), feed concentration ( $\text{mg/L}$ ), and permeate concentration ( $\text{mg/L}$ ), respectively.

### 3.4.2 Vacuum membrane distillation

Vacuum MD (VMD) was used in the study due to its higher thermal efficiency [19]. Polyvinylidene fluoride (PVDF) HF membrane was manufactured and provided by Econity, Republic of Korea. Mean pore size, liquid entry pressure, and porosity of the membranes were 0.1  $\mu\text{m}$ , 2.3 bar, and 63%, respectively. The HF membranes were used as received without any modification and treatment. Thirteen such HF membranes with length of 0.2 m were used to make membrane modules for a total surface area of 0.0106  $\text{m}^2$ , which was placed in the VMD set-up illustrated in **Figure 28**. The membrane modules had an internal diameter of 8 mm.



**Figure 28.** Schematic diagram of vacuum membrane distillation in this study

### **3.5 Analytic methods used in experiments**

#### **3.5.1 Scanning Electron Microscope (SEM) and energy dispersive X-ray spectroscopy (EDX)**

The morphologies of all membrane samples were examined by a scanning electron microscope (SEM, Supra 55vp from Carl Zeiss AG), while the energy-dispersive X-ray spectroscopy was used to determine the existing elements on the membrane foulants. ImageJ software (National Institutes of Health, USA) was used to analyze the SEM images to work out the average fiber diameter, surface pore size and their distributions, and three SEM images from different spots of the membrane samples were used for each fiber and pore size analysis.

#### **3.5.2 Membrane thickness**

Membrane thickness was measured with digital micrometre (IP65, Mitutoyo) and the average value of ten randomly picked spots was calculated for each sample.

#### **3.5.3 Contact angle**

Contact angles (CA), a major indicator of hydrophobicity, were measured by Theta Lite 100 (Attension) following sessile drop method. A water droplet around 5–8 ml was released from a needle tip onto the membrane surface. A motion camera was mounted to capture the images at a rate of 12 frames per second. Through the recorded videos, contact angles were analysed with the aid of specific software. To ensure experimental reproducibility, each set of samples were measured in triplicate and the average value of them was taken.

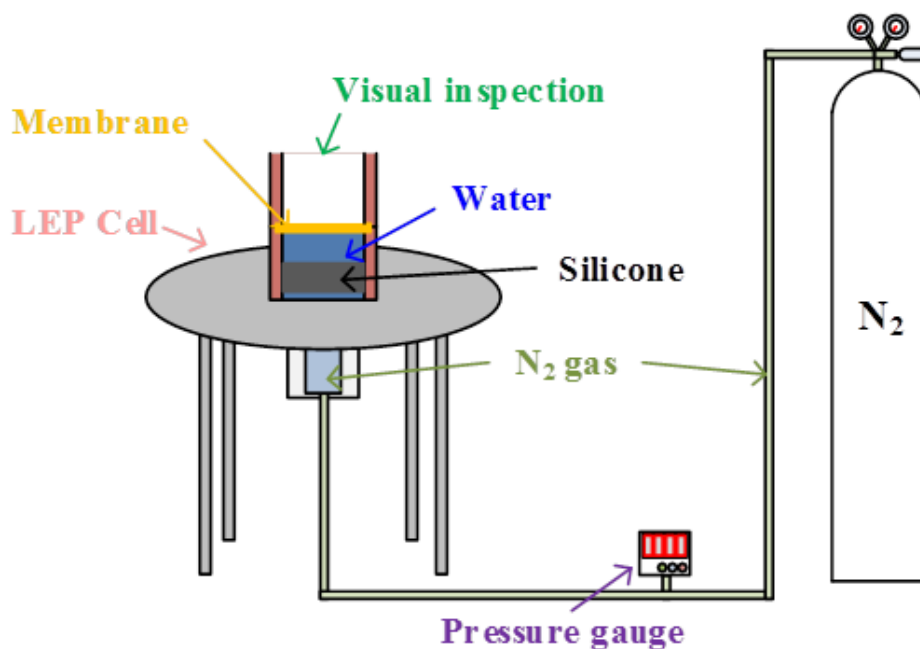
#### **3.5.4 Mechanical strength**

Mechanical properties including maximum stress, strain, and Young's modulus were measured with bench-type tensile tester (Lloyds). Average values of three runs were taken for each sample.

#### **3.5.5 Liquid entry pressure (LEP)**

LEP test was carried on the as-spun and heat-press membrane samples with a lab-assembled apparatus **Figure 29**. A digital gauge was connected to a hollow stainless plate with a pipe, and

nitrogen gas was released from the other end of pipe. On the stainless plate, there was a stainless cylinder container that was filled up with deionized (DI) water. The set-up had an effective surface area of 7 cm<sup>2</sup>. The samples were fixed on the top of cylinder by a stainless cap and a lock catch was used to secure the set-up. Pressure displayed on the gauge was recorded when the first water droplet came out through the membrane during the process of steadily releasing out nitrogen gas. Each sample was tested in triplicate and average data was recorded.



**Figure 29.** Schematic setup of the LEP apparatus (Woo, Kim, et al. 2016)

### 3.5.6 Pore size

The pore size and pore size distribution of membranes were measured by capillary flow porometry (CFP-1200-AEXL). All samples were firstly wetted by Galwick (a wetting liquid with a low surface tension of 15.9 dynes/cm) and tested under the pre-set conditions. Then the dried samples were applied with N<sub>2</sub> gas to determine the gas permeability under same conditions. The final average pore size and its distribution were automatically calculated with both data sets of wet and dry tests by the specific software.



### 3.5.7 Porosity

Membrane porosity was defined as the volume of the pores divided by the total volume of the membranes. It was determined by a gravimetric method in this study. After the membranes were immersed in ethanol (Univar 1170 from Ajax Finechem Pty. Ltd.) for adequate time to ensure that the pores fully filled up, the weight ( $w_1$ , g) of membrane with ethanol was measured after the residual liquid on the surface was removed. Then the membrane samples were left still in the open air for some time and got weighed ( $w_2$ , g) when all the ethanol within them had fully evaporated (i.e., dry condition). The porosity then could be worked out with the following equation:

$$\varepsilon_m = \frac{(w_1 - w_2)/\rho_e}{w_1 - w_2/\rho_e + w_2/\rho_{ph}} \quad (8)$$

, where  $\rho_e$  was the density of the ethanol ( $\text{g/m}^3$ ) and  $\rho_{ph}$  was the density of the PH ( $\text{g/m}^3$ ).

### 3.5.8 Fourier-transform infrared (FT-IR)

Fourier-transform infrared (FT-IR) spectroscopy (Varian 2000, Agilent, Santa Clara, CA, USA) was used to investigate the PVDF-HFP phases of the virgin membrane and thermally treated membranes. Each spectrum was acquired with signal averaging 32 scans at a resolution of  $8 \text{ cm}^{-1}$ , in transfer mode by pressing the sample with KBr to a pellet. It was also used to determine what specific types of organic compounds forming the membrane foulant layers by comparing the spectrum peaks.

### 3.5.9 X-ray diffraction (XRD)

X-ray diffraction (XRD) (Siemens D5000, Siemens, Karlsruhe, Germany) was carried out over Bragg angles ranging from  $10^\circ$  to  $30^\circ$  ( $\text{Cu K}\alpha$ ,  $\lambda = 1.54059 \text{ \AA}$ ). It was mainly used to determine the amorphous and crystal phases of the PVDF-HFP membranes before and after thermal treatment.

### 3.5.10 Total organic carbon (TOC)

Total organic carbon (TOC) was measured using a high-performance TOC analyzer (multi N/C3100®) which was purchased from Analytikjena, Germany. It was used to determine the organic carbon concentration in the solutions.

## **CHAPTER 4**

### **Wastewater Reclamation Utilizing Membrane**

### **Distillation with Resource Recovery**

## 4.1 Introduction

The on-site treatment of domestic wastewater is consistently gaining interests because it requires less energy consumption without the need of wastewater transportation to the central treatment plants (Leong et al. 2017; Teh et al. 2015). In addition, the potential use of the reclaimed water for non-potable purposes reduces the stress in local water supply, and hence the cost of freshwater production and transportation (Oviedo-Ocana et al. 2017). The decentralized wastewater treatment system also has strong potentials for use in remote areas in the developing countries (Massoud, Tarhini & Nasr 2009).

Biological treatment is the preferred technology to remove the high strength organic compounds in the wastewater for its high efficiency and low operation costs. However, conventional wastewater treatment technologies used in the centralized treatment plant are not feasible to be implemented in the treatment facilities owing to its large footprint and long retention time. Therefore, a novel technology should be specifically designed with high-performance (stable long-term operation and cost-efficient) and small footprint. The rapid development of membrane technology led to the maturity of membrane bioreactor (MBR), which is widely used for municipal and industrial wastewater treatment. The feasibility of applying a smaller size MBR system to treat local waste has been investigated. In one study, high total organic compounds (TOC) removal ratio ranging from 80 to 95% over 180 days was found in the MBR system designed for a hotel (Atanasova et al. 2017). In another study implementing an MBR for a single house, COD and anionic surfactant removal of 87% and 80% were achieved, respectively (Fountoulakis et al. 2016). In terms of economic feasibility in a multi-storied residential building, MBR-based system was proven feasible when the building size exceeded sufficient floors, and it would become more practical when cluster MBR-based system is introduced to building compounds (Friedler & Hadari 2006).

Although MBR has large capability to recycle the wastewater locally, the process still requires high energy consumption, especially for the aeration process to supply oxygen to the aerobic microorganisms as well as for mitigation of membrane fouling (Hernandez Rojas et al. 2005). In addition, owing to its rapid membrane fouling issues, MBR systems incurred more maintenance costs for the chemical cleaning, membrane replacement, and relative labor costs. Also, the effluent of the MBR in most cases still need further treatment even for non-potable usage (Melin et al. 2006).

Membrane distillation (MD) is an emerging membrane technology known for its high permeation performance and relatively low energy consumption; its energy efficiency can be improved when low grade heat sources such as solar and waste heat are available (Tijing et al. 2015c; Wijekoon et al. 2014). Thermophilic bioreactor presents high compatibility with MD system as the input heat into the reactor promotes both the bacterial production activity and MD separation process. A theoretically 100% non-volatile rejection can be achieved by the thermophilic MD-BR system, which can potentially lead to much less requirement of post-treatment of the effluent (Gryta et al. 2013). The other advantage of MD-BR is that the permeation process is not induced by external pressure, so theoretically it suffers less membrane breakage and fouling issues. Overall, the hybrid MD-BR system can potentially perform better than MBR-only system for wastewater treatment with less energy consumption. MD-BR is a high-solids retention MBR technology similar to osmotic membrane bioreactor (OMBR), another popular novel MBR system (Luo et al. 2017). In terms of system design, MD-BR has advantage over OMBR as there is no need of re-concentration of the diluted draw solution, which requires additional energy consumption and physical footprint. Furthermore, unlike OMBR, MD-BR is much less prone to the increase in the salinity in the reactor, which can exacerbate the permeation performance of OMBR processes (Song et al. 2018; Zhang, Gray & Li 2013).

To date, there are a few studies that were carried out for preliminary experiments on aerobic MD-BR in lab-scale system. It was found that a single-step MD-BR system could produce high quality permeate water comparable to the one from MBR-RO system with stable flux (Phattaranawik et al. 2008; Phattaranawik et al. 2009). The MD-BR also removed most of the trace organic compounds in the wastewater (Wijekoon et al. 2014). However, membrane wetting and fouling occurred during long-term operations, and the accumulation of salinity could potentially negatively affect the microorganism activities (Goh et al. 2013b; Wijekoon et al. 2014).

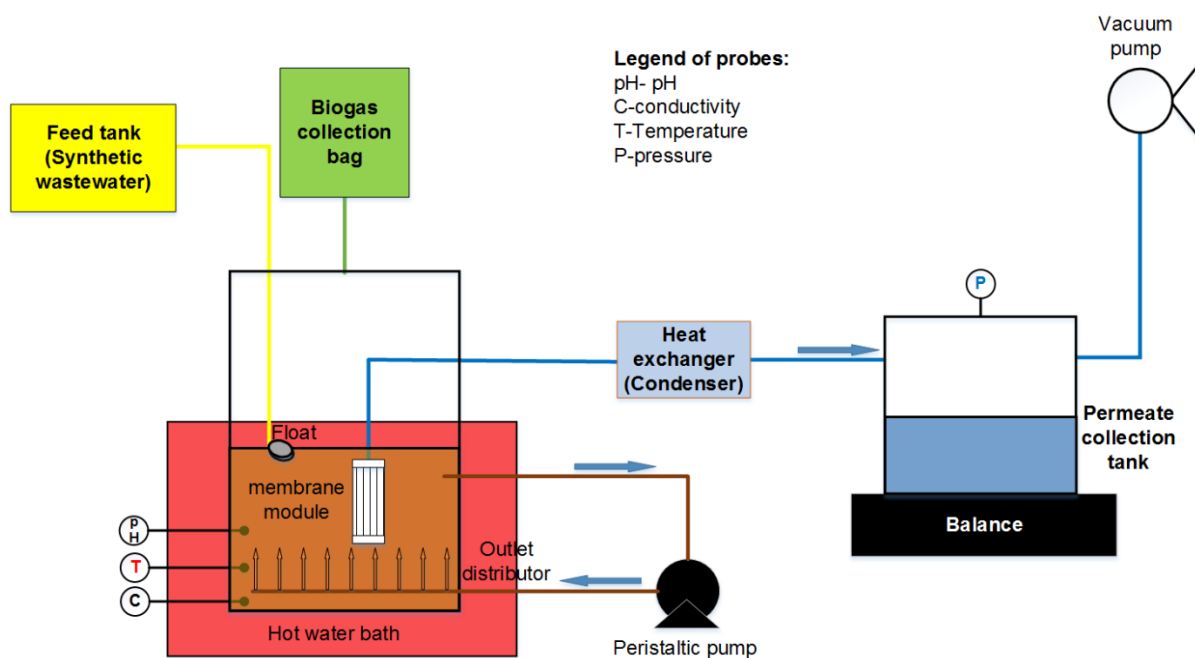
Compared with aerobic bioreactors, anaerobic bioreactors has higher capacities to treat the wastewater and they can recover biogas in addition (Goh et al. 2015; Jeison & van Lier 2008; Xia et al. 2016). To our best knowledge, no other study has been carried out on the design and investigation of an anaerobic MD-BR (referred herein onwards as anMDBR). Therefore, in this study, a lab-scale anMDBR was specifically designed for the treatment of local domestic wastewater utilizing sub-merged HF membranes; it was a set-up with minimal footprint and

highest packing density, Moreover, renewable energy source such as biogas could possibly be collected from thermophilic anaerobic bioreactors, contributing to less greenhouse gas emission (Wijekoon, Visvanathan & Abeynayaka 2011). The thermophilic anMDBR system has very high flexibilities and can work in scenarios ranging from small village in developing countries to large multi-storied residential towers in the developed countries. The potential greenhouse emission reduction by renewable-energy-producing anMDBR will benefit the society. As a preliminary investigation on the thermophilic anMDBR system, the objectives of this study were to investigate the effects of temperature and feed salinity on the membrane permeation performance (i.e., flux and permeate quality) of the anMDBR system in the treatment of domestic wastewater, and to evaluate its potentials in recovery of biogas and volatile fatty acids (VFA).

## **4.2 Experimental method**

### **4.2.1 Set-up**

A customized lab-scale anaerobic bioreactor (2 L) set-up was used in this study (**Figure 30**). The bioreactor was maintained at target temperatures (45, 55, and 65 °C in this study) using hot water baths (JSWB-30T, JSR, Republic of Korea) set at desired temperatures. Vacuum MD (VMD) was selected as the MD configuration in the thermophilic anMDBR system for the sake of its relatively higher thermal efficiency than other MD configurations (Tijing et al. 2015a). A vacuum pressure of 50 mbar was maintained during VMD operation directed at the membrane lumen side to draw the water vapor out of the membrane module, and the vapor was then condensed by a heater-exchanger and the condensate was collected. The recirculation rate was fixed at 15 mL/min. A float valve system was adopted in the bioreactor design to maintain the water level in the bioreactor, so the synthetic feed water could be supplemented into the reactor from the feed tank accordingly. It was designed in this way as anMDBR had a variable flux performance depending on the bioreactor temperatures and fouling rates. Biogas was collected from the fully sealed bioreactor using Tedlar® PLV gas sampling bag purchased from Sigma-Aldrich.



**Figure 30.** Schematic diagram of the anaerobic membrane distillation bioreactor used in the present study.

#### 4.2.2 MD and anMDBR

The thermophilic anaerobic biomass obtained from Central Park residential complex, Sydney were acclimatized at various target temperatures (45, 55, and 65°C) in the batch mode for four weeks before the start of the experiments. The MD and anMDBR shared identical system design (**Figure 1**), running parameters, and feed solutions, except the 10% (v/v) of incubated biomass added into the anMDBR bioreactor. The anMDBR system could be regarded as unsteady state as they were not fully stabilized. Organic loading meant the new synthetic wastewater was supplied to the bioreactor while the permeate left the bioreactor through MD process. Generally, the organic loading rate was decreasing due to the decrease in the flux caused by membrane fouling. Nevertheless, we designed the experiments in this way so that we can control the initial environment of the bioreactor to better understand the effects of temperature and salinity on the permeation performance, especially in terms of their roles in membrane fouling. We extracted 40 mL of samples from the MD and anMDBR system daily to analyze total organic carbon (TOC), conductivity and VFAs. The hydraulic retention time (HRT) varies with flux ranging from 48-120 hours. Synthetic wastewater with COD: N: P ratio of 250:5:1 was feed into the bioreactor. The recipe includes 1,500 mg/L of glucose, 20 mg/L of ammonium sulphate, 10 mg/L of potassium phosphate, and 50 mg/L of Urea, leading to

1,632 COD mg/L of the synthetic wastewater (Hussain, Kumar & Mehrotra 2015). Also, trace nutrients of calcium chloride, magnesium sulphate, manganese chloride, zinc sulphate, ferric chloride, cupric sulphate, and cobalt chloride of 0.368, 5, 0.275, 0.44, 1, 0.391, and 0.42 mg/L, respectively, were added into the synthetic wastewater to promote the growth of the biomass. Oxygen was depleted from the synthetic wastewater in the bioreactors by the injection of nitrogen gas. Milli-Q water was used to prepare the solutions to avoid potential foulants of calcium carbonate from the tap water, and the dissolved oxygen in the synthetic wastewater was purged using nitrogen gas before being feed into the bioreactors.

#### **4.2.3 Analytical methods**

MP-AES 4100 (Agilent, USA) was applied to measure the cations in the MD permeate. Biogas 5000 (Geotech, USA), a portable gas analyzer was used to analyze the components of the collected biogas from the bioreactors. Gas chromatography-mass spectrometry (GC-MS) was used to determine the concentrations of the VFA by using GC-2010 plus (Shimadzu, Japan). The VFA was extracted twice using methyl-tert-butyl ether (MTBE) before being analyzed by the GC-MS, following the method described in a previous study (Banel & Zygmunt 2011). Zeta potential was measured using Zetasizer NanoZS90 (Malvern, UK) and the average value of three measurements were taken for each sample.

#### **4.2.4 Mass transfer resistance**

To evaluate the mass transfer and its resistance of the vacuum membrane distillation in the anMDBR, various flow models had been considered, including the Knudsen flow model, the Poiseuille flow model, the diffusion-in-air flow model, or their combination. As the molecular diffusion model did not fit VMD configurations because of a low value of the partial pressure in the pores, the Knudsen and Poiseuille models were more appropriate. Due to the high pressure in the VMD configuration, the mean free path of water molecules could reach high values varying between 3.0 and 3.4  $\mu\text{m}$ . This means that the Knudsen number, which was defined as the ratio between the mean free path and the pore size, ranged from 30 to 34, as the pore size of the membranes used in this study was 0.1  $\mu\text{m}$ . Therefore, we could conclude that the molecule-pore wall collisions were dominant over the molecule-molecule collisions. So, a Knudsen type diffusion of water molecules passing through the membranes are assumed based on Dusty Gas Model, and the MD coefficient  $B'$  can be addressed as below:

$$B' = 1.064 \cdot \frac{r\varepsilon}{\delta\tau} \cdot \left(\frac{M}{RT}\right)^{1/2} \quad (9)$$

where  $B'$  is the membrane coefficient,  $r$  is the pore size (0.1  $\mu\text{m}$ ),  $\varepsilon$  is the fractional void volume of the membrane (0.7),  $\delta$  is the membrane thickness (265  $\mu\text{m}$ ),  $\tau$  is the pore tortuosity (assumed 2),  $M$  is the water molecular mass (0.018 kg/mol),  $R$  is the gas constant, and  $T$  is the temperature at the membrane surface (liquid/vapor interface).

In the Knudsen model, a linear relationship between the water flux,  $N$ , and water vapor pressure difference,  $\Delta P'$ , is described as below:

$$N = B' \Delta P' = B' [P_v(T'_w) - P_0] \quad (10)$$

, where  $B'$  was MD coefficient,  $P_0$  is the pressure in the vacuum side, and  $P_v(T'_w)$  is the water vapor pressure at the membrane shell surface at the relative temperature.

Then, Antoine's equation addressed below was introduced to find the related temperature with the vapor pressure at the membrane surface.

$$P_v(T) = \exp\left(23.1964 - \frac{3816.44}{T - 46.13}\right) \quad (11)$$

The iterative method following equations (9) to (11) was used to work out the mass transfer resistance (Mengual, Khayet & Godino 2004). Firstly, we supposed a temperature at the membrane surface in equation (1), then the obtained value of  $B'$  was put into equation (2) to get a value of pressure difference, and Antoine equation was used to get a new value of  $T'_w$ . The process was repeated multiple times until a consistent  $T'_w$  was achieved.

Cake formation model for mass transfer (or fouling) resistance was applied, and individual mass transfer resistances were worked out using following equation (Goh et al. 2015). Resistance,  $R$ , was defined as the inverse of MD coefficient,  $B'$ .

$$R_t = R_m + R_{tp} + R_c \quad (12)$$

, where  $R_t$  is total mass transfer resistance,  $R_m$  is membrane resistance,  $R_{tp}$  is temperature polarization resistance, and  $R_c$  is cake layer resistance.



#### 4.2.5 Removal ratio and enrichment factor, $\beta$

To determine the removal efficiency of TOC or inorganic salts, following equations are used to calculate removal ratio and enrichment factor  $\beta$ :

$$Removal\% = 1 - \frac{C_p}{C_l} \quad (13)$$

, where  $C_p$  is the TOC/inorganic salts concentration in the permeate and  $C_l$  is the relative compounds concentration in the mixed liquor.

To determine whether VFAs were concentrated or diluted in the permeate from anMDBR, enrichment factor  $\beta$  was introduced, addressed below:

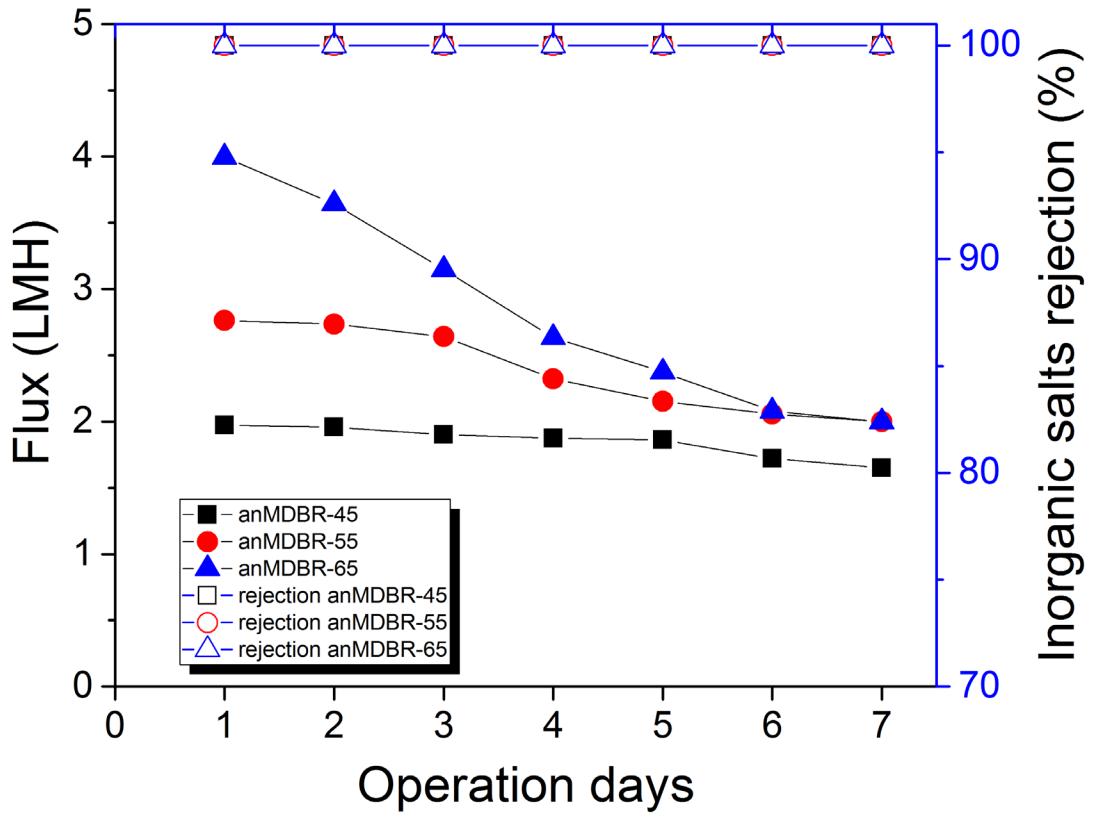
$$Enrichment\ factor\ \beta = \frac{C_{p2}}{C_l} \quad (14)$$

, where  $C_{p2}$  is the VFAs concentration in the permeate and  $C_l$  is the relative compounds concentration in the mixed liquor.

### 4.3 Effects of bioreactor (feed side) temperature (45, 55, & 65 °C) on anMDBR performance

#### 4.3.1 Flux comparison and inorganic compounds rejection for 7 days

The difference of temperature between the membrane feed and permeate sides is one of the main parameters determining the permeation performance of MD. Moreover, the increase in the reactor temperature from 45 to 65 °C could potentially promote the activity of the microorganisms, leading to higher TOC removal efficiency. However, more organic fouling could occur at higher temperature, which would negatively affect the mass transfer of vapor due to increased fouling. Therefore, it is essential to understand the effects of the reactor temperature on the MD performance and permeate quality. Also, the biomass activity in the reactors was assessed regarding organic compounds removal efficiency. In this study, three bioreactor temperatures, 45, 55, and 65 °C were selected because anaerobic microbes proliferated at an optimal temperature of 45 to 65 °C (Goh et al. 2015). For ease of discussion, the anMDBRs maintained at temperatures of 45, 55, and 65 °C are referred herein as anMDBR-45, anMDBR-55, and anMDBR-65, respectively.



**Figure 31.** Anaerobic membrane distillation bioreactor flux performance at various bioreactor temperatures. (anMDBR-45, anMDBR-55, and anMDBR-65 are membrane distillation bioreactor operated at 45, 55, and 65 °C, respectively)

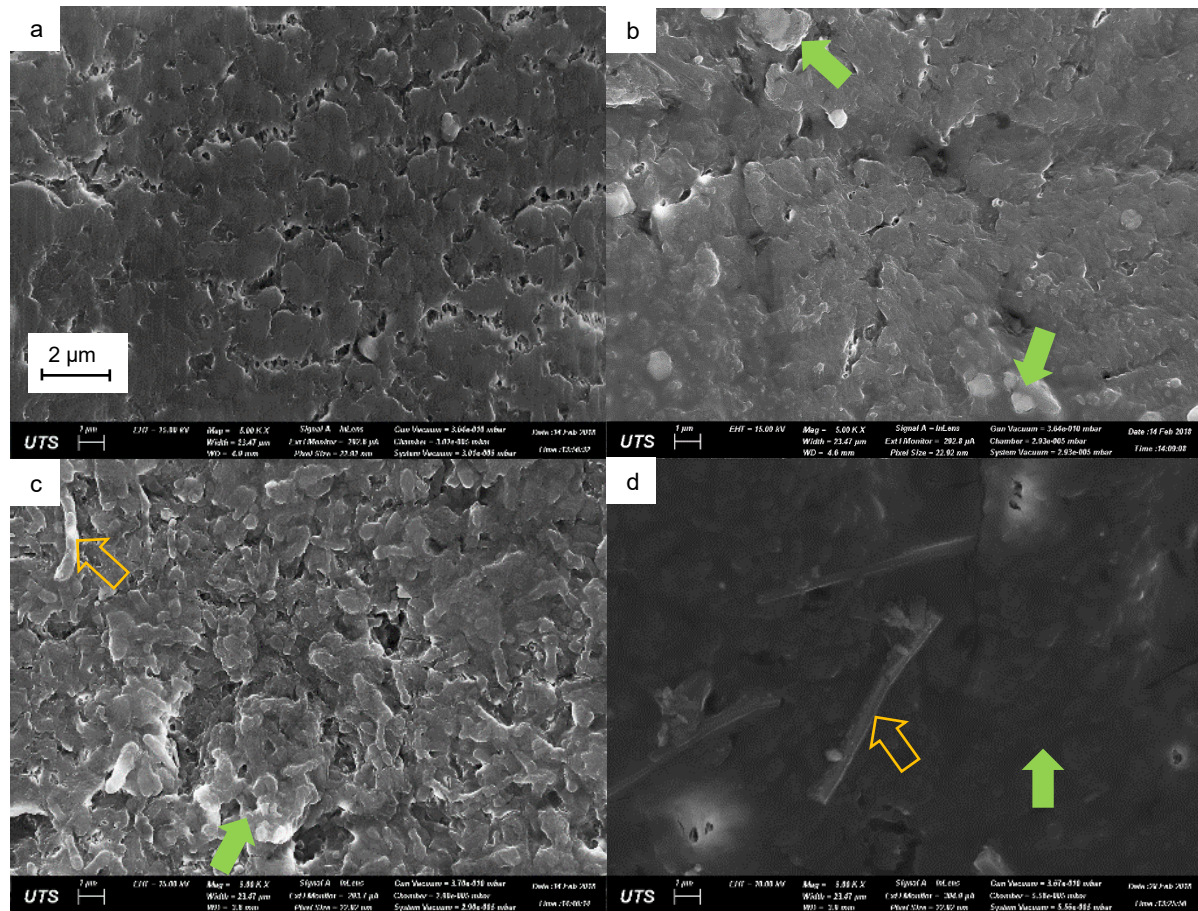
**Figure 31** shows that the increase in the reactor temperature strongly affects the flux performance of anMDBR due to the greatly increased vapor pressure generated onto the interface of the membrane surface. A 20 °C increase in the feed temperature from 45 to 65 °C doubles the initial flux from 2 to 4 LMH. However, a big flux decline (50%) from its initial flux was observed at day 7 when the bioreactor was running at 65 °C, while the bioreactor at 45 °C has a much smaller decline (16%) after 7-day of operation. The observations of the flux decline in the permeate were consistent with previous finding (Goh et al. 2013b; Jeison & van Lier 2008). Formation of cake layer fouling on the membrane surface was the main contributor to the reduction of the flux, composed of suspended or dissolved organic substances which were caused by the products of the microbial activities. Also, larger declines of flux in the

bioreactor at higher temperatures could be caused by the extra release of the microbial products due to promoted activities of the microorganisms (Gao et al. 2012). Comparison of MD and anMDBR treating same synthetic wastewater were addressed in section 4.4.3 to specifically evaluate the effects of biomass on the membrane fouling and flux decline.

Despite the severe membrane fouling, the membrane wetting did not occur in the anMDBR during 7-day operation, as the trace inorganic ions (Na, K, Fe, etc.) were not detected in the permeate using MP-AES. All the anMDBR systems achieved a high inorganic rejection of 99.99%.

By using the float valve, the organic loading rate was proportional to the permeation flux as the feed inlet rate equaled permeation flux while the organic strength was constant. Therefore, as the MD flux was in declining trend during 7-day operation, the organic loading rate ranged from 0.42 to 0.50 kg COD/m<sup>3</sup>·day for anMDBR-45, from 0.51 to 0.70 kg COD/m<sup>3</sup>·day for anMDBR-55, and from 0.51 to 1.01 kg COD/m<sup>3</sup>·day for anMDBR-65. Considering the smaller organic loading rate shock, anMDBR-45 was favored for the process.

### 4.3.2 Membrane fouling analysis in membrane distillation bioreactors



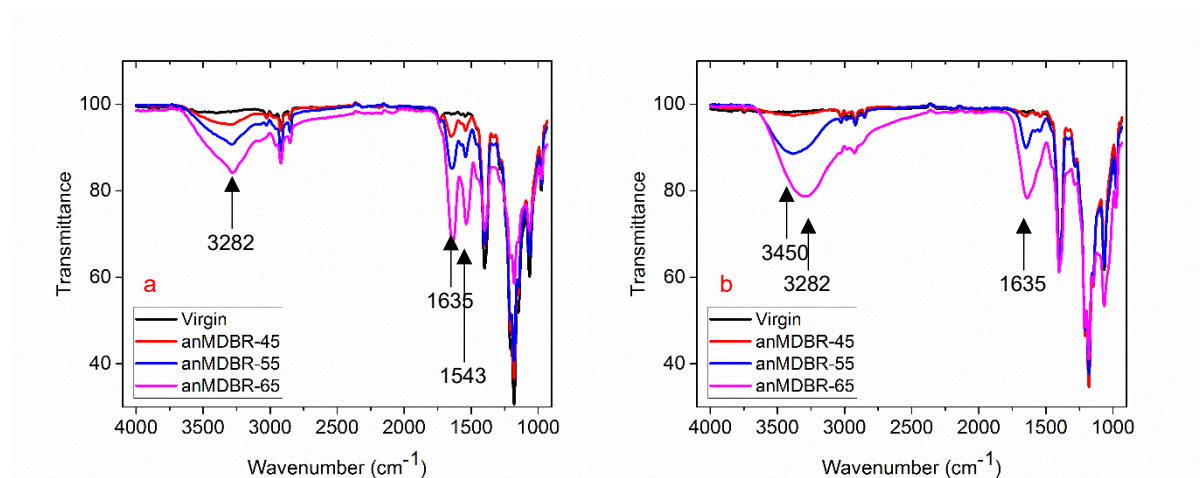
**Figure 32.** SEM images of the shell sides of hollow fiber membrane surfaces for: (a) virgin membrane, and for anMDBR at various temperatures after 7-day operation: (b)45°C, (c)55°C, (d)65°C

The study on the morphology of fouled membrane surfaces supported that the membrane fouling caused larger decline of flux at higher bioreactor temperatures (see **Figure 32**). The membrane morphology from anMDBR-45 after 7-day operation looks nearly identical as with the virgin membrane shown in **Figure 32a**. However, some organic foulants started to adhere onto the membrane surface (see solid arrows in **Figure 32b**). The anMDBR-55 membrane showed hierarchical cake layers on the shell side of the membrane surfaces (**Figure 32c**) owing to increased microbial products and reduced colloidal particle size (Gao et al. 2012; Lin et al. 2013). Nevertheless, the cake layers were porous and not very compact as the original polymer structure could still be observed underneath. Also, some bar-shape deposit started to appear on the foulant layers (see hollow arrow in Fig. 32c), which were believed to be inorganic scaling.

Then, further increase in the bioreactor temperature to 65 °C (i.e., anMDBR-65) resulted in a very dense non-porous fouling layer on the membrane surface (**Figure 32d**), which could be contributed by dramatically decreased colloidal particle size and increased microbial products concentration. And it could lead to a large increase in the fouling resistance as Gao et al. (2012) stated. More bar-shape structures could be seen merging into the fouling layer, which were likely salt crystals as EDX results indicated. The interaction of organic and inorganic fouling were investigated in previous study and it was found that a complex of foulant layer formed by combination of organic compounds and inorganic salts grew on the membrane surface as a result (Meng, Ye, et al. 2014).

The study of the contact angle proved the change of hydrophobicity of membrane surface after 7-day operation. The contact angles of the fouled membranes from bioreactors at various temperatures were nearly identical at 80°, dropping from 110° for the virgin membrane. The large decrease in the contact angles caused by the adherence of organic compounds on the membrane surfaces agreed with the previous study (Goh et al. 2013b). However, the contact angles of lumen surfaces showed very distinct results. Contact angle of membrane lumens from anMDBR-45 was similar with the virgin membranes (105°). But further increase in the bioreactor temperatures decreased the contact angles of the lumen surface, with anMDBR-55 decreasing to CA=86.5°. It was assumed that the foulants had passed through membrane shell surfaces and reached the underneath layers of the lumen side. Increase in the bioreactor temperature to 65 °C (anMDBR-65) led to the further decreased contact angle value of 59.4°, which was even lower than the shell contact angle from the same membrane. It was recognized that the hydrophobic foulants tend to form into a cake layer on the membrane surface due to the hydrophobic interaction between the foulants and PVDF membrane (Liang et al. 2008); while the amphiphilic organic compounds passed through the membranes by mechanism of adsorption-desorption-adsorption illustrated by Meng, and then adhered to the inner pores of HF membranes, reaching the lumen sides. (Meng, Ye, et al. 2014; Yao, Woo, Tijing, Choi, et al. 2017). The membrane wetting found in previous MDBR study was highly likely caused by the amphiphilic organic compounds (Goh et al. 2013b); membrane wetting did not occur in this

study as there was no direct contact of the permeate and membrane lumen side in the VMD configuration.



**Figure 33.** FTIR analysis of shell and lumen sides of hollow fiber membranes after 7 days' operation (a. FTIR analysis on the shell sides of the membranes; b. on the lumen sides)

FTIR studies were carried out on the membrane surface to gain insight of the surface chemical properties. **Figure 33** indicates that the components of the foulants deposited on the shell and lumen sides were very different and the bioreactor temperatures could intensify the severity of fouling degree (**Figure 33**). On the shell sides, the FTIR spectrum (**Figure 33a**) showed one sharp peak at  $3282\text{ cm}^{-1}$ , assigned to the aliphatic amine group (Sahinkaya, Yurtsever & Çınar 2017). And the sharp double peaks at  $1635\text{ cm}^{-1}$  and  $1543\text{ cm}^{-1}$  are unique to the protein secondary structures (Zhang et al. 2012). The peaks strongly suggested the presence of the proteins, products of the microorganisms, forming the cake layers on the shell surface of the membrane during anMDBR process; it shared similar analysis of fouling layers in MBR (Luna et al. 2014). The proteins could be found on the membrane surface from the bioreactors at all tested temperatures, and increase in the bioreactor temperature clearly intensified the severity of fouling, which agreed with the change of the morphology (**Figure 32**). On the other hand, the FTIR analysis on the lumen of the HF membranes suggested that a different category of organic compounds passed through the membranes (**Figure 33b**). A broad peak from  $3280$  to  $3450\text{ cm}^{-1}$  could be contributed by both N-M bonds and O-H bonds (Rondon et al. 2015; Wang et al. 2008), and only one peak at  $1635\text{ cm}^{-1}$  appeared without  $1543\text{ cm}^{-1}$ . These peaks strongly suggest the presence of humic substance, another category of sludge products, on the lumen side of the membranes (Rodrigues et al. 2009). It was well recognized that the humic substance,

despite their low volatility, could pass through the membrane and reached the permeate side in MD through a mechanism called “adsorption-desorption-adsorption” (Meng, Ye, et al. 2014; Naidu, Jeong & Vigneswaran 2015). The humic substances were not detected on the lumen side of the membrane from anMDBR-45, but enormously at anMDBR-55 and anMDBR-65, which agreed with trend of their relative contact angles. Also, significant weight percentage of inorganic salts were detected by EDX analysis on the lumen side which indicated that the liquid water started to pass through the membranes. Nevertheless, pore wetting had not occurred yet as inorganic salts were not detected in the permeate; a potential membrane wetting might occur if extra operation time was applied.

**Table 6.** Mass transfer resistance analysis between bioreactors operated at various temperatures

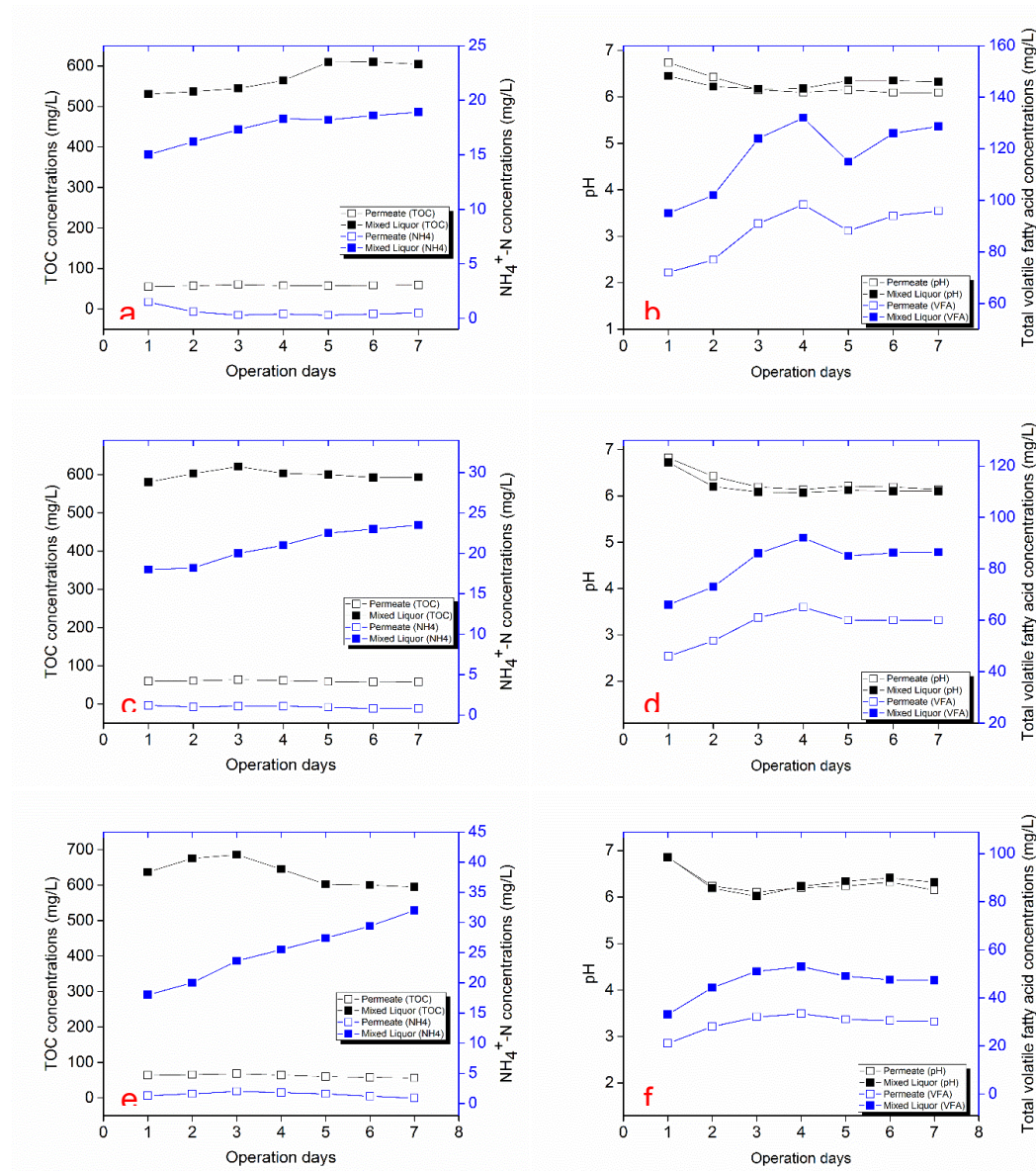
	anMDBR@45°C	anMDBR@55°C	anMDBR@65°C
<b>R<sub>m</sub> (Pa·m<sup>2</sup>·h/ kg)</b>	748.1	749.1	749.0
<b>R<sub>tp</sub> (Pa·m<sup>2</sup>·h/ kg)</b>	1594.8	3135.8	4260.5
<b>R<sub>c</sub> (Pa·m<sup>2</sup>·h/ kg)</b>	410.2	1439.3	5018.9
<b>R<sub>t</sub> (Pa·m<sup>2</sup>·h/ kg)</b>	<b>2753.1</b>	<b>5324.1</b>	<b>10028.4</b>
<b>R<sub>c</sub>/R<sub>t</sub></b>	14.9%	27.0%	50.0%

To determine how fouling resistance contributing to the decrease in the permeate performance compared with other resistance, analysis on mass transfer resistance after 7-day operation were conducted (Table 6). For anMDBR-45, the fouling (cake layer) resistance was 410.2 which was much lower than temperature polarization resistance and membrane resistance; it was only accountable for 14.9% of the total resistance. However, much more severe membranes fouling occurred at higher bioreactors temperatures as the cake layer resistance was accountable for 50% of the total resistance at anMDBR-65. The increased cake resistance agreed with the non-porous surface morphology found in **Figure 32d**. A similar trend was found by Goh (2013). It was worth noting that the increase in the bioreactors temperatures also led to significantly increased temperature polarization resistance because of no water velocity on HF membrane surface in submerge-mode. We concluded that anMDBR operated at higher temperatures



suffered more mass transfer resistance which led to big drop in mass transfer efficiency; hence, we suggested that the optimal temperature was 45 °C for anMDBR in this study.

### 4.3.3 Change of TOC, NH<sub>4</sub>, pH, and VFA concentrations in the permeate and mixed liquor at various feed temperatures



**Figure 34.** Total organic compounds and N-NH<sub>4</sub> concentrations in permeate and mixed liquor at (a)45°C; (c)55°C; (e)65°C, pH and total volatile fatty acid concentrations in permeate and mixed liquor at b)45°C; (d)55°C; (f)65°C



**Figure 34** shows that the anaerobic bioreactor performs well regarding TOC digestion as the TOC concentrations in the mixed liquor remains stable regardless of the bioreactor temperatures. On the other hand, low but significant concentrations (around 60 mg/L) of TOC existed in the permeate. Although MD could remove 99.99% non-volatile impurities, the volatile organic compounds had low partial pressure close to water vapor so they could penetrate the membranes easily in MD system (Alkhudhiri, Darwish & Hilal 2012). The TOC concentrations in the permeate was not affected by the bioreactor temperatures. Also, the decreasing pH in both mixed liquor and permeate suggested the volatile organic compounds was maintained slightly acidic. To our best knowledge, there was no such observations in the literature regarding MD-BR that significant concentrations of TOC found in the permeate while membrane wetting did not occur. We suspected the presence of volatile fatty acids (VFAs) led to the increase in the TOC concentrations in the permeate, the intermediate products produced by acidogenesis in the anaerobic bioreactors (Khan et al. 2016). The GC-MS measurement confirmed the existence of the VFAs in the permeate. Acetic acid, propanoic acid, butyric acid, and isovaleric acid were detected, while acetic acid had the highest concentration among all VFAs. The detailed components of each VFA in both mixed liquor and permeate are discussed in section 4.5.1. The increase in the bioreactor temperatures led to a decrease in the total VFA concentrations because the higher operation temperatures promoted the thermophilic methanogens activities which mitigated the build-up of VFA (Hu & Stuckey 2006; Lettinga 1995).

Trace of ammonium was detected in the permeate in low concentrations (<2 mg/L) while high concentrations of  $\text{N-NH}_4^+$  was found in the mixed liquor, contributed by ammonium sulphate and the hydrolyzed urea. The main reason of low mass transfer of  $\text{N-NH}_4^+$  was that the slightly acidic environment in the bioreactor causes ammonia mostly converted to the form of ammonium ions, which were non-volatile and hence could not penetrate the MD membrane (He et al. 2018; Yang et al. 2017). The anaerobic bioreactor could not nitrify the ammonium in the mixed liquor and hence an accumulation of the  $\text{NH}_4^+\text{-N}$  occurred, and it was more viable at higher reactor temperatures due to their higher loading rate (Sui et al. 2014).

The zeta potentials of the colloids in the mixed liquor, ranging from -18.3 to -15.6 mV, were strongly dependent on its pH while bioreactor temperatures had minimal impact on it. The reduction of pH led to the increase in the zeta potential, which potentially caused more fouling issues as the floc particles became more likely coagulated (Meng et al. 2006). However, the

zeta potentials of the mixed liquors from anMDBR operated at various temperatures shared nearly identical value, so they did not contribute to the differences in the fouling behavior on the relative membranes in anMDBR.

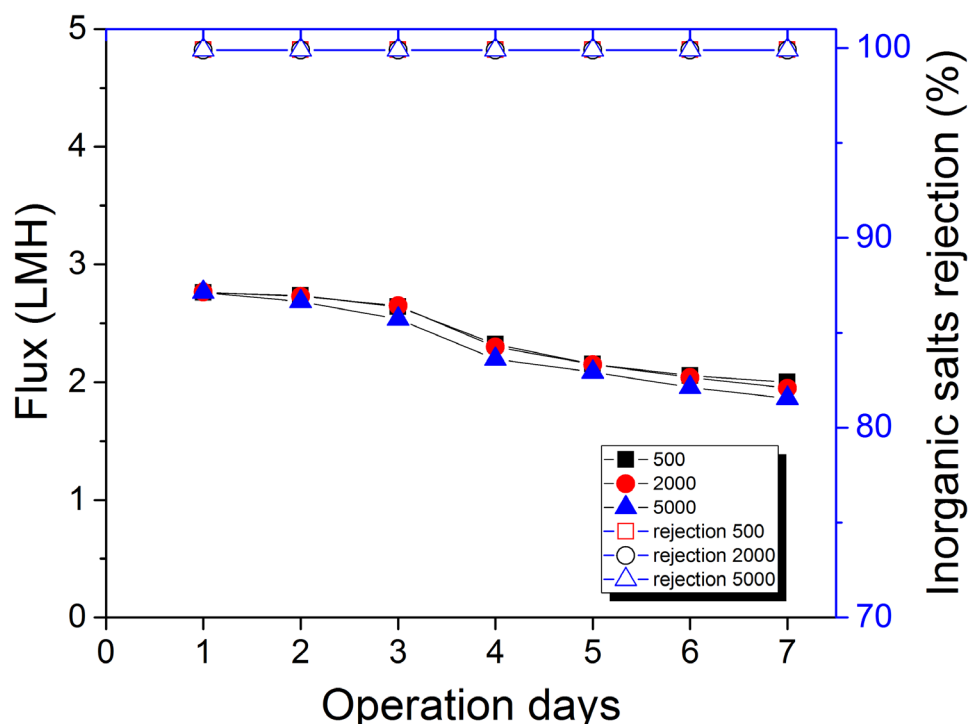
#### **4.4 Effects of various salinity on anMDBR**

The anMDBRs is a high-solid retention process. It was found that the accumulated high salinity could negatively affect the membrane performance in OMBR (Luo et al. 2017). To control the salinity in OMBR, microfiltration or ultrafiltration were incorporated into the process design, which raised the complexities and total costs of the systems (Pathak et al. 2017). Therefore, the effects of salinity in the anMDBR system should be investigated to determine whether the accumulated salinity would affect the permeation performance and hence whether the mitigation strategies should be introduced into the system design. In this study, to determine the effects of salinity, same synthetic wastewater was used for each experiment with various initial salinities of 500, 2000, and 5000  $\mu\text{S}/\text{cm}$  by adding sodium chloride into the relative mixed liquors, and 10% (v/v) of incubated biomass was added into the anMDBR bioreactor. The temperature of the mixed liquor in the anMDBR systems was maintained at 55 °C, and a vacuum pressure of 50 mbar had been applied onto the permeate side.

##### **4.4.1 Effects of bioreactor initial salinities on the permeate flux and membrane fouling morphologies**

Unlike its OMBR counterpart, the salinity had minimal impact on the anMDBR permeation performance as MD was recognized for its strong capabilities to treat very concentrated salty wastewater with high water recovery and stable performance (Tijing et al. 2015a). The anMDBR with three various salinities shared same salt rejection of 99.99%. The increase in the salinity from 500 to 5,000  $\mu\text{S}/\text{cm}$  showed insignificant effects on the flux performance (**Figure 35**).

Although the salinity has little effects on the flux performance, slight decrease in flux was observed when the salinity of the liquor mixed increased. It is found that that the increase in the sodium chloride concentrations greatly changes the morphology on the membrane surface, which tends to be more coiled and spherical in shape (Hong & Elimelech 1997; Liang et al. 2008; Wijekoon et al. 2014). Nevertheless, the foulant layers remained porous and they shared nearly identical mass transfer resistance so that the permeation flux kept very close under same



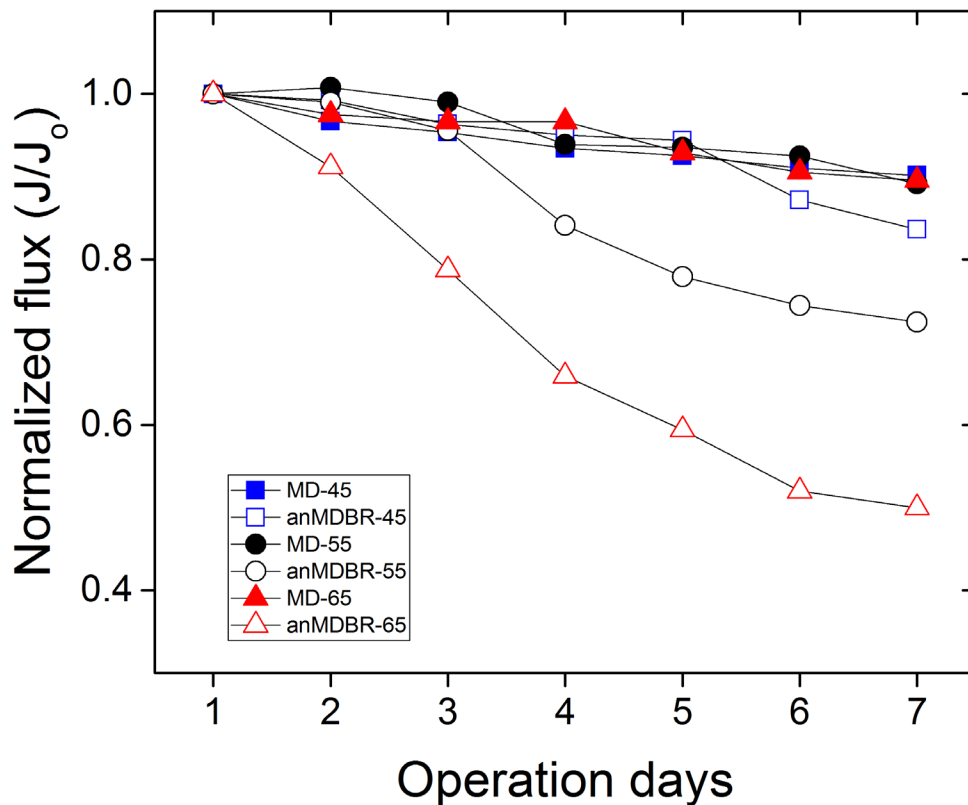
**Figure 35.** Flux of anMDBR-55 operated at various initial salinity

#### 4.4.2 Removal efficiency

As the reactors with higher initial salinity had slightly lower flux, its organic loading rate was lower resulting in slower TOC accumulation. However, the flux difference was not significant. On the other hand, the reactors with higher initial salinity also had slightly lower TOC in the permeate, which could be contributed by both the increased cake layer mass transfer resistance and lower VFAs yield owing to hindered bacterial activity (Luo et al. 2016).

#### 4.4.3 Performance of anMDBR compared with MD

To determine the effects of organic compounds produced by anaerobic bacterial especially regarding their adherence on the membrane surface, anMDBR was compared with MD using the same setup running at 45, 55, and 65 °C, except an addition of the biomass to the bioreactor. Vacuum pressures were all set at 50 mbar.



**Figure 36.** Flux comparison between membrane distillation and anaerobic membrane distillation bioreactor at various temperatures (MD-45 means MD operated at 45 °C; AnMDBR-45 means anMDBR operated at 45 °C; same rule of calling is used in the other items in the legend)

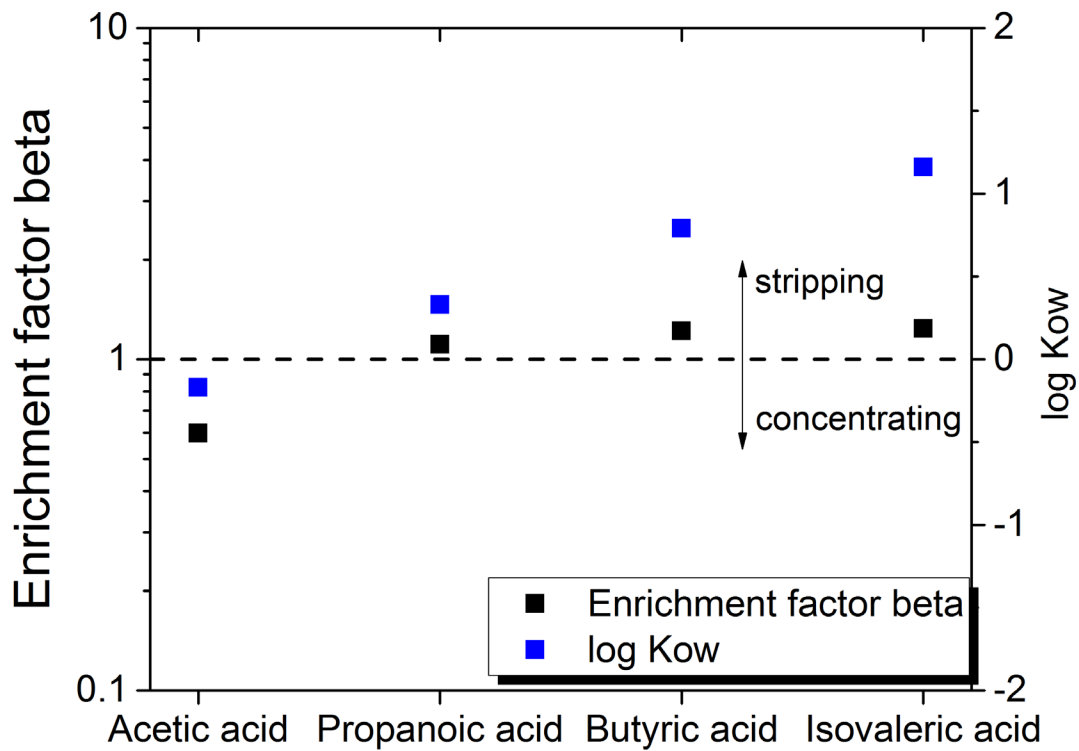
At same bioreactor temperatures, flux of anMDBR shares similar initial flux performance as their MD counterparts. However, the continuous operations of anMDBR showed a larger flux decline, and the increase in the bioreactor temperatures greatly intensify the reduction (**Figure 36**). While anMDBR-65 had a sharp flux decline of around 50% at day 7, MD-65 showed only a small drop of 11%, which was close to the reduction in MD operated at 45 and 55 °C. MD at various temperatures of mixed liquor shared similar flux drop mainly owing to the organic fouling: without the existence of biofilm, the increase in organic compounds concentration in anMDBRs with higher temperatures did not lead to a compact fouling layer on the membrane surface, contributing to little effect on the mass transfer resistance. The flux comparison between MD and AnMDBR supported the statement in section 4.3.1 that the protein produced

by the biomass greatly contributed to the sharp increase in the mass transfer resistance through the formation of non-porous compact cake layer on the membrane surface.

## **4.5 Bioresource recovery**

### **4.5.1 VFAs recovery from the permeate**

The separation of VFAs from the bioreactor to the permeate tank made it viable for its recovery. VFAs are regarded as valuable resources as it could be precursors of biopolymers replacing expensive chemicals, such as alcohols, aldehydes, ketones, and biofuels. Also, VFA could be used as green fuels, contributing to the decrease in the greenhouse emissions (Khan et al. 2016). Therefore, the potential production of VFA from the wastewater by employing anMDBR systems could supply extra economic benefits. Another advantage of VFA separation from bioreactors was to enhance the microorganism's growth as VFA was one of the major inhibitors in anaerobic bioreactors (Gryta et al. 2013). Currently, several methods including reactive distillation, sorption, and solvent extraction had been developed to recover the VFA from the source water containing low concentration VFA (Zhang et al. 2011). Among them, membrane electrodialysis had the strongest potential (Yu et al. 2000). However, the total VFA concentration in the source water (0.01 wt.%) from this study was relatively lower than the ones treated in the literature. Therefore, the recovery techniques required further studies for optimal efficiency.



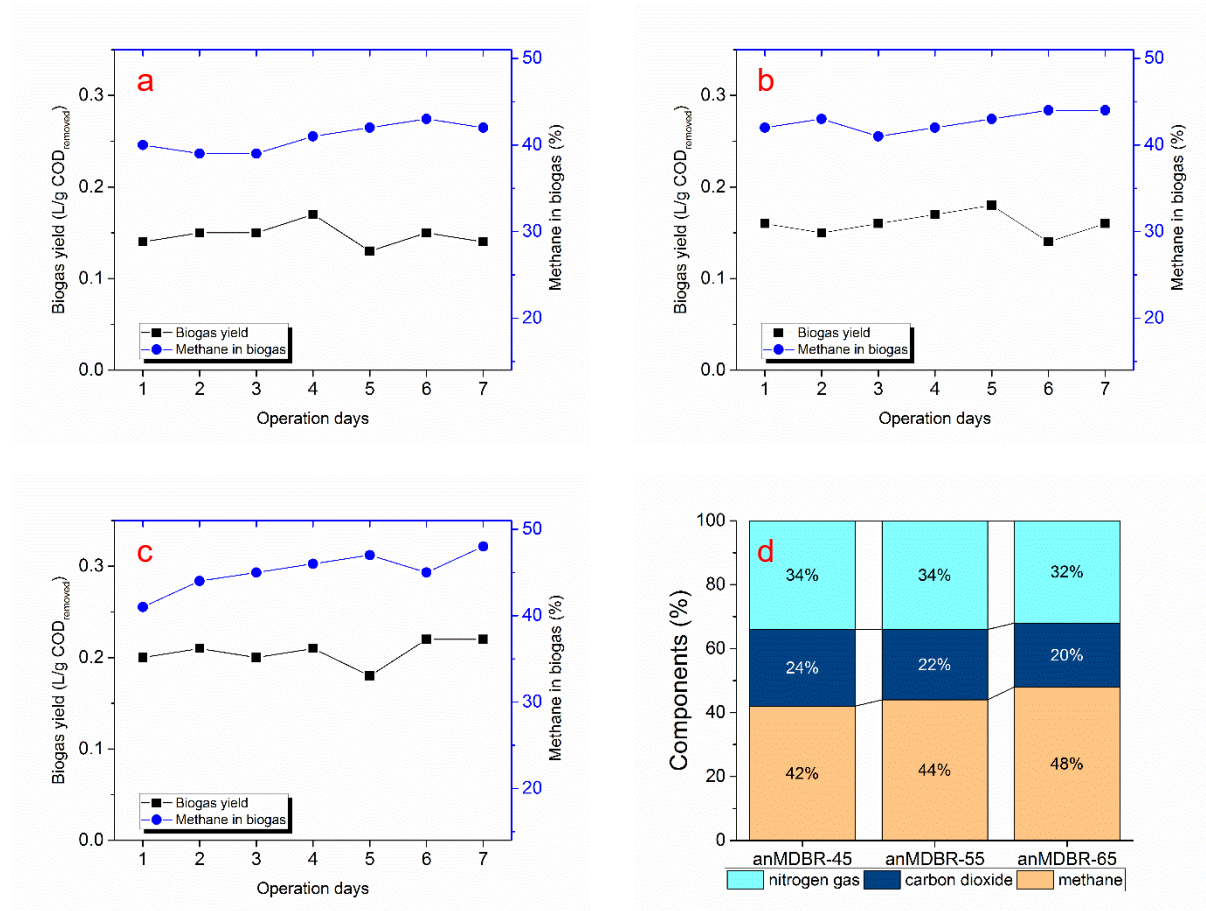
**Figure 37.** Enrichment ratio of each individual volatile fatty acid (VFA) and their relationship with the partition coefficient

The components of volatile fatty acid found in the permeate from anMDBR-55 at day 7 were analyzed. Acetic acid had highest concentration at 58.6 mg/L while higher concentration (97.9 mg/L) of acetic acid was found in the mixed liquor; on the other contrary, propanoic acid, butyric acid, and isovaleric acid had higher transport rate although they had higher boiling points than acetic acid. **Figure 37** shows that the latter three VFAs concentrate in the permeate tank while acetic acid was being diluted. This could be caused by their higher partition coefficient as a larger hydrophobic head in the compounds could enhance their transfer rate through the membrane (Yao, Woo, Tijing, Choi, et al. 2017). The mass transfer of VFAs in anMDBR greatly differed from the one in anaerobic MBR system where 98% VFA rejection was observed (Jeison & van Lier 2008).

#### 4.5.2 Biogas recovery from the thermophilic anMDBR

The final bioresource product of anMDBR is the biogas, and their successful recovery could contribute to improved energy efficiency of the system. The daily biogas volume was strongly correlated to the daily organic loading rate. As the COD feed rate was proportional to the MD permeation flux rate, anMDBR at higher temperature had higher organic loading rate than the ones at lower temperature. However, the anMDBR-65 gas production efficiency deteriorated due to a large decline in flux and hence organic loading rate in 7-day operation. The biogas yield was quite consistent regardless of the anMDBR temperatures for the 7-day operation, as well as the components of the biogas. **Figure 38(a-c)** show that the bioreactor operated at 65 °C has slightly higher biogas yield than the others, which can be due to the improved microbial activity. Also, at day 7, it had improved biogas quality with higher methane percentage at 48% compared with 42 and 44% from bioreactors operated at 45 °C and 55 °C, respectively (**Figure**

38d). However, the percentage of methane in our bioreactors was lower compared with others in the literature as they had not reached completely steady state as mentioned in section 4.2.2.



**Figure 38.** Biogas yield and methane percentage in bioreactors at (a) 45 °C; (b) 55 °C; (c) 65 °C, and (d) their biogas components at day 7

## 4.6 Conclusions

This study reports the first attempt to design and investigate the feasibility of a lab-scale anMDBR for the treatment of domestic wastewater. The performance of the anMDBR was evaluated in terms of permeate flux, TOC and inorganic compounds rejection, and bioresources recovery; the challenges of anMDBR operation was also evaluated in the light of flux decline and permeate quality. The following are the main conclusions from this study:

- (1) The system achieved high initial permeation flux at relatively low feed temperatures (45 to 65 °C) in the bioreactors using HF membranes in submerged mode, showing the potentials of anMDBR in terms of small footprints like their MBR counterpart.



- (2) High inorganic rejection (99.99%) was achieved in 7-day operation regardless of the tested anMDBR temperatures (45-65°C). However, TOC rejection was not high as volatile fatty acids (VFAs) were found in the permeate which require further treatment.
- (3) Bioreactors with higher operating temperatures had larger decrease in flux in 7-day operation. Specifically, anMDBR operated at 65 °C had a decline of 50% at day 7. Compact non-porous cake layers formed of proteins were observed on the membrane surface from anMDBR-65, contributing to a big increase in the mass transfer resistance. Also, we observed that liquid water started to pass through the membrane structures and reached the lumen of the HF membranes in 7-day operation although complete pore wetting had not occurred yet.
- (4) Salinity of the mixed liquor was found to show minimal impact on the permeation performance, making this high solid-retention system more feasible in real application than osmotic membrane bioreactors.
- (5) The potential recovery of biogas and VFAs from anMDBR could reduce the costs for its relatively high energy consumption. Higher anMDBR temperatures showed increased biogas yield and quality, but the differences were nearly negligible. Therefore, based from the results, we conclude that anMDBR temperature of 45 °C was the optimal temperature for the anMDBR system as it required least energy for heating and suffered minimal membrane fouling issues while maintaining strong capabilities of TOC reduction in the mixed liquor and bioresource production.
- (6) To realize the potentials of the anMDBR system, novel design of anti-fouling membranes was strongly needed. Prevention of adherence of hydrophobic and amphiphilic organic compounds, products from microorganisms in anaerobic reactors, on membrane surfaces require specific membrane surface properties different from “superhydrophobicity” normally required for desalination or “hydrophilicity” for the treatment of low surface tension wastewater. Also, techniques for VFA recovery at low concentration should be developed for anMDBR.

## **CHAPTER 5**

### **Behavior of Volatile Organic Compounds in Membrane Distillation**

## 5.1 Introduction

Coal seam gas (CSG), also called coal bed methane, is one type of unconventional natural gas resources stored in coal seams at a depth of 300-1000 m (Hamawand, Yusaf & Hamawand 2013). Fast replacing coals and conventional natural gas, CSG has been developed into one of most important energy resources for Australian economies (especially for Queensland), which is being greatly exported as liquefied natural gas (LNG) to Asian countries. Similarly, CSG has become an important energy source in the United States, Canada, and some other countries as well. Although CSG is considered as a relatively “greener” resource as it produced much less carbon dioxide after burning, the processes of gas exploration still pose great risks on the local ecological system. One of the biggest challenges is produced water management (Gordalla, Ewers & Frimmel 2013; Hamawand, Yusaf & Hamawand 2013). To mine the gas out of the coal bead, large amounts of water is required to be removed from the coal to reduce the hydrostatic pressure. Formation water, flow back water, and water condensing from the gas phase compose produced water. Formation water is the major contributor to the produced water, naturally occurring and being stored in oil and gas reservoirs. The water is often of brackish to saline quality (Dahm et al. 2011; Hamawand, Yusaf & Hamawand 2013).

Management of the produced water is a major challenge in energy industry due to its large amounts, complex chemical compositions, and limited disposal options. In Australia, direct reinjection of the produced water back into the deep underground well is banned, a technique commonly practiced in the United States (Nghiem et al. 2011). Therefore, currently most Australian exploration companies applied reverse osmosis (RO) on site to treat the produced water. The permeate water of RO is sold to local residents for irrigation (Averina, Rasul & Begum 2008; Nghiem et al. 2011). However, RO is not efficient to treat concentrated salty water, so still large amounts of brine could only be stored in the onsite evaporation ponds as short- or medium-term solution.

Membrane distillation (MD) has strong potentials to further treat the brine or produced water as salt concentration in the feed had minimal effects on its flux performance. Around 95% recovery of RO brine from the CSG produced water had been achieved through the RO-MD hybrid system (Duong et al. 2015c; Woo et al. 2017; Woo, Kim, et al. 2016). Regarding salt removal, the quality of the permeate was decent as MD has theoretically 100% rejection rate for non-volatile solutes (Alkhudhiri, Darwish & Hilal 2013a). Also, the flux performance is

less affected by the salinity of the feed. In terms of energy consumption, MD was found to be more efficient than the business as usual strategy (BAU) for treatment of the produced water. Tavakkoli et al. found that the operation cost of MD was roughly half of the BAU strategies when low-grade heat was available (Tavakkoli et al. 2017). However, MD had degraded permeate quality when treating wastewater containing VOCs, dissolved gas, or some small organic particles (Shaffer et al. 2013). Especially, when the VOCs are alcohol or having surfactant properties, membrane wetting will occur and lead to further deterioration of the permeate quality as the feed water can pass through the membrane directly via the wetted pores (Chew, Zhao, Loh, et al. 2017; Shaffer et al. 2013; Yao, Woo, Tijing, Cesarini, et al. 2017). Recently, some researchers studied the effect of the surfactant and oil existed in the produced water on the water recovery via MD and found that they had strong negative impact on the permeation flux and permeate quality (Chew, Zhao, Loh, et al. 2017; Eykens, De Sitter, et al. 2017b). However, none of researches has investigated the effect of VOCs in the produced water on the MD performance, which may share similar effects as the surfactant and oil.

It has been found that the compositions of the CSG produced water are highly dependent on the geology (Orem et al. 2014). In some mining wells, high concentrations of the volatile organic compounds (VOCs), mainly acetic acid, had been found in the produced water (Brantley et al. 2014); also, the produced water (also called flow back water) could contain large amounts of VOCs which had been artificially added into the pumping fluids for fracking, especially during initial stage of CSG mining (Orem et al. 2014). Those VOCs can hinder the MD process regarding permeate quality and water permeation performance (Alkhudhiri, Darwish & Hilal 2012). To address this challenge, this study aims to systematically study the effects of commonly found VOCs in the produced water and their mechanism of the membrane penetration. Here, acetic acid, ethylene glycol, isopropyl alcohol (IPA), and 2-Butoxyethanol (2-BE), which are commonly used in the fracking fluids or naturally occurring (Orem et al. 2014), had been extensively investigated regarding their roles in MD. A fundamental understanding of the effects of VOCs on water recovery from CSG produced water via MD can help new membrane and system design, which can further promote the realization of its potential in the application.

## 5.2 Experimental method

### 5.2.1 Chemicals

Acetic acid was purchased from Chem-supply, Australia. IPA was bought from Merck group, Germany while 2-BE and ethylene glycol were obtained from Sigma-Aldrich, USA. All the VOCs were used as received and their properties are displayed in **Table 7**. To accelerate the progress, 2000 ppm of the tested VOC was added into de-ionized (DI) water and the solution was stirred for 15 mins before MD experiment, individually.

**Table 7.** Properties of VOCs and concentrations of ion components of the synthetic produced water used in this study

<b>Volatile organic compounds</b>	<b>Molecular weight [g mol<sup>-1</sup>]</b>	<b>Surface tension [mNm<sup>-1</sup>] at 20°C</b>	<b>Boiling temperature [°C]</b>	<b>Vapor pressure at 20° [kPa]</b>	<b>Source/ usage</b>
<b>Acetic acid</b>	60.1	27.3	118.1	1.6	Natural occurring
<b>Isopropyl alcohol</b>	60.1	21.4	82.6	4.1	Added as corrosion inhibitor in fracking process
<b>2-Butoxyethanol</b>	118.2	26.6	171	0.1	Added as surfactant and active solvent in fracking process
<b>Ethylene glycol</b>	62.1	48.4	197.3	0.06	Added as friction reducer in fracking process

Water (for reference)	18.0	72.8	100	2.3	-			
Ions	Na <sup>+</sup>	HCO <sub>3</sub> <sup>-</sup>	Cl <sup>-</sup>	Mg <sup>2+</sup>		Si (SiO <sub>2</sub> )	CO <sub>3</sub> <sup>2-</sup>	SO <sub>4</sub> <sup>2-</sup>
Concentration (mgL <sup>-1</sup> )	6,840	4,740	7,770	17		75	30	20

Various chemicals were purchased for the preparation of synthetic CSG RO brine water. Sodium chloride was purchased from Ajax Finechem, Australia. Potassium chloride and sodium silicate solution were received from Chem-supply, Australia. Magnesium chloride, calcium chloride, sodium bicarbonate, sodium carbonate, and sodium sulphate decahydrate were purchased from Sigma Aldrich, USA. All the chemicals were used as received. Composition of the synthetic CSG RO brine is illustrated in **Table 7**. Properties of VOCs and concentrations of ion components of the synthetic produced water used in this study.

### 5.2.2 Vacuum membrane distillation (VMD) configuration

We conducted VMD process with various parameters to optimize the system. In the VMD experiments, feed flow rate was maintained at 400 ml/min by a gear pump purchased from Cole-Parmer Instrument Company, USA. Feed temperature was kept at 70 °C by a heat exchanger (DSB 193-11 F) provided by Daesung Engineering, South Korea. Another heat exchanger of same model set at 15 °C was used to condense the water vapor. Vacuum pressure was set at 850 mbar by a vacuum pump (PC 3001 Vario pro) from John Morris Scientific, Australia. Same setup was used in long-term operation test. For each experiment, a new membrane module was made, and before the start of each experiment, they were tested using DI water as feed for 3 h to make sure that they had identical flux performance. The permeate flux,  $J$ , was calculated as per Eq. (6). The salt rejection,  $R$ , is given in Eq. (7).

### 5.2.3 Characterizations

Total organic carbon (TOC) was measured using a high-performance TOC analyzer (multi N/C3100®) which was purchased from Analytikjena, Germany. Attenuated total reflection-

Fourier transform infrared spectroscopy (ATR-FTIR) (IRAffinity-1 with MIRacle 10) was purchased from Shimadzu, Japan, which had penetration depths from 1.2 to 2.4  $\mu\text{m}$  for detection spectrum from 2000 to 4000  $\text{cm}^{-1}$ . It was used to investigate the mechanism of VOC movements through the HF membranes by measuring the shell and lumen sides of the used membranes. Each spectrum was obtained with signal averaging 32 scans at a resolution of 4  $\text{cm}^{-1}$  in transfer mode by pressing the sample with KBr to a pellet (Yao, Woo, Tijing, Cesarini, et al. 2017). Contact angles of the virgin and used HF membranes were measured by Theta Lite 100 (Attension) using a sessile drop method (Woo, Tijing, et al. 2016; Yao et al. 2016). A water droplet around 5  $\mu\text{l}$  was released from a needle tip onto the flatted HF membrane surface. A motion camera was mounted to capture the videos at a rate of 12 frames per second. Using the Theta Lite software, contact angles were analyzed automatically. Each set of HF membrane samples were measured for three times and the average value of them was taken.

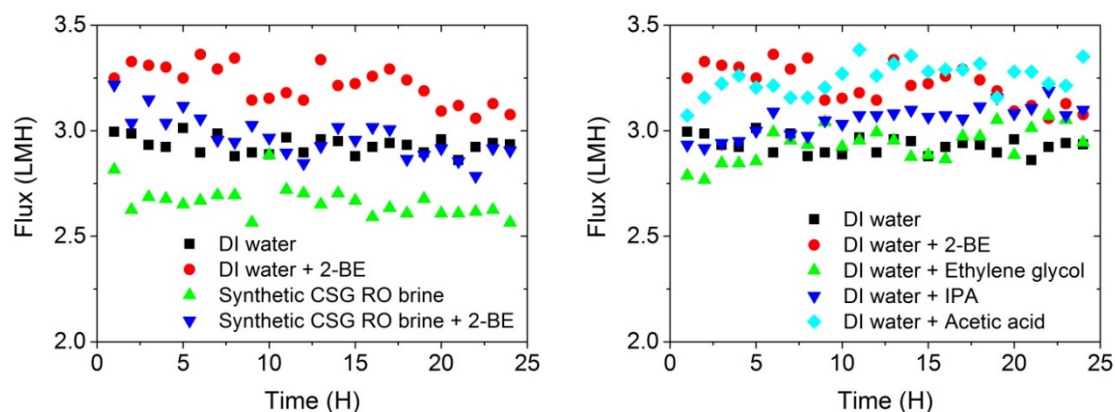
## **5.3 Results and discussions**

### **5.3.1 Optimization of VMD process**

First stage of this study is to determine the optimal running parameters of VMD in the treatment of the produced water. Three major parameters: vacuum pressure, feed temperature, and feed flow rate had been identified and extensively studied by using DI water as feed in baseline study. It was found that increasing feed temperature led to a great increase in permeate flux, as the flux was increased from 1.5 to 4.3 LMH when the temperature was increased from 60° to 70° while the flow rate was maintained at 400 L/min. Similarly, increasing vacuum pressure resulted in great increase in the flux. According to the experiments, it was concluded that feed temperature and vacuum pressure played more important roles than feed flow rate in terms of MD performance.

### 5.3.2 Effects of VOCs on MD performance

#### 5.3.3 VMD treatment of synthetic brine water



**Figure 39.** Effects of A) 2-butoxyethanol on flux when treating de-ionized water and synthetic produced water; B) various volatile organic compounds on flux when treating de-ionized water

To determine the effects of the VOCs on the VMD flux performance, 2-BE was first selected as a representative VOC to be added into the synthetic produced water for comparison because it was widely applied in the industries and has attracted lots of academic interests for its effect on the local ecological systems (Brantley et al. 2014; Gordalla, Ewers & Frimmel 2013; Orem et al. 2014). **Figure 39A** shows that the addition of 2-BE into the synthetic water increases the average flux of VMD treating DI water from 2.9 to 3.3 LMH in 24 h operation, which was due to the mass transport of 2-BE. Also, the declining trend of the flux could be observed, which could be caused by the partial pore wetting, and they will be further discussed in the latter sections. Addition of 2-BE into the synthetic produced water contributed to the increase in the overall permeation flux and its gradual declining trend, which was consistent with the result when 2-BE was added into the DI water as feed. The declining trend of flux was not observed when treating feed without 2-BE regardless of using DI or synthetic produced water as feed.

Concentrations of the feed and the permeate was measured before and after the VMD process, and it was found that a salt rejection of 99.99% was achieved regardless of the presence of 2-BE in the feed. Meanwhile, after treating synthetic produced water with 2-BE via VMD, a very high concentration of 2-BE could be found in the permeate, reaching 3260 ppm, which was

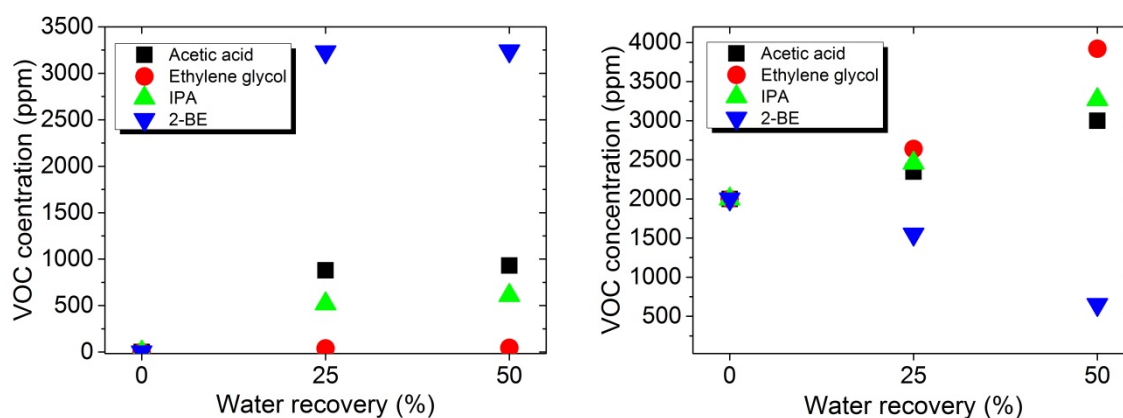


much higher than the initial concentration of 2000 ppm in the feed. The high mobility of 2-BE was reported in previous study concerning the impact of the fracking process on local ecological system, where it was used as a surfactant and active solvent (Brantley et al. 2014). However, it was still unexpected that 2-BE severely penetrated the membrane in VMD process considering that it had much lower vapor pressure than water (0.1 vs. 2.3 kPa at 20°C). Hence it is essential to study whether other common VOCs existing in the produced water posed similar challenges, and what characteristics of the VOCs, except vapor pressure, affect their mass transfer in the MD systems, along with their penetration mechanism (which will be addressed in section 5.5).

#### **5.3.4 Comparison of flux using various VOCs as feed**

Various popular VOCs used in fracking process namely acetic acid, 2-BE, ethylene glycol and IPA, had been investigated regarding their effects on the VMD flux performance. **Figure 39B** shows that the addition of VOCs in the DI water, except ethylene glycol, led to an obvious increase in the average flux (including water and VOCs, following all the same). The increase of the flux after the injection of IPA into the feed can be explained by the increase of partial pressures (García-Payo, Izquierdo-Gil & Fernández-Pineda 2000). Similarly, addition of ethylene glycol into feed led to lowest VMD performance because of its extremely low vapor pressure (Rodríguez et al. 2008). However, among all the tested VOCs, feed with acetic acid had highest average flux although acetic acid had much lower vapor pressure than IPA; its vapor pressure is even lower than water. Also, 2-BE, which had second lowest vapor pressure among all, shows high mobility in this study. It has highest initial flux and second highest average flux for 24 h operation. IPA was expected to result in highest flux increase as it had highest vapor pressure; however, it was outperformed by acetic acid and 2-BE, both having even lower vapor pressures than water. Therefore, the high flux of VMD treating feed water containing acetic acid and 2-BE indicated that there were some characteristics of VOC, other than boiling temperature, surface tension, and vapor pressure, contributing to their high mobility in VMD. Some researchers discussed about the mechanism of “adsorption-desorption” for some organic chemicals with hydroxyl and carboxylic group (Meng, Mansouri, et al. 2014; Naidu, Jeong & Vigneswaran 2015) when trying to explain the movement of certain types of organic compounds from feed to permeate side without membrane wetting occurring. This mechanism could explain the high mobility of 2-BE and acetic acid. It is also worth noting that

only the addition of 2-BE into DI water caused obvious decline in the VMD flux due to the potential membrane wetting caused by the VOCs.



**Figure 40.** Changes in concentrations of various volatile organic compounds in A) permeate; and B) feed sides

### 5.3.5 Mass transfer of VOC from feed to permeate

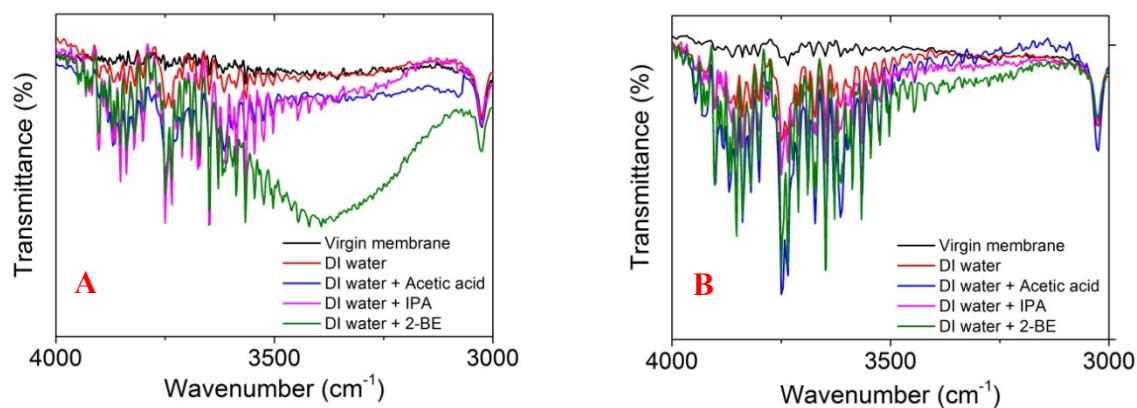
To confirm the mass transport of VOCs which led to increase in flux for feed containing VOCs, measurement of feed and permeate concentration of VOCs had been carried out individually at various water recovery rates. **Figure 40A** shows that concentrations of various VOCs (except 2-BE) in permeate solution increased when the water recovery increased. Owing to its higher boiling point, surface tension, and lowest vapor pressure, there was no mass transfer of ethylene glycol through the membrane during MD process as its concentration in the permeate was maintained ignorable while the one in the feed doubled. IPA and acetic acid shared similar mass transfer rate. Concentration of acetic acid was slightly higher in permeate than IPA although acetic acid had much lower vapor pressure. 2-BE had very different trends of concentration from the other VOCs. 2-BE concentrations in feed decreased rapidly during the VMD process (**Figure 40B**). When water recovery reached 50%, the 2-BE concentrations in permeate (3240 ppm) even exceeded the initial feed concentration (2000 ppm), which meant that the mobility of 2-BE was much higher than water in the MD process even though it had higher boiling temperature and lower vapor pressure. The “adsorption-desorption” mechanism might play an important role in the phenomenon, which involved the strong hydrogen bond between the 2-BE and water molecules. The mechanism of the VOCs’ behavior would be further discussed in the later sections of this paper.

Another series of VMD experiments with same concentrations of VOCs had been conducted, only replacing DI water with 1.0% NaCl as feed base. Nearly identical flux and VOCs mass transfer could be found after 24 h operation, and salt rejection of the VMD experiments were found to be 99.99%, indicating that the membrane pores were not wetted during the processes.

## 5.4 Effect of VOCs on the membranes

### 5.4.1 Penetration of VOCs and water into the membranes

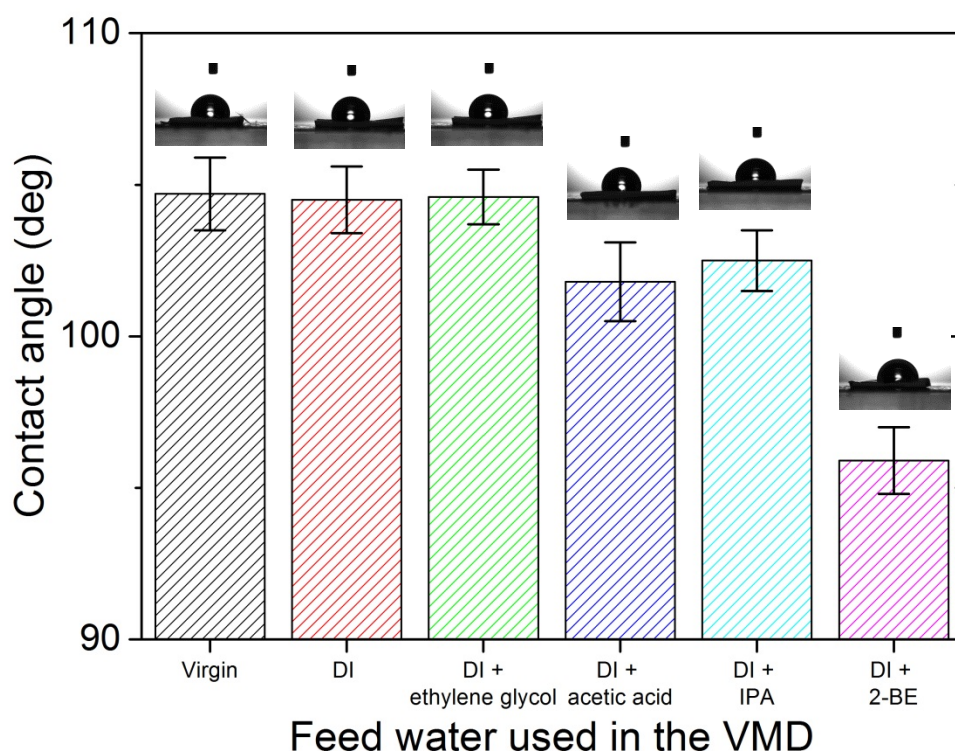
**Figure 41** shows the ATR-FTIR measurement of the shell and lumen sides of membrane samples that have treated VOCs feeds via VMD for 24 h. Ethylene glycol was not tested in this experiment set because of their low vapor pressure and failure to penetrate the membranes. The penetration depth of the FTIR ranged from 1.2 to 2.4  $\mu\text{m}$  for detection spectrum from 2000 to 4000  $\text{cm}^{-1}$ . Membranes that have treated DI water display smallest peak of absorption in the range of 3500 to 3700  $\text{cm}^{-1}$  (Brinkley & Gupta 1998), indicating free hydroxyl (OH) bonds stretching at very low concentration. The free OH bonds represented the trapped water vapor or VOC traces in the HF membrane pores. When analyzing HF membranes that had treated feed water containing acetic acid, IPA or 2-BE, much larger peaks could be observed in the range of 3500 to 3700  $\text{cm}^{-1}$  (Chew, Zhao, Loh, et al. 2017; Murphy & de Pinho 1995). It was contributed by the VOC traces trapped in the membrane pore. The deeper peaks indicate more VOC molecules trapped in the membrane pores on the shell side. Moreover, **Figure 41A** displays that when 2-BE was added into the feed, a large broad peak in the range of 3200-3600  $\text{cm}^{-1}$  appeared, which were H-bounded OH in stretching mode. It represented the liquid water [12,26]. Because of strong surfactant properties of 2-BE, the surface tension of the feed solution decreased greatly, leading to partial pore wetting on the membrane shell side. (Brinkley & Gupta 1998; Kaatze, Pottel & Schumacher 1992). It explained that the feed containing 2-BE had decreasing flux performance in VMD although the salt rejection was maintained high. **Figure 41B** shows the FTIR analysis of the lumen side of the operated HF membranes, indicating that higher amounts of acetic acid and 2-BE than IPA were trapped in the membrane pores at lumen side, while all three samples that had treated the VOCs shows deeper peak in the range of 3500 to 3700  $\text{cm}^{-1}$  than the one had treated DI water. Broad peaks in the range of 3200-3600  $\text{cm}^{-1}$  did not appear in the lumen side of the HF sample that had treated feed containing 2-BE, indicating that the liquid water had not reached the lumen side of the membrane after 24 h operation yet (Chew, Zhao, Loh, et al. 2017).



**Figure 41.** FTIR analysis of membranes after 24 h operation: (A) shell side (feed) (B) lumen side (permeate)

#### 5.4.2 Contact angle

Contact angle had been measured to investigate the effect of the VOCs on the HF membrane. **Figure 42** shows that after treating DI water, or ethylene glycol, the contact angle of the HF membranes hardly changed. After treating acetic acid and IPA, the contact angle of the membranes decreased slightly due to their weak surfactant properties, as some traces of the VOCs started to adhere on the membrane surface. On the other hand, treating feed with 2-BE could result in significant decrease in contact angle of the HF membranes (10%) owing to its relatively strong surfactant properties and partial pore wetting on the membrane surface (Orem et al. 2014).



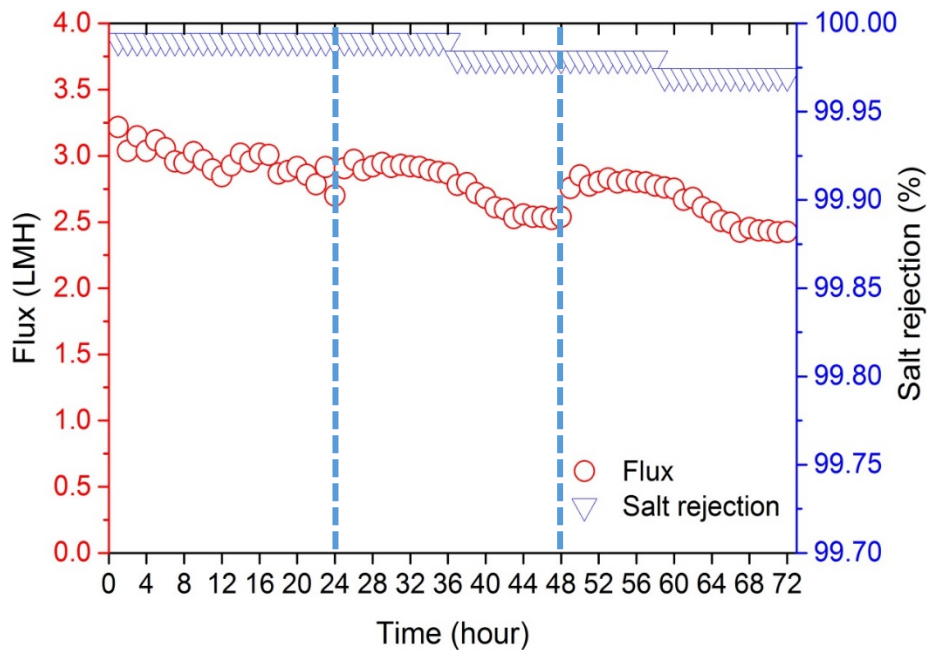
**Figure 42.** Contact angle of membranes after treating various VOCs for 24 h in VMD

## 5.5 Long-term operation performance with feed containing 2-BE

### 5.5.1 Flux

Surfactants in the feed water had been found to cause membrane wetting rapidly (Chew, Zhao, Loh, et al. 2017; Eykens, De Sitter, et al. 2017b). When treating feed that contained 2-BE for 24 h, partial pore wetting appeared. Therefore, a complete pore wetting was expected in long-term operation. Same VMD setup used in previous section were implemented for the long-term operation study. The setup was kept running for 72 h to treat 2L synthetic produced water containing 2000 ppm of 2-BE. Every 24 h the permeate container vessel was emptied and new 2L synthetic produced water with 2000 ppm 2-BE was filled into the feed container (water recovery <60%), and we recorded the flux only when the feed temperature became stabilized at 70° after replacing the feed. **Figure 43** shows that the flux had a gradual decreasing trend during 72 h VMD operation. It was caused by the decrease in 2-BE concentration in the feed

and partial pore wetting of the HF membranes as the existence of the salts had minimal effect on the decrease in the flux (**Figure 39A**). It was worth noting that after the feed concentration was increased back to 2000 ppm after 24 h operation, the flux recovered to some extent although it was still lower than the initial flux. This proved that the decrease in flux over time was caused by the decrease of 2-BE concentration in the feed. After 72 h operation, salt rejection of VMD dropped to 99.97%, which meant that complete pore wetting started to appear as average flux was decreasing comparing three periods of 24 h operation (Chew, Zhao, Loh, et al. 2017; Rezaei et al. 2017). Further measurement was carried out to confirm the status of the pore wetting, which was illustrated in next section.

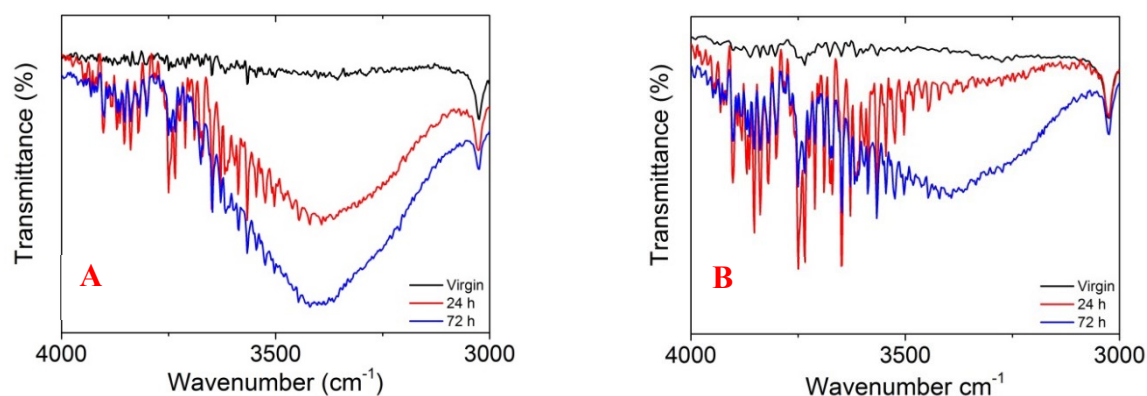


**Figure 43.** Flux of VMD treating synthetic CSG RO brine containing 2-BE for 72 h

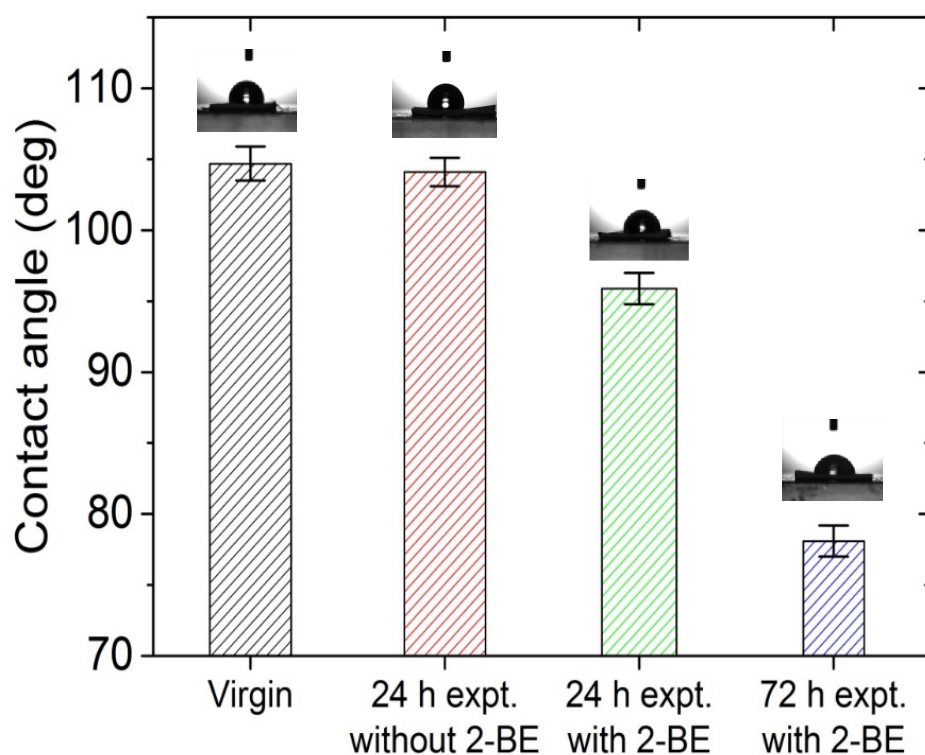
### 5.5.2 Penetration of 2-BE and water through the membrane

FTIR measurement was conducted on the HF membrane that had treated feed containing 2-BE for 72 h. Compared with membrane that treated same feed for 24 h, a deeper broad peak in the range of  $3200\text{--}3600\text{ cm}^{-1}$  could be observed on the membrane shell side, which meant that more severe pore wetting occurred as more liquid water had penetrated the membrane surface and stayed inside of the pores (**Figure 44A**) (Chew, Zhao, Loh, et al. 2017; Lin et al. 2015). Moreover, an analysis on the lumen side shows that the liquid water has further travelled and

reached the lumen side of the HF membranes (**Figure 44B**). This indicated that complete pore wetting started to occur as salt rejection was dropping as well.



**Figure 44.** FTIR analysis of both a) shell and b) lumen sides of membranes after 24 h and 72 h operations using feed with and without 2-BE addition.



**Figure 45.** Contact angle of HF membranes after treating synthetic produced water containing 2-BE after 24 and 72 h operation via VMD



### 5.5.3 Contact angle

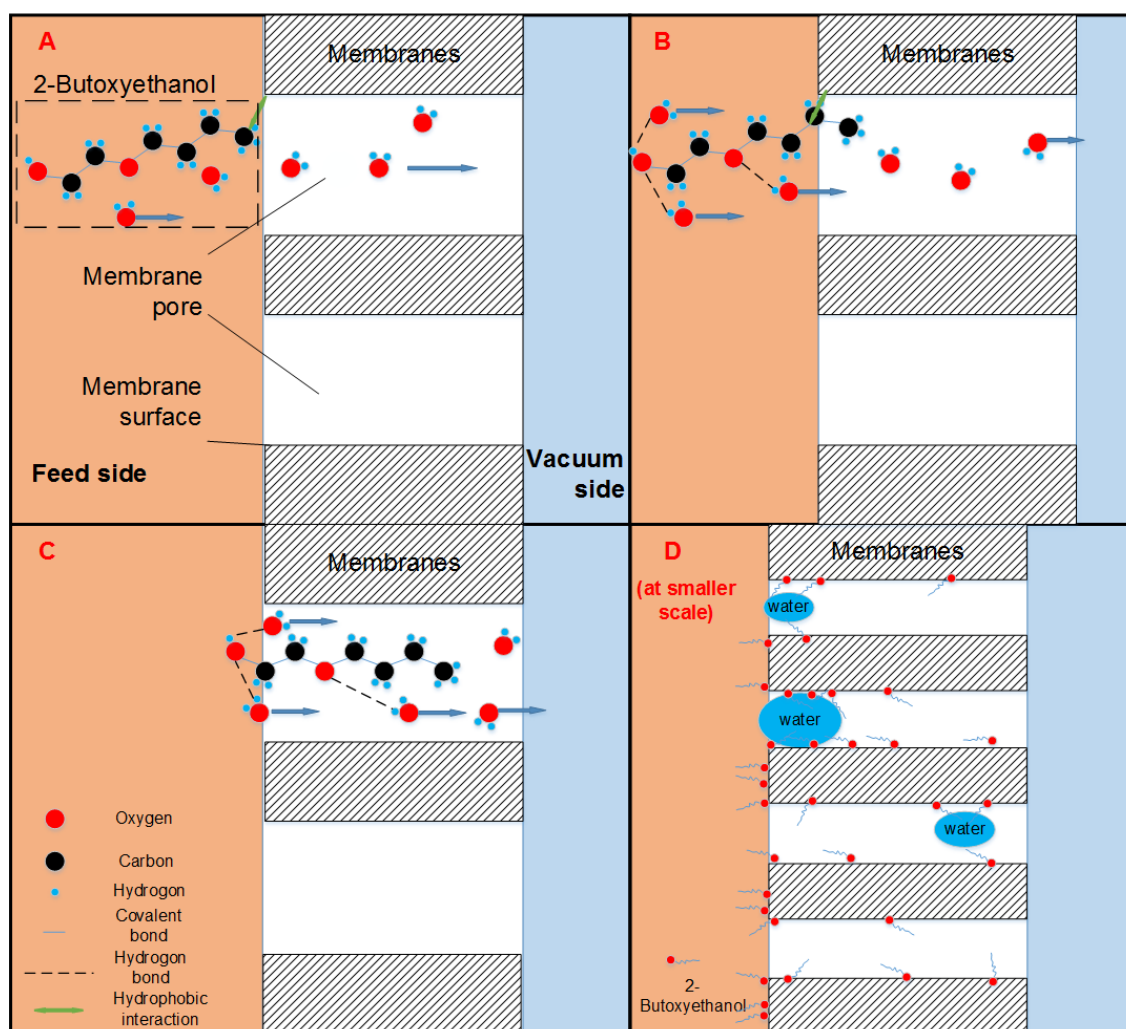
A contact angle measurement had been conducted on the HF membranes after 72 h VMD operation. The existence of minerals in the synthetic produced water had insignificant effect on the contact angle as a marginal decrease from 104.7° to 104.1° was noticed after 24 h operation (**Figure 45**). On the other hand, addition of 2-BE into the synthetic CSG RO brine caused the contact angle of membranes reduced from 104.7° to 95.9° after 24 h VMD operation, and it further dropped to 78.1° after 72 h operation. The decrease in contact angle was caused by both the surfactant properties of 2-BE which adhered on the membrane surface, and pore wetting caused by the 2-BE.

## 5.6 Mechanism of penetration of VOCs

Like some small organic particle, the “adsorption-desorption” mechanism was considered as the cause of the high mobility of the VOCs. In **Figure 46**, 2-BE was selected to explain the mechanism for its noticeable characteristics affecting mass transfer of VOC in MD. Firstly, **Figure 46A** shows that the hydrophobic head (usually an alkyl group of VOCs) of the 2-BE was attracted and attached on the surface of the hydrophobic membrane owing to their hydrophobic interactions (adsorption). Then hydrogen bonds between 2-BE and water molecule was formed. The intra-molecular hydrogen bonds between water and 2-BE were very strong because 3 bonds could be formed (2-BE had two acceptors and one donor) (Brinkley & Gupta 1998) (**Figure 46B**). Fast mass transfer of 2-BE was achieved as it was “pushed” by the water molecules (**Figure 46C**), the hydrophobic interaction was lost during the movement (desorption). The “adsorption-desorption” process can be repeated which promote the further travel of the VOCs through the membrane pores. Nevertheless, some 2-BE molecules would be trapped in the membrane pores due to its high molecule weight and boiling point. At a smaller scale, **Figure 46D** shows that, in MD, partial pore wetting started to appear on the membrane surface pores due to the relatively strong surfactant properties of 2-BE (Chew, Zhao, Loh, et al. 2017). Also, some liquid water may be trapped inside of the membrane pores due to engagement between the water molecule and large amounts of 2-BE previously trapped in the pores by hydrogen bonding. This mechanism applies to other VOCs that have surfactant property and ability to form hydrogen bonds with water. Acetic acid has slightly stronger surfactant strengths and ability to form hydrogen bonds than IPA, and this explained its higher mass transfer rate during VMD in this study even though acetic acid had much lower



vapor pressure than IPA. Also, surfactant strengths of acetic acid are much lower than 2-BE, so partial pore wetting did not occur during 24 h operation. Banat found similar phenomenon when studying on the recovery of dilute acetone-butanol-ethanol solvents from the aqueous solution through MD. Although butanol had the biggest molecular weight and lowest vapor pressure among the three solvents, the flux of butanol was significantly higher than acetone and ethanol at the same conditions (Banat & Al-Shannag 2000). The mechanism of the fast penetration of butanol can be explained as above because butanol has strong surfactant properties and can form hydrogen bonds with water molecules. Therefore, for mass transfer of the VOCs in MD system, strengths of surfactants properties and intra-molecular hydrogen bonding with water molecules seem to play same significant roles as the vapor pressure, which deserve further investigation.



**Figure 46.** Mechanism of the penetration of VOCs: A) 2-butoxyethanol (2-BE) molecules was attracted and adhered onto the membranes surface due to hydrophobic interactions between the

alkyl head on the 2-BE and the hydrophobic surface of the membrane polymer; B) three hydrogen bonds were formed between the 2-BE and water molecules; C) the water vapors “pushed” the 2-BE molecules moving forward through the membrane pores; D) pore wetting started to appear due to the surfactant properties of 2-BE

## 5.7 Conclusion

In this study, series of experiments had been conducted to systemically determine the impacts of various VOCs in feed solution on the VMD performance and membrane properties. Addition of 2-BE, acetic acid, and IPA into feed could increase the flux due to their mass transport. All the tested VOCs, except ethylene glycol, could easily penetrate the membranes as high concentrations of them were found in the permeate, without the occurrence of membrane wetting. High concentrations of the VOCs found in the permeate raised the concerns about pre- or post-treatment of VOCs. It was unexpected to find that 2-BE had highest mobility although it had second lowest vapor pressure among the tested VOCs; the concentration of 2-BE was much higher in the permeate than in the feed. Moreover, due to the strong surfactant property of 2-BE, liquid water had been found in the pores of the membrane that had treated feed containing 2-BE. Also, contact angle of the HF membranes was decreased due to existence of VOCs on the membrane surfaces and wetted pores. A longer operation time would see a further travel of the liquid water through the membranes, a progress from partial pore wetting to complete pore wetting, and the salt rejection hence dropped. Therefore, this study concluded that the VOCs existing in the produced water could have strong impacts on the quality of the final permeate and MD performance. It also found that the strengths of surfactant and intra-molecular hydrogen bond between the water and the VOCs play as important roles as the vapor pressure of the VOCs in MD operation in terms of their mass transfer. It explains that ethylene glycol, a VOC with no surfactant property, had no impact on MD performance and permeate quality, while 2-BE, a VOC with strong surfactant properties and capable of forming strong intra-molecular hydrogen bonds with water, had superior impact on MD flux and permeate quality, although they share close boiling point.

## **CHAPTER 6**

### **Improving Membrane Distillation Permeation Performance by Optimizing Non-solvent in Dope Solution**

## 6.1 Introduction

Membrane distillation (MD) is widely considered as one of the most promising next-generation membrane technologies as its unique mechanism demonstrates strong capacities in the desalination and wastewater treatment applications where traditional membrane technologies are impractical (Deshmukh et al. 2018; McGaughey, Gustafson & Childress 2017). However, MD has not been fully commercialized yet due to several major drawbacks; and one of them is its relatively low permeation performance, which makes this energy-intensive process even less competitive (Eykens, De Sitter, et al. 2017a).

Lack of membranes ideally designed for MD is the major reason for the low permeation performance (Li, Dong & Zhu 2018). Although many kinds of research have been conducted to develop MD membranes with higher permeation, the fabrication cost of these membranes is very high making them unviable for industrial upscaling (Zhang et al. 2018; Zhu, Jiang & Matsuura 2015). Therefore, a simple and effective approach is needed to develop high-performance MD membranes. An ideal MD membrane should have a highly hydrophobic surface, narrow pore size distribution and large porosity to achieve high permeation flux (Qiu et al. 2018; Shi et al. 2012). Considering the effect of heat loss in MD, it is also essential to optimize the membrane thickness to balance the trade-off between the flux performance and thermal efficiency (Wang, Teoh & Chung 2011).

Polyvinylidene fluoride (PVDF), a low-surface-tension thermoplastic fluoropolymer, is favored as the base material for MD membranes due to its low thermal conductivity, high chemical resistance, and mechanical strength (García-Payo, Essalhi & Khayet 2010; Venault et al. 2014). Unlike other non-reactive hydrophobic polymers, PVDF can be used to fabricate cost-effective membranes as it can be easily dissolved in various common solvents. Therefore, multiple fabrication approaches have been implemented using PVDF as the dope solution (Tao et al. 2013). Electrospinning is one of the fabrication methods that has been extensively employed to develop nanofibrous PVDF membranes with high permeation flux owing to their larger mean pore size and porosity. However, these electrospun nanofibrous membranes face wetting issues, which lead to a rapid salt rejection drop and a sudden flux increase owing to their low liquid entry pressure (LEP) (Liao et al. 2013b). Moreover, the electrospinning technique is not practical for mass production (Ahmed, Lalia & Hashaikh 2015).

Non-solvent induced phase separation (NIPS) process, is another method that has been comprehensively studied for MD membrane development. The PVDF MD membranes made via NIPS method generally have a smaller mean pore size and porosity than the nanofibrous membranes prepared with the same dope solution; thus, demonstrating lower permeation flux in MD (Buonomenna et al. 2007; Munirasu et al. 2017). In general, the NIPS PVDF membranes have finger-like macrovoids underneath their thick skin layers, and dense sponge structure for the bottom layers (Bonyadi & Chung 2009; Pinnau & Koros 1993). It has been reported that membranes with macrovoids have multiple disadvantages like high sensitivity to wetting, high tendency towards scaling and intra-pore salt precipitation, which lower membrane stability in long-term MD operation (Hung et al. 2016). Besides electrospinning and NIPS, thermally induced phase separation (TIPS) method was also employed for MD membrane fabrication. Jung et al. (2018) found that HF membranes with macrovoid-free bicontinuous (open pores) structure can be developed using TIPS method and proper diluent ratio as it allowed both liquid-liquid (L-L) and solid-liquid (S-L) demixing to occur at the right time (Jung et al. 2018). However, TIPS is not a cost-effective method due to its technical limitations (e.g., high heat energy consumption) (Sukitpaneenit & Chung 2009).

It is more cost-effective and practical to improve the NIPS method to obtain high-performance MD membranes. Wu et al. developed PVDF HF membrane with the incorporation of additives. Their results indicated improved permeation flux but still quite low (<10 LMH at feed temperature of 60 °C) (Wu, Jiang & Hu 2018). The main issues of NIPS membranes are their dense skin layer and the macrovoid structure underneath it. Thus, there is a need to optimize the NIPS membrane fabrication method to improve the membrane morphology and properties that could lead to improve MD performance, with the consideration of commercial perspectives (Zhang, Yang, et al. 2013).

To prepare NIPS PVDF membranes without macrovoids, the main strategy is to delay the L-L demixing rate (Smolders et al. 1992). Various techniques have been employed to delay the L-L demixing rate, such as increasing the polymer concentration or molecular weight, using weak coagulants, exposing the casting dope solution to water vapor before immersion into the cogulation bath, and decreasing the coagulant bath temperature (Buonomenna et al. 2007; Munirasu et al. 2017; Zhang, Yang, et al. 2013). However, these techniques either sacrifice membrane porosity or hinder mass production due to the high economic and environmental costs. Recently, Nejati et al. (2015) and Chang et al. (2017) reported that the L-L demixing rate

could be greatly decreased by using triethyl phosphate (TEP) as polymer solvent owing to its higher viscosity and lower affinity with water (Nejati et al. 2015; Yeow, Liu & Li 2003). Hence, it is possible to fabricate macrovoid-free membranes without using costly approaches. Although the membranes prepared using TEP as a polymer solvent have demonstrated better MD performance in both short and long-term operations, their improvement is limited due to their relatively dense skin layers and small surface porosity. These characteristics are common among PVDF membranes prepared using NIPS method and water as coagulant (Abed et al. 2012; Chang et al. 2017). Therefore, further improvement in the inner structure and surface morphology of the NIPS HF membranes is required to improve the permeation performance in MD process.

In this paper, the effect of various non-solvents (NSs) in the polymer dope solution on the inner structure and surface morphology of the membranes was investigated. The viscosity and water affinity of the dope solutions were controlled to manipulate the sequence of L-L and S-L demixing rates during the NIPS process to change the membrane morphology. Permeation performance of the HF membranes in MD was evaluated based on the improvement in membrane morphology and mean pore size. The results indicate that the optimization of the polymer, solvent, and NS compositions in the dope solution is essential to design high-performance (high flux with long-term stability) membranes for MD processes.

## **6.2 Experimental method**

### **6.2.1 Determination of dope solution recipes**

In the NIPS approach, the sequence of L-L demixing and S-L demixing strongly affects the membrane morphology (Lin et al. 2002). In general, S-L demixing (crystallization) takes a much slower pace than L-L demixing. If L-L demixing occurs at a very fast rate during the NIPS process, macrovoid structures are formed underneath the skin layer of the membrane and the remaining layers are dominated by sponge-like structures (cellular pores). On the other hand, if L-L demixing lags S-L demixing process, then large spherulitic crystal structures become dominant. Viscosity and water affinity of the PVDF dope solution were recognized to strongly influence the NIPS demixing process; hence, they were chosen to optimize the membrane morphology. The water affinity was determined by Hansen solubility (dipole force) of the liquid chemical. Generally, increasing solution viscosity or decreasing water affinity

leads to a delayed L-L demixing and promotes S-L demixing in NIPS process, so spherulitic crystal structures will become dominant (Chang et al. 2017; Mansourizadeh & Ismail 2011; Smolders et al. 1992). Therefore, in this study, high molecular weight PVDF was chosen for all the recipes as the dope solution has high viscosity even at low concentration. Triethyl phosphate (TEP) was used as a solvent due to its low water affinity and high compatibility with PVDF. To manipulate the demixing rate in phase inversion, NSs with various combination of viscosity and Hansen solubility (water affinity) were selected. In addition, the selected NSs must comply with the following requirements:

- (i) forms a homogenous polymer solution at 80 °C after mixing NS and remains stable for at least 10 h once the dope solution cools down to room temperature
- (ii) provides suitable dope solution viscosity for HF membrane fabrication
- (iii) has low toxicity and causticity; less harmful to the human and ecological system
- (iv) cost-effective

After careful consideration, toluene, acetone, and DBP were used as NS in the dope solution. The main properties of the chemicals used in the present study are listed in **Table 8**.

**Table 8.** Hansen solubility parameters at 25°C, molecular weight, density, partition coefficient, and viscosity of various chemicals used in this study

Materials	Viscosity (cP)	Hansen solubility, $\delta_p$ (J cm <sup>-3</sup> ) <sup>1/2</sup>	Molecular weight (g/mol)	Density (g mol <sup>-1</sup> )	Partition coefficient, log K <sub>ow</sub>
PVDF (HSV 900)	N/A	12.1	N/A	1.78	N/A
Water	0.89	16	18	1	-
N-Methyl-2- pyrrolidone (NMP)	1.65	12.3	99	1.03	-0.38

<b>Triethyl phosphate (TEP)</b>	1.46	11.5	182	1.07	0.8
<b>Toluene*</b>	0.56	1.4	92	0.87	2.73
<b>Acetone*</b>	0.31	10.4	58	0.78	-0.24
<b>Dibutyl phthalate (DBP)*</b>	19.6	8.6	278	1.05	4.5

\*NSs used in this study

## 6.2.2 Preparation of dope solution and fabrication of PVDF hollow fiber membranes

PVDF was used as the base polymer in this study. Homogenous polymer dope solutions were prepared by dissolving dry PVDF powder (11 wt.%) in the mixture of TEP (89 wt.%) and NS at 80 °C under continuous stirring for 72 h. The various combinations of TEP and NS used to prepare the dope solutions, and the names of corresponding HF membranes are listed in **Table 9**. A control sample, NMP0, was also prepared same way with TEP0, except that NMP was used as solvent instead of TEP.

**Table 9.** Name conventions and dope solution compositions for hollow fiber membrane fabrication in this study.

Sample	NS chemical	Dope concentration (wt.%)			
		PVDF	NMP	TEP	NS
<b>NMP0</b>	-	11	89.0	-	-
<b>TEP0</b>	-		-	89.0	-
<b>TEPA-1</b>	Acetone		-	80.1	8.9



<b>TEPA-2</b>	Acetone		-	71.2	17.8
<b>TEPD-1</b>	DBP		-	80.1	8.9
<b>TEPD-2</b>	DBP		-	71.2	17.8
<b>TEPT-1</b>	Toluene		-	80.1	8.9
<b>TEPT-2</b>	Toluene		-	71.2	17.8

The prepared dope solutions were then poured into the syringe pump (Model 500D, Teledyne Isco, USA) and left to degas at room temperature for 24 h before spinning. All the HF membranes were fabricated using the dry-jet wet spinning process. **Table 10** lists the detailed spinning parameters, which were kept constant for the fabrication of all HF membranes. The as-spun HF membranes were stored in a distilled water tank for three days after the phase inversion process. The water was changed daily to completely remove the residue chemicals from the membranes. After three days, the membranes were dried at room temperature.

**Table 10.** PVDF hollow fiber spinning conditions

Dope extrusion rate (mL/min)	5.0
Bore fluid flow rate (mL/min)	1.9
External coagulant and bore fluid	Tap water
Air gap (cm)	2
Dope solution temperature (°C)	25
Coagulant bath and spinneret temperature (°C)	25

Ten fibers of each PVDF HF membrane fabricated with various dope solutions were used to make modules having a total surface area of 82 cm<sup>2</sup>. The internal diameter of the membrane module was 8 mm.

### **6.2.3 Characterizations**

The viscosity of the PVDF dope solutions was measured at room temperature using a dial viscometer with spindle #4 (LVT, Brookfield, USA). The readings were taken after full stabilization was achieved. The value of viscosity was interpreted from the table provided by the manufacturer.

The membrane surface roughness was measured using atomic force microscopy (AFM, Dimension 3100 Scanning Probe Microscope, Bruker) in tapping mode. A scanning area of 10.0 μm x 10.0 μm was used for all the membrane samples. Each sample was scanned three times at randomly chosen locations to obtain the average root mean square roughness (R<sub>q</sub>).

The mean pore size of the HF membrane samples was measured using a PMI liquid-liquid permeameter (LLP-1100A, Porous Materials, Inc.) with a resolution of 1 in 60,000 and a flow resolution of 0.0001 cc/min. Isobutanol was used as the fluid to measure the mean pore size. An average value for the mean pore size was obtained from three measurements taken for each HF membrane sample.

Differential scanning calorimetry (DSC) was conducted using DSC 2000 (TA Instruments) to measure the heat flow of the polymer samples during the melting process. Crystallinity was calculated based on the obtained enthalpy. Average of three measurements were reported for each sample.

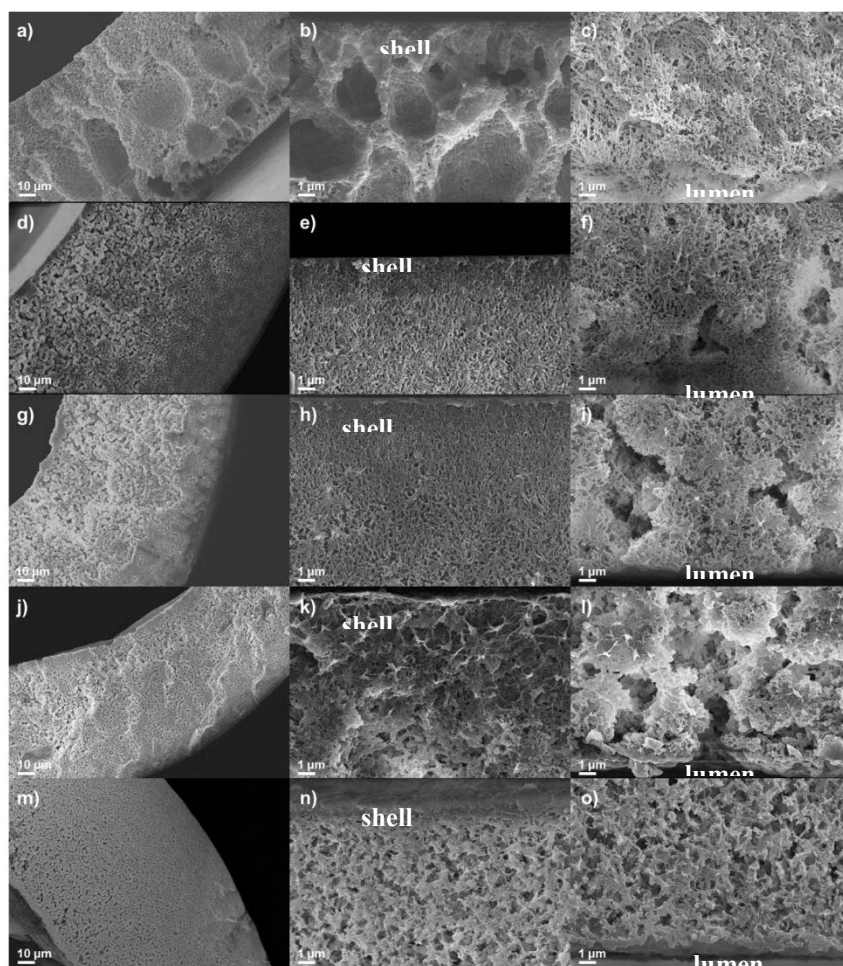
The mechanical properties of the HF membrane samples were measured by a bench-type material tester (Lloyd Instruments, Ametek) with a starting gauge length of 25 mm and a stretching rate of 50 mm/min. Average values were obtained from five tests conducted for each sample.

## **6.3 Results and discussion**

### **6.3.1 Effect of various NS on the inner structure of the hollow fiber membranes**

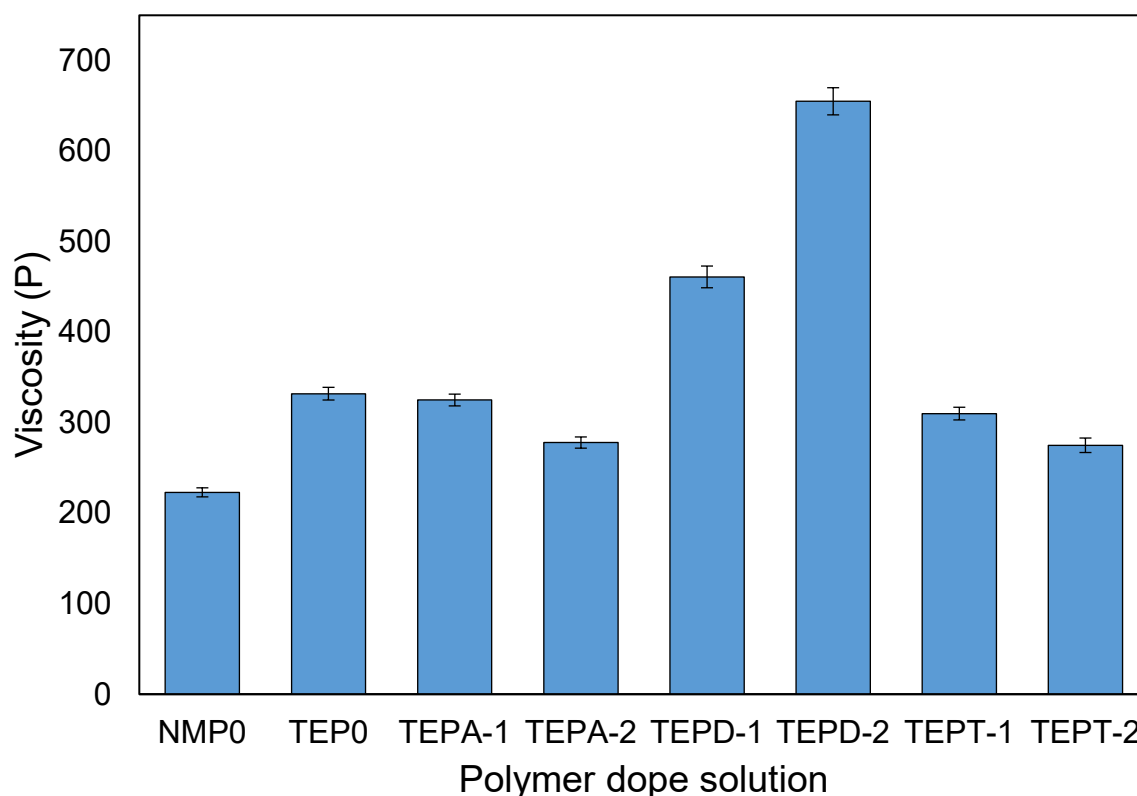
The inner structures of HF membranes were determined by the dope solutions, and they can be indirectly adjusted by the change of solvent and NS.

**Figure 47(a-c)** shows that the HF membranes using NMP as solvent (NMP0) consisted of asymmetric inner structures: the membranes have large macrovoids underneath their thick skin layers, and dense sponge structure for the bottom layers. On the other hand, the formation of macrovoids structures was prevented when replacing NMP with TEP as solvents in the dope solution. **Figure 47(d-f)** illustrates the morphology of TEP0 with macrovoid-free fibrous structures at shell and spherulitic structures at lumen, composed of large open pores. Nejati et al. obtained a flat sheet membrane with similar asymmetric morphology using TEP as the dope solvent. He suggested that the initial L-L demixing created a less permeable wall to NS diffusion which delayed the demixing in the sublayers and led to the spherulitic morphology at bottom layers (Nejati et al. 2015).



**Figure 47.** SEM images displaying the cross-section of hollow fiber membranes cast from (a-c) 11 wt.% PVDF in NMP; (d-f) 11 wt.% PVDF in TEP; 11 wt.% PVDF in TEP with 17.8 wt.% NS of (g-i) acetone; (j-l) DBP and (m-o) toluene.

The optimization of the HF membrane inner structures is expected to improve MD permeation performance, which can be achieved by manipulating the viscosity and water affinity of the polymer solutions by incorporating various NS like acetone, DBP and toluene into the dope solution. Acetone has a much lower viscosity than TEP, so the addition of 20 wt.% acetone into the polymer solution results in the reduction of dope solution viscosity from 33,200 to 27,800 cP. In addition to the decreased viscosity, the polymer solutions containing acetone have increased water affinity because of the low partition coefficient of acetone. Therefore, a faster L-L demixing occurred in HF membranes prepared using acetone-containing dope solution, so TEPA-2 had a different morphology from TEP0. TEPA-2 (**Figure 47i**) shared similar membrane inner structure with that of TEP0 (**Figure 47f**), which is dominant with large spherulitic crystal structures at the lumen side of HF membranes; however, it had denser and thicker layers comprising fibrous structures at the shell sides of the HF membrane. Moreover, with decreased membrane thickness, the inner diameters of TEPA-2 was larger than TEP0 due to the promoted L-L demixing (**Table 11**) (Chang et al. 2017). In general, a membrane fabricated with a faster L-L demixing has thinner membrane thickness. However, the improvement in MD performance using TEPA-1 and TEPA-2 were not expected as the benefits of a decrease in membrane thickness can be offset by the potential decrease in the porosity and pore size due to the change in the morphology.



**Figure 48.** Viscosity of various dope solutions

The addition of NS of DBP into the polymer solution led to a significantly different HF membrane structure from TEP0 and TEPA-2. The dope solution incorporated with DBP has a significantly higher viscosity (**Figure 48**) and lower water affinity (**Table 8**); thereby, leading to a greatly promoted S-L demixing (crystallization). **Figure 47j-l** shows that TEPD-2 is composed of large spherulitic crystal nodes through the whole cross-section of the HF membrane. Unlike TEP0 and TEPA-2, the spherulitic structures with large open pores were also dominant at the shell side. The spherulitic structures were also observed by Sukipaneenit and Chung when weak coagulant(e.g., ethanol) was used in the coagulation bath, as the L-L demixing rate was greatly reduced and crystallization became dominant (Sukitpaneenit & Chung 2009). A membrane containing large open pores is likely to have a low LEP, and is prone to wetting in MD.

On the other hand, HF membranes fabricated with the polymer dope solution containing toluene produced very distinct HF membrane structure. The polymer solution of TEPT-2 had reduced viscosity of 27,500 cP and reduced water affinity owing to its low partition coefficient.

As such, the usage of a dope solution containing toluene led to a unique NIPS process that resulted in the formation of inner structures. Different from the asymmetric morphology of TEP0, a symmetric inner structure was observed in the toluene based HF membranes (**Figure 47m-o**). The large spherulitic crystal structures with open pores, as can be found in TEP0, TEPA-2, and TEPD-2, were not observed in TEPT-2. The HF membrane confirmed a uniform bicontinuous structure comprising of interlinked small spherulitic crystal structures, which had pores with the same size through the membranes. The absence of the large spherulitic crystal structures with open pores at the lumen side (**Figure 47l**) occurred due to the presence of toluene in the dope solution. For comparison, TEPA-2, having low dope viscosity, had large spherulitic crystal structures at the lumen side. It is assumed that the combination of both decreased water affinity and viscosity would contribute to a balance between the L-L demixing and S-L demixing, which would promote the diffusion of the dope solution into the coagulants without fast solidification. Therefore, all portions of the dope solution have the same diffusion and solidification rate, which results in the formation of bicontinuous structures. In the literature, our work is the first study to successfully fabricate HF membranes with macrovoid-free bicontinuous inner morphology without using weak coagulant like ethanol in the coagulation bath.

### 6.3.2 Porosity and pore size distribution

Table 11 shows the porosity and pore size distribution of the HF membranes. The formation of various membrane structures was strongly affected by the NIPS process, which was manipulated by adjusting the viscosity and water affinity of the polymer dope solution (García-Payo, Essalhi & Khayet 2010; Li, Xu & Yu 2010; Tao et al. 2013). Owing to its fastest L-L demixing rate, NMP0 possessed the lowest porosity and smallest mean pore size among all the samples despite its macrovoid formations. On the other hand, HF membranes fabricated using dope solution with TEP solvent showed higher porosity. It is because higher viscosity and lower water affinity of dope solutions led to the formation of spherulitic crystal structures by the slow S-L demixing (Ahmad, Otitoju & Ooi 2018; Lin et al. 2006). Addition of acetone as NS reduced the viscosity and increased the water affinity of the dope solution, which resulted in the formation of fibrous structure layers at the shell side (**Figure 47h**). Thus, TEPA-1 and TEPA-2 demonstrated reduced porosity and mean pore size. In contrast, TEPD-2 had the highest mean pore size among all the samples due to its spherulitic crystal structures that resulted from the much-delayed L-L demixing. On the other hand, the addition of toluene into

the polymer solution increased the porosity of the HF membranes because of its bicontinuous structures with open pores. The toluene-based membranes also demonstrated higher porosity (86.2% for TEPT-2), which contributed to the improvement of mass transfer efficiency in MD.

**Table 11.** Comparison of porosity, mean pore size, thickness, and inner and outer diameters of hollow fiber membranes using various dope solutions

Sample	Porosity (%)	Mean pore size ( $\mu\text{m}$ )	$\Phi_{\text{outer}}$ ( $\mu\text{m}$ )	$\Phi_{\text{inner}}$ ( $\mu\text{m}$ )	Thickness ( $\mu\text{m}$ )
NMP0	$75.1 \pm 0.9$	$0.0263 \pm 0.0009$	$1072 \pm 13$	$796 \pm 15$	$138 \pm 10$
TEP0	$81.8 \pm 1.0$	$0.0477 \pm 0.0012$	$968 \pm 16$	$618 \pm 15$	$175 \pm 12$
TEPA-1	$80.5 \pm 1.2$	$0.0395 \pm 0.0011$	$978 \pm 12$	$642 \pm 15$	$168 \pm 12$
TEPA-2	$78.5 \pm 1.2$	$0.0263 \pm 0.0015$	$972 \pm 12$	$662 \pm 16$	$155 \pm 9$
TEPD-1	$81.6 \pm 1.5$	$0.3520 \pm 0.0021$	$966 \pm 17$	$640 \pm 21$	$163 \pm 15$
TEPD-2	$80.3 \pm 1.7$	$0.4242 \pm 0.0028$	$940 \pm 25$	$650 \pm 22$	$145 \pm 12$
TEPT-1	$83.2 \pm 1.5$	$0.0772 \pm 0.0020$	$1079 \pm 12$	$719 \pm 16$	$180 \pm 14$
TEPT-2	$86.2 \pm 1.4$	$0.0815 \pm 0.0019$	$1099 \pm 14$	$719 \pm 16$	$190 \pm 13$

The thickness of the HF membrane varied although the same procedure was used to prepare all the dope solutions and membranes. NMP0 had the lowest thickness among all the samples owing to the fast L-L demixing promoted by the low viscosity and high water affinity of the dope solution. Whereas, TEPT-2 experienced elevated diffusion of the dope solution and S-L demixing process causing it to be the thickest among all the samples.

### 6.3.3 Polymer crystallinity and mechanical strength

The degree of the crystallinity in the PVDF membrane is dependent on the level of crystallization during the NIPS process, which can be critically affected by the addition of NSs into the dope solution. As a semi-crystalline polymer, PVDF can stay at either crystalline or amorphous state, and the demixing mechanism plays a critical role during the phase inversion. A fast L-L demixing of the polymer solution with a strong NS usually forms PVDF at the amorphous state (Wu, Jiang & Hu 2018). For this reason, NMP0 had the highest amount of PVDF polymer at amorphous state with the lowest crystallinity of 35% (**Table 12**). NMP0 also showed the highest tensile strength and strain at break among all the samples. Generally, a fast L-L demixing rate in polymer dope solution forms membranes with dense fibrous sponge structures, which have higher mechanical strength and lower crystallinity (Zhang, Yang, et al. 2013). On the other hand, when the L-L demixing is delayed during the phase inversion process, the inner structure of the membranes will change from fibrous sponge structure to spherulitic crystal structure. Membranes with spherulitic crystal structures have low tensile strength and elongation at break; as such, they are more fragile (Chang et al. 2017). Replacing NMP with TEP as a solvent in the polymer solution led to the delayed L-L demixing; therefore, the crystallinity of TEP0 greatly increased but its mechanical strength deteriorated.

TEPA-2 demonstrated improved tensile strength (from 2 to 2.2 MPa) and strain (from 0.57 to 0.62) while its crystallinity decreased, which was consistent with its fibrous structure morphology (**Figure 49**). The fibrous structures resulted from using acetone as an NS, which increased the L-L demixing rate by lowering the viscosity and increasing the water affinity of the dope solution. On the other hand, the addition of DBP into dope solution formed membranes with large spherulitic crystal structures that resulted in high Young's modulus of 8.8 MPa and low elongation of 0.16. The high viscosity and low water affinity of DBP considerably hindered the L-L demixing process, and S-L demixing became dominant in the phase inversion process. Hence, the crystallinity of TEPD-2 is also the highest (50%) among all the tested samples. Bonyadi and et al. (2009) also found that the delayed demixing resulted in high Young's modulus of the fabricated membranes (Bonyadi & Chung 2009). Any further decrease in the tensile strength and elongation at break of the HF membranes caused by phase inversion may damage the mechanical integrity.



The addition of toluene into the polymer solution exhibited similar effects to that of DBP on the HF membrane properties. As a result of the slower L-L demixing rate, the crystallinities of TEPT-1 and TEPT-2 were slightly higher than those of TEP0 despite the lack of large spherulitic crystal structures. The membranes also had decreased tensile strengths and strains at break compared with TEP0, but they were much higher than those of the HF membranes prepared using a dope solution containing DBP as NS. This is because the distinct bicontinuous structures were well interconnected with the nodes. It can be concluded that TEPT-2 containing bicontinuous inner structures with high mean pore sizes can still maintain mechanical integrity, which makes it suitable for MD applications.

**Table 12.** Comparison of mechanical strength and crystallinities of hollow fiber membranes using various dope solutions

<b>Sample</b>	<b>Crystallinity (%)</b>	<b>Tensile strength at break (MPa)</b>	<b>Strain at break</b>	<b>Young's modulus (MPa)</b>
<b>NMP0</b>	35.2 ± 1.3	2.83 ± 0.03	0.65 ± 0.03	4.35 ± 0.17
<b>TEP0</b>	43.5 ± 2.0	2.04 ± 0.02	0.57 ± 0.05	3.60 ± 0.33
<b>TEPA-1</b>	41.3 ± 1.6	2.17 ± 0.03	0.60 ± 0.05	3.63 ± 0.24
<b>TEPA-2</b>	40.3 ± 0.6	2.28 ± 0.01	0.62 ± 0.03	3.68 ± 0.12
<b>TEPD-1</b>	46.4 ± 2.2	1.92 ± 0.01	0.35 ± 0.01	5.51 ± 0.18
<b>TEPD-2</b>	50.6 ± 2.1	1.45 ± 0.02	0.16 ± 0.01	9.07 ± 0.16
<b>TEPT-1</b>	44.9 ± 1.5	1.95 ± 0.02	0.44 ± 0.02	4.43 ± 0.16

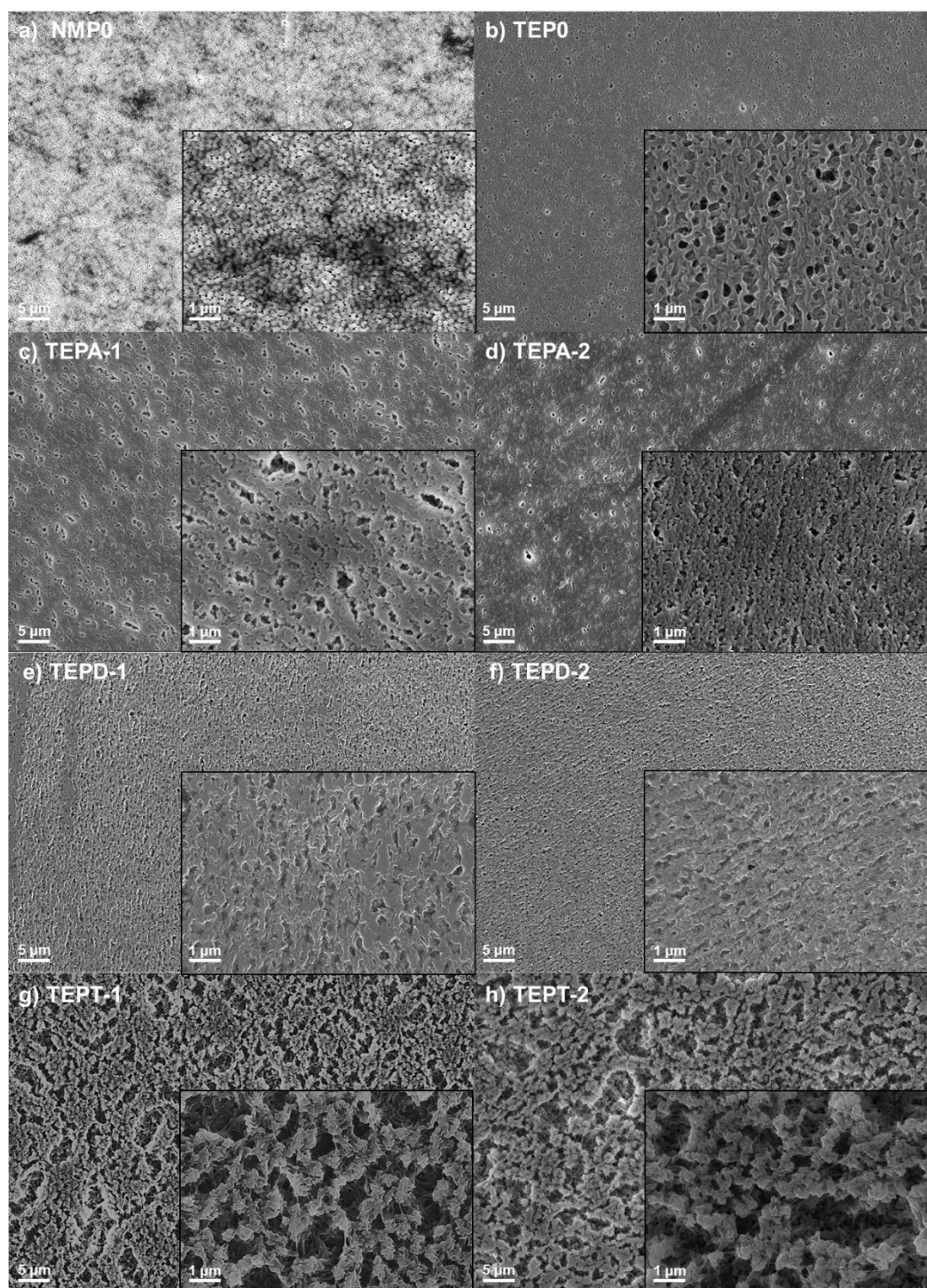
<b>TEPT-2</b>	$46.6 \pm 2.3$	$1.76 \pm 0.01$	$0.32 \pm 0.01$	$5.51 \pm 0.15$
---------------	----------------	-----------------	-----------------	-----------------

### 6.3.4 Surface morphology, contact angle, and surface roughness

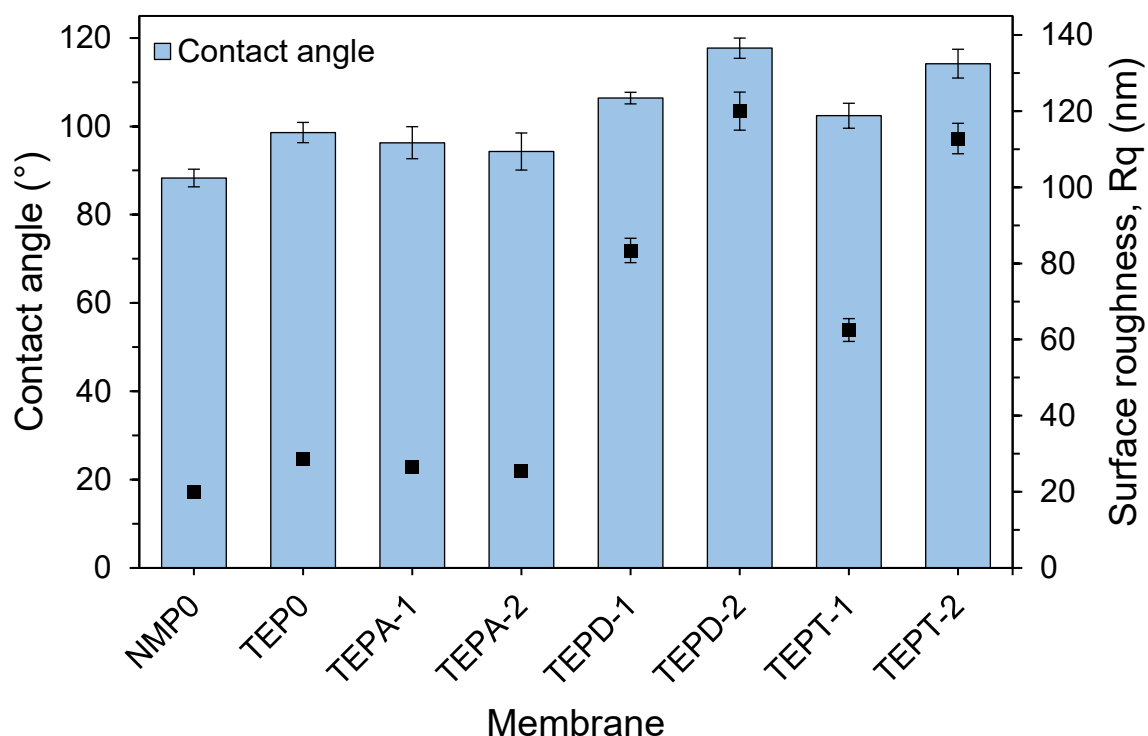
**Figure 49** shows the surface morphology (shell skin) of the HF membranes that are greatly affected by the phase inversion process. A slow L-L demixing usually results in a delayed solidification of the surface layer, so the skin layer has larger surface pore sizes and rough surface. TEPO (**Figure 49b**) consisted of significantly larger surface pores than NMP0 (**Figure 49a**). In general, the surface hydrophobicity depends on the surface roughness; increasing the surface roughness increases the surface hydrophobicity which is represented by the contact angle of water droplet (Franken et al. 1987). For NMP0, a fast L-L demixing process caused a fast solidification of the surface layer, resulting in a smooth membrane surface with a roughness of 20.1 nm and a lower contact angle of 88.3° (**Figure 50**). Similar results can be found in the literature where the membranes prepared using NMP as solvent had lower contact angles (Chang et al. 2017). In the same way, the addition of acetone into the PVDF dope solution decreased the surface pore size and contact angles as acetone promoted the L-L demixing by decreasing the viscosity of the PVDF solution (**Figure 49c, d**).

On the other hand, **Figure 49e, f** shows that the addition of DBP into the polymer solution leads to a dense skin at the shell side of the membrane despite its increased mean pore size. It is assumed that the significant increase in the solution viscosity would greatly delay the L-L demixing, suggesting that the NS coagulant (water) would diffuse slowly through the dope solution and form smaller pores on the shell skin. Despite its dense surface skin, the mean pore sizes of TEPD-1 and TEPD-2 were much higher than the ones of other samples due to its spherulitic structures under the shell skin. TEPD-2 obtained the highest surface roughness of 120.0 nm and contact angle of 117.7° owing to the high surface peaks formed during the NIPS process dominated by S-L demixing process. In contrast, the membranes fabricated from the toluene containing dope solution displayed very distinct surface morphology. **Figure 49g, h** illustrates that both TEPT-1 and TEPT-2 have more porous skins than the ones observed in other samples due to their delayed L-L demixing. Further increase in the weight ratio of toluene in the dope solution brought about an increase in the surface pore size. The surface roughness and contact angle of TEPT-2 are the second highest (112.8 nm) among all the samples. The

porous surface layer with an improved hydrophobicity can contribute to a higher mass transfer rate in MD for TEPT-2.



**Figure 49.** SEM images displaying the surface morphology of hollow fiber membranes cast from (a) 11 wt.% PVDF in NMP; (b) 11 wt.% PVDF in TEP; 11 wt.% PVDF in TEP with NS of (c), (d) acetone; (e), (f) DBP; (g), (h) toluene.



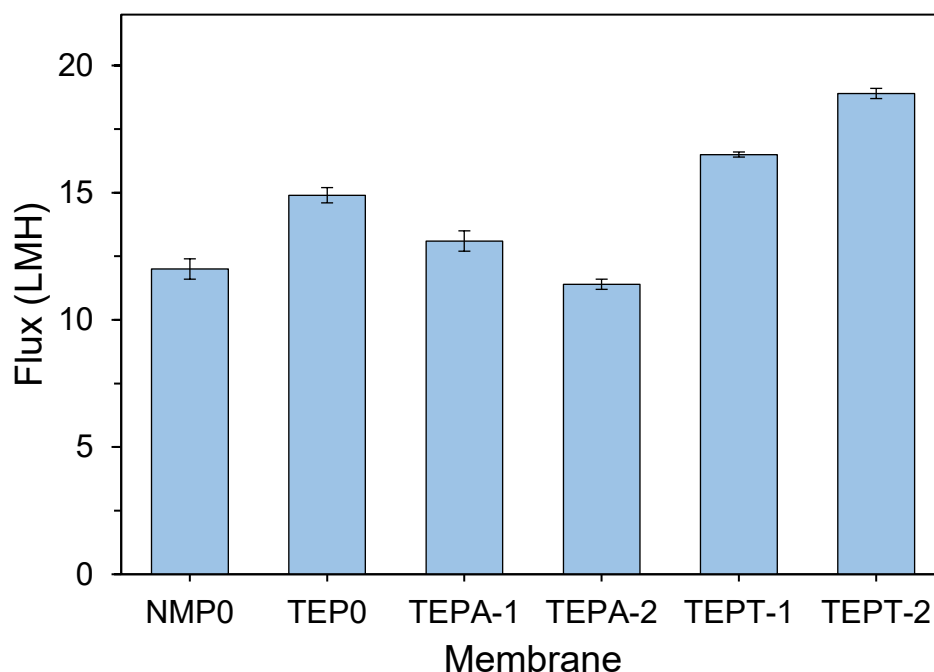
**Figure 50.** Contact angle of hollow fiber membrane shell surface by using dope solutions containing various NSs

### 6.3.5 MD flux performance

#### 6.3.5.1 Comparison of MD performance using various membranes

**Figure 51** shows the flux permeation of different membranes in direct contact membrane distillation. Given that the same high salt rejection of 99.99% is observed, the HF membrane samples demonstrate various permeation performance as their morphologies and properties are significantly different. TEP0 has higher water flux than NMP0 possibly due to its increased porosity and mean pore size. TEPA-2 had a lower flux than NMP0 although they consisted of similar porosity, mean pore size and contact angles. The increased thickness of TEPA-2 could be the main contributor to the increased mass transfer resistance. On the other hand, the addition of DBP into the dope solution presented large mean pore sizes, which is highly susceptible to pore wetting. Consequently, both TEPD-0 and TEPD-1 suffered from rapid

wetting within half an hour of starting the operation; hence their results are not demonstrated in **Figure 51**. TEPT-2 showed an improved permeation performance over TEP0, which had a significant increase from 14.9 to 18.9 LMH. The much-improved inner structure with large porosity and mean pore size offset the large thickness of TEPT-2; in addition, this membrane had much reduced mass transfer resistance at membrane surface due to its porous skin layer (**Figure 49h**). Therefore, TEPT-2 had the highest flux among all the membrane samples.

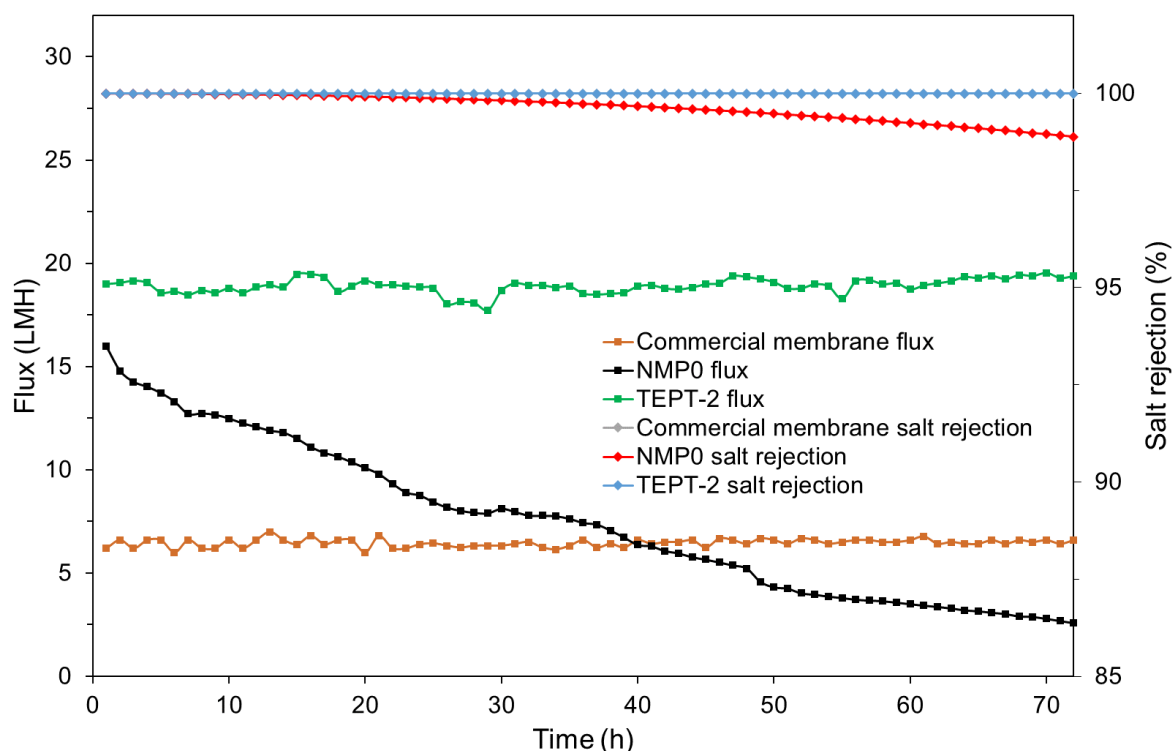


**Figure 51.** Flux permeation comparison of membrane samples prepared by using dope solutions containing various NS in direct contact membrane distillation

#### 6.3.5.2 Long-term operation of membrane distillation

**Figure 52** presents the flux performances of a commercial membrane and the membranes using a dope solution of PVDF in NMP and TEP. To test the operational viability of the samples in long-term applications, the permeation performance of TEPT-2 was tested and compared with the control group of NMP0 and the commercial HF membranes in the same configuration for 72 h. The commercial HF membranes demonstrated a stable low flux of 6.4 LMH. On the other hand, NMP0 had a higher initial flux, but the flux and salt rejection steadily decreased during the 72-h operation. The deteriorated permeation performance can be caused by the partial pore wetting. On the other hand, TEPT-2 had a high and stable flux for 72 h operation

owing to its bicontinuous structure and porous skin morphology. TEPT-2 showed no sign of wetting as it maintained a high salt rejection of 99.99%. The performance test results confirm that the addition of toluene into the dope solution produces high-performance HF membranes with improved flux, while maintaining high rejection of inorganic salts in the feed. This fabrication strategy can be easily applied, which makes it feasible for mass production of high-performance MD membranes.



**Figure 52.** Flux performance of the commercial membrane, NMP0 and TEPT-2

## 6.4 Conclusions

The effects of various NSs in the dope solution on the membrane inner structure and surface morphology of HF membranes were investigated to improve the MD performance. The viscosity and water affinity of the dope solution were controlled to manipulate the sequence of L-L and S-L demixing rates of NIPS process to obtain various membrane morphology. Permeation performance of the HF membranes in MD was evaluated based on the improvement in membrane morphology and mean pore size. The sequence of L-L and S-L demixing rates between solvent and coagulant in NIPS was determined from the viscosity and water affinity of the dope solution. The mixing of NSs with various properties into the dope solution resulted

in very different morphologies and properties of the membrane samples. The results indicated that a bicontinuous inner structure with porous shell skins could be achieved by adding toluene into the dope solution. TEPT-2 demonstrated significant improvement in the porosity and mean pore size while maintaining mechanical integrity without the formation of macrovoids. Using this membrane, a high flux of  $18.9 \text{ kg/m}^2\cdot\text{h}$  with a salt rejection of 99.99% was achieved in DCMD process at  $60^\circ\text{C}/20^\circ\text{C}$  (feed/permeate) when tested for 72 h.

## **CHAPTER 7**

### **Improving Permeation Performance of Membrane Distillation by Heat-Pressing on Membranes**



## 7.1 Introduction

Water and energy have been recognized as the top two major challenges in the world today and in the coming future. Nowadays, lots of freshwater resources are becoming unrenewable due to climate change and massive human activities. Moreover, the water shortage issues are much more serious in some countries with arid climate and poor economic conditions, so lack of clean water is a great threat to the hygiene of local residents (Tijing, Woo, et al. 2014).

Desalination is a viable option to obtain stable freshwater supply for coastal countries, and currently reverse osmosis (RO) is widely applied in desalination due to its relatively high efficiency. However, the capital and maintenance costs of RO plants are high and large amounts of electrical energy are required for generating high pressure in the process. In addition, RO has great negative impact on global environment by carbon dioxide as the generation of electrical energy is very likely fossil-fuel based. RO brine disposal is another major issue that is widely concerned by the society due to their impact on the local ecological system. Therefore, development of new generations of technology is strongly needed for replacement of RO technology (Alkhudhiri, Darwish & Hilal 2012).

Membrane distillation (MD) has been considered as a promising next-generation technology for desalination because of its higher efficiency and permeation performance independent on the salt concentration (Tijing et al. 2015a; Woo et al. 2015). The potential usage of low-grade heat such as industrial waste heat or solar heat makes it a more attractive option. The MD mechanism is based on a separation process where water vapor molecules at feed side pass through pores of a hydrophobic membrane and condense at permeate side (Alkhudhiri, Darwish & Hilal 2013b; Boubakri, Hafiane & Bouguecha 2014; Geng et al. 2014; Tian et al. 2014). The driving force of the MD is generated by the temperature difference of vapors between both sides of the membrane (Fan & Peng 2012). Evaporation occurs at the membrane interface with the contact of hot solution (Dong et al. 2014b). The vapor molecular then diffuses through the pores to the other side of interface where it condenses by cool permeate side (Tomaszewska, Gryta & Morawski 1994).

However, as an emerging technology, MD has not yet been widely applied in the global water industry due to lack of suitable membranes for long-term operation. Qualities such as strong resistance against wetting and fouling with long term stability are lacking in current available

membranes on the market (Francis et al. 2014). At the moment, membranes designed for microfiltration are utilized in MD and they are mainly made of polyvinylidene fluoride (PVDF) due to its high hydrophobicity, high solubility in common solvent, and high resistance against chemicals and heat (Dong et al. 2014a; Hwang et al. 2011). Non-solvent-induced phase separation (NIPS) and thermally induced phase separation (TIPS) are the two most common approaches exercised to fabricate membranes. However, these membranes does not fit for MD processes due to their low flux performance and susceptibility to wetting (Ge et al. 2014; Goh et al. 2013a; Nghiem & Cath 2011; Song & Jiang 2013). Thus, recently there is an increasing trend on membrane fabrication with new approaches for MD. Zhang et al. noted that the main challenges for membranes used in MD are to design features including porous structure and superhydrophobic surface for high filtration performance, as well as high mechanical properties for long-term operation (Song & Jiang 2013; Zhang, Li & Gray 2011).

Electrospun membranes possess some appropriate advantages involving high hydrophobicity, high porosity, adjustable pore size, and membrane thickness, which make them attractive candidates as MD membrane (Alkhudhiri, Darwish & Hilal 2012; Feng et al. 2013a). Compared to NIPS and TIPS, electrospinning is a relatively simple technique to fabricate membrane. By applying high electric fields on a polymer solution, millions of fibers are formed joining together to become nonwoven membrane sheet and collected on the foils (Feng et al. 2013a; Tijing, Choi, et al. 2014). Though electrospun membranes have many attractive properties for MD, however, they had some drawbacks limiting its performance, including relatively big pore sizes, low mechanical properties, and low LEP compared to the membranes fabricated by casting methods. Thus, there is a requirement to improve these characteristics without sacrificing high porosity and hydrophobicity by some membrane modification approaches (Tijing, Choi, et al. 2014). For this reason, post-treatment processes, one type of membrane modification procedures, has been widely applied on the electrospun membrane to enhance its morphology and characteristics including robustness and capability against wetting (Lalia, Guillen-Burrieza, et al. 2013a; Liao, Wang & Fane 2014). Previous studies indicated that “heat-press” could enhance the desalination performance by changing mechanical and morphological structure of the membranes in a favorable way (Liao et al. 2013a; Tijing, Choi, et al. 2014). It is expected that higher LEP, higher mechanical strength, lesser thickness, smaller average pore size and more uniform distribution of the pore size can be obtained through this technique.

Though a few studies have utilized heat-press to modify their MD membranes, the post-treatment approach is still not fully investigated (i.e., only few heat-press conditions were used) especially for electrospun membranes. Hence, in this study, the effect of different heat-press conditions such as temperature, pressure, and duration are comprehensively investigated to determine their effects on the electrospun membrane properties and MD performance. The optimal heat-press condition set is then identified and applied on electrospun membranes with various initial thicknesses to check the improvement. MD tests with as-spun, heat-pressed and commercial membranes are conducted and compared regarding permeation flux and salt rejection.

## **7.2 Experimental method**

### **7.2.1 Membrane fabrication by electrospinning**

PVDF-HFP at 20 wt.% was dissolved in a mixed solvent composed of acetone and DMAc (1:4 acetone/DMAc ratio). To obtain homogenous polymer solution, the mixture was magnetic stirred for 24 h. The prepared PVDF-HFP solution was then supplied in a 12 ml plastic syringe fitted with a 21G nozzle (internal diameter = 0.51  $\mu$ m).

### **7.2.2 Heat-press post-treatment**

After electrospinning, the as-spun membranes were removed from the collector and initially dried at 50 °C for 2 h inside an air flow oven (OTWMHD24, Labec, Australia). Membranes were then fully covered by foils, placed between flat metal plates with dead weight placed on the top plate, and put in a pre-heated oven. In each stage, various conditions (heat-press temperatures of 140, 150, 160, 170 °C; pressing pressure of 0.7, 2.2, 6.5, and 9.8 kPa; and heat-press duration of 1, 2, 4 and 8 h) were applied to the membrane as detailed with their name conventions in **Table 13**. The samples were investigated and compared separately in three consecutive stages classified by the conditions for deeply understanding their effects.

### **7.2.3 Experiment design**

As shown in **Table 13**, the experiments could be classified into four stages in this study. In Stage 1, four various temperatures were selected and tested. The applied pressure was pre-set to be 2.2 kPa (7 kg dead weight using metal plates over a 15 mm x 20 mm membrane) and 2 h was selected as the duration of the process. Then, in Stage 2 (i.e., effect of heat-press pressure),

the treatment temperature was fixed at 150 °C; then four various pressures were chosen in a wide range to check their effects. The duration of heat-pressure was pre-set to be 2 h. In Stage 3, the temperature and pressure were set at 150 °C and 2.2 kPa respectively, and the duration varied from 1 h to 8 h. Characteristics of post-treated membranes in each stage were addressed and compared. In Stage 4, optimal heat-press conditions were applied on the membranes with various thicknesses, in the range between 103 to 395  $\mu\text{m}$ . Both as-spun and heat-pressed membranes were characterized. Selected as-spun and heat-pressed membrane samples from Stage 4 were applied in the DCMD for desalination, and their permeation performances (flux and salt rejection) were compared with the commercial membranes (GVHP).

**Table 13.** Heat-press conditions and name conventions used in the present study.

Electrospun membrane samples		Heat-press conditions			
		Temperature (°C)	Pressure (kPa)	Duration (h)	Thickness ( $\mu\text{m}$ )
As spun	Neat	-	-	-	45
Stage 1	M0	140			43
	M1	150	2.2	2	39
	M2	160			31
	M3	170			melted
Stage 2	M1-A		0.7		40
	M1-B	150	2.2	2	68
	M1-C		6.5		37
	M1-D		9.8		37
Stage 3	M1-B-1			1	38
	M1-B-2	150	2.2	2	38
	M1-B-3			4	37
	M1-B-4			8	36

Stage 4	PH1	-	-	-	103
	PH2				147
	PH3				224
	PH4				395
	PH1'				90
	PH2'				129
	PH3'	150	6.5	8	195
	PH4'				343

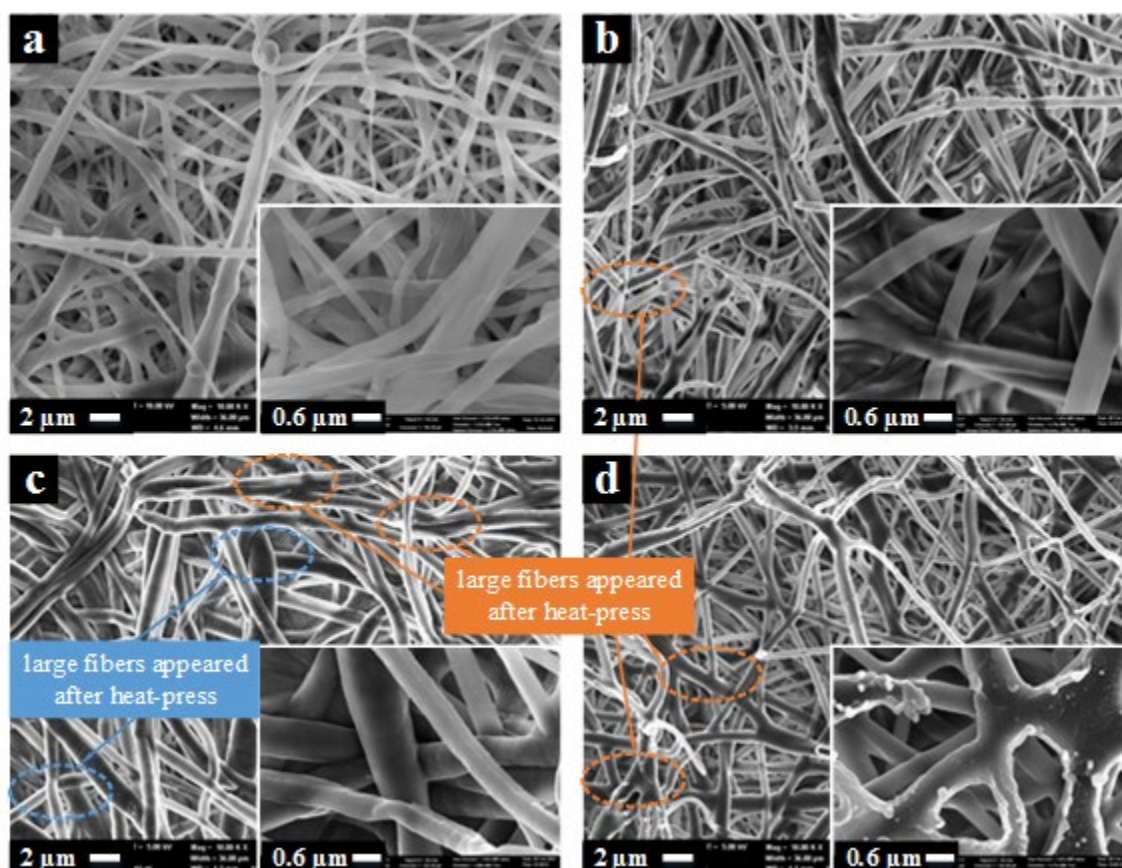
## 7.3 Results and discussion

### 7.3.1 Effect of heat-press temperature on the membranes

PVDF-HFP was used in this study and its melting point was 155-160 °C described in the “properties” section on the official product webpage of Sigma-Aldrich (*Properties* 2015). The existence of co-polymer (HFP) reduces the melting point of the PVDF-HFP hence it has a slightly lower melting temperature than pure PVDF, as HFP had lower surface tension(Ma et al. 2005).

In the stage 1 of the experiment, various temperatures were applied on the membranes. The samples were names as M0, M1 and M2, which meant that heat-press temperatures of 140°C, 150 °C and 160 °C were applied respectively.

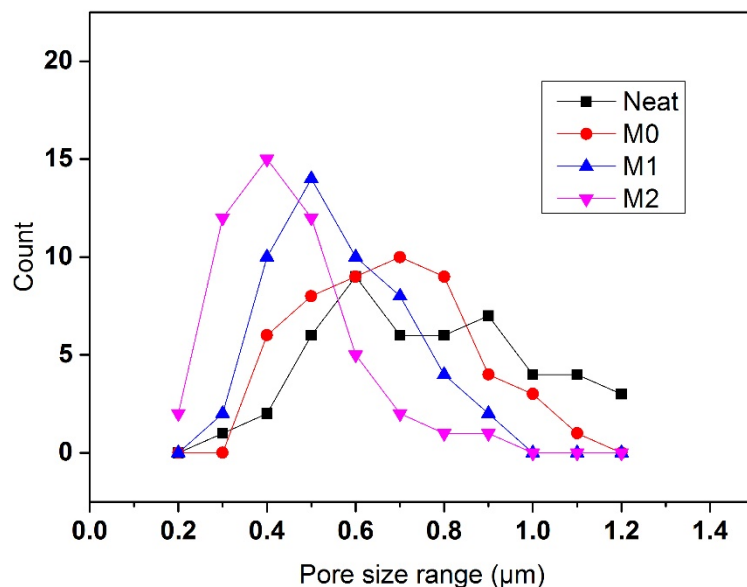
### 7.3.1.1 Effect of temperature on morphology



**Figure 53.** SEM images of as-spun and heat-pressed PVDF-HFP membrane at magnifications of 10K and 50K: (a)as-spun neat membrane (Neat); membranes heat-pressed under (b)140 °C (M0); (c)150 °C (M1); (d)160 °C (M2).

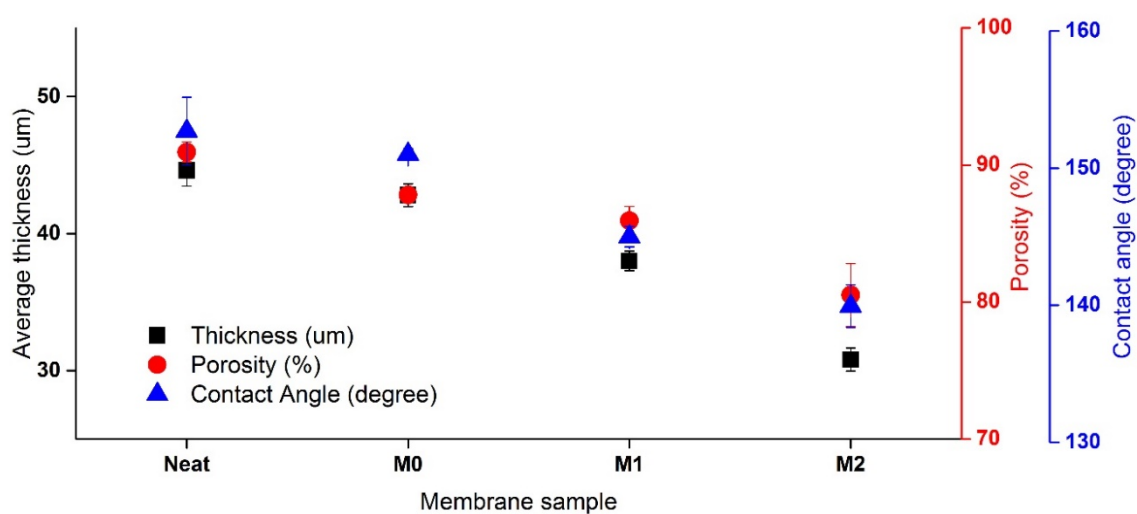
**Figure 53** displayed the morphologies of as-spun and heat-pressed membrane (as-spun, membrane heat-pressed under 140 °C, 150 °C and 160 °C) under various temperatures at two magnifications. We could find that some of the fibers fused together when heat-press was applied, and there would be more fused fibers with the increase of the heat-press temperature. It could be observed optically on the SEM images that the heat-pressed electrospun fibers were obviously “fatter” than as-spun membranes, and the average surface pore size decreases as the fibers widened and block some passage of the pore. The change of morphology was also observed by Wu (Wu, Wang & Field 2014). The measured surface pore size distributions were displayed in **Figure 54** which showed an obvious trend that increasing temperature could narrow the pore size distribution and decrease the average pore size. Similarly, Liao and Wu applied heat-press treatment with similar processes and conditions on PVDF electrospun

membranes to achieve smaller pore size of electrospun membranes. However, they did not conduct the experiment with other temperatures (Liao et al. 2013a; Wu, Wang & Field 2014).



**Figure 54.** Fiber distributions of as-spun and membrane samples heat-pressed under various temperatures.

### 7.3.1.2 Effect of temperature on the characteristics



**Figure 55.** Effects of temperature on thickness, porosity and contact angle

Details of average fiber and surface pore sizes clearly showed an increasing trend of fiber size and decreasing trend of surface pore size when heat-press temperatures were raised (**Table 14**).

The thickness of the heat-pressed membranes was affected by the heating temperature greatly inversely. Membranes without heat treatment had a thickness of 46  $\mu\text{m}$ . When heat-pressed at 140  $^{\circ}\text{C}$ , the membrane's thickness decreased to 41  $\mu\text{m}$ . Further increase of the heating temperature to 150  $^{\circ}\text{C}$  could make the membrane even thinner. The decrease of the thickness was caused when multiple layers of fiber in membrane fused together to form much denser structures, and increasing temperature could increase the compaction level (Tijing, Woo, et al. 2014). However, when the temperature reached 160  $^{\circ}\text{C}$ , the thickness decreases sharply to 31  $\mu\text{m}$ . It was believed that partially melting occurs and some regions of the internal fibrous network was melt together (Liao et al. 2013a). Samples of M3 was totally melt as the temperature was above the melting temperature, hence there was no characterization of it. Porosity of membrane shared a similar decreasing trend as the thickness. Neat had the highest porosity of 92% while the M2 had the lowest porosity of 80% (**Table 14**). The reduction of the porosity was due to the loss of some voids due to compaction.

**Figure 55** and **Table 14** showed that the contact angle kept decreasing steadily as the applied temperature increased. However, when the temperature continued increasing up to 160  $^{\circ}\text{C}$ , the contact angle dropped significantly to 139.9  $^{\circ}\text{C}$ , indicating that partially melting of polymer on the surface could occur, which could be noticed on **Figure 53**. The change of contact angle was because that if the applied temperature was near the melting point of the polymer the morphology of membrane would be greatly changed leading to much smaller pore size and low contact angle. Generally the surface of the membranes became less rough during the post-treatment, which meant that the membrane surface would become less hydrophobic (Lalia, Guillen-Burrieza, et al. 2013a; Liao et al. 2013a).

**Table 14.** Characteristics of the membranes after heat-press at different temperatures

Sample	Neat	M0	M1	M2
Fiber size ( $\mu\text{m}$ )	0.387 $\pm$ 0.119	0.553 $\pm$ 0.187	0.686 $\pm$ 0.239	0.747 $\pm$ 0.295
Surface pore size ( $\mu\text{m}$ )	0.501 $\pm$ 0.210	0.480 $\pm$ 0.100	0.451 $\pm$ 0.090	0.407 $\pm$ 0.099



<b>Thickness (<math>\mu\text{m}</math>)</b>	44.6 $\pm$ 1.1	42.8 $\pm$ 0.8	39.2 $\pm$ 0.4	30.8 $\pm$ 0.8
<b>Porosity (%)</b>	90.9 $\pm$ 0.7	87.8 $\pm$ 0.2	85.9 $\pm$ 1.0	80.5 $\pm$ 2.3
<b>Contact angle (<math>^{\circ}\text{C}</math>)</b>	152.7 $\pm$ 2.5	151.0 $\pm$ 0.4	148.1 $\pm$ 2.2	140.0 $\pm$ 1.6
<b>Young's modulus (MPa)</b>	11.7 $\pm$ 5.4	31.1 $\pm$ 5.8	40.9 $\pm$ 2.6	103.9 $\pm$ 8.2
<b>Stress at break (MPa)</b>	3.09 $\pm$ 0.18	10.64 $\pm$ 0.55	12.11 $\pm$ 0.35	16.09 $\pm$ 1.26
<b>Strain at break</b>	0.66 $\pm$ 0.05	1.30 $\pm$ 0.08	1.56 $\pm$ 0.19	0.84 $\pm$ 0.15
<b>LEP (kPa)</b>	71 $\pm$ 9	65 $\pm$ 7	83 $\pm$ 4	64 $\pm$ 6

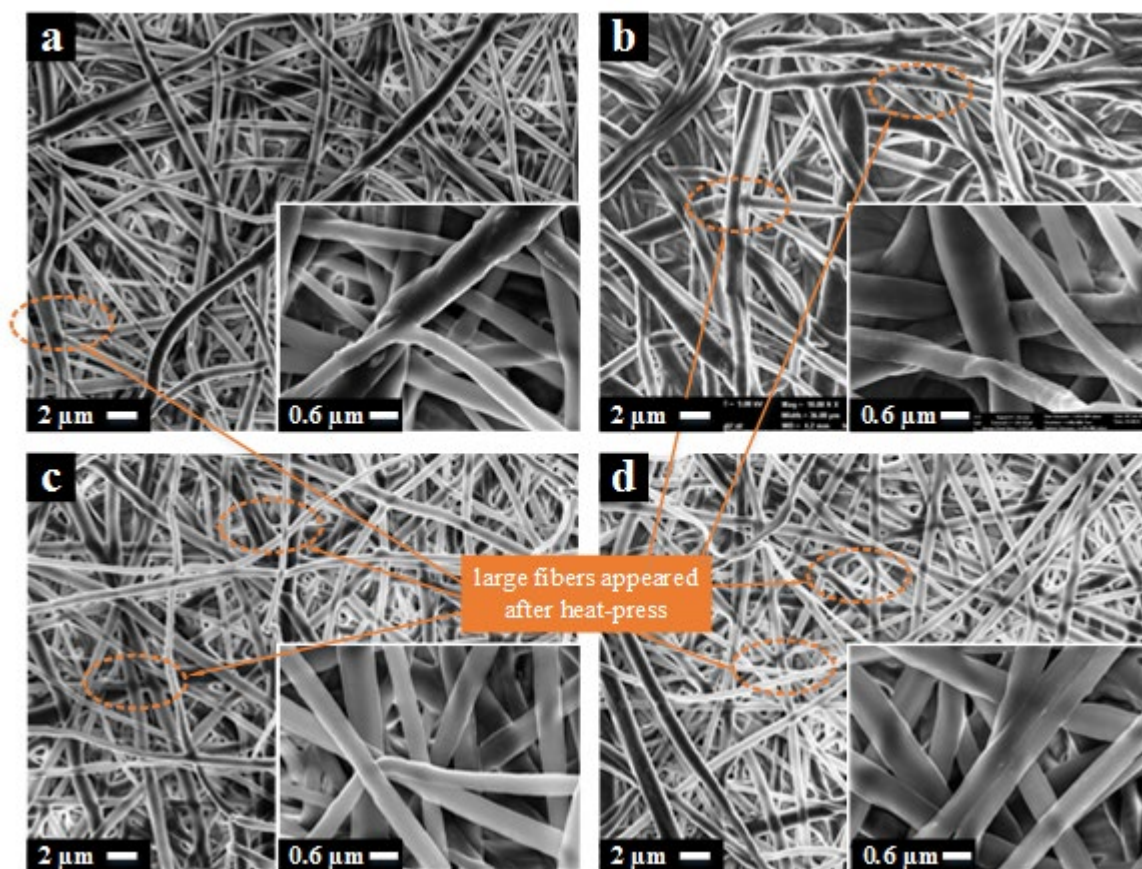
At higher treating temperatures, more fibers could be observed to be fused at interlay points, and they could contribute to both decreased pore size and increase of mechanical strengths. Maximum stress and young's modulus were investigated, and it was found that both parameters increased when temperature was raised. Higher tensile strength and young's modulus could be achieved with higher heat-press temperature. Especially, M2 had a much higher young's modulus than other samples, due to its greatly changed morphology after the membrane fibers melted partially forming bulk polymer. LEP was greatly improved after heat-press, indicating better resistance against wetting and improved robustness(Ahmed, Lalia & Hashaikeh 2015). LEP of M0 was found to be lower than neat membrane. It was because that the membrane was not sufficiently heat-pressed hence the morphology such as surface pore size was not enhanced. However, the reduction of the thickness after heat-press could decrease the LEP greatly (Guillen-Burrieza et al. 2015). It explained that LEP of M2 was lower than M1 as well.

### 7.3.2 Effect of heat-press pressure on the membranes

Heat-press pressure played an important role in affecting the morphology and characteristic of the membrane and increasing pressure in heat-press progress was expected to influence the membrane properties in a favorable way.

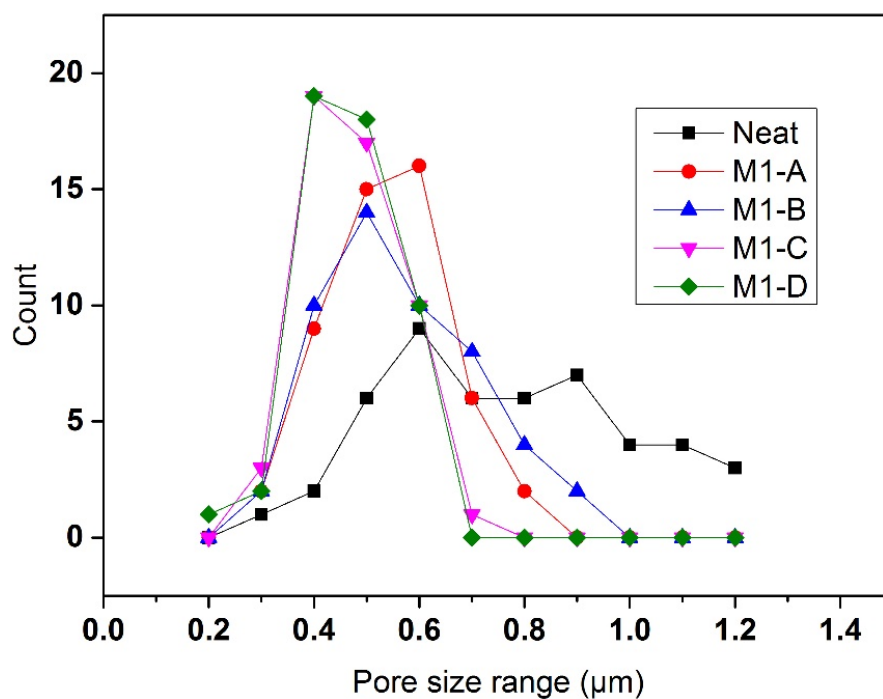
Keeping the heating temperature at 150  $^{\circ}\text{C}$  and treatment duration for 2 h, four metal plates with mass of 2 kg, 7 kg, 20 kg and 30 kg were applied on the membrane samples individually, which were converted to be 0.7 kPa, 2.2 kPa, 6.5 kPa and 9.8 kPa as pressure respectively. The samples were then named as M1-A, M1-B, M1-C and M1-D respectively.

### 7.3.2.1 Effect of pressure on the morphology



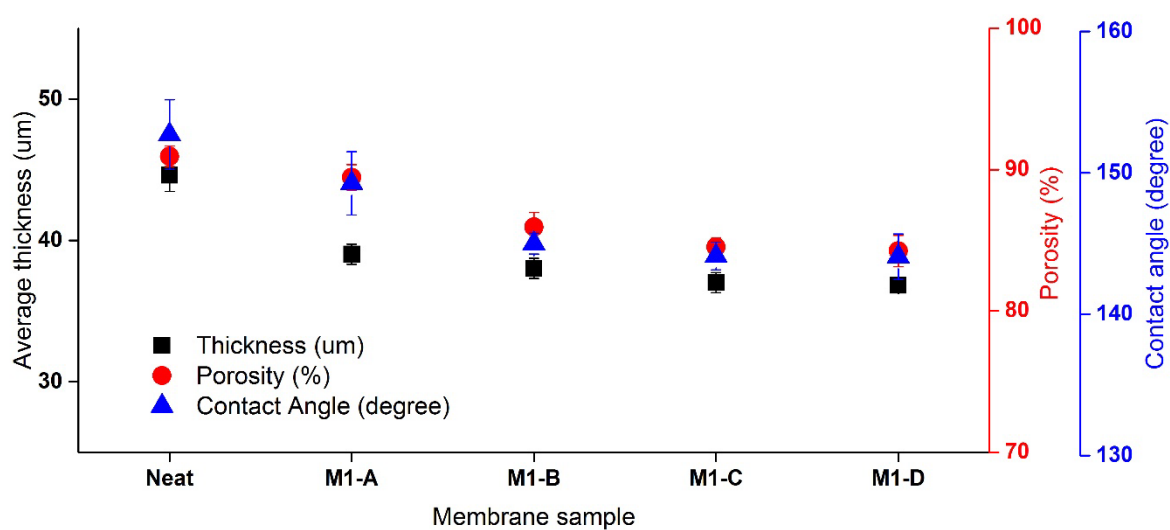
**Figure 56.** SEM images of heat-pressed PH membrane at magnifications of 10K and 50K: membranes heat-pressed under (a) 0.7 kPa (M1-A); (b) 2.2 kPa (M1-B); (c) 6.5 kPa (M1-C); (d) 9.8 kPa (M1-D).

**Figure 56** showed the morphologies of heat-pressed membranes under various pressures. It could be seen that although their surface structures shared similar features as fiber sizes looked nearly identical, more fused joints could be found in heat-pressed membranes under higher pressures. It was assumed that the external pressure could help the fibers fusing with each other. Analysis of surface pore sizes (**Figure 57**) indicated that further increasing the pressures could narrow the surface pore distributions and reduce the average pore size. However, sample M1-C and M1-D shared identical distributions and average pore size, which both were more favored than the other two samples.



**Figure 57.** Fiber distributions of as-spun and membrane samples heat-pressed under various pressures.

### 7.3.2.2 Effect of pressure on the characteristics



**Figure 58.** Effects of pressure on thickness, porosity and contact angle

We could observe that increasing pressure resulted in larger fiber size and smaller surface pore size. However, when the applied pressure was further increased beyond value of 2.2 kPa, the effect of heat-press pressure on fiber sizes tended to become minimal (**Table 15**). It was also found that the difference of fiber size between M1-C and M1-D was insignificant. The two membrane samples shared very similar average size of 0.704  $\mu\text{m}$  and 0.726  $\mu\text{m}$  respectively, and their surface pore size was nearly identical. It was concluded that further increasing the pressure beyond certain values had no benefits on the characteristics of the membranes. In other researchers' work, pressure applied on the samples were mentioned in the papers. However, we could find that only glass plates were applied on the membranes, and similar increase of fiber size and decrease of pore size could be found (Lalia, Guillen-Burrieza, et al. 2013a; Liao et al. 2013a). This meant that a moderate pressure higher than certain values should be sufficient for the heat-press treatment.

As displayed in **Figure 58**, heat-press pressure had similar effects on thickness, porosity and contact angle, as all of three characteristics decreased when the applied pressure increased. However, the trend of the decreasing was not as strong as the trend of temperature effects discussed in last section. Additionally, M1-C and M1-D shared very similar values of thickness, porosity and contact angle, which meant the membranes might have reached its maximum compaction level.

**Table 15.** Characteristics of the membranes after heat-press at different pressures

Sample	Neat	M1-A	M1-B	M1-C	M1-D
<b>Fiber size (<math>\mu\text{m}</math>)</b>	0.387 $\pm$ 0.119	0.629 $\pm$ 0.179	0.686 $\pm$ 0.239	0.704 $\pm$ 0.201	0.726 $\pm$ 0.199
<b>Surface pore size (<math>\mu\text{m}</math>)</b>	0.501 $\pm$ 0.210	0.485 $\pm$ 0.109	0.451 $\pm$ 0.090	0.421 $\pm$ 0.090	0.420 $\pm$ 0.128
<b>Thickness (<math>\mu\text{m}</math>)</b>	44.6 $\pm$ 1.1	39.5 $\pm$ 0.7	38.0 $\pm$ 0.9	37.1 $\pm$ 0.4	36.8 $\pm$ 0.4
<b>Porosity (%)</b>	90.9 $\pm$ 0.7	89.4 $\pm$ 0.9	85.9 $\pm$ 1.3	84.5 $\pm$ 0.6	84.2 $\pm$ 1.1
<b>Contact angle (<math>^{\circ}</math>)</b>	152.7 $\pm$ 2.5	149.3 $\pm$ 2.2	145.0 $\pm$ 0.8	144.1 $\pm$ 1.0	144.1 $\pm$ 1.6
<b>Young's modulus (MPa)</b>	11.7 $\pm$ 5.4	36.5 $\pm$ 6.6	40.9 $\pm$ 2.6	48.5 $\pm$ 4.0	48.7 $\pm$ 6.0

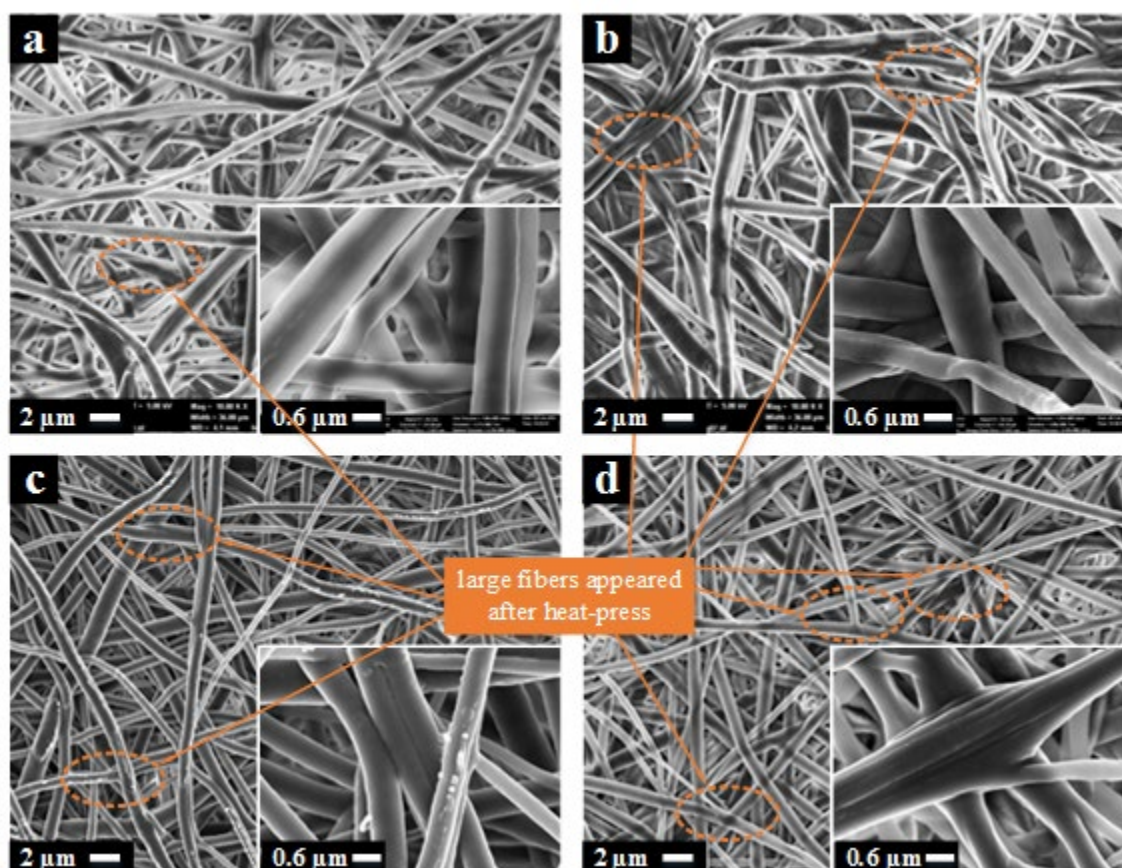
<b>Stress at break (MPa)</b>	3.09±0.18	11.90±1.21	12.11±0.35	13.29±1.85	13.50±0.85
<b>Strain at break</b>	0.66±0.05	1.30±0.08	1.56±0.19	1.42±0.38	1.38±0.19
<b>LEP (kPa)</b>	71±9	73±8	83±4	93±4	89±3

**Table 15** also shown that increasing pressure could enhance the mechanical properties greatly, M1-C had a young's modulus of 48.5 MPa which was much higher than M1-A. M1-C also had a higher tensile stress, which was the results of changed morphology after heat-press (Tijing, Woo, et al. 2014). However, when the pressing mass was further increased beyond 6.5 kPa, the increase of both young's modulus and maximum stress could be negligible. Effect of heat-press pressure on LEP shared similar trend with pressure on tensile strength, as increasing pressure could increase LEP for some degree. However, further increasing pressure beyond 6.5 kPa had no significant effect on the LEP, as we could see M1-C and M1-D had very similar LEP values.

### 7.3.3 Effect of heat-press duration on the membranes

The effect of heat-press duration was not extensively studied in previous studies. In recent relevant studies, there were two common approaches of heat-press process: the membrane samples were (1) placed in an pre-heated oven for 1 h; (2) heat-pressed by extremely hot iron for very short periods (e.g. 1-2) s (Liao et al. 2013a; Wu, Wang & Field 2014). Hence, there was a strong need to explore the effect of durations comprehensively. It was expected that the micro-fibers could be better fused if the polymer films were heat-pressed for longer duration, so both the morphology and characteristics might be improved. Thus, four durations: 1 h, 2 h, 4 h and 8 h were applied in post-treatment to investigate their effects, and the relevant samples were named M1-B-1, M1-B-2, M1-B-3 and M1-B-4, respectively.

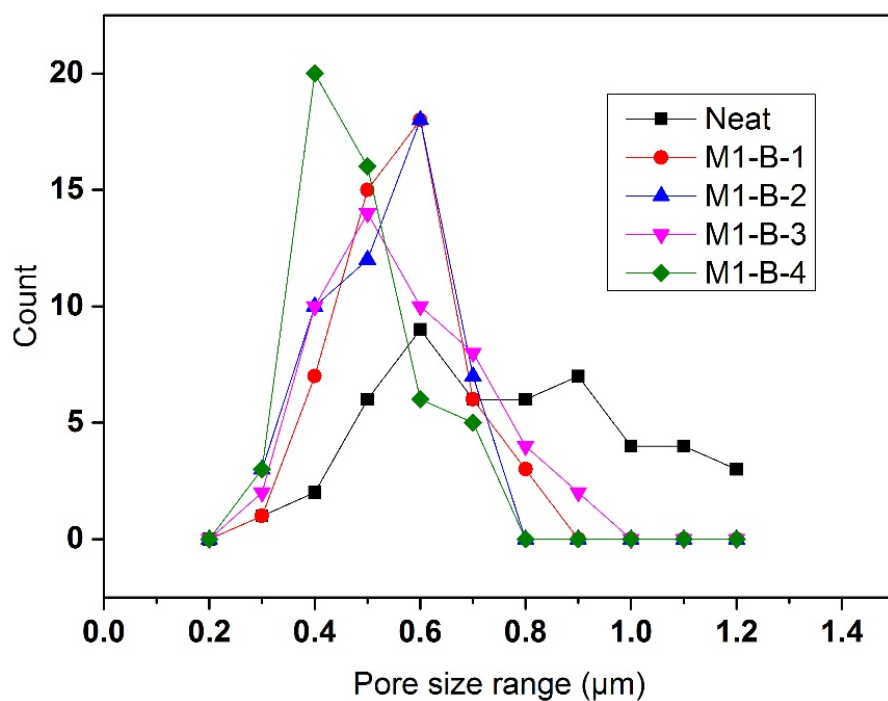
### 7.3.3.1 Effect of duration on the morphology



**Figure 59.** SEM images of heat-pressed PVDF-HFP membrane at magnifications of 10K and 50K: membranes heat-pressed for (a)1 h (M1-B-1); (b)2 h (M1-B-2); (c)4 h (M1-B-3); (d)8 h (M1-B-4).

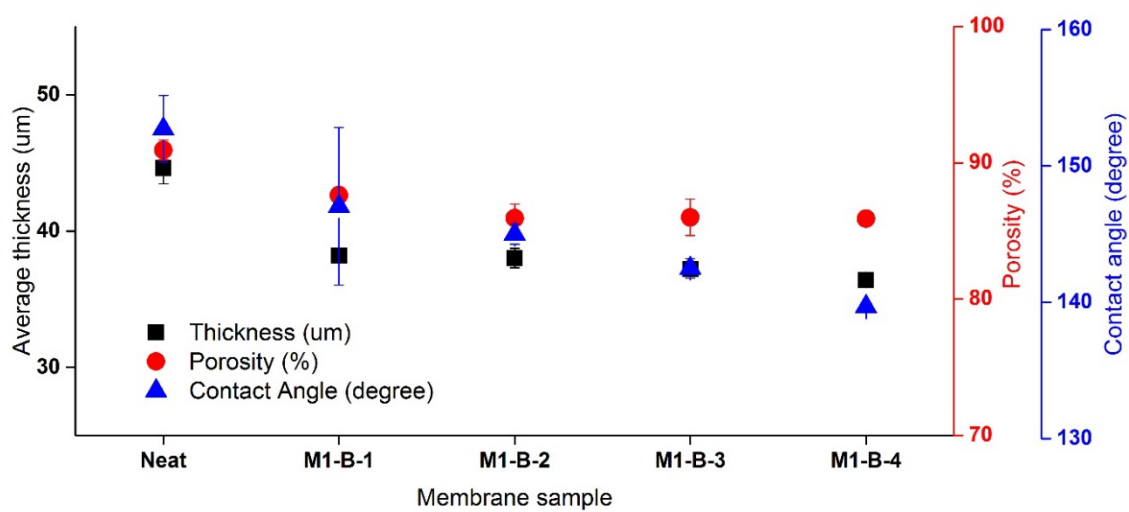
In **Figure 59**, we could find that when increasing the durations of heat-press, there would be more fiber fused with each other in the morphology. M1-B-4 had most fused fibers than the other samples and a large fused joint could be seen in the fused joint in 50K view of **Figure 59d**, which rarely be found in other samples. Also, heat-pressed membrane for longer duration tended to have even larger fiber size and smaller surface pore size. It was clearly displayed in **Figure 60** that membranes heat-pressed for 8 h had the narrowest distributions of surface pore size and smallest average pore size.





**Figure 60.** Fiber distributions of as-spun and membrane samples heat-pressed for various durations.

### 7.3.3.2 Effect of duration on the characteristics



**Figure 61.** Effects of pressure on thickness, porosity and contact angle

Fiber size and surface pore were strongly affected by the duration of the heat-press, as it was observed that when membrane samples were heat-pressed for 8 h, it had the largest fiber size of 0.800  $\mu\text{m}$  and smallest surface pore size (**Table 16**).

**Figure 63** demonstrates that contact angle, porosity and thickness of membranes samples heat-pressed for various durations shared comparable trends. When the durations increased, the values of these characteristics decreased. Thickness and contact angle were affected by the duration more severely. However, it was interesting to point that further increase of duration beyond 2 h had meant that a moderate pressure higher than certain values should be sufficient for the heat-press treatment influence on the porosity.

**Table 16.** Characteristics of the membranes after heat-press at different durations

Sample	Neat	M1-B-1	M1-B-2	M1-B-3	M1-B-4
Fiber size ( $\mu\text{m}$ )	0.387 $\pm$ 0.119	0.656 $\pm$ 0.212	0.686 $\pm$ 0.239	0.692 $\pm$ 0.258	0.800 $\pm$ 0.285
Surface pore size ( $\mu\text{m}$ )	0.501 $\pm$ 0.210	0.477 $\pm$ 0.122	0.451 $\pm$ 0.090	0.447 $\pm$ 0.119	0.397 $\pm$ 0.104
Thickness ( $\mu\text{m}$ )	44.6 $\pm$ 1.1	38.2 $\pm$ 0.4	38.0 $\pm$ 0.9	37.2 $\pm$ 0.4	36.4 $\pm$ 0.5
Porosity (%)	90.9 $\pm$ 0.7	87.6 $\pm$ 0.3	84.5 $\pm$ 0.6	86.0 $\pm$ 1.3	85.9 $\pm$ 0.5
Contact angle ( $^{\circ}\text{C}$ )	152.7 $\pm$ 2.5	147.0 $\pm$ 5.8	145.0 $\pm$ 0.8	142.5 $\pm$ 0.7	140.0 $\pm$ 0.2
Young's modulus (MPa)	11.7 $\pm$ 5.4	27.9 $\pm$ 4.8	40.9 $\pm$ 2.6	41.8 $\pm$ 7.9	45.7 $\pm$ 7.6
Stress at break (MPa)	3.09 $\pm$ 0.18	11.26 $\pm$ 0.52	12.11 $\pm$ 0.35	12.55 $\pm$ 0.16	13.28 $\pm$ 0.65
Strain at break	0.66 $\pm$ 0.05	1.54 $\pm$ 0.11	1.56 $\pm$ 0.19	1.55 $\pm$ 0.08	1.39 $\pm$ 0.26
LEP (kPa)	71 $\pm$ 9	58 $\pm$ 4	83 $\pm$ 4	82 $\pm$ 4	90 $\pm$ 7

The mechanical properties were affected by the heat-press duration in a positive way also. M1-B-1 had a lower tensile strength, indicating that the membrane was not sufficiently compacted

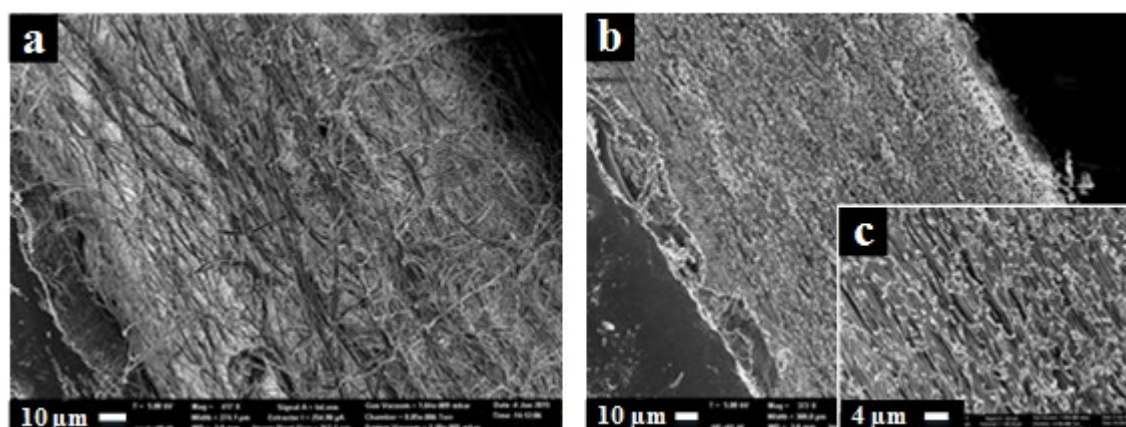


and the electrospun fibers were not fused in micro view relatively. **Table 16** also showed that M1-B-4 had highest young's modulus and maximum stress, indicating longer heat-press duration could increase the mechanical properties positively. Heat-press duration could affect the LEP as well. We could see that M1-B-4 had highest LEP of 90 kPa. It was interesting to state that M1-B-1 had LEP lower than neat membrane. It could be explained that the decrease of thickness could affect the LEP of membrane negatively, while the membrane fibers did not have sufficient time being fused together to deliver higher resistance against fiber deformations under high pressures (Lalia et al. 2014).

### 7.3.4 Effect of heat-press on membrane with various thickness

In previous stages, it could be found that samples of M1, M1-C and M1-B-4 had better pore size distribution, LEP and mechanical properties in each of their belonging group, and their relative controllable parameters were 150 °C Celsius, pressure of 6.5 kPa and duration of 8 h, respectively. It was assumed that the optimal heat-press condition recipe could be achieved with the combination of the individual optimal individual. Hence, the combination of 150°C, 6.5 kPa and 8 h was considered as the optimal heat-press condition set in this study. In stage 4, four membranes samples with increasing thicknesses from 103 to 395  $\mu\text{m}$  were applied with the optimal conditions. Then, four pairs of membranes before and after heat-press would be investigated to determine its effect on morphology and characteristics, which was named as PH1, PH1', PH2, PH2', PH3, PH3', PH4 and PH4'.

#### 7.3.4.1 Effect of heat press on morphology and characteristics



**Figure 62.** SEM cross section images of as-spun (a: 400k) and heat-pressed membrane (b: 350k; c: 1500k)

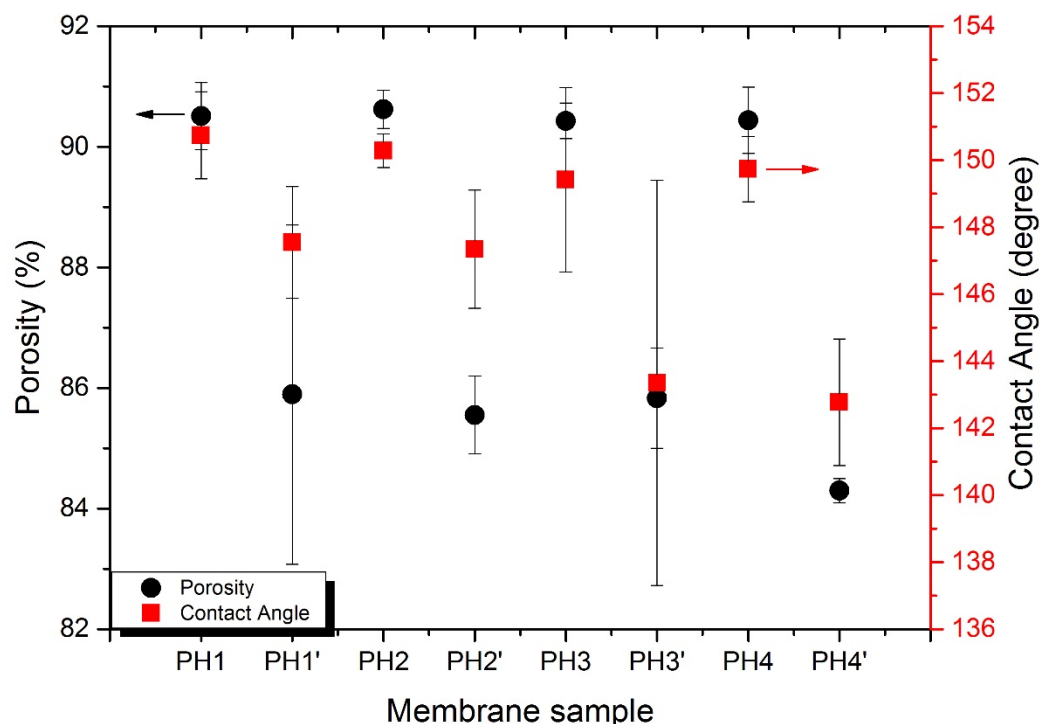
**Figure 62** showed that the cross-section of membranes before and after heat-press with optimal conditions. More uniform and denser morphology could be observed in heat-pressed membranes which could contribute to higher LEP. Besides, the thickness of heat-pressed membrane was obviously lower. The increase of fiber size and decrease of surface pore size after heat-press were not dependent on the thickness of the membranes, as fiber and pore sizes of membranes shared similar values, before or after heat-press (**Table 17**). The trends of fiber and pore size change were similar with Wu's study (Wu, Wang & Field 2014).

**Table 17.** Thickness of various membrane samples before and after heat-press

Sample	Average ( $\mu\text{m}$ )	Reduction percentage after heat-press based from initial
PH1	103.4 $\pm$ 1.1	
PH1'	89.8 $\pm$ 1.1	13.15%
PH2	146.8 $\pm$ 3.0	
PH2'	129.0 $\pm$ 2.9	12.13%
PH3	224.4 $\pm$ 4.4	
PH3'	194.8 $\pm$ 1.9	13.19%
PH4	395.2 $\pm$ 3.5	
PH4'	343.2 $\pm$ 2.3	13.16%

From **Table 17**, it could be observed that the reduction of heat-press membrane was consistent in membrane samples with various thicknesses. The results agreed with the experiment in previous stages when membrane with thickness of 45  $\mu\text{m}$  was heat-pressed into 37  $\mu\text{m}$ , indicating a reduction around 15% based from initial. However, the reduction percentage was relatively smaller than the ones in other researches. In Wu's research the reduction was around 25% (Wu, Wang & Field 2014), and in Liao's and Lalia's studies, the reduction could be over 50% (Lalia, Guillen-Burrieza, et al. 2013a; Liao, Wang & Fane 2014). It was assumed that the difference of heat-press approaches and polymer material leading to the thickness reduction

difference.



**Figure 63.** Effects of heat-press with optimal conditions on porosity and contact angles of membranes with various thicknesses

**Figure 63** showed that porosity and contact angle share similar decreasing trend after heat-press. Samples with various thickness would had decreased porosity and contact angle. PH1' had a decreased contact angle from 151 to 148 °C, and a decreased porosity from 91 to 87%, while PH4' had a decreased contact angle from 150 to 143 °C, and a decreased porosity from 90 to 84%. The difference of the characteristics decrease between membrane samples with greatest difference of thickness was insignificant, so we could conclude that thickness of membrane hardly affects the effect of heat-press on these two characteristics.

We could also observe that increasing thickness of membranes could enhance the mechanical strengths of membrane slightly, while the mechanical properties could be enhanced greatly after heat-press. It was also needed to note that the maximum stresses at break increased greatly after heat-press, however, the maximum strains at break decreased, indicating the polymers turned from elastic to more plastic materials. Also, heat-press could improve the LEP of membranes with various thicknesses. The improvement was consistent which was around 25%.

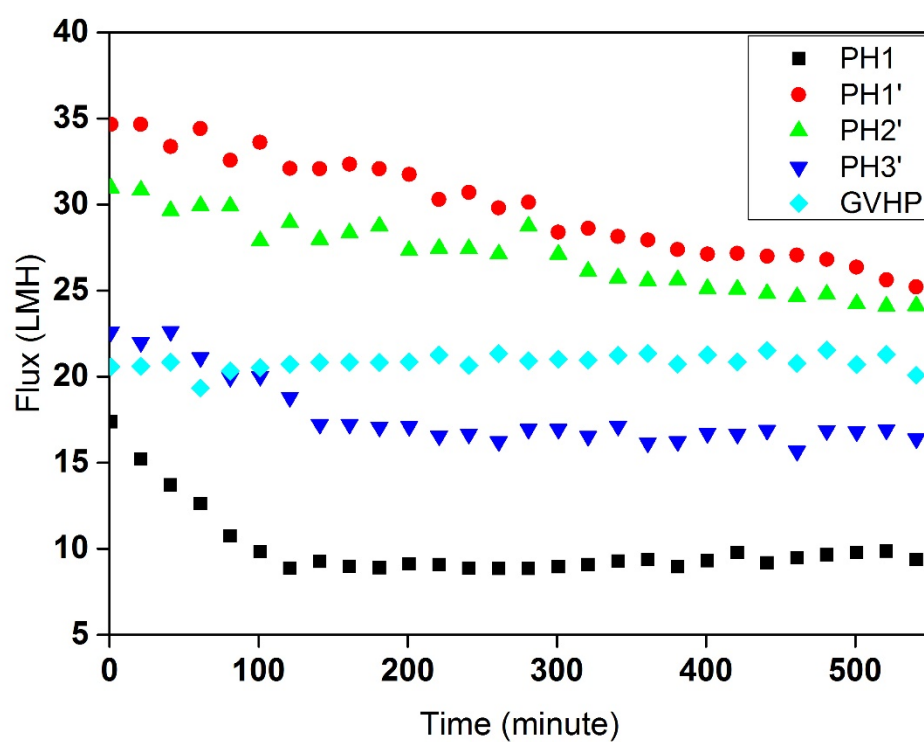
**Table 18.** Characteristics of the membranes with various thicknesses after heat-press

Sample name	a	b	c	d
<b>Before heat-press</b>	<b>PH1</b>	<b>PH2</b>	<b>PH3</b>	<b>PH4</b>
Fiber size ( $\mu\text{m}$ )	0.428 $\pm$ 0.237	0.454 $\pm$ 0.290	0.433 $\pm$ 0.264	0.399 $\pm$ 0.225
Surface pore size ( $\mu\text{m}$ )	0.652 $\pm$ 0.291	0.620 $\pm$ 0.235	0.613 $\pm$ 0.254	0.611 $\pm$ 0.163
Porosity (%)	90.5 $\pm$ 0.6	90.6 $\pm$ 0.3	90.4 $\pm$ 0.3	90.4 $\pm$ 0.6
Contact angle ( $^{\circ}\text{C}$ )	150.7 $\pm$ 1.3	150.3 $\pm$ 0.5	149.4 $\pm$ 2.8	149.7 $\pm$ 1.0
Young's modulus (MPa)	15.7 $\pm$ 9.4	16.2 $\pm$ 1.8	16.4 $\pm$ 5.9	20.6 $\pm$ 0.6
Stress at break (MPa)	6.74 $\pm$ 0.32	6.60 $\pm$ 0.13	6.31 $\pm$ 0.38	10.13 $\pm$ 0.47
Strain at break	1.54 $\pm$ 0.08	1.20 $\pm$ 0.02	1.25 $\pm$ 0.12	1.87 $\pm$ 0.01
LEP (kPa)	76.5 $\pm$ 2.2	79.0 $\pm$ 1.2	88.0 $\pm$ 2.0	93.0 $\pm$ 2.5
<b>After heat-press</b>	<b>PH1'</b>	<b>PH2'</b>	<b>PH3'</b>	<b>PH4'</b>
Fiber size ( $\mu\text{m}$ )	0.676 $\pm$ 0.257	0.758 $\pm$ 0.273	0.697 $\pm$ 0.244	0.638 $\pm$ 0.224
Surface pore size ( $\mu\text{m}$ )	0.423 $\pm$ 0.207	0.393 $\pm$ 0.156	0.380 $\pm$ 0.168	0.353 $\pm$ 0.147
Porosity (%)	85.9 $\pm$ 2.8	85.6 $\pm$ 0.7	85.8 $\pm$ 0.8	84.3 $\pm$ 0.2
Contact angle ( $^{\circ}\text{C}$ )	147.6 $\pm$ 1.7	147.3 $\pm$ 1.8	143.4 $\pm$ 6.1	142.8 $\pm$ 1.9
Young's modulus (MPa)	44.7 $\pm$ 12.9	36.4 $\pm$ 12.2	30.6 $\pm$ 4.0	40.0 $\pm$ 2.3
Stress at break (MPa)	13.29 $\pm$ 0.33	13.61 $\pm$ 1.07	14.23 $\pm$ 1.89	15.91 $\pm$ 1.04
Strain at break	0.86 $\pm$ 0.01	1.09 $\pm$ 0.03	0.95 $\pm$ 0.42	1.40 $\pm$ 0.16
LEP (kPa)	97.0 $\pm$ 1.4	99.5 $\pm$ 0.7	108.5 $\pm$ 1.5	116.0 $\pm$ 2.4

### 7.3.5 MD performance of heat-pressed membrane with various thicknesses

Selected membrane samples were compared in terms of permeation flux and salt rejection in DCMD module for desalination, with feed temperature of 60 °C and permeate temperature of 20 °C. One neat membrane samples (PH1), three heat-pressed membrane samples (PH1', PH2' & PH3') and commercial PVDF membrane GVHP were selected to determine the effect of the optimal heat-press. PH4' were not tested due to their unsuitable high thickness. **Figure 64** showed that commercial membrane shared similar flux with the as-spun membrane. And, after heat-press, the permeation performance of electrospun membrane increased greatly. Part of the reason of flux improvement was contributed by the decrease of thickness after heat-press (Wu, Wang & Field 2014). Improvement of surface pore size distribution, tensile strength and LEP contributed more to the enhanced permeation performance, as we could see that PH2' had better permeation flux with thicker thickness than PH1. It was considered that the improvement of mechanical strength could help electrospun fibers having higher strength against deformation which might result in the increasing pore size and hence decreasing of flux. It could also prevent water stay in the “holes” between the fiber layers, which could increase mass transfer resistance greatly (Liao et al. 2013a).

Generally, membranes after heat-press at optimal settings had much better performance than the ones before heat-press. Heat-pressed membranes had a stable trend of flux and salt rejection while as-spun had decreasing flux and salt rejection in short time. It was also found that heat-pressed membranes with thickness between 37 - 130  $\mu\text{m}$  shared similar permeation performance. PH1' and PH2' showed declined flux during the MD process caused by gradual partial pore wetting due to their relatively low membrane thicknesses. However, when membrane thickness further increased, the flux would decline rapidly. This phenomenon agreed with Wu's study that increasing thickness could decrease transmembrane flux (Wu, Wang & Field 2014). Therefore, thickness of electrospun membrane beyond 200  $\mu\text{m}$  even after heat-press was not favored for DCMD due to its greatly decreased permeability.



**Figure 64.** Comparison of DCMD permeation performance of selected membrane samples

### 7.3.5.1 Comparison of permeation performance of heat-pressed and commercial membranes with their Characteristics and MD setting up parameters

**Table 19.** Comparison of Heat-pressed MD flat-sheet membranes for desalination with commercial PVDF membrane

Membrane	Solvent	Method of heat-press	Mean pore size (μm)	Thickness (μm)	Porosity (%)	Feed solution	Feed velocity (m s <sup>-1</sup> )	Feed temperature (°C)	Permeate temperature (°C)	Permeate velocity (m s <sup>-1</sup> )	Permeation flux (LMH)	Salt rejection (%)
<b>5% PVDF with LiCl<sub>2</sub> as additive [23]</b>	DMF/acetone	placed under glass plate in an oven at 170 °C for 1 h	0.21	42	54	3.5 wt.% NaCl solution	0.07	50	20	0.14	20.6	-
<b>10% PVDF-HFP [22]</b>	DMAc/acetone	applied iron on both top and bottom surfaces at 200 °C for 1-2 s	0.26	110	55-60%	1 wt.% NaCl solution	0.32	50	24	0.32	20-22	98
<b>5% PVDF [27]</b>	DMF/acetone	placed under glass plate in an oven at 170 °C for 1 h	-	27-58	80-84%	10 wt.% NaCl solution	0.31	65	20	0.31	10-30	-

<b>20% PVDF-HFP (in this study)</b>	DMAc/acetone	placed under metal plates in oven at 150 °C for 8 h	0.42	90	86%	3.5 wt.% NaCl solution	0.07	60	20	0.07	29	99.99
<b>Millipore GVHP PVDF (in this study)</b>	-	-	0.22	110	-	3.5 wt.% NaCl solution	0.07	60	20	0.07	22	99.98



In this study, membranes heat-pressed under optimal conditions had better performance in MD for desalination than the heat-pressed membranes in previous researches and commercial PVDF membranes, regarding both salt rejection and permeation flux (**Table 19**).

## **7.4 Conclusion**

(1) Heat-press temperature had crucial effects on the membrane morphology and characteristics. Increasing heat-press temperature could make more fibers fused together and improve the pore size distributions, and the mechanical properties and LEP were improved greatly. However, temperature above melting points (155 °C) was not desired as the post-treatment could make the membrane partially melt and its internal open pore structure could be damaged, which would have resulted in worse pore size, porosity and mass transfer coefficient.

(2) Heat-press pressure played less important role in affecting the membrane morphology and characteristics. Increasing pressure could result in more fused fibers, narrower pore size distribution and higher tensile strength and LEP. However, the improvement was somehow not so great. And when the pressure exceeded certain value, the improvement would be ignorable as the membrane reached its maximum compaction level.

(3) Heat-press duration affected the morphology and characteristics of membranes greatly. Increasing temperature could greatly cause more fibers fused at interlay points, and the pore size distribution was narrowed with significantly decreased average pore size. The mechanical strength and LEP was improved greatly also.

(4) Membrane samples with various thicknesses were heat-pressed with optimal conditions (150 °C, 6.5kPa& 8 h), and it was found that effects on morphology and characteristics were consistent regardless of the thickness. MD tests with selected membranes were also conducted, and it was found that membranes after heat-press had greatly improved permeation performance, while thickness of membrane still played an important role in permeation.

Overall, heat-press treatment with reasonable conditions could successfully improve the characteristics of the membranes, and hence permeation performance in MD. Heat-press temperature and duration had dominant roles in the post-treatment, while pressure had relatively minor role. Thickness of heat-pressed membranes between 37 and 130  $\mu\text{m}$  was considered as the optimal range due to their relatively high permeability, contributed by their

relatively small surface pore size and thin thickness. Thickness of electrospun membrane beyond 200  $\mu\text{m}$  was considered not appropriate as mass transfer coefficient impressively decreased after thickness was increased beyond certain level. It was estimated that other polymer could be improved by heat-press with proper conditions in terms of morphology, LEP and tensile strength. In conclusion, heat-press technique was strongly recommended for electrospun polymer membrane to enhance their morphology and characteristics impressively as required by relative applications.

## **CHAPTER 8**

### **Improving Membrane Properties for Membrane Distillation by Annealing**

## 8.1 Introduction

Shortage of water is one of the biggest concerns in the future society while human population is increasing steadily. Desalination is becoming the major approach for coastal areas short of fresh water. Currently reverse osmosis (RO) is widely applied for the treatment process owing to its relatively high efficiency. However, there are two main issues in RO: high energy consumption and brine treatment, and the difficulty to address the issues is increasing as RO has already reached state-of-art. Therefore, new generations of technology are strongly needed to develop for replacement of RO technology (Alkhudhiri, Darwish & Hilal 2012; Tijing, Woo, et al. 2014). Among them, MD is one of the most promising technologies.

As an emerging technology, MD has not yet been widely applied in the global water industry owing to lack of suitable membranes for long-term operation. Qualities such as strong resistance against wetting and fouling is lacking in current available membranes on the market (Francis et al. 2014). At the moment, membranes designed for microfiltration are utilized in MD and they are mainly made of polyvinylidene fluoride (PVDF) owing to its high hydrophobicity, high solubility in common solvent, and high resistance against chemicals and heat (Dong et al. 2014b; Hwang et al. 2011).

Electrospun membranes possess some appropriate advantages involving high hydrophobicity, high porosity, adjustable pore size, and membrane thickness, which make them attractive candidates as MD membrane (Alkhudhiri, Darwish & Hilal 2012; Feng et al. 2013b). Compared to NIPS and TIPS, electrospinning is a relatively simple technique to fabricate membrane. By applying high electric fields on a polymer solution, millions of fibers are formed joining together to become nonwoven membrane sheet and collected on the foils (Feng et al. 2013b; Tijing, Choi, et al. 2014). Though electrospun membranes have many attractive properties for MD, however, they had some drawbacks limiting its performance, including relatively big pore sizes, low mechanical properties, and LEP compared to the membranes fabricated by casting methods. Thus, there is a requirement to improve these characteristics without sacrificing high porosity and hydrophobicity by some membrane modification approaches (Tijing, Choi, et al. 2014). For this reason, post-treatment processes, one type of membrane modification procedures, are applied on the electrospun membrane to enhance its morphology and characteristics regarding robustness and capability against wetting (Lalia, Guillen-Burrieza, et al. 2013b; Liao, Wang & Fane 2014). In our previous study, effects of

heat-press conditions have been fully studied. It has been found that temperature and duration played more important roles than pressure. The properties of the electrospun membrane had been impressively improved. Although the contact angle and porosity decreased, the LEP and hence permeation performance in desalination improved greatly. In this study, to further improve the properties of the electrospun membranes, annealing, a commonly applied thermal treatment used in material modification, was applied on the heat-pressed PVDF membrane at first time. Favourable change of the properties could be achieved, and the MD performance was further improved.

## 8.2 Experimental method

### 8.2.1 Heat-press treatment

After electrospinning, the as-spun membranes were removed from the collector and initially dried at 50 °C for 2 h inside an air flow oven (OTWMHD24, Labec, Australia). Membranes were then fully covered by foils, placed between flat metal plates with dead weight placed on the top plate, and put in a pre-heated oven. Then, heat-press temperatures of 150 °C, pressing pressure (i.e., dead weight on top of the membrane) of 6.5 kPa, and heat-press duration of 24 h were applied to the membranes.

### 8.2.2 Annealing

After heat-pressing, membrane annealing was realized by removing the dead weight on the membranes and leaving the pressed membranes in the oven at 120 °C (where temperature had been gradually decreased by 10 °C per hour) for another 1-3 days. After these day(s), the membranes were slowly cooled by reducing temperature in the oven by 10 °C per hour, until room temperature. Along with their thickness, the samples were named in **Table 20** as below:

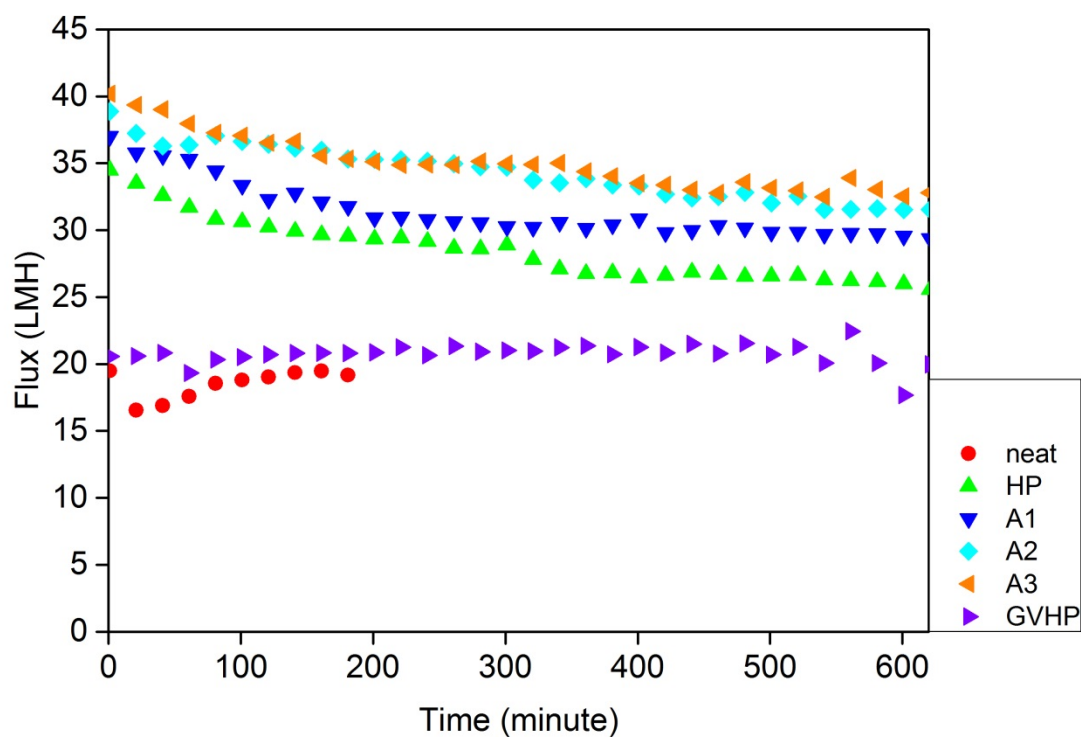
**Table 20.** Sample naming and their thicknesses

Sample name	Description	Membrane thickness (μm)
Neat	As-spun electrospun PVDF-HFP membranes	51

<b>HP</b>	Neat membrane heat-pressed at 150 °C under 6.5 kPa for 24 h	39
<b>A1</b>	HP membranes annealed for 1 day at 120°C	37
<b>A2</b>	HP membranes annealed for 2 days at 120°C	34
<b>A3</b>	HP membranes annealed for 3 days at 120 °C	34

## 8.3 Results and discussion

### 8.3.1 DCMD performance

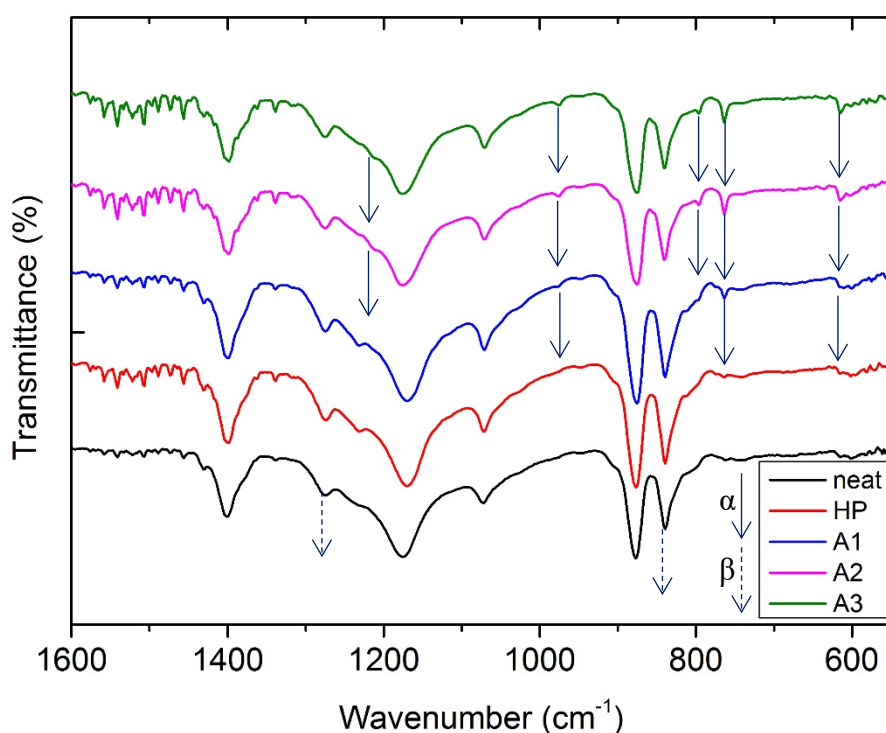


**Figure 65.** Comparison of flux performance between post-treated& as spun electrospun membranes and commercial ones (feed: 60 °C, permeate: 20 °C)

All the heat-pressed and annealed membrane had a salt rejection of 99.99%, while the neat membrane suffered rapid wetting 30 minutes immediately after operation started as permeate conductivity increased beyond 10 mS/cm. The wetting of electrospun membranes could be

judged based on the steady increase in the flux and the conductivity of permeate. **Figure 65** showed that heat-pressed showed improved flux and wetting resistance; however, it had a noticeable decreasing trend during the 10 h operation. Annealed membranes showed noticeable higher flux than the heat-pressed membrane although they shared the same membrane thickness. Moreover, the annealed membrane showed a more stable trend of flux in 10 h operation than HP, indicating better wetting resistance. Membrane annealed for 2 and 3 days shared similar performance, and both performed better than the membrane annealed for 1 day. Flux of commercial membrane (GVHP) was shown here for comparison. A2 and 3, having superb average flux of 35 LMH in 10 h operation, were 75% higher than GVHP (20 LMH).

### 8.3.2 Increased crystallinity and appearance of $\alpha$ phase after annealing



**Figure 66.** FT-IR spectra of as-spun and thermal treated electrospun membranes

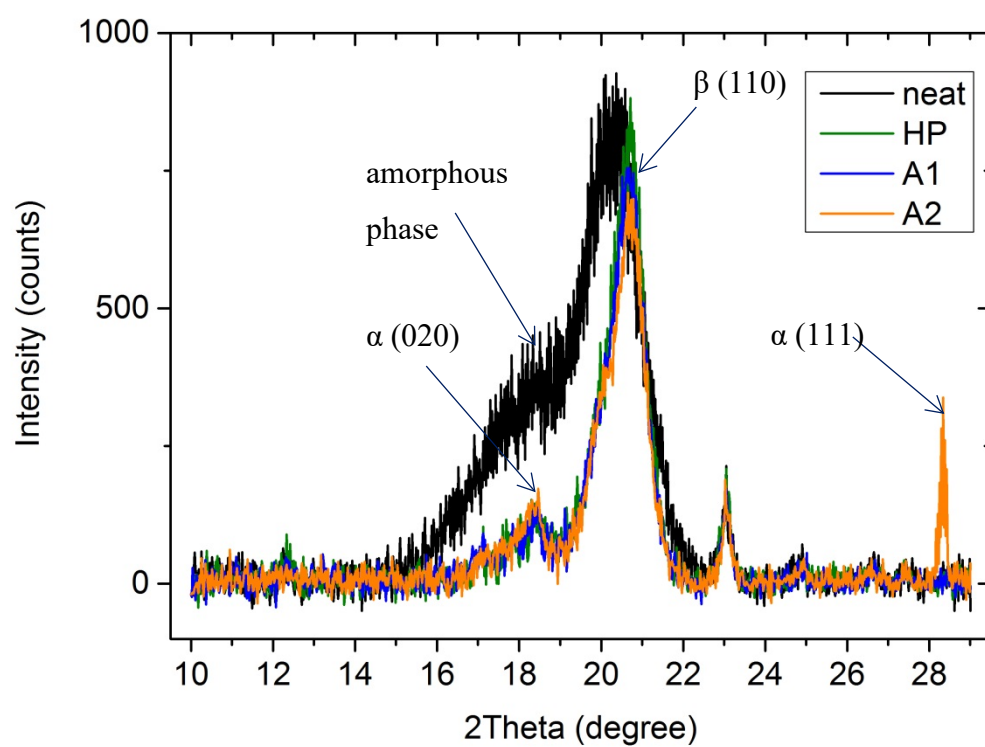
FT-IR spectra of  $\alpha$  and  $\beta$  phases of PVDF in PVDF-HFP copolymer had been investigated comprehensively. It was found that the bands in terms of  $\beta$  phase of PVDF appeared at 840 and 1278  $\text{cm}^{-1}$  (Du, Zhu & Xu 2006; Liu, Lu & Wu 2013) in all the as-spun and thermal treated membrane, as shown in **Figure 66**, while the bands related to  $\alpha$  phase of PVDF appeared at

615, 765, 795, 975 and 1212  $\text{cm}^{-1}$  (Du, Zhu & Xu 2006; Liu, Lu & Wu 2013; Salimi & Yousefi 2003), and they were only found in the annealed membranes. The phase of PVDF in neat membrane was basically  $\beta$  only as the peak representing  $\alpha$  phase rarely appeared. Two factors contributed to the  $\beta$  phase as-spun membranes: 1. the existence of HFP copolymer in the polymer chains (Du, Zhu & Xu 2006); 2. stretching and pulling of the electrospun fiber during the whipping process in electrospinning (Esterly 2002; Salimi & Yousefi 2003). After the neat membrane had been heat-pressed, the transmitter of wave at band of 840  $\text{cm}^{-1}$ , representing  $\beta$  phase, increased from 63.6 to 53.0%, while the band in terms of  $\alpha$  phase did not appear after heat-press treatment. The increase in transmitter of  $\beta$  phase bands showed the increase in crystallinity of the membrane as amorphous phase of PVDF was converted into  $\beta$  phase due to the mechanical deformation, caused by the pressure applied on the membranes during heat-pressing (Esterly 2002; Salimi & Yousefi 2003). Vineet et al. found that annealing PVDF above 80° led to an increase in both total crystallinity and  $\alpha$  phase PVDF percentage (Du, Zhu & Xu 2006; Tiwari & Srivastava 2014). Du et al. also pointed out that annealing of membrane resulted in the transformation of some regions of PVDF phase from  $\beta$  to  $\alpha$  (Du, Zhu & Xu 2006). In this study, bands in terms of  $\alpha$  phase started to appear at 615, 765, and 975  $\text{cm}^{-1}$  after one-day annealing, and more obviously at 615, 765, 795, 975 and 1212  $\text{cm}^{-1}$  after 2 and 3 days annealing, while the transmitter of wave at band of 840  $\text{cm}^{-1}$  decreased back to 62.1% which was same value as in the neat membrane. It is worth noting that membrane annealed for 3 days had nearly identical FT-IR results of spectra as the one annealed for 2 days, which means 2 days annealing could be long enough for sufficient annealing. The appearance of  $\alpha$  phase PVDF in the membrane was favorable for MD process owing to its non-polar properties because it led to decreased dipolar interaction between water molecular and membranes (Aqeel et al. 2015). The existence of  $\alpha$  phase PVDF could increase the liquid entry pressure and hence wetting resistance, contributing to better permeation performance. Saffarini et al. stated that annealing could also affect the microstructure evolution (Saffarini et al. 2013). By increasing the crystallinity and releasing the internal stresses caused by the heat-pressing, the thermal stability of the membrane could be improved, preventing LEP dropping rapidly owing to distortion at high feed temperature, so the performance of MD in long-term operation with electrospun membranes adequately annealed could be improved greatly.



### 8.3.3 Further detection of phase conversion by XRD

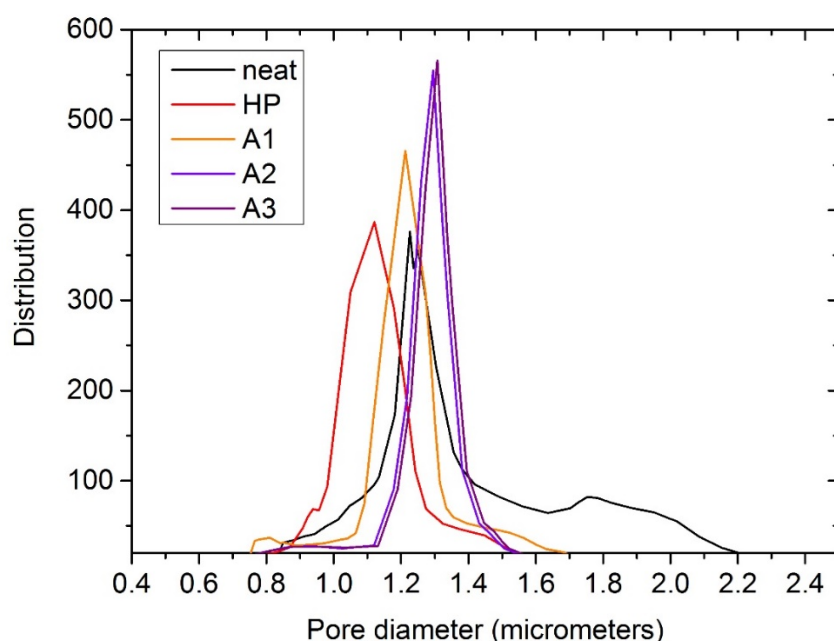
To further confirm the change of PVDF crystal phase in PH membranes, X-ray diffraction was conducted on these membrane samples. **Figure 67** showed the amorphous and both  $\alpha$  and  $\beta$  crystalline phases of PVDF in the PVDF-HFP electrospun membranes with or without post-treatment. It could be clearly seen that the as spun electrospun membrane had much more regions containing amorphous phase of PVDF as the peaks representing  $\alpha$  and  $\beta$  phase have been merged, leading to a much broader and weaker peak. After heat-treatment, PVDF of amorphous state reduced greatly as two sharp peaks at  $18.4^\circ$  and  $20.8^\circ$  appears, representing  $\alpha$  (020) and  $\beta$  (110) respectively (Du, Zhu & Xu 2006; Liu, Lu & Wu 2013). The sharp increase in the crystallinity of the PVDF-HFP membrane resulted in a great change of the membrane properties, especially contact angle (CA) and LEP which would be discussed in later sections. Annealing of the heat-pressed membrane could further improve the crystalline structure of PVDF-HFP membrane in favored way. Due to the non-polar structure, membrane composing more regions of  $\alpha$  phase PVDF has higher hydrophobicity, leading to higher wetting resistance. While the total crystallinity nearly maintained unchanged, annealing heat pressed membrane for one day at  $120^\circ\text{C}$  could convert  $\beta$  phase to  $\alpha$  phase as the relative peaks varied. After the membranes were further annealed for another day, both  $\alpha$  phase and crystallinity was increased, leading to the increase in thermal and mechanical stability (Liu, Lu & Wu 2013). More interestingly, a sharp new peak with high intensity at  $28.1^\circ$  appeared, which was very close to  $\alpha$  (111) having a 2-theta angle of  $27.8^\circ$ . Considering the various new peaks representing  $\alpha$  phase PVDF crystal appeared at FT-IR in A2 membranes, we assumed that the peak at  $2\theta$  angle of  $28.1^\circ$  was  $\alpha$  (111) (Esterly 2002; Liu, Lu & Wu 2013). The high intensity of  $\alpha$  (111) means a big increase of  $\alpha$  phase PVDF as well as total crystallinity, so we believed that more amorphous phase of PVDF along with  $\beta$  phase were converted to  $\alpha$  phase. A3 (membrane annealed for 3 days with slow cooling) showed identical spectra of XRD results as A2, so it was not shown on **Figure 67** for tidiness.



**Figure 67.** XRD patterns ( $2\theta$  spectra) of as-spun and thermal treated electrospun membranes

### 8.3.4 Improvement of membrane properties

#### 8.3.4.1 Pore size distribution and porosity



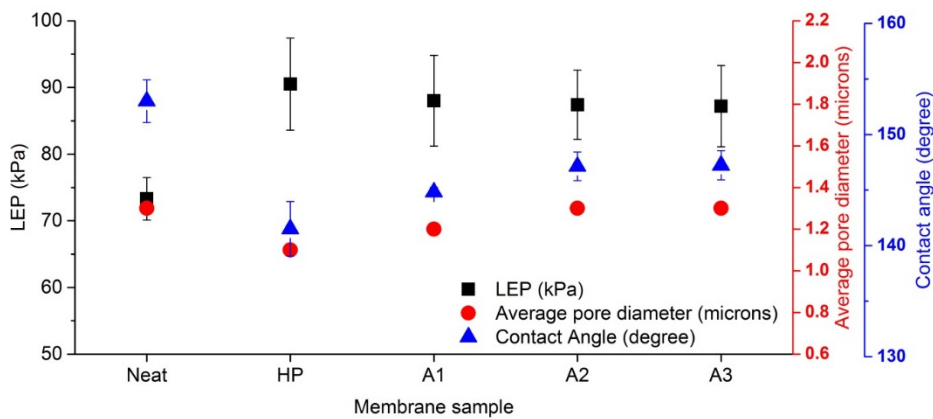
**Figure 68.** Pore diameter distribution of as spun and post-treated electrospun membranes

**Figure 68** showed the pore size distribution of membranes before and after heat treatment. The as-spun membrane had an average pore diameter of 1.3  $\mu\text{m}$  and a much wider range (from 0.8 – 2.2  $\mu\text{m}$ ) than the other samples. The heat-pressed membrane (HP) had the smallest average pore size (1.1  $\mu\text{m}$ ) and a much-decreased range of pore diameter compared with the neat ones because the fibers were deformed and widened under high pressure at 150°. Annealing the HP membranes for 1 day could further narrow the pore size distribution although the mean pore diameter increased from 1.1 to 1.2  $\mu\text{m}$ . The increase in pore size was due to the further decrease in the membrane thickness from 39 to 37  $\mu\text{m}$  which might be caused by the release of internal stress generated during heat-press; the other possible cause could be the supplementary merging of crystalline phase of PVDF which was converted from amorphous phase during annealing. The results were consistent with the study of Saffarini et al., as it was found that an increase in annealing temperature would lead to an increase in average pore size of the membranes (Saffarini et al. 2013). Further annealing for another day could decrease the range of the pore diameter greatly and a sharp peak appeared, although the average mean pore size

was further increased to 1.3  $\mu\text{m}$  (which was same as the neat membrane). An increased average pore diameter led to an increase in the flux performance (Manawi et al. 2014), justifying that MD applied with A2 and A3 membranes had the highest flux performance than the other samples. In literature, the pore size distribution of MD membranes generally lied between 0.2 and 1  $\mu\text{m}$  as the increase in maximum pore size would greatly decreased the LEP, leading to wetting problems (Camacho et al. 2013b). Narrowing the range of pore diameter greatly improved the wetting resistance as LEPs of A2 and A3 were much higher than the one of neat membranes. The other factor regarding improvement of wetting resistance is regarding evolution of crystalline structure in micro-view, which was fully discussed in last two sections. The heat-pressing process turned the amorphous state of PVDF into crystalline phases, which had much higher thermal and mechanical stability (Liu, Lu & Wu 2013); and annealing process help some of amorphous and  $\beta$  phase PVDF being converted into  $\alpha$  phase, which had higher hydrophobicity owing to its non-polar structure. Both factors contributed to A2's high wetting resistance in MD process even though it had highest average pore size (same as the neat ones). A high average pore size led to high flux performance which was favored for MD applications. A3 had nearly identical pore diameter distribution as A2; therefore, annealing for 2 days was sufficient for the improvement.

The porosity of neat and thermal treated membranes did not have significant difference. The porosity of neat, HP, A1, A2, A3 were 91%, 86%, 86%, 87%, and 87%, respectively, somehow following the trend of contact angle (CA). However, their difference was too minimal to affect the MD flux performance.

### 8.3.5 Improvement of liquid entry pressure (LEP) and hydrophobicity



**Figure 69.** Comparison of LEP, CA and average pore diameter of as-spun, heat-pressed, and annealed membranes

Comparison of membrane properties of LEP, CA and pore size between as spun and post-treated membranes had been investigated. Consistent with previous study (Yao et al. 2016), **Figure 69** showed that the LEP of the neat membrane had the lowest LEP, leading to rapid wetting in DCMD. After the membrane was heat-pressed, the LEP increased dramatically from 73 to 91 kPa owing to the vastly decreased average pore diameter and increased crystallinity, although the contact angle decreased greatly from 153° to 142° owing to the reduced roughness. Annealing the HP membranes did not result in significant change of LEP as the effect of increased pore sizes was offset by the increase in the hydrophobicity of the membranes, indicated by the increased CA. A2 shared nearly identical LEP as HP while it had highest pore size (1.3  $\mu\text{m}$ ) owing to a greatly increased CA of 147°. The 2-days annealing was proved to be sufficient for the property improvement as A3 shared nearly identical LEP, CA and average pore diameter as A2.

## 8.4 Conclusion

In the present study, we successfully fabricated electrospun nanofiber membranes and modified them by post-treatments (heat-pressing and annealing). Especially, effects of annealing on the electrospun membranes have been extensively investigated. Based on the results, it was found that the sufficiently annealed electrospun membranes had increased average pore size, which contributed to its much higher flux in DCMD than the other membrane samples. An average flux 35 LMH could be achieved for annealed membranes while a flux of 20 LMH was obtained by using commercial PVDF membranes in the same DCMD setup during 10 h operation. Also, the increase in  $\alpha$  phase of PVDF led to the increase in the hydrophobicity of the membrane, so the high LEP after heat-pressing was maintained unchanged although the average pore diameter increased. The other key factor in terms of wetting resistance was the greatly narrowed pore size distribution, membrane annealed for 2 and 3 days had the narrowest distribution among all the samples. In summary, annealing technique is strongly recommended for electrospun nanofiber membrane compared with heat-pressing technique and without post-treatment to improve their characteristics such as LEP, CA and pore size for membrane distillation process.

## **CHAPTER 9**

### **Conclusions and Recommendations**

## 9.1 Conclusions

The overall aim of my PhD study is to develop highly efficient membrane system to treat wastewater with special designed membranes. MD has many advantages over conventional MF such as high quality permeates and potentially high energy efficiency because MD has unique mechanism which makes it capable of treating wastewater that other technologies are struggling to deal with. So, there are lots of potentials in replacing MF in MBR with MD. Hereby, following research objectives have been developed to meet the aims: 1. to develop the first thermophilic anMDBR for the treatment of municipal wastewater. 2. to improve the permeation performance of HF membranes. 3. to investigate the behavior of organic compounds in MD processes regarding fouling and mass transfer.

During my PhD studies, I have successfully developed the first anMDBR system in lab-scale. High inorganic and organic compounds rejection of 99.99% could be achieved using this system. Based on the results, I recommend 45 °C as optimal bioreactor temperatures for its stable flux performance and resource recovery. It was found that salinity of the mixed liquor had minimal impact on anMDBR. The potential recovery of biogas and VOCs offered economic benefits. Some challenges were realized when developing anMDBR system: 1. Permeation flux was very low (~2 LMH). 2. Impact of volatile organic compounds (VOCs). 3. Fouling issues. Hence, following solutions have been suggested: 1. Development of membrane with high permeability. 2. Study of VOCs behavior. 3. New membrane design for anti-fouling properties. Therefore, in next stage of study, I developed first HF membranes with bicontinuous structure and porous skin without using weak solvent in coagulation bath. The bicontinuous morphology improved permeation performance in membrane distillation due to high porosity and mean pore size. Also, I found that non-solvents in the dope solution affect the morphology of HF membranes. It can be concluded that this is a simple and cost-effective technique, which is suitable for mass production. Then I investigated the behavior of VOCs in feed tank. It was found that VOCs with surfactant properties existing in the feed have high mobility and cause rapid wetting. Also, the total flux of VMD was increased with the addition of VOCs into the feed. And VOCs showed negative impacts on the permeate quality as they penetrated membranes. I also conducted some researches regarding permeation performance improvement using heat-treatment and optimal conditions had been determined.

The remaining challenge is fouling issues. Therefore, we need to develop MD membranes with anti-fouling properties. One of main potential solutions is to develop membranes with special wettability. This special surface wettability expands the application of MD towards treatment of challenging feed solutions, or those containing oils or low surface tension components. The present thesis has compiled and analyzed the various studies related to membranes with special surface wettability for MD and the improvement membrane properties via various methods. The fundamental concepts regarding surface wettability have been thoroughly discussed to aid in the membrane design. Individual special wettability is also defined in association with the fundamental concepts, and the insights of their benefits and issues are offered. The relative approaches to achieve the special wettability have been summarized based on membrane substrates, which is classified for detailed comparison and analysis.

## **9.2 Recommendations**

Membranes with high fouling and wetting resistance are required for the success of MD applications such as anMDBR, especially for membrane distillation bioreactors. Therefore, membranes with special wettability should be developed:

(1) Omniphobic and Janus (omniphobic-on-hydrophilic) membranes are developed to deal with highly saline produced water which usually contains surfactants and low surface tension liquid (e.g. oil water emulsion). They can be used in anMDBR. The surface-modified membranes have significantly increased organic fouling resistance. However, the omniphobic property highly relies on the hierarchical morphology (especially re-entrant structures). The air trapped on the surface structures plays an important role in omniphobic membranes. As the trapped air may escape from air pockets during continuous MD operations, the membranes will gradually lose its omniphobicity. Therefore, new morphology design such as repulsive air-spring structures should be developed for MD membranes to maintain omniphobicity in long-term operation. Another issue is the wide use of fluorination during surface modification to reduce surface tension. Environment-friendly chemicals should be developed for the achievement of omniphobic membranes;

(2) Janus (hydrophilic-on-hydrophobic) membranes have been developed targeting low surface tension saline wastewater. The hydrophilic layer exhibits high underwater oil resistance. Some researchers found such membrane have higher oil resistance than omniphobic membranes as it



completely prevents hydrophobic interaction. They could be used in an MDBR due to their high resistance against low surface tension compounds. However, surface charge of the Janus (hydrophilic-on-hydrophobic) membrane should be wisely controlled based on the charge of organic compounds in wastewater for electrostatic repulsion, so that the Janus membranes can maintain underwater oleophobicity for longer time. It is concluded that, in MD experiments, both omniphobic or Janus membrane can only mitigate the impacts of surfactants at low concentration in limited time, which means the control of organic concentration in bioreactor and membrane cleaning strategies should also be optimized.

(3) There are challenges for omniphobic and Janus membrane. The attachment between substrates and coating layers should be strong enough against routine water flush and chemical cleaning in real operational scenarios. However, few studies have investigated the robustness of the surface-modified membranes, which should be one of the main areas for research in future study. Another issue is the limitation of substrates. The mean pore size of substrates should not be too small as it will significantly decrease after surface modification, so electrospun and inorganic membranes are preferred. However, the energy consumption of these two fabrication techniques are intensive which greatly increase production costs.

Nevertheless, membranes with special wettability have bright future for MD applications if the challenges mentioned above are well addressed. Some potential technical advances and novel approaches, which may contribute to this emerging technology are highlighted as below.

(1) The re-entrant structures on membrane surfaces are critical for the achievement of superhydrophobic and omniphobic surface. Currently, its achievement is mainly dependent on depositing micro/nano particles on/in the surface. Novel top-down techniques (e.g., templating) or bottom-up techniques (e.g. carbon quantum dots) can be successful candidates for the construction of more stable re-entrant structures;

(2) As nanotechnology plays an important role in material science supporting membrane fabrication, its advance can bring novel nanomaterials with unprecedented benefits as additive in either substrates or coating layers for special wettability with improved permeability or fouling resistance;

(3) Conventional surface modification method such as lithograph and templating can be implemented for hierarchical surface structures. Only one group of researchers have developed

superhydrophobic surface by casting dope solutions on prepared PDMS substrate (Zhao et al. 2018). These top-down one-step methods can prevent the bonding issues between coating layers and substrates;

(4) Similarly, novel fabrication technique (e.g. 3D printing) opens possibilities of one-step fabrication of membranes with special wettability, dealing with weak bonding issues between coating layers and substrates;

(5) Membrane designs taking consideration of routine cleaning procedures in advance. As membrane wetting and fouling are inevitable in MD, membranes with high flux recovery after cyclical water flush and chemical cleaning are attractive in practice;

(6) MD in conjunction with other technologies to form a hybrid wastewater treatment system will mitigate the negative impacts on membranes due to improved control of foulants and wetting agents.

## REFERENCES

- Abed, M.R.M., Kumbharkar, S.C., Groth, A.M. & Li, K. 2012, 'Ultrafiltration PVDF hollow fibre membranes with interconnected bicontinuous structures produced via a single-step phase inversion technique', *Journal of Membrane Science*, vol. 407-408, pp. 145-54.
- Ahmad, A.L., Otitoju, T.A. & Ooi, B.S. 2018, 'Hollow fiber (HF) membrane fabrication: A review on the effects of solution spinning conditions on morphology and performance', *Journal of Industrial and Engineering Chemistry*.
- Ahmed, F.E., Lalia, B.S. & Hashaiekeh, R. 2015, 'A review on electrospinning for membrane fabrication: Challenges and applications', *Desalination*, vol. 356, pp. 15-30.
- Al-Obaidani, S., Curcio, E., Macedonio, F., Di Profio, G., Al-Hinai, H. & Drioli, E. 2008, 'Potential of membrane distillation in seawater desalination: thermal efficiency, sensitivity study and cost estimation', *Journal of Membrane Science*, vol. 323, no. 1, pp. 85-98.
- Alkhudhiri, A., Darwish, N. & Hilal, N. 2012, 'Membrane distillation: a comprehensive review', *Desalination*, vol. 287, pp. 2-18.
- Alkhudhiri, A., Darwish, N. & Hilal, N. 2013a, 'Produced water treatment: application of air gap membrane distillation', *Desalination*, vol. 309, pp. 46-51.
- Alkhudhiri, A., Darwish, N. & Hilal, N. 2013b, 'Treatment of saline solutions using Air Gap Membrane Distillation: Experimental study', *Desalination*, vol. 323, no. 0, pp. 2-7.
- An, A.K., Guo, J., Lee, E.-J., Jeong, S., Zhao, Y., Wang, Z. & Leiknes, T. 2017, 'PDMS/PVDF hybrid electrospun membrane with superhydrophobic property and drop impact dynamics for dyeing wastewater treatment using membrane distillation', *Journal of Membrane Science*, vol. 525, pp. 57-67.
- An, X., Liu, Z. & Hu, Y. 2018, 'Amphiphobic surface modification of electrospun nanofibrous membranes for anti-wetting performance in membrane distillation', *Desalination*, vol. 432, pp. 23-31.
- Aqeel, S.M., Wang, Z., Than, L., Sreenivasulu, G. & Zeng, X. 2015, 'Poly (vinylidene fluoride)/poly (acrylonitrile)-based superior hydrophobic piezoelectric solid derived by aligned carbon nanotubes in electrospinning: fabrication, phase conversion and surface energy', *RSC advances*, vol. 5, no. 93, pp. 76383-91.
- Atanasova, N., Dalmau, M., Comas, J., Poch, M., Rodriguez-Roda, I. & Buttiglieri, G. 2017, 'Optimized MBR for greywater reuse systems in hotel facilities', *J Environ Manage*, vol. 193, pp. 503-11.
- Attia, H., Alexander, S., Wright, C.J. & Hilal, N. 2017, 'Superhydrophobic electrospun membrane for heavy metals removal by air gap membrane distillation (AGMD)', *Desalination*, vol. 420, pp. 318-29.
- Attia, H., Johnson, D.J., Wright, C.J. & Hilal, N. 2018, 'Robust superhydrophobic electrospun membrane fabricated by combination of electrospinning and electrospraying techniques for air gap membrane distillation', *Desalination*, vol. 446, pp. 70-82.
- Averina, A., Rasul, M. & Begum, S. 2008, 'Management of coal seam gas (CSG) by-product water: a case study on spring gully mine site in Queensland, Australia', *2nd International Conference on Waste Management, Water Pollution, Air Pollution, Indoor Climate (WWAI'08)*, Corfu, Greece, pp. 26-8.
- Banat, F. & Al-Shannag, M. 2000, 'Recovery of dilute acetone-butanol-ethanol (ABE) solvents from aqueous solutions via membrane distillation', *Bioprocess Engineering*, vol. 23, no. 6, pp. 643-9.

- Banel, A. & Zygmunt, B. 2011, 'Application of gas chromatography-mass spectrometry preceded by solvent extraction to determine volatile fatty acids in wastewater of municipal, animal farm and landfill origin', *Water Sci Technol*, vol. 63, no. 4, pp. 590-7.
- Boban, M., Golovin, K., Tobelmann, B., Gupte, O., Mabry, J.M. & Tuteja, A. 2018, 'Smooth, All-Solid, Low-Hysteresis, Omniphobic Surfaces with Enhanced Mechanical Durability', *ACS applied materials & interfaces*, vol. 10, no. 14, pp. 11406-13.
- Bonyadi, S. & Chung, T.-S. 2009, 'Highly porous and macrovoid-free PVDF hollow fiber membranes for membrane distillation by a solvent-dope solution co-extrusion approach', *Journal of Membrane Science*, vol. 331, no. 1-2, pp. 66-74.
- Bonyadi, S. & Chung, T.S. 2007, 'Flux enhancement in membrane distillation by fabrication of dual layer hydrophilic-hydrophobic hollow fiber membranes', *Journal of Membrane Science*, vol. 306, no. 1, pp. 134-46.
- Boo, C., Lee, J. & Elimelech, M. 2016, 'Omniphobic Polyvinylidene Fluoride (PVDF) Membrane for Desalination of Shale Gas Produced Water by Membrane Distillation', *Environmental Science & Technology*, vol. 50, no. 22, pp. 12275-82.
- Boubakri, A., Bouguecha, S.A.-T., Dhaouadi, I. & Hafiane, A. 2015, 'Effect of operating parameters on boron removal from seawater using membrane distillation process', *Desalination*, vol. 373, pp. 86-93.
- Boubakri, A., Hafiane, A. & Bouguecha, S.A.T. 2014, 'Application of response surface methodology for modeling and optimization of membrane distillation desalination process', *Journal of Industrial and Engineering Chemistry*, vol. 20, no. 5, pp. 3163-9.
- Boulay, A.-M., Bare, J., Benini, L., Berger, M., Lathuillière, M.J., Manzardo, A., Margni, M., Motoshita, M., Núñez, M. & Pastor, A.V. 2018, 'The WULCA consensus characterization model for water scarcity footprints: assessing impacts of water consumption based on available water remaining (AWARE)', *The International Journal of Life Cycle Assessment*, vol. 23, no. 2, pp. 368-78.
- Brantley, S.L., Yoxtheimer, D., Arjmand, S., Grieve, P., Vidic, R., Pollak, J., Llewellyn, G.T., Abad, J. & Simon, C. 2014, 'Water resource impacts during unconventional shale gas development: The Pennsylvania experience', *International Journal of Coal Geology*, vol. 126, pp. 140-56.
- Brinkley, R.L. & Gupta, R.B. 1998, 'Intra-and intermolecular hydrogen bonding of 2-methoxyethanol and 2-butoxyethanol in n-hexane', *Industrial & engineering chemistry research*, vol. 37, no. 12, pp. 4823-7.
- Buonomenna, M.G., Macchi, P., Davoli, M. & Drioli, E. 2007, 'Poly(vinylidene fluoride) membranes by phase inversion: the role the casting and coagulation conditions play in their morphology, crystalline structure and properties', *European Polymer Journal*, vol. 43, no. 4, pp. 1557-72.
- Camacho, L., Dumée, L., Zhang, J., Li, J.-d., Duke, M., Gomez, J. & Gray, S. 2013a, 'Advances in membrane distillation for water desalination and purification applications', *Water*, vol. 5, no. 1, pp. 94-196.
- Camacho, L.M., Dumée, L., Zhang, J., Li, J.-d., Duke, M., Gomez, J. & Gray, S. 2013b, 'Advances in membrane distillation for water desalination and purification applications', *Water*, vol. 5, no. 1, pp. 94-196.
- Cassie, A. & Baxter, S. 1944, 'Wettability of porous surfaces', *Transactions of the Faraday society*, vol. 40, pp. 546-51.
- Cerneaux, S., Strużyńska, I., Kujawski, W.M., Persin, M. & Larbot, A. 2009, 'Comparison of various membrane distillation methods for desalination using hydrophobic ceramic membranes', *Journal of membrane science*, vol. 337, no. 1-2, pp. 55-60.

- Chang, J., Zuo, J., Zhang, L., O'Brien, G.S. & Chung, T.-S. 2017, 'Using green solvent, triethyl phosphate (TEP), to fabricate highly porous PVDF hollow fiber membranes for membrane distillation', *Journal of Membrane Science*, vol. 539, pp. 295-304.
- Chen, L.-H., Huang, A., Chen, Y.-R., Chen, C.-H., Hsu, C.-C., Tsai, F.-Y. & Tung, K.-L. 2018, 'Omniphobic membranes for direct contact membrane distillation: Effective deposition of zinc oxide nanoparticles', *Desalination*, vol. 428, pp. 255-63.
- Chew, N.G.P., Zhao, S., Loh, C.H., Permogorov, N. & Wang, R. 2017, 'Surfactant effects on water recovery from produced water via direct-contact membrane distillation', *Journal of Membrane Science*, vol. 528, pp. 126-34.
- Chew, N.G.P., Zhao, S., Malde, C. & Wang, R. 2017, 'Superoleophobic surface modification for robust membrane distillation performance', *Journal of Membrane Science*, vol. 541, pp. 162-73.
- Chew, N.G.P., Zhao, S., Malde, C. & Wang, R. 2018, 'Polyvinylidene fluoride membrane modification via oxidant-induced dopamine polymerization for sustainable direct-contact membrane distillation', *Journal of Membrane Science*, vol. 563, pp. 31-42.
- Choi, W., Tuteja, A., Mabry, J.M., Cohen, R.E. & McKinley, G.H. 2009, 'A modified Cassie–Baxter relationship to explain contact angle hysteresis and anisotropy on non-wetting textured surfaces', *Journal of colloid and interface science*, vol. 339, no. 1, pp. 208-16.
- Chul Woo, Y., Chen, Y., Tijing, L.D., Phuntsho, S., He, T., Choi, J.-S., Kim, S.-H. & Kyong Shon, H. 2017, 'CF<sub>4</sub> plasma-modified omniphobic electrospun nanofiber membrane for produced water brine treatment by membrane distillation', *Journal of Membrane Science*, vol. 529, pp. 234-42.
- Crick, C.R. & Parkin, I.P. 2011, 'Water droplet bouncing—a definition for superhydrophobic surfaces', *Chemical Communications*, vol. 47, no. 44, pp. 12059-61.
- Dahm, K.G., Guerra, K.L., Xu, P. & Drewes, J.E. 2011, 'Composite geochemical database for coalbed methane produced water quality in the Rocky Mountain region', *Environ Sci Technol*, vol. 45, no. 18, pp. 7655-63.
- Deng, L., Ye, H., Li, X., Li, P., Zhang, J., Wang, X., Zhu, M. & Hsiao, B.S. 2018, 'Self-roughened omniphobic coatings on nanofibrous membrane for membrane distillation', *Separation and Purification Technology*, vol. 206, pp. 14-25.
- Deshmukh, A., Boo, C., Karanikola, V., Lin, S., Straub, A.P., Tong, T., Warsinger, D.M. & Elimelech, M. 2018, 'Membrane distillation at the water-energy nexus: limits, opportunities, and challenges', *Energy & Environmental Science*, vol. 11, no. 5, pp. 1177-96.
- Dong, Y., Ma, L., Tang, C.Y., Yang, F., Quan, X., Jassby, D., Zaworotko, M.J. & Guiver, M.D. 2018, 'Stable Superhydrophobic Ceramic-Based Carbon Nanotube Composite Desalination Membranes', *Nano Letters*, vol. 18, no. 9, pp. 5514-21.
- Dong, Z.-Q., Ma, X.-h., Xu, Z.-L., You, W.-T. & Li, F.-b. 2014a, 'Superhydrophobic PVDF–PTFE electrospun nanofibrous membranes for desalination by vacuum membrane distillation', *Desalination*, vol. 347, no. 0, pp. 175-83.
- Dong, Z.-Q., Ma, X.-h., Xu, Z.-L., You, W.-T. & Li, F.-b. 2014b, 'Superhydrophobic PVDF–PTFE electrospun nanofibrous membranes for desalination by vacuum membrane distillation', *Desalination*, vol. 347, pp. 175-83.
- Dong, Z.-Q., Wang, B.-J., Ma, X.-h., Wei, Y.-M. & Xu, Z.-L. 2015, 'FAS Grafted Electrospun Poly(vinyl alcohol) Nanofiber Membranes with Robust Superhydrophobicity for Membrane Distillation', *ACS Applied Materials & Interfaces*, vol. 7, no. 40, pp. 22652-9.

- Dow, N., García, J.V., Niadoo, L., Milne, N., Zhang, J., Gray, S. & Duke, M. 2017, 'Demonstration of membrane distillation on textile waste water: assessment of long term performance, membrane cleaning and waste heat integration', *Environmental Science: Water Research & Technology*, vol. 3, no. 3, pp. 433-49.
- Drioli, E., Ali, A. & Macedonio, F. 2015, 'Membrane distillation: recent developments and perspectives', *Desalination*, vol. 356, pp. 56-84.
- Du, C.-H., Zhu, B.-K. & Xu, Y.-Y. 2006, 'The effects of quenching on the phase structure of vinylidene fluoride segments in PVDF-HFP copolymer and PVDF-HFP/PMMA blends', *Journal of materials science*, vol. 41, no. 2, pp. 417-21.
- Duong, H.C., Chivas, A.R., Nelemans, B., Duke, M., Gray, S., Cath, T.Y. & Nghiem, L.D. 2015a, 'Treatment of RO brine from CSG produced water by spiral-wound air gap membrane distillation—a pilot study', *Desalination*, vol. 366, pp. 121-9.
- Duong, H.C., Chivas, A.R., Nelemans, B., Duke, M., Gray, S., Cath, T.Y. & Nghiem, L.D. 2015b, 'Treatment of RO brine from CSG produced water by spiral-wound air gap membrane distillation - A pilot study', *Desalination*, vol. 366, pp. 121-9.
- Duong, H.C., Chivas, A.R., Nelemans, B., Duke, M., Gray, S., Cath, T.Y. & Nghiem, L.D. 2015c, 'Treatment of RO brine from CSG produced water by spiral-wound air gap membrane distillation — A pilot study', *Desalination*, vol. 366, pp. 121-9.
- El-Abbassi, A., Hafidi, A., García-Payo, M.C. & Khayet, M. 2009, 'Concentration of olive mill wastewater by membrane distillation for polyphenols recovery', *Desalination*, vol. 245, no. 1-3, pp. 670-4.
- Esterly, D.M. 2002, 'Manufacturing of Poly (vinylidene fluoride) and Evaluation of its Mechanical Properties'.
- Eykens, L., De Sitter, K., Dotremont, C., De Schepper, W., Pinoy, L. & Van Der Bruggen, B. 2017, 'Wetting resistance of commercial membrane distillation membranes in waste streams containing surfactants and oil', *Applied Sciences*, vol. 7, no. 2, p. 118.
- Eykens, L., De Sitter, K., Dotremont, C., Pinoy, L. & Van der Bruggen, B. 2017a, 'Membrane synthesis for membrane distillation: A review', *Separation and Purification Technology*, vol. 182, pp. 36-51.
- Eykens, L., De Sitter, K., Dotremont, C., Pinoy, L. & Van der Bruggen, B. 2017b, 'Wetting resistance of commercial membranes in waste streams containing surfactants and oil in membrane distillation', *Applied Sciences*, vol. 7, pp. 118-30.
- Fan, H. & Peng, Y. 2012, 'Application of PVDF membranes in desalination and comparison of the VMD and DCMD processes', *Chemical Engineering Science*, vol. 79, no. 0, pp. 94-102.
- Feng, C., Khulbe, K.C., Matsuura, T., Tabe, S. & Ismail, A.F. 2013a, 'Preparation and characterization of electro-spun nanofiber membranes and their possible applications in water treatment', *Separation and Purification Technology*, vol. 102, pp. 118-35.
- Feng, C., Khulbe, K.C., Matsuura, T., Tabe, S. & Ismail, A.F. 2013b, 'Preparation and characterization of electro-spun nanofiber membranes and their possible applications in water treatment', *Separation and Purification Technology*, vol. 102, no. 0, pp. 118-35.
- Fountoulakis, M.S., Markakis, N., Petousi, I. & Manios, T. 2016, 'Single house on-site grey water treatment using a submerged membrane bioreactor for toilet flushing', *Sci Total Environ*, vol. 551-552, pp. 706-11.
- Francis, L., Ghaffour, N., Alsaadi, A.S., Nunes, S.P. & Amy, G.L. 2014, 'Performance evaluation of the DCMD desalination process under bench scale and large scale module operating conditions', *Journal of Membrane Science*, vol. 455, no. 0, pp. 103-12.

- Franken, A., Nolten, J., Mulder, M., Bargeman, D. & Smolders, C. 1987, 'Wetting criteria for the applicability of membrane distillation', *Journal of Membrane Science*, vol. 33, no. 3, pp. 315-28.
- Friedler, E. & Hadari, M. 2006, 'Economic feasibility of on-site greywater reuse in multi-storey buildings', *Desalination*, vol. 190, no. 1-3, pp. 221-34.
- Fürstner, R., Barthlott, W., Neinhuis, C. & Walzel, P. 2005, 'Wetting and self-cleaning properties of artificial superhydrophobic surfaces', *Langmuir*, vol. 21, no. 3, pp. 956-61.
- Gao, W.J., Qu, X., Leung, K.T. & Liao, B.Q. 2012, 'Influence of temperature and temperature shock on sludge properties, cake layer structure, and membrane fouling in a submerged anaerobic membrane bioreactor', *Journal of Membrane Science*, vol. 421-422, pp. 131-44.
- García-Payo, M., Izquierdo-Gil, M.A. & Fernández-Pineda, C. 2000, 'Air gap membrane distillation of aqueous alcohol solutions', *Journal of Membrane Science*, vol. 169, no. 1, pp. 61-80.
- García-Payo, M., Izquierdo-Gil, M.A. & Fernández-Pineda, C. 2000, 'Wetting study of hydrophobic membranes via liquid entry pressure measurements with aqueous alcohol solutions', *Journal of colloid and interface science*, vol. 230, no. 2, pp. 420-31.
- García-Payo, M.C., Essalhi, M. & Khayet, M. 2010, 'Effects of PVDF-HFP concentration on membrane distillation performance and structural morphology of hollow fiber membranes', *Journal of Membrane Science*, vol. 347, no. 1-2, pp. 209-19.
- Ge, J., Peng, Y., Li, Z., Chen, P. & Wang, S. 2014, 'Membrane fouling and wetting in a DCMD process for RO brine concentration', *Desalination*, vol. 344, no. 0, pp. 97-107.
- Geng, H., He, Q., Wu, H., Li, P., Zhang, C. & Chang, H. 2014, 'Experimental study of hollow fiber AGMD modules with energy recovery for high saline water desalination', *Desalination*, vol. 344, no. 0, pp. 55-63.
- Goh, S., Zhang, J., Liu, Y. & Fane, A.G. 2013a, 'Fouling and wetting in membrane distillation (MD) and MD-bioreactor (MDBR) for wastewater reclamation', *Desalination*, vol. 323, no. 0, pp. 39-47.
- Goh, S., Zhang, J., Liu, Y. & Fane, A.G. 2013b, 'Fouling and wetting in membrane distillation (MD) and MD-bioreactor (MDBR) for wastewater reclamation', *Desalination*, vol. 323, pp. 39-47.
- Goh, S., Zhang, J., Liu, Y. & Fane, A.G. 2015, 'Membrane Distillation Bioreactor (MDBR) - A lower Green-House-Gas (GHG) option for industrial wastewater reclamation', *Chemosphere*, vol. 140, pp. 129-42.
- Gordalla, B.C., Ewers, U. & Frimmel, F.H. 2013, 'Hydraulic fracturing: a toxicological threat for groundwater and drinking-water?', *Environmental earth sciences*, vol. 70, no. 8, pp. 3875-93.
- Gryta, M., Grzechulska-Damszel, J., Markowska, A. & Karakulski, K. 2009, 'The influence of polypropylene degradation on the membrane wettability during membrane distillation', *Journal of Membrane Science*, vol. 326, no. 2, pp. 493-502.
- Gryta, M., Markowska-Szczupak, A., Bastrzyk, J. & Tomczak, W. 2013, 'The study of membrane distillation used for separation of fermenting glycerol solutions', *Journal of Membrane Science*, vol. 431, pp. 1-8.
- Gude, V.G. 2016, 'Desalination and sustainability—an appraisal and current perspective', *Water research*, vol. 89, pp. 87-106.
- Gude, V.G. 2017, 'Desalination and water reuse to address global water scarcity', *Reviews in Environmental Science and Bio/Technology*, vol. 16, no. 4, pp. 591-609.

- Guillen-Burrieza, E., Servi, A., Lalia, B.S. & Arafat, H.A. 2015, 'Membrane structure and surface morphology impact on the wetting of MD membranes', *Journal of Membrane Science*, vol. 483, no. 0, pp. 94-103.
- Hamawand, I., Yusaf, T. & Hamawand, S.G. 2013, 'Coal seam gas and associated water: A review paper', *Renewable and Sustainable Energy Reviews*, vol. 22, pp. 550-60.
- He, Q., Tu, T., Yan, S., Yang, X., Duke, M., Zhang, Y. & Zhao, S. 2018, 'Relating water vapor transfer to ammonia recovery from biogas slurry by vacuum membrane distillation', *Separation and Purification Technology*, vol. 191, pp. 182-91.
- Hernandez Rojas, M.E., Van Kaam, R., Schetrite, S. & Albasi, C. 2005, 'Role and variations of supernatant compounds in submerged membrane bioreactor fouling', *Desalination*, vol. 179, no. 1-3, pp. 95-107.
- Hong, S. & Elimelech, M. 1997, 'Chemical and physical aspects of natural organic matter (NOM) fouling of nanofiltration membranes', *Journal of Membrane Science*, vol. 132, no. 2, pp. 159-81.
- Hu, A.Y. & Stuckey, D.C. 2006, 'Treatment of dilute wastewaters using a novel submerged anaerobic membrane bioreactor', *Journal of environmental engineering*, vol. 132, no. 2, pp. 190-8.
- Huang, C.-Y., Ko, C.-C., Chen, L.-H., Huang, C.-T., Tung, K.-L. & Liao, Y.-C. 2018, 'A simple coating method to prepare superhydrophobic layers on ceramic alumina for vacuum membrane distillation', *Separation and Purification Technology*, vol. 198, pp. 79-86.
- Huang, Y.-X., Wang, Z., Jin, J. & Lin, S. 2017, 'Novel Janus Membrane for Membrane Distillation with Simultaneous Fouling and Wetting Resistance', *Environmental Science & Technology*, vol. 51, no. 22, pp. 13304-10.
- Hubadillah, S.K., Dzarfan Othman, M.H., Sheikh Abdul Kadir, S.H., Jamalludin, M.R., Harun, Z., Abd Aziz, M.H., Rahman, M.A., Jaafar, J., Nomura, M., Honda, S., Iwamoto, Y. & Fansuri, H. 2019, 'Removal of As(iii) and As(v) from water using green, silica-based ceramic hollow fibre membranes via direct contact membrane distillation', *RSC Advances*, vol. 9, no. 6, pp. 3367-76.
- Hung, W.-L., Wang, D.-M., Lai, J.-Y. & Chou, S.-C. 2016, 'On the initiation of macrovoids in polymeric membranes – effect of polymer chain entanglement', *Journal of Membrane Science*, vol. 505, pp. 70-81.
- Hussain, A., Kumar, P. & Mehrotra, I. 2015, 'NITROGEN AND PHOSPHORUS REQUIREMENT IN ANAEROBIC PROCESS: A REVIEW', *Environmental Engineering & Management Journal (EEMJ)*, vol. 14, no. 4.
- Hwang, H.J., He, K., Gray, S., Zhang, J. & Moon, I.S. 2011, 'Direct contact membrane distillation (DCMD): Experimental study on the commercial PTFE membrane and modeling', *Journal of Membrane Science*, vol. 371, no. 1–2, pp. 90-8.
- Jeison, D. & van Lier, J.B. 2008, 'Feasibility of thermophilic anaerobic submerged membrane bioreactors (AnSMBR) for wastewater treatment', *Desalination*, vol. 231, no. 1-3, pp. 227-35.
- Jung, J.T., Wang, H.H., Kim, J.F., Lee, J., Kim, J.S., Drioli, E. & Lee, Y.M. 2018, 'Tailoring nonsolvent-thermally induced phase separation (N-TIPS) effect using triple spinneret to fabricate high performance PVDF hollow fiber membranes', *Journal of Membrane Science*, vol. 559, pp. 117-26.
- Kaatze, U., Pottel, R. & Schumacher, A. 1992, 'Dielectric spectroscopy of 2-butoxyethanol/water mixtures in the complete composition range', *Journal of Physical Chemistry*, vol. 96, no. 14.



- Kang, G.D. & Cao, Y.M. 2014, 'Application and modification of poly(vinylidene fluoride) (PVDF) membranes - A review', *Journal of Membrane Science*, vol. 463, pp. 145-65.
- Khan, M.A., Ngo, H.H., Guo, W.S., Liu, Y.W., Zhou, J.L., Zhang, J., Liang, S., Ni, B.J., Zhang, X.B. & Wang, J. 2016, 'Comparing the value of bioproducts from different stages of anaerobic membrane bioreactors', *Bioresour Technol*, vol. 214, pp. 816-25.
- Khayet, M. 2011, 'Membranes and theoretical modeling of membrane distillation: a review', *Advances in colloid and interface science*, vol. 164, no. 1-2, pp. 56-88.
- Khayet, M., Godino, P. & Mengual, J.I. 2000, 'Theory and experiments on sweeping gas membrane distillation', *Journal of Membrane Science*, vol. 165, no. 2, pp. 261-72.
- Khayet, M. & Matsuura, T. 2003, 'Determination of surface and bulk pore sizes of flat-sheet and hollow-fiber membranes by atomic force microscopy, gas permeation and solute transport methods', *Desalination*, vol. 158, no. 1-3, pp. 57-64.
- Khayet, M., Mengual, J.I. & Matsuura, T. 2005, 'Porous hydrophobic/hydrophilic composite membranes: Application in desalination using direct contact membrane distillation', *Journal of Membrane Science*, vol. 252, no. 1, pp. 101-13.
- Kim, Y., Li, S., Francis, L., Li, Z., Linares, R.V., Alsaadi, A.S., Abu-Ghdaib, M., Son, H.S., Amy, G. & Ghaffour, N. 2019, 'Osmotically and Thermally Isolated Forward Osmosis–Membrane Distillation (FO–MD) Integrated Module', *Environmental science & technology*, vol. 53, no. 7, pp. 3488-98.
- Krupenkin, T.N., Taylor, J.A., Schneider, T.M. & Yang, S. 2004, 'From rolling ball to complete wetting: the dynamic tuning of liquids on nanostructured surfaces', *Langmuir*, vol. 20, no. 10, pp. 3824-7.
- Kujawa, J. 2019, 'From nanoscale modification to separation - The role of substrate and modifiers in the transport properties of ceramic membranes in membrane distillation', *Journal of Membrane Science*, vol. 580, pp. 296-306.
- Kujawa, J., Al-Gharabli, S., Kujawski, W. & Knozowska, K. 2017, 'Molecular grafting of fluorinated and nonfluorinated alkylsiloxanes on various ceramic membrane surfaces for the removal of volatile organic compounds applying vacuum membrane distillation', *ACS applied materials & interfaces*, vol. 9, no. 7, pp. 6571-90.
- Kujawa, J. & Kujawski, W. 2016, 'Functionalization of ceramic metal oxide powders and ceramic membranes by perfluoroalkylsilanes and alkylsilanes possessing different reactive groups: Physicochemical and tribological properties', *ACS applied materials & interfaces*, vol. 8, no. 11, pp. 7509-21.
- Kwon, M.H., Shin, H.S. & Chu, C.N. 2014, 'Fabrication of a super-hydrophobic surface on metal using laser ablation and electrodeposition', *Applied Surface Science*, vol. 288, pp. 222-8.
- Lalia, B.S., Guillen-Burrieza, E., Arafat, H.A. & Hashaikh, R. 2013a, 'Fabrication and characterization of polyvinylidene fluoride-co-hexafluoropropylene (PVDF-HFP) electrospun membranes for direct contact membrane distillation', *Journal of Membrane Science*, vol. 428, pp. 104-15.
- Lalia, B.S., Guillen-Burrieza, E., Arafat, H.A. & Hashaikh, R. 2013b, 'Fabrication and characterization of polyvinylidene fluoride-co-hexafluoropropylene (PVDF-HFP) electrospun membranes for direct contact membrane distillation', *Journal of Membrane Science*, vol. 428, no. 0, pp. 104-15.
- Lalia, B.S., Guillen, E., Arafat, H.A. & Hashaikh, R. 2014, 'Nanocrystalline cellulose reinforced PVDF-HFP membranes for membrane distillation application', *Desalination*, vol. 332, no. 1, pp. 134-41.

- Lalia, B.S., Kochkodan, V., Hashaikheh, R. & Hilal, N. 2013, 'A review on membrane fabrication: Structure, properties and performance relationship', *Desalination*, vol. 326, pp. 77-95.
- Lee, E.-J., Deka, B.J., Guo, J., Woo, Y.C., Shon, H.K. & An, A.K. 2017, 'Engineering the re-entrant hierarchy and surface energy of PDMS-PVDF membrane for membrane distillation using a facile and benign microsphere coating', *Environmental Science & Technology*, vol. 51, no. 17, pp. 10117-26.
- Lee, J., Boo, C., Ryu, W.-H., Taylor, A.D. & Elimelech, M. 2016, 'Development of Omniphobic Desalination Membranes Using a Charged Electrospun Nanofiber Scaffold', *ACS Applied Materials & Interfaces*, vol. 8, no. 17, pp. 11154-61.
- Leong, J.Y.C., Oh, K.S., Poh, P.E. & Chong, M.N. 2017, 'Prospects of hybrid rainwater-greywater decentralised system for water recycling and reuse: A review', *Journal of Cleaner Production*, vol. 142, pp. 3014-27.
- Lettinga, G. 1995, 'Anaerobic digestion and wastewater treatment systems', *Antonie van Leeuwenhoek*, vol. 67, no. 1, pp. 3-28.
- Li, J.-M., Xu, Z.-K., Liu, Z.-M., Yuan, W.-F., Xiang, H., Wang, S.-Y. & Xu, Y.-Y. 2003, 'Microporous polypropylene and polyethylene hollow fiber membranes. Part 3. Experimental studies on membrane distillation for desalination', *Desalination*, vol. 155, no. 2, pp. 153-6.
- Li, Q., Xu, Z.-L. & Yu, L.-Y. 2010, 'Effects of mixed solvents and PVDF types on performances of PVDF microporous membranes', *Journal of Applied Polymer Science*, vol. 115, no. 4, pp. 2277-87.
- Li, X., Wang, C., Yang, Y., Wang, X., Zhu, M. & Hsiao, B.S. 2014, 'Dual-biomimetic superhydrophobic electrospun polystyrene nanofibrous membranes for membrane distillation', *ACS Applied Materials and Interfaces*, vol. 6, no. 4, pp. 2423-30.
- Li, X., Yu, X., Cheng, C., Deng, L., Wang, M. & Wang, X. 2015, 'Electrospun Superhydrophobic Organic/Inorganic Composite Nanofibrous Membranes for Membrane Distillation', *ACS Applied Materials & Interfaces*, vol. 7, no. 39, pp. 21919-30.
- Li, Y., Dong, S. & Zhu, L. 2018, 'Preparation of novel poly(vinylidene fluoride)/TiO<sub>2</sub> photocatalysis membranes for use in direct contact membrane distillation', *Journal of Nanoparticle Research*, vol. 20, no. 3.
- Liang, S., Zhao, Y., Liu, C. & Song, L. 2008, 'Effect of solution chemistry on the fouling potential of dissolved organic matter in membrane bioreactor systems', *Journal of Membrane Science*, vol. 310, no. 1-2, pp. 503-11.
- Liao, Y., Loh, C.-H., Wang, R. & Fane, A.G. 2014, 'Electrospun Superhydrophobic Membranes with Unique Structures for Membrane Distillation', *ACS Applied Materials & Interfaces*, vol. 6, no. 18, pp. 16035-48.
- Liao, Y., Wang, R. & Fane, A.G. 2013, 'Engineering superhydrophobic surface on poly(vinylidene fluoride) nanofiber membranes for direct contact membrane distillation', *Journal of Membrane Science*, vol. 440, pp. 77-87.
- Liao, Y., Wang, R. & Fane, A.G. 2014, 'Fabrication of Bioinspired Composite Nanofiber Membranes with Robust Superhydrophobicity for Direct Contact Membrane Distillation', *Environmental Science & Technology*, vol. 48, no. 11, pp. 6335-41.
- Liao, Y., Wang, R., Tian, M., Qiu, C. & Fane, A.G. 2013a, 'Fabrication of polyvinylidene fluoride (PVDF) nanofiber membranes by electro-spinning for direct contact membrane distillation', *Journal of Membrane Science*, vol. 425-426, pp. 30-9.

- Liao, Y., Wang, R., Tian, M., Qiu, C. & Fane, A.G. 2013b, 'Fabrication of polyvinylidene fluoride (PVDF) nanofiber membranes by electro-spinning for direct contact membrane distillation', *Journal of Membrane Science*, vol. 425, pp. 30-9.
- Lin, D.-J., Chang, C.-L., Chen, T.-C. & Cheng, L.-P. 2002, 'Microporous PVDF membrane formation by immersion precipitation from water/TEP/PVDF system', *Desalination*, vol. 145, no. 1, pp. 25-9.
- Lin, D.-J., Chang, H.-H., Chen, T.-C., Lee, Y.-C. & Cheng, L.-P. 2006, 'Formation of porous poly(vinylidene fluoride) membranes with symmetric or asymmetric morphology by immersion precipitation in the water/TEP/PVDF system', *European Polymer Journal*, vol. 42, no. 7, pp. 1581-94.
- Lin, H., Peng, W., Zhang, M., Chen, J., Hong, H. & Zhang, Y. 2013, 'A review on anaerobic membrane bioreactors: applications, membrane fouling and future perspectives', *Desalination*, vol. 314, pp. 169-88.
- Lin, P.-J., Yang, M.-C., Li, Y.-L. & Chen, J.-H. 2015, 'Prevention of surfactant wetting with agarose hydrogel layer for direct contact membrane distillation used in dyeing wastewater treatment', *Journal of Membrane Science*, vol. 475, pp. 511-20.
- Lin, S., Nejati, S., Boo, C., Hu, Y., Osuji, C.O. & Elimelech, M. 2014, 'Omniphobic membrane for robust membrane distillation', *Environmental Science & Technology Letters*, vol. 1, no. 11, pp. 443-7.
- Liu, J., Lu, X. & Wu, C. 2013, 'Effect of Preparation Methods on Crystallization Behavior and Tensile Strength of Poly (vinylidene fluoride) Membranes', *Membranes*, vol. 3, no. 4, pp. 389-405.
- Liu, T. & Kim, C.-J. 2014, 'Turning a surface superrepellent even to completely wetting liquids'.
- Lonsdale, H. 1982, 'The growth of membrane technology', *Journal of membrane science*, vol. 10, no. 2-3, pp. 81-181.
- Lu, C., Su, C., Cao, H., Ma, X., Duan, F., Chang, J. & Li, Y. 2018, 'F-POSS based Omniphobic Membrane for Robust Membrane Distillation', *Materials Letters*, vol. 228, pp. 85-8.
- Lu, K.J., Zuo, J., Chang, J., Kuan, H.N. & Chung, T.-S. 2018, 'Omniphobic Hollow-Fiber Membranes for Vacuum Membrane Distillation', *Environmental Science & Technology*, vol. 52, no. 7, pp. 4472-80.
- Lu, X., Peng, Y., Ge, L., Lin, R., Zhu, Z. & Liu, S. 2016, 'Amphiphobic PVDF composite membranes for anti-fouling direct contact membrane distillation', *Journal of Membrane Science*, vol. 505, pp. 61-9.
- Lu, X., Peng, Y., Qiu, H., Liu, X. & Ge, L. 2017, 'Anti-fouling membranes by manipulating surface wettability and their anti-fouling mechanism', *Desalination*, vol. 413, pp. 127-35.
- Luna, H.J., Baêta, B.E.L., Aquino, S.F. & Susa, M.S.R. 2014, 'EPS and SMP dynamics at different heights of a submerged anaerobic membrane bioreactor (SAMBR)', *Process Biochemistry*, vol. 49, no. 12, pp. 2241-8.
- Luo, W., Phan, H.V., Hai, F.I., Price, W.E., Guo, W., Ngo, H.H., Yamamoto, K. & Nghiem, L.D. 2016, 'Effects of salinity build-up on the performance and bacterial community structure of a membrane bioreactor', *Bioresource Technology*, vol. 200, pp. 305-10.
- Luo, W., Phan, H.V., Xie, M., Hai, F.I., Price, W.E., Elimelech, M. & Nghiem, L.D. 2017, 'Osmotic versus conventional membrane bioreactors integrated with reverse osmosis for water reuse: Biological stability, membrane fouling, and contaminant removal', *Water Res*, vol. 109, pp. 122-34.

- Ma, M., Hill, R.M., Lowery, J.L., Fridrikh, S.V. & Rutledge, G.C. 2005, 'Electrospun Poly(Styrene-block-dimethylsiloxane) Block Copolymer Fibers Exhibiting Superhydrophobicity', *Langmuir*, vol. 21, no. 12, pp. 5549-54.
- Ma, Z., Hong, Y., Ma, L. & Su, M. 2009, 'Superhydrophobic Membranes with Ordered Arrays of Nanospiked Microchannels for Water Desalination', *Langmuir*, vol. 25, no. 10, pp. 5446-50.
- Manawi, Y.M., Khraisheh, M., Fard, A.K., Benyahia, F. & Adham, S. 2014, 'Effect of operational parameters on distillate flux in direct contact membrane distillation (DCMD): Comparison between experimental and model predicted performance', *Desalination*, vol. 336, no. 0, pp. 110-20.
- Mansourizadeh, A. & Ismail, A.F. 2011, 'Preparation and characterization of porous PVDF hollow fiber membranes for CO<sub>2</sub> absorption: Effect of different non-solvent additives in the polymer dope', *International Journal of Greenhouse Gas Control*, vol. 5, no. 4, pp. 640-8.
- Marmur, A. 2003, 'Wetting on hydrophobic rough surfaces: to be heterogeneous or not to be?', *Langmuir*, vol. 19, no. 20, pp. 8343-8.
- Marmur, A. 2004, 'The lotus effect: superhydrophobicity and metastability', *Langmuir*, vol. 20, no. 9, pp. 3517-9.
- Marmur, A. 2008, 'From hydrophilic to superhydrophobic: theoretical conditions for making high-contact-angle surfaces from low-contact-angle materials', *Langmuir*, vol. 24, no. 14, pp. 7573-9.
- Massoud, M.A., Tarhini, A. & Nasr, J.A. 2009, 'Decentralized approaches to wastewater treatment and management: applicability in developing countries', *J Environ Manage*, vol. 90, no. 1, pp. 652-9.
- McGaughey, A.L., Gustafson, R.D. & Childress, A.E. 2017, 'Effect of long-term operation on membrane surface characteristics and performance in membrane distillation', *Journal of Membrane Science*, vol. 543, pp. 143-50.
- McGinnis, R.L. & Elimelech, M. 2008, 'Global challenges in energy and water supply: the promise of engineered osmosis', ACS Publications.
- McHale, G. 2007, 'Cassie and Wenzel: were they really so wrong?', *Langmuir*, vol. 23, no. 15, pp. 8200-5.
- Melin, T., Jefferson, B., Bixio, D., Thoeye, C., De Wilde, W., De Koning, J., van der Graaf, J. & Wintgens, T. 2006, 'Membrane bioreactor technology for wastewater treatment and reuse', *Desalination*, vol. 187, no. 1-3, pp. 271-82.
- Meng, F., Zhang, H., Yang, F., Li, Y., Xiao, J. & Zhang, X. 2006, 'Effect of filamentous bacteria on membrane fouling in submerged membrane bioreactor', *Journal of Membrane Science*, vol. 272, no. 1-2, pp. 161-8.
- Meng, S., Mansouri, J., Ye, Y. & Chen, V. 2014, 'Effect of templating agents on the properties and membrane distillation performance of TiO<sub>2</sub>-coated PVDF membranes', *Journal of Membrane Science*, vol. 450, pp. 48-59.
- Meng, S., Ye, Y., Mansouri, J. & Chen, V. 2014, 'Fouling and crystallisation behaviour of superhydrophobic nano-composite PVDF membranes in direct contact membrane distillation', *Journal of Membrane Science*, vol. 463, pp. 102-12.
- Mengual, J., Khayet, M. & Godino, M. 2004, 'Heat and mass transfer in vacuum membrane distillation', *International Journal of Heat and Mass Transfer*, vol. 47, no. 4, pp. 865-75.
- Miwa, M., Nakajima, A., Fujishima, A., Hashimoto, K. & Watanabe, T. 2000, 'Effects of the surface roughness on sliding angles of water droplets on superhydrophobic surfaces', *Langmuir*, vol. 16, no. 13, pp. 5754-60.

- Munirasu, S., Banat, F., Durrani, A.A. & Haija, M.A. 2017, 'Intrinsically superhydrophobic PVDF membrane by phase inversion for membrane distillation', *Desalination*, vol. 417, pp. 77-86.
- Murphy, D. & de Pinho, M.N. 1995, 'An ATR-FTIR study of water in cellulose acetate membranes prepared by phase inversion', *Journal of Membrane Science*, vol. 106, no. 3, pp. 245-57.
- Naidu, G., Jeong, S. & Vigneswaran, S. 2015, 'Interaction of humic substances on fouling in membrane distillation for seawater desalination', *Chemical Engineering Journal*, vol. 262, pp. 946-57.
- Nejati, S., Boo, C., Osuji, C.O. & Elimelech, M. 2015, 'Engineering flat sheet microporous PVDF films for membrane distillation', *Journal of Membrane Science*, vol. 492, pp. 355-63.
- Nghiem, L.D. & Cath, T. 2011, 'A scaling mitigation approach during direct contact membrane distillation', *Separation and Purification Technology*, vol. 80, no. 2, pp. 315-22.
- Nghiem, L.D., Ren, T., Aziz, N., Porter, I. & Regmi, G. 2011, 'Treatment of coal seam gas produced water for beneficial use in Australia: a review of best practices', *Desalination and Water Treatment*, vol. 32, no. 1-3, pp. 316-23.
- Öktem, H., Erzurumlu, T. & Kurtaran, H. 2005, 'Application of response surface methodology in the optimization of cutting conditions for surface roughness', *Journal of Materials Processing Technology*, vol. 170, no. 1, pp. 11-6.
- Onda, T., Shibuichi, S., Satoh, N. & Tsujii, K. 1996, 'Super-Water-Repellent Fractal Surfaces', *Langmuir*, vol. 12, no. 9, pp. 2125-7.
- Onishi, V.C., Fraga, E.S., Reyes-Labarta, J.A. & Caballero, J.A. 2018, 'Desalination of shale gas wastewater: Thermal and membrane applications for zero-liquid discharge', *Emerging Technologies for Sustainable Desalination Handbook*, Elsevier, pp. 399-431.
- Orem, W., Tatu, C., Varonka, M., Lerch, H., Bates, A., Engle, M., Crosby, L. & McIntosh, J. 2014, 'Organic substances in produced and formation water from unconventional natural gas extraction in coal and shale', *International Journal of Coal Geology*, vol. 126, pp. 20-31.
- Oviedo-Ocana, E.R., Dominguez, I., Ward, S., Rivera-Sanchez, M.L. & Zaraza-Pena, J.M. 2017, 'Financial feasibility of end-user designed rainwater harvesting and greywater reuse systems for high water use households', *Environ Sci Pollut Res Int*.
- Owens, D.K. & Wendt, R. 1969, 'Estimation of the surface free energy of polymers', *Journal of applied polymer science*, vol. 13, no. 8, pp. 1741-7.
- Pathak, N., Chekli, L., Wang, J., Kim, Y., Phuntsho, S., Li, S., Ghaffour, N., Leiknes, T. & Shon, H. 2017, 'Performance of a novel baffled osmotic membrane bioreactor-microfiltration hybrid system under continuous operation for simultaneous nutrient removal and mitigation of brine discharge', *Bioresource Technology*, vol. 240, pp. 50-8.
- Peng, P., Fane, A. & Li, X. 2005, 'Desalination by membrane distillation adopting a hydrophilic membrane', *Desalination*, vol. 173, no. 1, pp. 45-54.
- Phattaranawik, J., Fane, A.G., Pasquier, A.C. & Bing, W. 2008, 'A novel membrane bioreactor based on membrane distillation', *Desalination*, vol. 223, no. 1-3, pp. 386-95.
- Phattaranawik, J., Fane, A.G., Pasquier, A.C.S., Bing, W. & Wong, F.S. 2009, 'Experimental study and design of a submerged membrane distillation bioreactor', *Chemical Engineering & Technology*, vol. 32, no. 1, pp. 38-44.

- Pinnau, I. & Koros, W.J. 1993, 'A qualitative skin layer formation mechanism for membranes made by dry/wet phase inversion', *Journal of Polymer Science Part B: Polymer Physics*, vol. 31, no. 4, pp. 419-27.
- Properties 2015, Sigma-aldrich, viewed 11/06/2015 2015, <<http://www.sigmaaldrich.com/catalog/product/aldrich/427179?lang=en&region=AU>>.
- Qiu, H., Peng, Y., Ge, L., Villacorta Hernandez, B. & Zhu, Z. 2018, 'Pore channel surface modification for enhancing anti-fouling membrane distillation', *Applied Surface Science*, vol. 443, pp. 217-26.
- Qtaishat, M., Matsuura, T., Kruczek, B. & Khayet, M. 2008, 'Heat and mass transfer analysis in direct contact membrane distillation', *Desalination*, vol. 219, no. 1-3, pp. 272-92.
- Quist-Jensen, C.A., Macedonio, F., Horbez, D. & Drioli, E. 2017, 'Reclamation of sodium sulfate from industrial wastewater by using membrane distillation and membrane crystallization', *Desalination*, vol. 401, pp. 112-9.
- Ray, S.S., Gandhi, M., Chen, S.-S., Chang, H.-M. & Cao, D.-T. 2018, 'Anti-wetting behaviour of Superhydrophobic Octadecyltrimethoxysilane blended PVDF/Recycled Carbon Black Composite Membrane for enhanced desalination', *Environmental Science: Water Research & Technology*.
- Razmjou, A., Arifin, E., Dong, G., Mansouri, J. & Chen, V. 2012, 'Superhydrophobic modification of TiO<sub>2</sub> nanocomposite PVDF membranes for applications in membrane distillation', *Journal of Membrane Science*, vol. 415-416, pp. 850-63.
- Ren, L.-F., Xia, F., Shao, J., Zhang, X. & Li, J. 2017, 'Experimental investigation of the effect of electrospinning parameters on properties of superhydrophobic PDMS/PMMA membrane and its application in membrane distillation', *Desalination*, vol. 404, pp. 155-66.
- Rezaei, M., Warsinger, D.M., Duke, M.C., Matsuura, T. & Samhaber, W.M. 2018, 'Wetting phenomena in membrane distillation: Mechanisms, reversal, and prevention', *Water research*, vol. 139, pp. 329-52.
- Rezaei, M., Warsinger, D.M., Lienhard V, J.H. & Samhaber, W.M. 2017, 'Wetting prevention in membrane distillation through superhydrophobicity and recharging an air layer on the membrane surface', *Journal of Membrane Science*, vol. 530, pp. 42-52.
- Rodrigues, A., Brito, A., Janknecht, P., Proença, M.F. & Nogueira, R. 2009, 'Quantification of humic acids in surface water: effects of divalent cations, pH, and filtration', *Journal of Environmental Monitoring*, vol. 11, no. 2, pp. 377-82.
- Rodríguez, A., Serrano, L., Moral, A., Pérez, A. & Jiménez, L. 2008, 'Use of high-boiling point organic solvents for pulping oil palm empty fruit bunches', *Bioresource Technology*, vol. 99, no. 6, pp. 1743-9.
- Rondon, H., El-Cheikh, W., Boluarte, I.A., Chang, C.Y., Bagshaw, S., Farago, L., Jegatheesan, V. & Shu, L. 2015, 'Application of enhanced membrane bioreactor (eMBR) to treat dye wastewater', *Bioresour Technol*, vol. 183, pp. 78-85.
- Saffarini, R.B., Mansoor, B., Thomas, R. & Arafat, H.A. 2013, 'Effect of temperature-dependent microstructure evolution on pore wetting in PTFE membranes under membrane distillation conditions', *Journal of membrane science*, vol. 429, pp. 282-94.
- Sahinkaya, E., Yurtsever, A. & Çınar, Ö. 2017, 'Treatment of textile industry wastewater using dynamic membrane bioreactor: Impact of intermittent aeration on process performance', *Separation and Purification Technology*, vol. 174, pp. 445-54.
- Salimi, A. & Yousefi, A. 2003, 'Analysis method: FTIR studies of  $\beta$ -phase crystal formation in stretched PVDF films', *Polymer Testing*, vol. 22, no. 6, pp. 699-704.

- Shaffer, D.L., Arias Chavez, L.H., Ben-Sasson, M., Romero-Vargas Castrillón, S., Yip, N.Y. & Elimelech, M. 2013, 'Desalination and reuse of high-salinity shale gas produced water: drivers, technologies, and future directions', *Environmental science & technology*, vol. 47, no. 17, pp. 9569-83.
- Shan, H., Liu, J., Li, X., Li, Y., Tezel, F.H., Li, B. & Wang, S. 2018, 'Nanocoated amphiphobic membrane for flux enhancement and comprehensive anti-fouling performance in direct contact membrane distillation', *Journal of Membrane Science*, vol. 567, pp. 166-80.
- Shi, F., Ma, Y., Ma, J., Wang, P. & Sun, W. 2012, 'Preparation and characterization of PVDF/TiO<sub>2</sub> hybrid membranes with different dosage of nano-TiO<sub>2</sub>', *Journal of Membrane Science*, vol. 389, pp. 522-31.
- Singh, R. & Hankins, N. 2016, *Emerging membrane technology for sustainable water treatment*, Elsevier.
- Smolders, C., Reuvers, A., Boom, R. & Wienk, I. 1992, 'Microstructures in phase-inversion membranes. Part 1. Formation of macrovoids', *Journal of Membrane Science*, vol. 73, no. 2-3, pp. 259-75.
- Song, X., Xie, M., Li, Y., Li, G. & Luo, W. 2018, 'Salinity build-up in osmotic membrane bioreactors: Causes, impacts, and potential cures', *Bioresour Technol.*
- Song, Z.W. & Jiang, L.Y. 2013, 'Optimization of morphology and performance of PVDF hollow fiber for direct contact membrane distillation using experimental design', *Chemical Engineering Science*, vol. 101, no. 0, pp. 130-43.
- Su, C., Li, Y., Dai, Y., Gao, F., Tang, K. & Cao, H. 2016, 'Fabrication of three-dimensional superhydrophobic membranes with high porosity via simultaneous electrospraying and electrospinning', *Materials Letters*, vol. 170, pp. 67-71.
- Subramanian, N., Qamar, A., Alsaadi, A., Gallo, A., Ridwan, M.G., Lee, J.-G., Pillai, S., Arunachalam, S., Anjum, D., Sharipov, F., Ghaffour, N. & Mishra, H. 2019, 'Evaluating the potential of superhydrophobic nanoporous alumina membranes for direct contact membrane distillation', *Journal of Colloid and Interface Science*, vol. 533, pp. 723-32.
- Sui, Q., Liu, C., Dong, H. & Zhu, Z. 2014, 'Effect of ammonium nitrogen concentration on the ammonia-oxidizing bacteria community in a membrane bioreactor for the treatment of anaerobically digested swine wastewater', *Journal of bioscience and bioengineering*, vol. 118, no. 3, pp. 277-83.
- Sukitpaneenit, P. & Chung, T.-S. 2009, 'Molecular elucidation of morphology and mechanical properties of PVDF hollow fiber membranes from aspects of phase inversion, crystallization and rheology', *Journal of Membrane Science*, vol. 340, no. 1-2, pp. 192-205.
- Tang, N., Jia, Q., Zhang, H., Li, J. & Cao, S. 2010, 'Preparation and morphological characterization of narrow pore size distributed polypropylene hydrophobic membranes for vacuum membrane distillation via thermally induced phase separation', *Desalination*, vol. 256, no. 1-3, pp. 27-36.
- Tao, M.-m., Liu, F., Ma, B.-r. & Xue, L.-x. 2013, 'Effect of solvent power on PVDF membrane polymorphism during phase inversion', *Desalination*, vol. 316, pp. 137-45.
- Tavakkoli, S., Lokare, O.R., Vidic, R.D. & Khanna, V. 2017, 'A techno-economic assessment of membrane distillation for treatment of Marcellus shale produced water', *Desalination*, vol. 416, pp. 24-34.
- Teh, X.Y., Poh, P.E., Gouwanda, D. & Chong, M.N. 2015, 'Decentralized light greywater treatment using aerobic digestion and hydrogen peroxide disinfection for non-potable reuse', *Journal of Cleaner Production*, vol. 99, pp. 305-11.

- Tian, R., Gao, H., Yang, X.H., Yan, S.Y. & Li, S. 2014, 'A new enhancement technique on air gap membrane distillation', *Desalination*, vol. 332, no. 1, pp. 52-9.
- Tijing, L.D., Choi, J.-S., Lee, S., Kim, S.-H. & Shon, H.K. 2014, 'Recent progress of membrane distillation using electrospun nanofibrous membrane', *Journal of Membrane Science*, vol. 453, pp. 435-62.
- Tijing, L.D., Woo, Y.C., Choi, J.-S., Lee, S., Kim, S.-H. & Shon, H.K. 2015a, 'Fouling and its control in membrane distillation—a review', *Journal of Membrane Science*, vol. 475, pp. 215-44.
- Tijing, L.D., Woo, Y.C., Choi, J.-S., Lee, S., Kim, S.-H. & Shon, H.K. 2015b, 'Fouling and its control in membrane distillation—A review', *Journal of Membrane Science*, vol. 475, no. 0, pp. 215-44.
- Tijing, L.D., Woo, Y.C., Choi, J.S., Lee, S., Kim, S.H. & Shon, H.K. 2015c, 'Fouling and its control in membrane distillation-A review', *Journal of Membrane Science*, vol. 475, pp. 215-44.
- Tijing, L.D., Woo, Y.C., Johir, M.A.H., Choi, J.-S. & Shon, H.K. 2014, 'A novel dual-layer bicomponent electrospun nanofibrous membrane for desalination by direct contact membrane distillation', *Chemical Engineering Journal*, vol. 256, pp. 155-9.
- Tijing, L.D., Woo, Y.C., Shim, W.-G., He, T., Choi, J.-S., Kim, S.-H. & Shon, H.K. 2016, 'Superhydrophobic nanofiber membrane containing carbon nanotubes for high-performance direct contact membrane distillation', *Journal of Membrane Science*, vol. 502, pp. 158-70.
- Tiwari, V. & Srivastava, G. 2014, 'Effect of thermal processing conditions on the structure and dielectric properties of PVDF films', *Journal of Polymer Research*, vol. 21, no. 11, pp. 1-8.
- Tomaszewska, M., Gryta, M. & Morawski, A.W. 1994, 'A study of separation by the direct-contact membrane distillation process', *Separations Technology*, vol. 4, no. 4, pp. 244-8.
- Tufa, R.A., Curcio, E., Brauns, E., van Baak, W., Fontananova, E. & Di Profio, G. 2015, 'Membrane distillation and reverse electrodialysis for near-zero liquid discharge and low energy seawater desalination', *Journal of Membrane Science*, vol. 496, pp. 325-33.
- Van der Bruggen, B. 2013, 'Integrated membrane separation processes for recycling of valuable wastewater streams: nanofiltration, membrane distillation, and membrane crystallizers revisited', *Industrial & Engineering Chemistry Research*, vol. 52, no. 31, pp. 10335-41.
- Vazquez, G., Alvarez, E. & Navaza, J.M. 1995, 'Surface tension of alcohol water+ water from 20 to 50. degree. C', *Journal of chemical and engineering data*, vol. 40, no. 3, pp. 611-4.
- Venault, A., Chang, Y., Wu, J.-R. & Wang, D.-M. 2014, 'Influence of solvent composition and non-solvent activity on the crystalline morphology of PVDF membranes prepared by VIPS process and on their arising mechanical properties', *Journal of the Taiwan Institute of Chemical Engineers*, vol. 45, no. 3, pp. 1087-97.
- Wang, J., Zheng, L., Wu, Z., Zhang, Y. & Zhang, X. 2016, 'Fabrication of hydrophobic flat sheet and hollow fiber membranes from PVDF and PVDF-CTFE for membrane distillation', *Journal of membrane science*, vol. 497, pp. 183-93.
- Wang, K., Abdalla, A.A., Khaleel, M.A., Hilal, N. & Khraisheh, M.K. 2017, 'Mechanical properties of water desalination and wastewater treatment membranes', *Desalination*, vol. 401, pp. 190-205.



- Wang, K., Hou, D., Wang, J., Wang, Z., Tian, B. & Liang, P. 2018, 'Hydrophilic surface coating on hydrophobic PTFE membrane for robust anti-oil-fouling membrane distillation', *Applied Surface Science*, vol. 450, pp. 57-65.
- Wang, P. & Chung, T.S. 2015, 'Recent advances in membrane distillation processes: Membrane development, configuration design and application exploring', *Journal of Membrane Science*, vol. 474, pp. 39-56.
- Wang, P., Teoh, M.M. & Chung, T.S. 2011, 'Morphological architecture of dual-layer hollow fiber for membrane distillation with higher desalination performance', *Water Res*, vol. 45, no. 17, pp. 5489-500.
- Wang, Z., Chen, Y. & Lin, S. 2018, 'Kinetic Model for Surfactant-Induced Pore Wetting in Membrane Distillation', *Journal of Membrane Science*.
- Wang, Z., Chen, Y., Sun, X., Duddu, R. & Lin, S. 2018, 'Mechanism of pore wetting in membrane distillation with alcohol vs. surfactant', *Journal of Membrane Science*, vol. 559, pp. 183-95.
- Wang, Z., Hou, D. & Lin, S. 2016a, 'Composite Membrane with Underwater-Oleophobic Surface for Anti-Oil-Fouling Membrane Distillation', *Environmental Science and Technology*, vol. 50, no. 7, pp. 3866-74.
- Wang, Z., Hou, D. & Lin, S. 2016b, 'Composite membrane with underwater-oleophobic surface for anti-oil-fouling membrane distillation', *Environmental science & technology*, vol. 50, no. 7, pp. 3866-74.
- Wang, Z., Jin, J., Hou, D. & Lin, S. 2016, 'Tailoring surface charge and wetting property for robust oil-fouling mitigation in membrane distillation', *Journal of Membrane Science*, vol. 516, pp. 113-22.
- Wang, Z. & Lin, S. 2017, 'Membrane fouling and wetting in membrane distillation and their mitigation by novel membranes with special wettability', *Water research*, vol. 112, pp. 38-47.
- Wang, Z., Wu, Z., Yin, X. & Tian, L. 2008, 'Membrane fouling in a submerged membrane bioreactor (MBR) under sub-critical flux operation: Membrane foulant and gel layer characterization', *Journal of Membrane Science*, vol. 325, no. 1, pp. 238-44.
- Warsinger, D.M., Swaminathan, J., Guillen-Burrieza, E. & Arafat, H.A. 2015, 'Scaling and fouling in membrane distillation for desalination applications: a review', *Desalination*, vol. 356, pp. 294-313.
- Wijekoon, K.C., Hai, F.I., Kang, J., Price, W.E., Guo, W., Ngo, H.H., Cath, T.Y. & Nghiem, L.D. 2014, 'A novel membrane distillation-thermophilic bioreactor system: biological stability and trace organic compound removal', *Bioresour Technol*, vol. 159, pp. 334-41.
- Wijekoon, K.C., Visvanathan, C. & Abeynayaka, A. 2011, 'Effect of organic loading rate on VFA production, organic matter removal and microbial activity of a two-stage thermophilic anaerobic membrane bioreactor', *Bioresour Technol*, vol. 102, no. 9, pp. 5353-60.
- Wirth, D. & Cabassud, C. 2002, 'Water desalination using membrane distillation: comparison between inside/out and outside/in permeation', *Desalination*, vol. 147, no. 1-3, pp. 139-45.
- Woo, Y.C., Chen, Y., Tijing, L.D., Phuntsho, S., He, T., Choi, J.-S., Kim, S.-H. & Shon, H.K. 2017, 'CF<sub>4</sub> plasma-modified omniphobic electrospun nanofiber membrane for produced water brine treatment by membrane distillation', *Journal of Membrane Science*, vol. 529, pp. 234-42.
- Woo, Y.C., Kim, Y., Shim, W.-G., Tijing, L.D., Yao, M., Nghiem, L.D., Choi, J.-S., Kim, S.-H. & Shon, H.K. 2016, 'Graphene/PVDF flat-sheet membrane for the treatment of RO

- brine from coal seam gas produced water by air gap membrane distillation', *Journal of Membrane Science*, vol. 513, pp. 74-84.
- Woo, Y.C., Kim, Y., Yao, M., Tijting, L.D., Choi, J.-S., Lee, S., Kim, S.-H. & Shon, H.K. 2018, 'Hierarchical Composite Membranes with Robust Omniphobic Surface Using Layer-By-Layer Assembly Technique', *Environmental Science & Technology*, vol. 52, no. 4, pp. 2186-96.
- Woo, Y.C., Lee, J.J., Tijting, L.D., Shon, H.K., Yao, M. & Kim, H.-S. 2015, 'Characteristics of membrane fouling by consecutive chemical cleaning in pressurized ultrafiltration as pre-treatment of seawater desalination', *Desalination*, vol. 369, no. 0, pp. 51-61.
- Woo, Y.C., Tijting, L.D., Shim, W.-G., Choi, J.-S., Kim, S.-H., He, T., Drioli, E. & Shon, H.K. 2016, 'Water desalination using graphene-enhanced electrospun nanofiber membrane via air gap membrane distillation', *Journal of Membrane Science*, vol. 520, pp. 99-110.
- Wu, H., Mansouri, J. & Chen, V. 2013, 'Silica nanoparticles as carriers of antifouling ligands for PVDF ultrafiltration membranes', *Journal of Membrane Science*, vol. 433, pp. 135-51.
- Wu, H.Y., Wang, R. & Field, R.W. 2014, 'Direct contact membrane distillation: An experimental and analytical investigation of the effect of membrane thickness upon transmembrane flux', *Journal of Membrane Science*, vol. 470, no. 0, pp. 257-65.
- Wu, P., Jiang, L.Y. & Hu, B. 2018, 'Fabrication of novel PVDF/P(VDF-co-HFP) blend hollow fiber membranes for DCMD', *Journal of Membrane Science*, vol. 566, pp. 442-54.
- Xia, T., Gao, X., Wang, C., Xu, X. & Zhu, L. 2016, 'An enhanced anaerobic membrane bioreactor treating bamboo industry wastewater by bamboo charcoal addition: Performance and microbial community analysis', *Bioresour Technol*, vol. 220, pp. 26-33.
- Xie, M., Shon, H.K., Gray, S.R. & Elimelech, M. 2016, 'Membrane-based processes for wastewater nutrient recovery: Technology, challenges, and future direction', *Water Research*, vol. 89, pp. 210-21.
- Xu, Y., Zhu, B.-K. & Xu, Y.-y. 2006, 'Pilot test of vacuum membrane distillation for seawater desalination on a ship', *Desalination*, vol. 189, no. 1-3, pp. 165-9.
- Xu, Z., Liu, Z., Song, P. & Xiao, C. 2017, 'Fabrication of super-hydrophobic polypropylene hollow fiber membrane and its application in membrane distillation', *Desalination*, vol. 414, pp. 10-7.
- Yan, H., Lu, X., Wu, C., Sun, X. & Tang, W. 2017, 'Fabrication of a super-hydrophobic polyvinylidene fluoride hollow fiber membrane using a particle coating process', *Journal of Membrane Science*, vol. 533, pp. 130-40.
- Yang, C., Li, X.-M., Gilron, J., Kong, D.-f., Yin, Y., Oren, Y., Linder, C. & He, T. 2014, 'CF<sub>4</sub> plasma-modified superhydrophobic PVDF membranes for direct contact membrane distillation', *Journal of Membrane Science*, vol. 456, pp. 155-61.
- Yang, H.C., Hou, J., Chen, V. & Xu, Z.K. 2016, 'Janus membranes: exploring duality for advanced separation', *Angewandte Chemie International Edition*, vol. 55, no. 43, pp. 13398-407.
- Yang, X., Pang, H., Zhang, J., Liubinas, A. & Duke, M. 2017, 'Sustainable waste water deammonification by vacuum membrane distillation without pH adjustment: Role of water chemistry', *Chemical Engineering Journal*, vol. 328, pp. 884-93.
- Yang, X., Wang, R., Shi, L., Fane, A.G. & Debowski, M. 2011, 'Performance improvement of PVDF hollow fiber-based membrane distillation process', *Journal of Membrane Science*, vol. 369, no. 1-2, pp. 437-47.

- Yao, M., Woo, Y.C., Tijing, L., Cesarini, C. & Shon, H.K. 2017, 'Improving Nanofiber Membrane Characteristics and Membrane Distillation Performance of Heat-Pressed Membranes via Annealing Post-Treatment', *Applied Sciences*, vol. 7, no. 1, p. 78.
- Yao, M., Woo, Y.C., Tijing, L.D., Choi, J.-S. & Shon, H.K. 2017, 'Effects of volatile organic compounds on water recovery from produced water via vacuum membrane distillation', *Desalination*.
- Yao, M., Woo, Y.C., Tijing, L.D., Choi, J.-S. & Shon, H.K. 2018, 'Effects of volatile organic compounds on water recovery from produced water via vacuum membrane distillation', *Desalination*, vol. 440, pp. 146-55.
- Yao, M., Woo, Y.C., Tijing, L.D., Shim, W.-G., Choi, J.-S., Kim, S.-H. & Shon, H.K. 2016, 'Effect of heat-press conditions on electrospun membranes for desalination by direct contact membrane distillation', *Desalination*, vol. 378, pp. 80-91.
- Yeow, M., Liu, Y. & Li, K. 2003, 'Isothermal phase diagrams and phase-inversion behavior of poly (vinylidene fluoride)/solvents/additives/water systems', *Journal of Applied Polymer Science*, vol. 90, no. 8, pp. 2150-5.
- Yong, J., Chen, F., Yang, Q., Huo, J. & Hou, X. 2017, 'Superoleophobic surfaces', *Chemical Society Reviews*, vol. 46, no. 14, pp. 4168-217.
- Yu, L., Guo, Q., Hao, J. & Jiang, W. 2000, 'Recovery of acetic acid from dilute wastewater by means of bipolar membrane electrodialysis', *Desalination*, vol. 129, no. 3, pp. 283-8.
- Yuan, Y. & Lee, T.R. 2013, 'Contact angle and wetting properties', *Surface science techniques*, Springer, pp. 3-34.
- Zhang, H., Li, B., Sun, D., Miao, X. & Gu, Y. 2018, 'SiO<sub>2</sub>-PDMS-PVDF hollow fiber membrane with high flux for vacuum membrane distillation', *Desalination*, vol. 429, pp. 33-43.
- Zhang, J., Gray, S. & Li, J.-D. 2013, 'Predicting the influence of operating conditions on DCMD flux and thermal efficiency for incompressible and compressible membrane systems', *Desalination*, vol. 323, pp. 142-9.
- Zhang, J., Li, J.-D. & Gray, S. 2011, 'Effect of applied pressure on performance of PTFE membrane in DCMD', *Journal of Membrane Science*, vol. 369, no. 1-2, pp. 514-25.
- Zhang, J., Loong, W.L.C., Chou, S., Tang, C., Wang, R. & Fane, A.G. 2012, 'Membrane biofouling and scaling in forward osmosis membrane bioreactor', *Journal of Membrane Science*, vol. 403-404, pp. 8-14.
- Zhang, J., Song, Z., Li, B., Wang, Q. & Wang, S. 2013, 'Fabrication and characterization of superhydrophobic poly (vinylidene fluoride) membrane for direct contact membrane distillation', *Desalination*, vol. 324, pp. 1-9.
- Zhang, P.-Y., Yang, H., Xu, Z.-L., Wei, Y.-M., Guo, J.-L. & Chen, D.-G. 2013, 'Characterization and preparation of poly (vinylidene fluoride)(PVDF) microporous membranes with interconnected bicontinuous structures via non-solvent induced phase separation (NIPS)', *Journal of Polymer Research*, vol. 20, no. 2, p. 66.
- Zhang, X., Li, C., Wang, Y., Luo, J. & Xu, T. 2011, 'Recovery of acetic acid from simulated acetaldehyde wastewaters: Bipolar membrane electrodialysis processes and membrane selection', *Journal of membrane science*, vol. 379, no. 1-2, pp. 184-90.
- Zhao, F., Ma, Z., Xiao, K., Xiang, C., Wang, H., Huang, X. & Liang, S. 2018, 'Hierarchically textured superhydrophobic polyvinylidene fluoride membrane fabricated via nanocasting for enhanced membrane distillation performance', *Desalination*, vol. 443, pp. 228-36.
- Zheng, R., Chen, Y., Wang, J., Song, J., Li, X.-M. & He, T. 2018, 'Preparation of omniphobic PVDF membrane with hierarchical structure for treating saline oily wastewater using

- direct contact membrane distillation', *Journal of Membrane Science*, vol. 555, pp. 197-205.
- Zhong, W., Hou, J., Yang, H.C. & Chen, V. 2017, 'Superhydrophobic membranes via facile bio-inspired mineralization for vacuum membrane distillation', *Journal of Membrane Science*, vol. 540, pp. 98-107.
- Zhu, H., Wang, H., Wang, F., Guo, Y., Zhang, H. & Chen, J. 2013, 'Preparation and properties of PTFE hollow fiber membranes for desalination through vacuum membrane distillation', *Journal of membrane science*, vol. 446, pp. 145-53.
- Zhu, J., Jiang, L. & Matsuura, T. 2015, 'New insights into fabrication of hydrophobic/hydrophilic composite hollow fibers for direct contact membrane distillation', *Chemical Engineering Science*, vol. 137, pp. 79-90.
- Zhu, Z., Liu, Y., Hou, H., Shi, W., Qu, F., Cui, F. & Wang, W. 2018, 'Dual-Bioinspired Design for Constructing Membranes with Superhydrophobicity for Direct Contact Membrane Distillation', *Environmental Science and Technology*, vol. 52, no. 5, pp. 3027-36.
- Zhu, Z., Liu, Z., Zhong, L., Song, C., Shi, W., Cui, F. & Wang, W. 2018, 'Breathable and asymmetrically superwetable Janus membrane with robust oil-fouling resistance for durable membrane distillation', *Journal of Membrane Science*, vol. 563, pp. 602-9.
- Zuo, G. & Wang, R. 2013, 'Novel membrane surface modification to enhance anti-oil fouling property for membrane distillation application', *Journal of membrane science*, vol. 447, pp. 26-35.
- Zuo, J., Bonyadi, S. & Chung, T.-S. 2016, 'Exploring the potential of commercial polyethylene membranes for desalination by membrane distillation', *Journal of Membrane Science*, vol. 497, pp. 239-47.
- Zuo, J., Chung, T.-S., O'Brien, G.S. & Kosar, W. 2017, 'Hydrophobic/hydrophilic PVDF/Ultem® dual-layer hollow fiber membranes with enhanced mechanical properties for vacuum membrane distillation', *Journal of Membrane Science*, vol. 523, pp. 103-10.